Order Number 9402447

Non-linear finite element analysis of reinforced concrete beams repaired by plate bonding

Ziraba, Yasin Naku, Ph.D.

King Fahd University of Petroleum and Minerals (Saudi Arabia), 1993

U·M·I
300 N. Zeeb Rd.
Ann Arbor, MI 48106

NON-LINEAR FINITE ELEMENT ANALYSIS OF REINFORCED CONCRETE BEAMS REPAIRED BY PLATE BONDING

BY

YASIN NAKU ZIRABA

A Thesis Presented to the

FACULTY OF THE COLLEGE OF GRADUATE STUDIES

KING FAHD UNIVERSITY OF PETROLEUM & MINERALS

DHAHRAN, SAUDI ARABIA

In Partial Fulfillment of the
Requirements for the Degree of

DOCTOR OF PHILOSOPHY

In

CIVIL ENGINEERING

JUNE, 1993

KING FAHD UNIVERSITY OF PETROLEUM AND MINERALS
DHAHRAN 31261, SAUDI ARABIA

COLLEGE OF GRADUATE STUDIES

This dissertation, written by YASIN NAKU ZIRABA *under the direction of his Dissertation Advisor and approved by his Dissertation Committee, has been presented to and accepted by the Dean of the College of Graduate Studies, in partial fulfillment of the requirements for the degree of*

DOCTOR OF PHILOSOPHY IN CIVIL ENGINEERING

Dissertation Committee

Prof M. H. Baluch
Dissertation Advisor

DR. I. A. Basunbul
Dissertation Co-Advisor

Prof A. K. Azad
Member

Dr. A. M. Sharif
Member

Dr. G. J. Al-Sulaimani
Member

Dr. Q. K. Ghori
Member

Dr. A. M. Sharif
Department Chairman

Dr. Ala H. Al-Rabeh
Dean College of Graduate Studies

Date: JUNE, 1993

DISSERTATION ABSTRACT

Full Name : YASIN NAKU ZIRABA

Title of Study : NON-LINEAR FINITE ELEMENT ANALYSIS OF REINFORCED CONCRETE BEAMS REPAIRED BY PLATE BONDING

Major Field : STRUCTURAL ENGINEERING

Date of Degree : JUNE 1993

This thesis presents a non-linear finite element model for the flexure shear response of RC beams strengthened externally by epoxy bonded steel and glass fiber reinforced plastics (GFRP). The salient features include (i) the introduction of a thin, six-noded element to simulate behavior of the concrete/epoxy glue/plate interface and (ii) a scheme of loading a virgin RC beam to a prescribed displacement to simulate damage, unloading and then reloading the damaged RC beam repaired by an external plate. Results are presented for RC beams repaired by plates of varying thickness and a transmutation of failure mode is noted from classical flexure for the case of external reinforcement in the form of thin plates to a unique concrete cover rip off failure for thicker plates.

Using experimental-numerical approach, and based on data from a specially designed half beam specimen and experimental results from other specimen geometries, combined with their respective non-linear finite element idealizations, a classical Mohr-Coulomb failure law together with a tension cut-off is suggested for the material characterization of the steel/glue/concrete interface.

Drawing on results of numerical and experimental studies, a rational design approach for plated RC beams is crystallized by interpreting major modes of failure including (i) flexural, (ii) interface separation and (iii) concrete cover rip-off. New expressions for peak interface shear and peeling stresses as well as a predictor equation for shear resistance of plated RC beams are presented for use as design aids.

DOCTOR OF PHILOSOPHY DEGREE
KING FAHD UNIVERSITY OF PETROLEUM AND MINERALS
Dhahran, Saudi Arabia
JUNE 1993

خلاصة الرسالة

اسم الطالـــب : ياسين ناكو زيرابا
عنوان الدراسة : تحليل الجسور الخرسانية بواسطة الألواح الخارجية .
التخصـــــص : هندسة إنشائية .
تاريخ الشهادة : يونيو ١٩٩٣م .

تقدم هذه الأطروحة نموذج تحليلي بواسطة (FE) أجهادات الأنثناء القصي في الجسور الخرسانية المقواه بواسطة الألواح الفولاذية أو ألواح الألياف الزجاجية والتي تم لصقها خارجياً باللدائن ومن المميزات المهمة لهذا النموذج هو : ١ - أستعمال وحدة ذات ستة رؤوس لمحاكاة العلاقة بين اللدائن والخرسانة والألواح . ٢ - خطة لتحميل جسر خرساني جديد إلى مرحلةالضرر ثم إعادة ومواصلة التحميل بعد عملية التقوية. نتائج الأبحاث أشتملت علي جسور مقواه بألواح ذات سماكات مختلفة ، مع متابعة لتطور الفشل الأقصى من فشل الانثناء إلى فشل الغطاء الخرساني لأسياخ التسليح في حالة استعمال الألواح السميكة .

وبأستخدام النموذج الرياضي المرتبط بنتائج الفحوصات التي تمت على عينات تمثل نصف الكمرة الخرسانية فقد تم تطوير نموذج محاكاة للفشل حسب نظرية موهر - كولومب وكذلك فقد تم تحديد مناطق نهاية الشد للألواح الخارجية حسب مؤشراء الألواح واللدائن المستعملة .

وبالقياس لنتائج الأبحاث المخبرية ومحاكاتها بالنموذج الرياضي فقد تم الحصول على تمثيل شامل لحالات الفشل المختلفة ومنها : ١ - فشل الأنثناء . ٢ - سلخ الألواح عن الخرسانة . ٣ - سلخ غطاء الخرسانة عن أسياخ التسليح . كما تم تمثيل قوى القص بصورة جيدة في النموذج الرياضي مما سيمكن مستخدمي هذا النموذج المتطور من أستخدامه في أغراض التصميم .

درجة الدكتوراة في الفلسفة
جامعة الملك فهد للبترول والمعادن
الظهران ، المملكة العربية السعودية
التاريخ : يونيو ١٩٩٣م

This dissertation is dedicated

to

My Parents, Wife and Children

ACKNOWLEDGEMENT

Firstly, I thank ALLAH, All Paraise is for Him, for bestowing me with the strength and health to complete this work. Then acknowledgement is due to King Fahd University of Petroleum & Minerals for the support given to this research and the opportunity given to me to pursue graduate study.

I acknowledge, with deep gratitude and appreciation, the inspiration, encouragement and guidance given to me by my major advisor, Prof. M. H. Baluch. I am also indebted to the other committee members Dr. I. Basunmbul, Prof. A. K. Azad, Dr. A. M. Sharif, Dr. G. J. Al-Sulaimani and Dr. Q. K. Ghori for the valuable comments and suggestions they made to improve this work.

I would also like to express my thanks to the extensive computer facilities provided by the Data Processing Center at KFUPM. Thanks are also due to all the technical personel in the research laboratories who assisted greatly in the experimental part of the research.

I must acknowledge the help of Dr. M. S. A. Abbasi who provided the initial skeleton of the non-linear finite program and who helped greatly in its initial development.

Finally, I thank my parents, wife and children for their support and patience.

Contents

List of Tables

List of Figures

Chapter 1

General Introduction

1.1 Introduction

The need to maintain, repair and upgrade structures has now come to be recognized as being just as important as their design and construction. The level of maintenance, particularly in the Kingdom, is expected to rise due to the extensive deterioration of structures experienced in the Gulf Peninsula.

The increase in vehicular loading, as has been seen in the Kingdom [1,2,3], may render the load carrying capacity of existing highway bridges inadequate. There is therefore an urgent need to strengthen the bridges to carry the extra load. In some cases strengthening becomes necessary due to poor construction and workmanship which may result into cross sectional strengths originally calculated not being achieved, or if individual reinforcing bars are incorrectly placed. In yet other situations, changed use of the structure may create internal forces that exceed the limiting capacity of the member. Strengthening repair may also become necessary after structural damage due to settlements, explosions, vehicular impacts, fire etc.

Depending on the type of structure, a number of techniques have been used in the past to achieve the desired improvement, and in case of concrete

structures, some of the most common methods include

- Replacing non-structural toppings with structural elements or by lighter materials to reduce the dead loads
- Introducing extra supports
- Adding extra reinforcement by stapling and guniting
- Prestressing either externally or internally.

The cost of such work as well as the long periods of time and the disruption involved can often be considerable. Evacuation of all or part of a building, or road closures in case of bridges, may be necessary while the work is being carried out and all these add to the cost.

With the advent and development of strong epoxy adhesives in recent years, strengthening of concrete structures by bonding external plates has come to be recognized as an effective and convenient method of improving structural performance. The gluing of steel plates to the surface of the concrete ensures composite action with the original member and helps in carrying the live load or live and dead load if propping or some other load relieving method is used. This technique has the virtues of being relatively simple in application, quick to carry out with minimum disruption to the functions of the facility, and when completed the changes to the structural dimensions are only of the order of a few millimeters.

Some of the most important and interesting features regarding the behavior of reinforced concrete beams strengthened with externally bonded plates are summarized in the list below:

- Full composite action can be achieved between a concrete member and a steel plate by the use of a suitable epoxy glue.
- Plating can be used to increase flexural capacity of R/C beams weak in flexure due to inadequate main reinforcement or to increase the

shear capacity of those beams weak in shear due to inadequate provision of stirrups.

- Plate bonding has a considerable reducing effect on crack widths and deflections.

- In situations where failure of a flexurally strengthened reinforced concrete member is by yielding of the plate (i.e. when plates are sufficiently thin), the ultimate strength of the structure can be accurately predicted by using conventional R/C theory.

- When it is necessary to use relatively thick plates, failure may occur by horizontal cracking and plate separation starting at the plate ends. In this case, the plates do not reach their yield stress and failure is sudden, brittle and without warning. This failure mode precipitated by an interface failure occurs when the interface shear stress exceeds the shear strength of the concrete-glue-steel interface.

The last aspect of the repair by plate bonding technique is of considerable concern to practicing engineers and forms the basis of some of the theoretical and experimental research being carried out at universities worldwide including KFUPM.

Due to the various factors involved, the problem of premature failure, which though is of such practical significance, does not lend itself readily to straightforward strength of materials analysis. Yet the vast potential of this technique as an effective repair and strengthening tool, has led to rapid field implementation based on actual laboratory findings. The understanding of fundamental behavior however has lagged behind. The main thrust of this thesis is to help bridge this gap and is achieved by using a finite element approach for the analysis of the problem.

1.2 Aims and Objectives of the Project

The overall objective of this work is to use finite element as a numerical tool to (i) analyze and understand the structural response including failure mechanisms of reinforced concrete beams strengthened by epoxy bonded steel plates and (ii) develop a criteria for the rational design of such repaired R/C beams. The specific objectives of the study include:

- Development of a computaional model in the form of a non-linear finite element program so as to adequately predict load-deflection response, the ultimate load and state of stress in the critical zone of plate curtailment.
- Experimental determination of the material properties of the glued interface and hence construction of a material model needed as input to the computational analysis.
- Verification of the program by comparing the numerical results to existing experimental data. The experimental data relating to beams bonded by cither steel plates or by glass fiber composite plates is derived from experiments conducted at KFUPM and other researchers elsewhere, particularly at University of Sheffield in the UK.

1.2.1 Finite Element Program

To be able to accurately simulate the structural response of a reinforced concrete member, the finite element model must be capable of simulating material nonlinearity including

- concrete cracking in tension and associated tension stiffening
- plasticity of concrete in compression
- plasticity of reinforcing steel

- nonlinearity due to bond-slip
- shear degradation of concrete.

For beams strengthened with external plates, special elements must be formulated to model nonlinear material characteristics unique to the steel-glue-concrete interface.

The program used in this study takes into account all of the above material nonlinearities by using an iterative approach in the computation algorithm to achieve an acceptable solution at any given load increment. The required degradation is achieved by updating the element stiffness matrix at any iteration and at the same time redistributing resulting stresses to be compatible with the appropriate constitutive law. Each component of the plate bonded reinforced concrete beam is modeled by a different element type, for which the stiffness matrix at any given iteration is derived.

1.2.2 Material Properties of the Glued Interface

Several test configurations are needed to permit the construction of a universal material law for the glued steel/concrete interface capable of simulating the associated characteristic failure mechanisms. Failure of the glue interface normally occurs in the concrete at low shear stresses if accompanied by tensile normal stresses acting transversely to the interface, and at relatively higher shear stresses when the normal stresses are compressive.

Double lap shear tests such as those used in experiments by Charif [4] as well as single lap tests of the type described in this work generally do fail at higher shear stresses due to the interface transverse normal stresses which are compressive. On the other hand an R/C beam under a four point loading and whose tensile face is bonded an external plate fails at much lower shear stresses as a result of transverse tensile or peeling forces simultaneously occurring at the zone of plate curtailment.

Whereas it is possible to determine the peak shear stress at failure as well as the shear stiffness of the interface, measurement of the accompanying transverse normal stress is practically impossible. In this project, a numerical-experimental technique is used to assess the normal stress at failure of the various test configurations leading to the derivation of a 'Mohr-Coulomb' type material law for the glue interface.

1.2.3 Program Verification

To verify that the finite element program developed simulated the structural response of a plate bonded beam, comparison between the numerical results and documented experimental data was made. In this respect data from experiments conducted at KFUPM and at the University of Sheffield was used.

Aspects of structural response compared include deflections, ultimate loads, cracking patterns, strains and stresses in the bonded plate and internal reinforcement as well as the overall failure mechanism.

1.2.4 Design Guidelines

In order to arrive at a rational design criteria for the plate bonded reinforced concrete beam, a parametric study must be undertaken to determine the influence of the various variables. In this project the parameters studied included

- bonding plate geometry. Aspects studied in this case were the plate thickness and width, position of plate curtailment and also the effect of the plate taper in the zone plate curtailment.
- the effect of level of damage prior to repair, on the load capacity and other structural properties of the plate bonded reinforced concrete beam

- type of ultimate failure as influenced by amount of main steel reinforcement

The concept of design for plated beams hinges on the relative plate thickness where for beams strenthened or repaired with thin plates, failure of is dominated by extensive flexural concrete cracking and steel yielding and ultimate failure defined by the crushing of concrete in the compression zone. In this case, the design can be based on strain compatibility and the use of a rectangular compression stress block similar to the ACI method for RC beams in flexure. As the plate thickness increases however, the interface stresses at the plate curtailment zone increase and if the allowable strength values for the interface are exceeded, the plate may separate resulting in premature failure.

If the bonding adhesive is weak or if the gluing is not properly done, this type of failure may be characterized by plate debonding initially emanating from the plate curtailment. As the plate debonding proceeds away from the support and as the effective plate length is reduced, the peak peeling stresses progressively increase till such a value that a shear critical crack develops leading to sudden failure.

If the glueing is strong enough so as to prevent plate debonding, cracking emanates from the location of plate curtailment. The existence of peak peeling and shear stresses at the plate curtailment zone in addition to the bending stress results in a biaxial tensile stress state forcing the crack to move in essentially horizontal direction just below the level of internal reinforcement where the section is weakest. Failure ensues when the moving horizontal crack joins an existing shear flexural crack, culminating in a steep vertical ascent towards the point of loading.

To determine the external plate thickness sufficient to strengthen or repair an RC beam therefore, the design procedure should consist of three steps namely: **Step I:** The plated beam should be designed for flexure

assuming plate yielding and concrete crushing on the compression side. **Step II:** The interface stresses must be checked to ensure they are within limits to avoid plate debonding. **Step III:** The shear capacity of the plated beam must be checked to safeguard the beam against sudden failure due to concrete cover rip-off.

1.3 Thesis Outline

Chapter 2 of this thesis presents a literature review of the state of the art related to this work in three broad categories namely;

- Study related to the bonding of plates to damaged reinforced concrete beams. This includes the experimental study of the parameters that affect plate bonded beams and application of the repair technique to actual practical problems in the field.
- Approximation techniques based on strength of materials and partial interaction theory to determine stress concentrations at the plate curtailment.
- Laboratory determination of the mechanical properties of the glued steel-concrete interface.

Chapter 3 contains explanations regarding the material model used in this work and details the constitutive relations for the different components of the externally bonded reinforced concrete beam at all load levels including the failure criteria.

In chapter 4, the finite element model is presented where the governing differential equations are derived using the minimization of the total potential energy. For each of the element type, the finite element discretization, the strain-displacement relations as well as the numerical integration schemes are discussed.

Chapter 5 describes the experimental configurations used in this study to investigate the mechanical properties of the glue interface and techniques used to derive a characteristic material law. The technique is built around a non-linear finite element discretization of various test specimens used to characterize interface behavior.

Techniques used to implement the material and finite element models as described in chapters 3 and 4 respectively, into a working computer program are presented in chapter 6.

In chapter 7 the ability of the finite element program developed in chapter 6 to predict the structural response of a reinforced concrete beam externally strengthened or repaired with plates is verified. Results from the numerical computations are compared with experimental data derived from experiments done both at University of Sheffield and at KFUPM.

Chapter 8 contains explanations regarding the numerical experiments conducted to determine the influence of several parameters on the structural response and ultimate behavior of repaired and strengthened R/C beams.

Guidelines to assist in the rational design of plated beams are suggested in chapter 9. A regressed equation, based on considerable data obtained from numerical experiments is presented to allow for the determination of interface stresses. A predictor equation for the shear strength of plated beams is also presented in this chapter after a survey of experimental data reported by different researchers.

The general conclusions of the present work are presented in chapter 10.

Appendix A contains the users manual for the main program and Appendix B explains the use of a pre-processing program capable of generating an input file for the main program. Instructions for using the graphical post-processing program are contained in Appendix C.

Chapter 2

Literature Review

2.1 Introduction

The numerous advantages offered by plate bonding as a strengthening technique compared to other more traditional methods of repair have provided an impetus into experimental research to come up with some design guidelines for the confident use of the technique in the field. The results of such intensive experimental investigations have led to rapid field implementations even before fully understanding the fundamental mechanics of the plate bonded beam.

Computations of the ultimate loads and deflections of plated beams based on standard design codes as well as theoretical calculations based on strength of material approaches have been used and compared to experimental data. Numerical modelling has been restricted to finite difference approach in order to estimate the shear stress concentration occurring at the location of plate curtailment. No existing model analytical or numerical, has attempted to include aspects of material non-linearity which can play a significant role in the overall response.

In this chapter, a review of the literature related to this work is presented in three categories namely;

- Experimental study of the parameters that affect plate bonded beams and application of the repair technique to actual practical problems in the field.
- Approximate techniques based on strength of materials used to evaluate stress concentration at the plate curtailment. Methods employing the partial interaction theory with partial slip are also reviewed.
- Laboratory determination of the mechanical properties of the glued steel-concrete interface.

Literature related to application of finite elements to reinforced concrete beams and use of finite element techniques to model interfaces is reviewed in Chapter 3 and 4.

2.2 Plate Bonding of Damaged Beams

The attempt to use epoxy resins to form the shear connection between external steel plates and existing concrete for purposes of repair or strengthening was simultaneously pioneered in France [5] and South Africa [6] in the late 1960s and early 1970s. The technique of structural strengthening by plate bonding has also been used elsewhere including parts of Europe [7] and Japan [8], where at least 240 undercapacity bridges had been plated by 1975. In the United Kingdom the technique has been applied to highway bridges [9] as well as buildings. A list of known such applications as of 1987 is given in Table 4 of reference [10]. In the Gulf region, repair of structures by plate bonding has been used at ALBA aluminium smelting plant in Bahrain [7] and parking garages in Riyadh and Jeddah, Saudi Arabia [11].

2.2.1 Experimental Study of Beams Bonded with Steel Plates

Irwin [12], in his study on the use of plate bonding technique for strengthening beams in flexure, concluded that the crack widths of the plated beam were significantly reduced to almost half of those on the unplated beam, whereas the moment capacity did not increase to any great degree.

Experimental studies done by Macdonald [13] focused on the effects of several variables including adhesive properties, joint geometry, plate thickness and load cycling, on the structural performance of plated reinforced concrete beams. The results showed that the load to produce a crack of certain width in a plated beam was approximately double the load needed to produce the same size-crack in the unplated beam, but with no significant increase in the load carrying capacity. From observations in all cases, failure occurred in the plated beam by horizontal shear in the concrete adjacent to the steel plate, commencing at the end where the plate is terminated. Also, after the plate separation, subsequent failure seemed to occur by shear/compression failure of the concrete at a load similar to the failure load of the unplated beam. The important observations stated in Macdonald's study [13] may thus be summarized as:

- **Bonding of steel plates** increased the beam stiffness and resulted into more closely spaced flexural cracks. Ultimate loads were increased by 40 % and stiffness by 190 %.

- **Proportion of plates.** Narrow plates with large width b, and small thickness t, gave ductile failures with yielding of the plate and eventual crushing of concrete. The lower flexural stiffness of the plate reduced the peeling stresses. It is recommended that rapid shear failure may be prevented by using a b/t greater than 60.

- **Adhesive flexibility.** A flexible adhesive did not change the crack

pattern nor the load at first crack and whereas the more stiff adhesive resulted in a similar deflection response, more closely spaced cracking pattern was noticeable. He thus recommended [13] the use of a stiff adhesive.

- **Measured shear stresses.** Very low peak shear stress values of τ between 0.13 and 0.8 MPa were reported. This was however, attributed to inaccuracies of strain measurement.

- **Partial bonding** of the plates resulted in the same ultimate loads as full bonding although the cracking was more extensive.

Jones, Swamy and Ang [14] studied the influence of bonding steel plates on the behavior of under and over reinforced concrete beams. One parameter studied was the relative efficiency of different plate thickness for under-reinforced beams. Two over-reinforced beams with plates bonded on the tension and compression respectively were also included in the experimental investigation. Some of the important observations, results and conclusions from their study may be summarized as follows;

- **Modes of failure** were characterized by yielding of the rebars and plates for under-reinforced beams of depth 150 mm and bonded with thin plates of 1.5 and 3.0 mm., whereas beams reinforced with thicker plates of 5 and 10 mm. failed by plate separation followed by tearing commencing at the plate curtailment. The over-reinforced beams suffered a sudden failure due to crushing of concrete in compression.

- **Increase in ultimate loads** was 100 % for under-reinforced beams, 44 % for over-reinforced beams with plates on the tensile face and only, 22 % for over-reinforced beams with plates on the compression side.

- **Effect on cracking** was that the first crack was delayed by plate bonding but little effect on crack spacing. Crack lengths and widths were however reduced.

- **Measured shear stresses** of τ between 2.13 and 2.18 MPa were constant and thought to be function of concrete strength.

- **Plate on the compression face** buckled initiated by the crushing concrete.

- **In the theoretical analysis** a rectangular stress block with $0.6f_c'$ was used. Using the actual $\sigma - \varepsilon$ for steel, a strain compatibility for concrete with $\varepsilon_u = 0.0035$, the experimental cracking and ultimate loads were accurately predicted.

The effect of parameters such as plate thickness, glue thickness, layering and lapping of plates, variations in glue thickness and presence of stress concentrations in the adhesive layer, on the service and ultimate loads were studied in the experimental investigations performed by Swamy, Jones and Bloxham [15]. A total of 24 beams of width 155 mm and a total depth of 255 mm were tested and summarized below are the salient features the study;

- **First crack load.** Best results are obtained when the glue layer is as thin as possible. Other parameters such as plate lapping, stress concentrations in the adhesive layer as well as precracking did not seem to have any significant effect on the first crack load.

- **Flexural rigidity** was found not to be constant and varied with the applied load, degree of cracking, plate and glue thicknesses. Increasing the thickness of plates reduces deflections and plate strains. The same result seems to apply with glue thickness though to a lesser extent.

- **Ultimate load.** The increase in the ultimate loads between the plated and unplated beams was 10% – 16% for plate thicknesses less than or equal to 3 mm. For the beam plated with 6 mm, the ultimate loads decreased by 5% – 16%. Glue thickness had no visible effect on the ultimate loads for thin plates, but lead to slightly lower loads when thicker plates were used. Overall factor of safety between the service and ultimate loads was about 1.6.

- **Theoretical prediction of ultimate moments** was done using three different methods, namely

  1. CP110 without a partial factor of safety.
  2. strain compatibility assuming cracked glue, CP110 rectangular stress block and no partial factors of safety.
  3. same as no. 2 except the glue was assumed to be uncracked.

  It was concluded that ultimate moments may be predicted by conventional means except for beams with thick plates ($t_p \geq 6$ mm) since such beams are unable to develop the full flexural capacity.

- **Modes of failure.**

  - **Beams with 1.5 mm plate** failed in flexure with yielding of the main reinforcement and plate. No plate debonding was noticeable. Similar failure pattern was reported for beams with lapped plates, variable glue thickness and stress concentration risers in the glue layer and also for beams precracked before plating.
  - **Beams with 3 mm plates** experienced a flexure/shear-bond failure though flexural mode dominated the failure mechanism. No debonding was noticed though concrete below the internal reinforcement ripped away after initiation of the shear crack at the

plate end. Beams with lapped plates achieved full flexural capacity though the final failure mechanism was that of shear/bond.

- **Beams with 6 mm plates** had the concrete cover ripped off but no debonding in the glue layer was noticeable. The steel did not yield and results indicated that a thinner glue layer gives more efficient performance.

- **Limiting plate thickness** to prevent brittle premature failure should be such that the ratio of plate width to thickness b/t is less than 50. To avoid conditions of over reinforcing, the ratio x/d should be less than or equal to 0.4, where x is the depth to the neutral axis and d the effective depth.

Conclusions along similar lines were made in an earlier study by Jones, Swamy, Bloxham and Bouderblah [16].

Swamy, Jones and Chariff [17] in their investigation on the effect of plating structurally damaged RC beams considered two cases of strengthening. In one case, beams loaded up to 70 % of the ultimate load were unloaded and strengthened in the unloaded state while in the second case the beams were strengthened in the loaded state. The result was that strengthening of severely cracked beams is structurally efficient and beams were restored to flexural stiffness and strengths more superior to unplated beams. Other conclusions of the study include;

- **Flexible epoxy adhesive** will not crack before failure and thus is a full participant in the composite system.

- **Strengthening of predamaged unloaded beams** had no adverse effect on the the beam behavior though cracking effect was more pronounced on loads beyond the preload level.

- **Strengthening of predamaged beams under high stress** lead to higher strains and deformations but less than the unplated beams.

- **Anchorage stresses** were assessed using conventional elastic theory. The shear stress in the anchorage zone may be calculated as

$$\tau = \frac{VA\bar{y}}{Ib} \tag{2.1}$$

where

V max shear,

A area of transformed section using long term modular ratio,

$\bar{y}$ distance from the neutral axis to the mid-plane of plate,

b width of plate and

I second moment of area of the transformed section using long term modular ratio.

Then the maximum shear stress,

$$\tau_{max} = 2\tau \leq \tau_{ult} = \sqrt{2} f_t \tag{2.2}$$

where

τ_{ult} ultimate shear stress and

f_t the tensile strength of the concrete.

In summary, these investigations show that bonding of thin steel plates on the tension faces of concrete beams can lead to significant improvements in the structural performance under both service and ultimate load conditions. However, the investigations also show that premature failure may occur because of shear and normal stress concentrations at the ends of the steel plates resulting in debonding of the plate or ripping off of the concrete cover. Although bolts at the plate curtailment may help prevent the premature tearing off of the plate, glued anchor plates on the beam sides seem to produce the best performance with thick plates as found out by Jones, Swamy and Charif [18] and Charif [4].

2.2.2 Long Term Durability Study of Plated Beams

To study the long-term behavior of reinforced concrete structures strengthened with externally bonded reinforcement, the Swiss Federal Laboratories for Materials Testing and Research (EMPA) started in 1973 a special program of testing reinforced concrete beams strengthened by externally bonded steel plates, with a planned observation period of at least 15 years. Christoph [19] has reported the initial information obtained after one, three and five years of this study. The different parameters that have been studied in this research include the magnitude of the load, the type of weathering and the type of corrosion protection. The results showed that no significant damage has occurred in comparison with the original conditions.

To investigate the possibility of deterioration of the bond between steel and concrete due to weather, Calder [20,21,22] carried out prolonged exposure tests on plain concrete specimens one side of which was bonded a steel plate using a structural adhesive. Some of the specimens were left unloaded while others were subjected to sustained flexural loading. The exposure sites were chosen to represent three different environments, namely a high rainfall rural region with clean air, a highly polluted industrial area and a coastal marine environment. Some of the specimens were kept in a controlled laboratory environment at constant temperature and humidity.

The results of strengths and stiffnesses under a four point loading of the outdoor specimens exposed for various periods compared to those of similar beam specimens kept in the laboratory, showed that no significant damage has occurred, though attention needs to be given to alternative surface treatments. Similar results have been reported by Gemert [23] and Weder [24].

2.2.3 Theoretical Analysis of Plate Bonded Beams

In the sections below is presented theoretical and analytical techniques that have been used thus far in the literature to model the stress state in the adhesive layers in order to asses the failure mode and predict the ultimate loads of plated beams.

2.2.3.1 Bonded Plate Analysis using a Strength of Materials Approach

Formulations based on equilibrium of the force systems at the steel/glue concrete interface as well as the strain compatibility of the transverse section result into some of the basic design guidelines to be followed in the deign of plates for strengthening of reinforced concrete beams. In one such formulation, Jones, Swamy and Charif [18] evaluate the shear and peeling stresses in the zone of plate curtailment and their analysis is presented in the next sections below.

Glue/Plate Interface Shear Stress

Equilibrium, $\sum F_x = 0$ of a plate element as shown in figure 2.1 result in

$$T_p + dT_p - T_p - f_{bp} dx b_p = 0 \tag{2.3}$$

or

$$f_{bp} = \frac{1}{b_p} \frac{dT_p}{dx} \tag{2.4}$$

where f_{bp} is the glue/plate interface bond stress and b_p the plate width. Using the concept of equivalent section,

$$\frac{f_{sp}}{n_p} = \frac{T_p}{A_p n_p} = \frac{M y_p}{I_t} \tag{2.5}$$

where

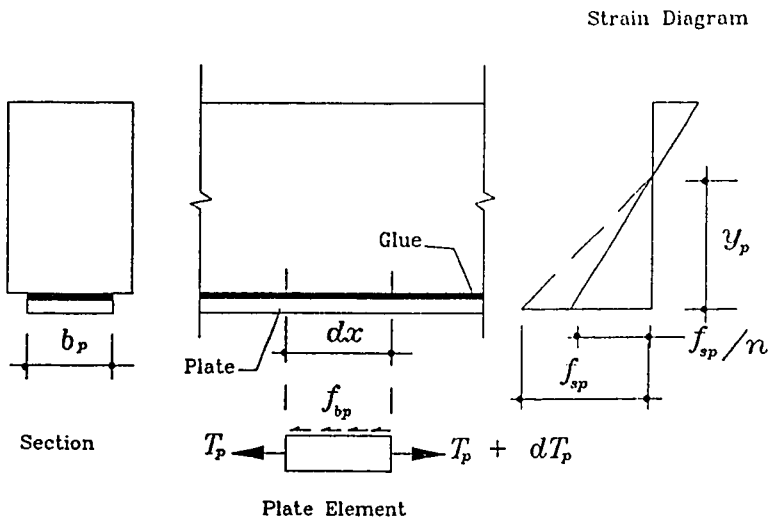

Figure 2.1: Shear stress in glue/plate interface

A_p cross-sectional area of plate

n_p modular ratio, $\frac{E_{plate}}{E_{concrete}} \simeq 8.0$

y_p distance from the neutral axis to the mid-plane of plate

I_t moment of inertia of the transformed section

f_{sp} the tensile stress in the plate.

The incremental form of equation 2.5 becomes

$$\frac{dT_p}{A_p n_p} = \frac{dM y_p}{I_t} \tag{2.6}$$

into which, if substituted $dM = V dx$ results in

$$\frac{dT_p}{dx} = \frac{V y_p A_p n_p}{I_t} \tag{2.7}$$

Using equation 2.7 into 2.4 yields the glue/plate interface bond stress as

$$f_{bp} = \frac{V y_p A_p n_p}{I_t b_p} \tag{2.8}$$

Glue/Concrete Interface Shear Stress

Equilibrium, $\sum F_x = 0$ of a plate-glue element as shown in figure 2.2 result in

$$f_{bc} b_p dx = (T_g + dT_g) - T_g + (T_p + dT_p) - T_p \tag{2.9}$$

or

$$f_{bc} = \frac{dT_g + dT_p}{b_p dx} \tag{2.10}$$

Also by analogy of equation 2.7

$$\frac{dT_g}{dx} = \frac{V y_g A_g n_g}{I_t} \tag{2.11}$$

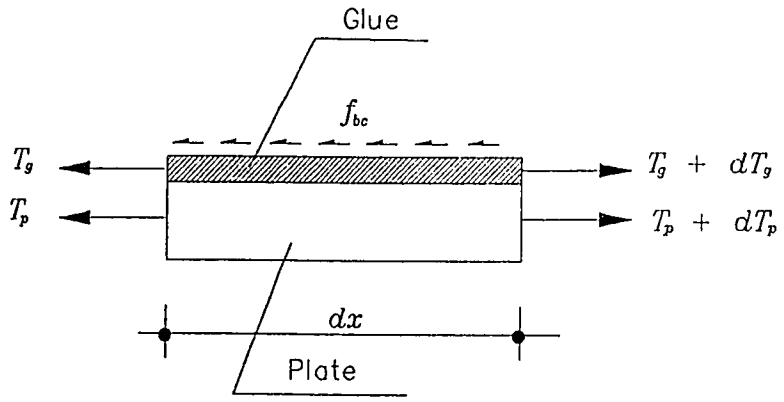

Figure 2.2: Shear stress in glue/concrete interface

A_g cross-sectional area of the glue layer

n_g modular ratio, $\frac{E_{glue}}{E_{concrete}} \simeq 0.03 - 0.30$

y_g distance from the neutral axis to the mid-plane of the glue layer

Comparing equations 2.7 and 2.11 results in $\frac{dT_p}{dT_g} \simeq \frac{n_p t_p}{n_g t_g}$ which is in the range of $12 - 270$. Assuming dT_g as small compared to dT_p, equation 2.10 becomes

$$f_{bc} = \frac{dT_p}{b_p dx} = f_{bp} \tag{2.12}$$

Effect of Plate Cut Off

I: Shear Stress

Assuming the plate is fully effective at section BB (see figure 2.3) and elastic theory applies at a distance $\bar{x}$ from the plate curtailment, the stress in the plate section at BB is given as

$$\sigma_p = \frac{V(L+\bar{x})y_p n_p}{I_t} \tag{2.13}$$

For average bond shear stress over length $\bar{x}$,

$$f_{bp}\bar{x}b_p = \sigma_p A_p \tag{2.14}$$

such that when used in equation 2.13, the shear stress becomes

$$\begin{aligned} f_{bp} &= \frac{V(L+\bar{x})y_p n_p}{I_t} A_p \frac{1}{\bar{x}b_p} \\ &= \left(1+\frac{L}{\bar{x}}\right)\frac{V y_p A_p n_p}{I_t b_p} \end{aligned} \tag{2.15}$$

When $L \simeq \bar{x}$, equation 2.15 compared to equation 2.8 shows considerable increase in the average bond stress near the region of plate cut off. Tests

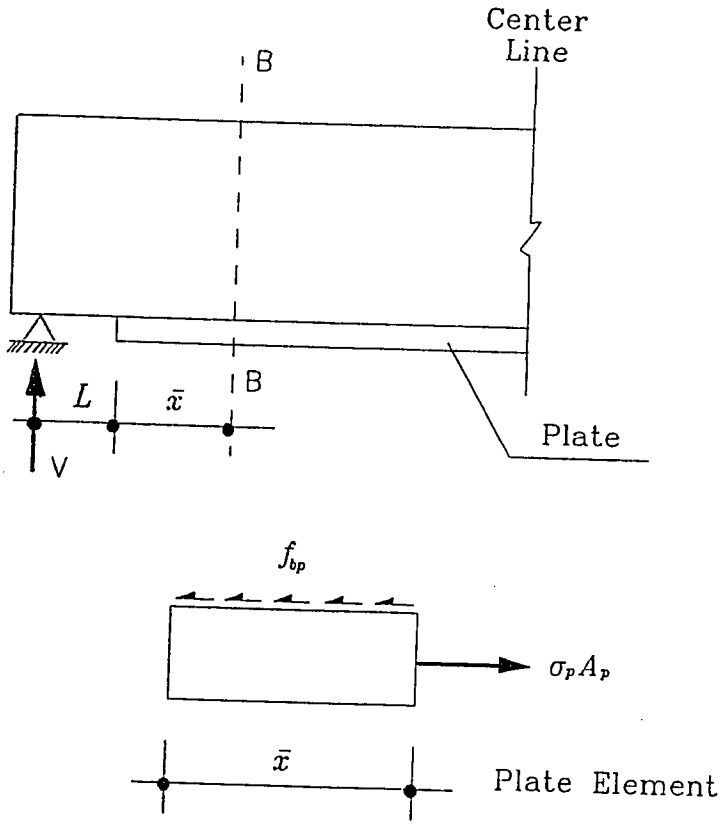

Figure 2.3: Development length at plate cut off

show this to be true [18], with non-uniform interface bond stresses and a high peak value near plate end. This f_{bp} increase plays a critical role in failure by plate separation.

II: Peeling Forces

The resultant of the interface stresse f_{pb} over an element length dx is given by (Figure 2.4a),

$$dF_a = f_{bp} b_p dx \tag{2.16}$$

Replacing the force system in Figure 2.4a with an equivalent single force and couple moment acting through the centroid of the plate results in

$$M_{xy} = b_p \left(t_g + \frac{t_p}{2} \right) f_{bp} \tag{2.17}$$

where M_{xy} is the twisting moment per unit length and as seen in Figure 2.4b is the total unbalanced peeling force due to the plate curtailment. Using equation 2.15 into 2.17 results in

$$M_{xy} = \frac{V y_p n_p A_p}{I_t} \left(t_g + \frac{t_p}{2} \right) \left(1 + \frac{L}{\bar{x}} \right) \tag{2.18}$$

Derived from a strength of materials approach, using elastic theory and equilibrium, equations 2.15 and 2.18 clearly indicate the basic guidelines to be followed in the design of plates for strengthening reinforced concrete beams. Equation 2.18 implies that peeling forces can be minimized by reducing A_p, t_g, t_p and L, and increasing $\bar{x}$. The latter can be attained by using flexible glue.

The experimental values of interface bond stress f_{bp} were very high in the anchorage zones near the ends of the plate, with a limiting value of $\sqrt{2} f_t$, where f_t is the tensile splitting strength of concrete. Theoretical stresses based on the simple elastic theory as given by equation 2.8 did not yield a consistent relationship to the measured values [18]. However, a

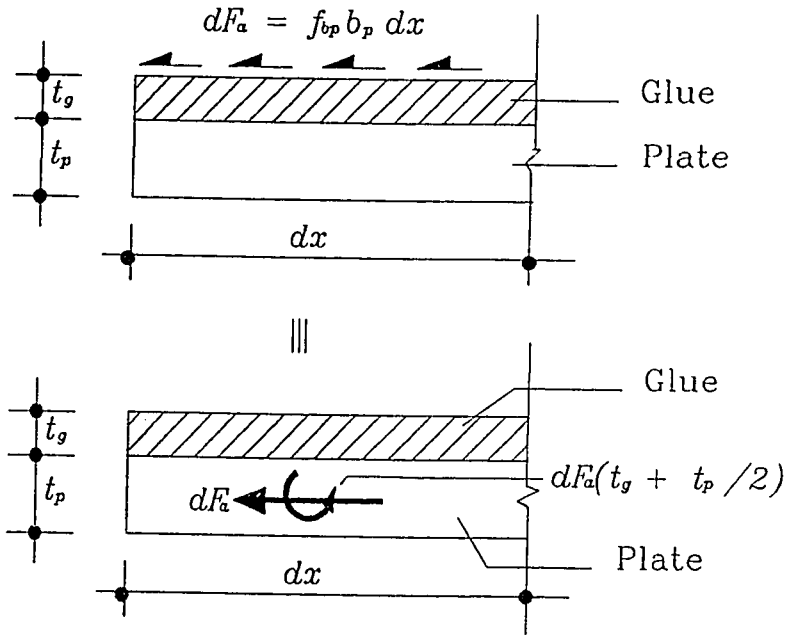

(a). Glue/Plate Element at Plate Curtailment

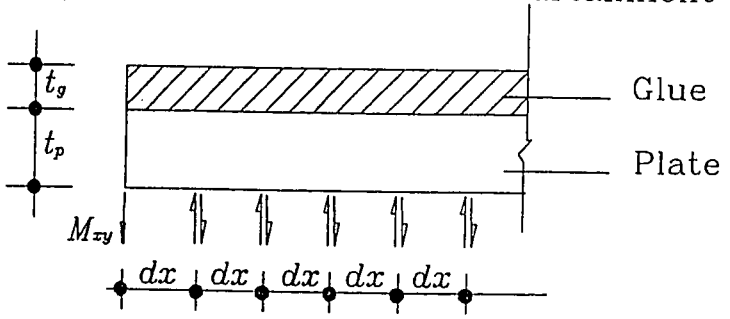

(b). Development of Peeling Force

Figure 2.4: Development of peeling forces near the plate cut off in glue/plate interface

magnification factor of 2 applied to the stress obtained theoretically gave a reasonable estimate of the peak values. This suggests an $\bar{x} \simeq L$ for the glue used in this particular set of experiments. A somewhat more rigorous but still elastic analysis was carried out by Roberts [25] and summarized in the sections below.

2.2.3.2 Approximate Analysis of Shear and Normal Stress Concentrations in the Adhesive layer of plated beams

The analysis presented by Roberts [25] is a superposition of three stages and diagrammatically illustrated in figure 2.5. In stage I, full composite action between the reinforced concrete beam and bonded plate is assumed and in the second and third stages, the solution is modified to take into account the actual boundary conditions due to plate curtailment.

Stage I

In the first stage of the analysis, the shear force per unit length, $\bar{\tau}_1$ in the adhesive layer, and the resultant normal force t_1 in the steel plate can be expressed using conventional theory and full composite action as

$$\bar{\tau}_1 = \frac{VQ}{I} = \frac{Fb_p d_p}{I}(h_p - h) \tag{2.19}$$

and

$$t_1 = \frac{Mb_p d_p}{I}(h_p - h) \tag{2.20}$$

where

$V = F$ the global shear force

M the global bending moment

b_p, d_p width, thickness of the bonding plate

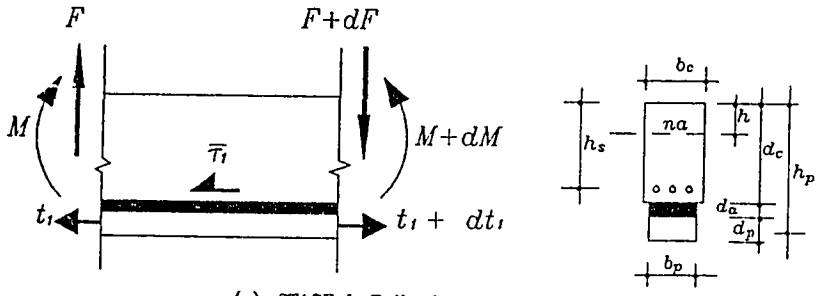

(a). STAGE I: Fully Composite

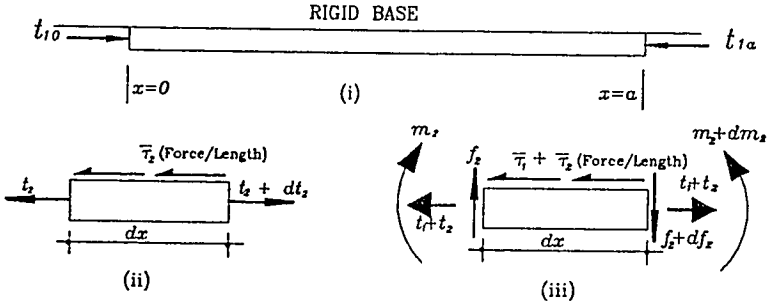

(b). STAGE II: Rigid Base, Glue Layer has only Shear Stiffness

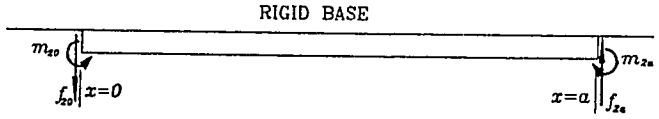

(c). STAGE III: Rigid Base, Glue Layer has only Normal Stiffness

Figure 2.5: The three stages of analysis according to Roberts

h_p depth to the center of the bonding plate

h depth to the neutral axis and

I the second moment of area of the transformed equivalent steel section about the neutral axis.

At the plate end where $x = 0$ or $x = a$, and $M = M_0$ or $M = M_a$, the respective quantities $\bar{\tau}_1$ and t_1 are denoted by $\bar{\tau}_{10}$, t_{10} and $\bar{\tau}_{1a}$, t_{1a}.

Stage II

In the second stage of the analysis, forces $-t_{10}$ and $-t_{1a}$ are applied to the plate since in reality, the resultant axial forces at plate ends are non-existent (see Figure 2.5b(i)). The approximate solution is achieved by assuming a steel plate bonded to a rigid concrete base through an adhesive layer with a finite shear stiffness. If $\bar{\tau}_2$ is the shear flow (force per unit length), then

$$\tau_{glue} = \frac{\bar{\tau}_2}{b_a} = G_a\gamma = G_a\frac{u_{rel}}{d_a}$$

or

$$\bar{\tau}_2 = \frac{G_a b_a}{d_a}u_{rel} = K_s u_{rel}$$

and

$$K_s = G_a\frac{b_a}{d_a} \tag{2.21}$$

where

τ_{glue} shear stress in the glue

γ shear strain in the glue layer

G_a shear modulus of the adhesive layer

b_a,d_a width and thickness of the adhesive layer and

u_{rel} relative deformation on the opposite sides of the glue layer.

From equilibrium (Figure 2.5b(ii)), the shear force in the adhesive layer is given as

$$\bar{\tau}_2 = \frac{dt_2}{dx} = K_s u \tag{2.22}$$

and the normal force as

$$t_2 = E_p b_p d_p \frac{du}{dx} \tag{2.23}$$

where

E_p is the elastic modulus of the plate and

u the plate displacement in the x direction.

Combining equations 2.22 and 2.23, the resulting governing differential equation becomes,

$$\frac{d^2u}{dx^2} - \alpha^2 u = 0$$

$$\alpha^2 = \frac{K_s}{E_p b_p d_p} \tag{2.24}$$

Solution of equation 2.24 using the boundary equations that $t_2 = -t_{10}$ at $x = 0$ and $t_2 = -t_{1a}$ at $x = a$ becomes

$$u = -\frac{t_{10} sinh\alpha x}{E_p b_p d_p \alpha} + \frac{t_{10} cosh\alpha a - t_{1a}}{E_p b_p d_p \alpha sinh\alpha a} cosh\alpha x \tag{2.25}$$

Using equation 2.25 into 2.22 the shear force per unit length becomes

$$\bar{\tau}_2 = \left(\frac{K_s}{E_p b_p d_p}\right)^{\frac{1}{2}} \left[-t_{10} sinh\alpha x + \frac{t_{10} cosh\alpha a - t_{1a}}{sinh\alpha a} cosh\alpha x\right] \tag{2.26}$$

Equilibrium of a steel differential element dx at end of solution stage II results in the shear force (see Figure 2.5b(iii))

$$f_2 = \frac{dm_2}{dx} + (\bar{\tau}_1 + \bar{\tau}_2)\frac{d_p}{2} \tag{2.27}$$

at $x = 0$, m_{20} may be ralated to the global curviture M_0 by the equation

$$m_{20} = M_0 \left[\frac{E_p I_p}{(E_p I_p + E_c I_c)} \right] \tag{2.28}$$

where I_p, I_c, are the second moment of area of plate and concrete about their respective centroidal axes, based on non-composite action. However, during the pursuit of the thesis, the expression used in equation 2.28 was found to be incorrect. Instead the value for m_{20} should be given as

$$m_{20} = M_0 \frac{I_p}{I} \tag{2.29}$$

where I is as defined in equations 2.19 and 2.20. This error would not affect the final result as the terms in which it plays a role are considered by the author [25] to be of minor significance.

Using equation 2.28 and 2.19 in 2.27 leads to

$$f_{20} = \left[\frac{E_p I_p}{(E_p I_p + E_c I_c)} \right] F_0 + (\bar{\tau}_{10} + \bar{\tau}_{20}) \frac{d_p}{2} \tag{2.30}$$

The moment m_{2a} and shear force f_{2a} can be similarly obtained for $x = a$.

Stage III

In the third stage of the analysis, moments $-m_{20}$, $-m_{2a}$, $-f_{20}$ and $-f_{2a}$ are applied at plate ends (see Figure 2.5c), and an approximate solution is obtained by assuming that the steel plate bonded to a rigid base by an adhesive layer with a finite normal stiffness. If $\bar{\sigma}$ is the normal force per unit length, then

$$\sigma_{glue} = \frac{\bar{\sigma}}{b_a} = E_a \varepsilon = E_a \frac{w_{rel}}{d_a}$$

or

$$\bar{\sigma} = \frac{E_a b_a}{d_a} w_{rel} = K_n w_{rel}$$

and

$$K_n = E_a \frac{b_a}{d_a} \tag{2.31}$$

where

σ_{glue} transverse normal stress in the glue

ε transverse normal strain in the glue layer

E_a Younge's modulus of the adhesive layer and

w_{rel} relative normal deformation on the opposite sides of the glue layer.

Using the fact that

$$\bar{\sigma_3} = K_n w \tag{2.32}$$

where $w \equiv w_{rel}$, the resulting governing differential equation becomes

$$\frac{d^4w}{dx^4} + 4\gamma^4 w = 0$$

$$\gamma^4 = \frac{K_n}{4E_pI_p} \tag{2.33}$$

The solution of 2.33 assuming w tends to zero as x increases and also that at $x = 0$,

$$\begin{aligned} -E_pI_p\frac{d^2w}{dx^2} &= m_3 = -m_{20} \\ -E_pI_p\frac{d^3w}{dx^3} &= f_3 = -f_{20} \end{aligned} \tag{2.34}$$

becomes

$$w = \frac{e^{-\gamma x}}{2E_pI_p\gamma^4}\left[(f_{20}\gamma + m_{20}\gamma^2)cos\gamma x - m_{20}\gamma^2 sin\gamma x\right] \tag{2.35}$$

Using 2.35 in 2.32 leads to

$$\bar{\sigma_3} = 2e^{-\gamma x}\left[(f_{20}\gamma + m_{20}\gamma^2)cos\gamma x - m_{20}\gamma^2 sin\gamma x\right] \tag{2.36}$$

A mirror image problem may be used to obtain the solution at $x = a$. By superposition,

$$\begin{aligned} \bar{\tau} &= \bar{\tau_1} + \bar{\tau_2} \\ \bar{\sigma} &= \bar{\sigma_3} \end{aligned} \tag{2.37}$$

The adhesive shear and transverse normal stresses are obtained by dividing the forces per unit length in equation 2.37 by the adhesive width, b_a.

By omitting terms of minor significance in 2.36 and assuming $cosh\alpha a = sinh\alpha a$ in 2.25, the peak stresses at the plate end can be shown to be

$$\tau_0 = \left(F_0 + \left[\frac{K_s}{E_p b_p d_p} \right]^{\frac{1}{2}} M_0 \right) \frac{b_p d_p}{I b_a} (h_p - h) \tag{2.38}$$

and

$$\sigma_0 = \tau_0 d_p \left[\frac{K_n}{4 E_p I_p} \right]^{\frac{1}{4}} \tag{2.39}$$

2.2.3.3 Comparison of Roberts and Swamy Equations

The distance $\bar{x}$, from the plate curtailment beyond which full composite action, may be approximated by comparing equation 2.15 suggested by Jones, Swamy and Charif [17] and equation 2.38 proposed by Roberts [25] for the calculation of the peak shear stresses in the glue interface as

$$\bar{x} \approx \left(\frac{E_p b_p d_p}{K_s} \right)^{1/2} \tag{2.40}$$

Figure 2.6 shows the plot of the shear stresses as predicted by the two approximate formulae.

2.2.3.4 Techniques Based on Partial Interaction Theories of Composite Beams

Elastic models developed by Newmark [26] and Roberts [27] to study the influence of slip on composite beams with partial interaction may be modified for the analysis of a plate bonded beam. In that case, the beam is considered as a composite beam made up of a concrete part connected to the steel plate through a flexible glue adhesive so as to allow slip between the concrete and the steel plate.

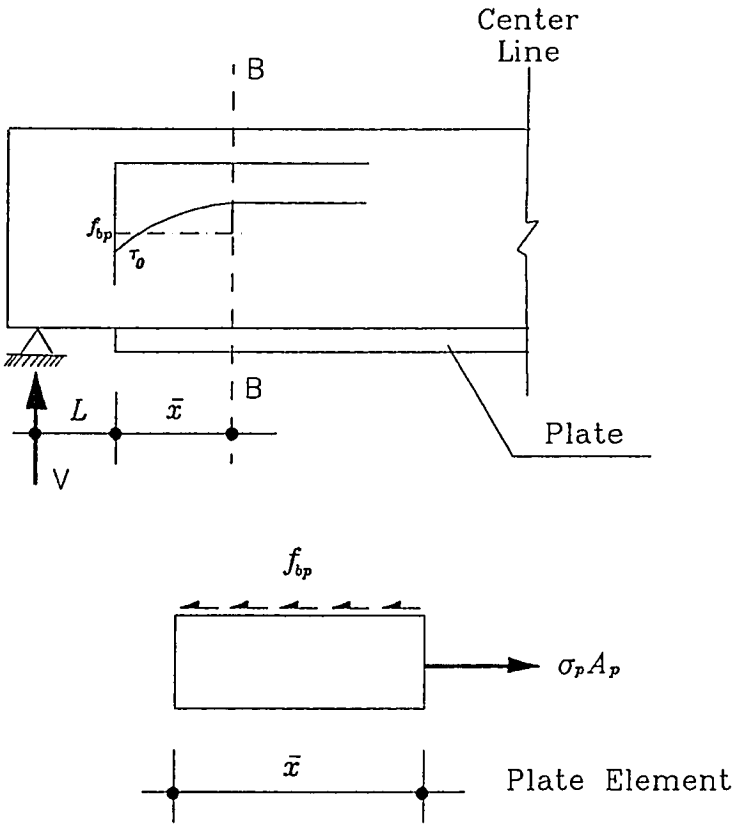

Figure 2.6: Comparison of Roberts and Swamy Equations

In the model suggested by Newmark [26] for concrete slab connected to a steel I-beam through shear connectors, the equilibrium and compatibility equations for a composite beam element are reduced to a single second order differential equation in terms of the axial force in concrete as

$$\frac{d^2F}{dx^2} - \frac{k}{s}\frac{\overline{EI}}{\overline{EA}\sum EI}F = \frac{k}{s}\frac{z}{\sum EI}$$

$$\sum EI = E_s I_s + E_b I_b$$

$$\overline{EI} = \sum EI + \overline{EA}z^2$$

$$\frac{1}{EA} = \frac{1}{E_s A_s} + \frac{1}{E_b A_b} \tag{2.41}$$

where

E_s,E_b elasticity modulus for slab and beam respectively,

A_s,A_b cross-sectional areas of slab and beam respectively,

k modulus of the shear connectors,

s spacing of the shear connectors,

z distance between the centroidal axes of the slab and beam and

F axial force acting at the centroids of the slab and beam.

A more general formulation is presented by Roberts [27] where in the derivations, the beam element consists of two materials a and b (see Figure 2.7) joined by a medium of negligible thickness but having finite normal and tangential stiffness. Assuming elastic behavior, equilibrium and compatibility relations for the beam element can be reduced to [27],

$$E_a A_a \frac{d^2u_a}{dx^2} + E_b A_b \frac{d^2u_b}{dx^2} = 0$$

$$E_a I_a \frac{d^4 w}{dx^4} + E_b I_b \frac{d^4 w}{dx^4} = p$$

$$E_a A_a \frac{d^2 u_a}{dx^2} - K_s (u_a - u_b - e\frac{dw}{dx}) = 0 \qquad (2.42)$$

The expressions in equation 2.42 are solved using finite difference for the composite beam with partial interaction. To solve the plate bonded beam with the plate curtailed short of the supports, Hussain [28] used a finite difference model in which the material properties of the plate and the adhesive are modified and set to zero as shown in Figure 2.8 [28], to simulate a non-existent plate in this region. For an elastic analysis, this approach does yield acceptable values for the interface shear and peeling stresses.

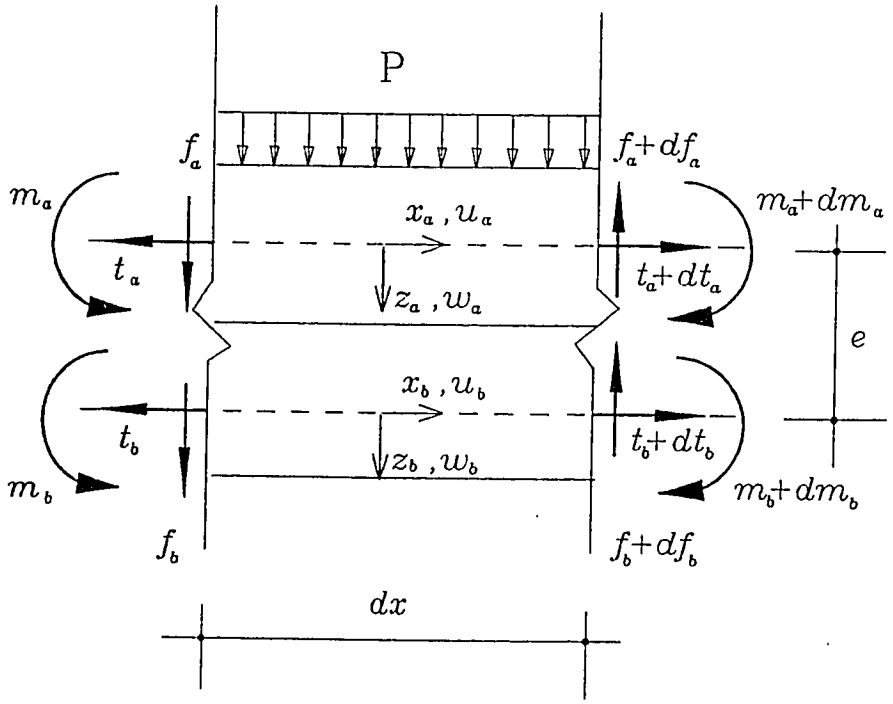

Figure 2.7: Partial interaction theory: Formulation according to Roberts [27]

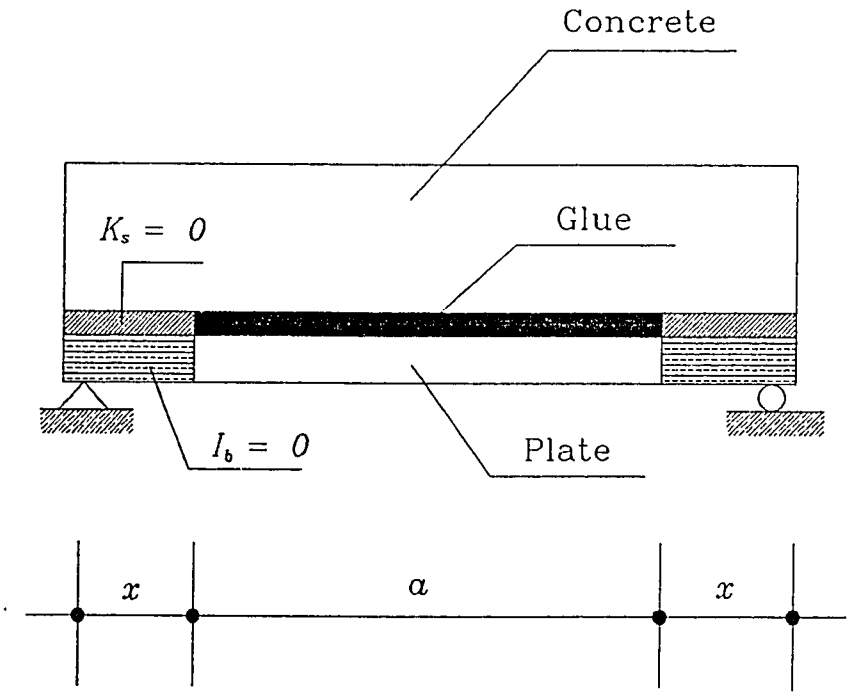

Figure 2.8: Modification to plate and glue properties to solve the plate bonded beam problem using the partial interaction theory [28]

Chapter 3

Material Modelling

3.1 Introduction

The failure of an externally plated RC beam can be precipitated not only by a premature interface failure but also due to various component materials reaching a limiting state of stress or strain, including

(i) significant cracking of concrete in tension in lightly to moderately reinforced concrete members,

(ii) yielding of internal reinforcement and external plate,

(iii) crushing of concrete in compression zone,

(iv) diagonal tension failure in RC members adequately reinforced against flexural failure and

(v) bond failure at the interface of concrete and internal reinforcement.

In order that a nonlinear finite element model depict the global behavior of the externally reinforced RC beam up to failure, which may be precipitated by a breakdown in any single component of the multi-phase structural system, limiting failure criteria describing the ultimate state of

each material must be defined. The constitutive relations at all levels of material stresses should also be established in order to evaluate the stiffness characteristics and at the same time adjust the stresses in the constituent components according to the material state.

The earliest published application of the finite element method to reinforced concrete structure was by Ngo and Scordelis in March 1967 [29]. Beams with predefined 'discrete cracks' were studied using a plane stress analysis in which the concrete and steel reinforcement were represented by two dimensional triangular finite elements or axial bar elements, and special linkage elements were used to connect the steel to the concrete. Scordelis, Ngo and Franklin [30] used this same approach to study shear in beams with diagonal tension cracks considering the effect of stirrups, dowel shear, aggregate interlock, and horizontal splitting along reinforcement near the support.

Because of the complications involved in using discrete crack modelling, an alternate approach was initiated to assist in design of the containment structures for gas cooled nuclear reactor [31]. It was necessary to model a large segment of the concrete containment vessel, its reinforcement and liner in order to study the overall behaviour of this structure to overload. The concrete model, therefore, had to locate zones of cracking and how crack development affected the overall behaviour of the structure. The consequence of these demands led to the development of a smeared crack model. Therefore in subsequent studies, emphasis was placed on the development of the smeared crack model.

Scordelis [32] in his state of the art report on 'Finite Element Analysis of Reinforced Concrete' presented the complicating factors in modelling, the experimental research that was needed and the future studies to be done.

From 1977 to 1985 several important events and publications occurred, which gave a strong impetus to research in this field. A state of the art report [33] published in May 1982 by the Task committee of the American

Society of Civil Engineers discusses in great detail topics such as Constitutive Relations and Failure Theories, Modelling of reinforcement and Representation of Bond, Concrete Cracking, Shear Transfer, Time dependent effects and Dynamic Analyses. It also includes numerical examples and compilations of finite element programs for nonlinear analysis of reinforced concrete structures.

In this chapter such relations as used in the present numerical model are described. The material behaviors are described for the materials of concrete, steel, including the internal flexural and shear reinforcement as well as the external plate and for the material behaviors of glued concrete/steel interface and steel/concrete bond.

3.2 Concrete

The behavior of concrete under predominantly compressive stresses is characteristically different from when it is subjected to tensile stresses. Under compression, concrete may flow plastically and as such, theories based on incremental plasticity have been used to model its material behavior. In tension however, cracking of the concrete and the accompanying tension stiffening and shear degradation are some of the major contributing factors to the material nonlinearities. In the sections below, these characteristics of concrete material behavior and how they are used in the present numerical model are described in more detail.

3.2.1 Behavior in Compression

3.2.1.1 Uniaxial Compression

The curves relating the stress to strain for concrete in compression for varying values of concrete strengths are shown in Figure 3.1, where it can be observed that up to 30% of the peak stress f_c' [34], a linear relation is exhib-

ited between the stress and strain. In the present model therefore, concrete is taken to be linear elastic up to a stress level of $0.3f_c'$. To more closely simulate the curves shown in Figure 3.1, a parabolic stress-strain relation is adopted up to a strain level corresponding to $2f_c'/E_0$ (see Figure 3.2) where E_0 is the initial elastic modulus. The stress is taken to be constant at a value of f_c' for increasing strains until the ultimate strain ε_u, where at crushing occurs and the concrete looses its stiffness and strength.

3.2.1.2 Yield Criterion

Since the actual behaviour and strength of concrete materials is quite complicated, no one mathematical model can be expected to completely describe the strength properties of real concrete under all conditions. And even if such a model is constructed it would be far too complex to be used in the analysis of practical problem. Therefore simpler models are used representing only those characteristics that are essential to the problem at hand. Models normally employed are Drucker Prager, Modified Drucker Prager [37], and the Mohr Coulomb [38].

The yield criterion is normally written in terms of stress invariants as

$$F(I_1, J_2, J_3, \chi) = 0 \tag{3.1}$$

where

I_1 is the first stress invariant,

J_2, J_3, are the second and third deviatoric stress invariants and

χ is the hardening parameter.

Equation 3.1 is more amenable to computer implementation if it is defined in the principle stress space (σ_1, σ_2, σ_3), and in terms of variables ξ, ρ and θ where

$$\xi = I_1/\sqrt{3}$$

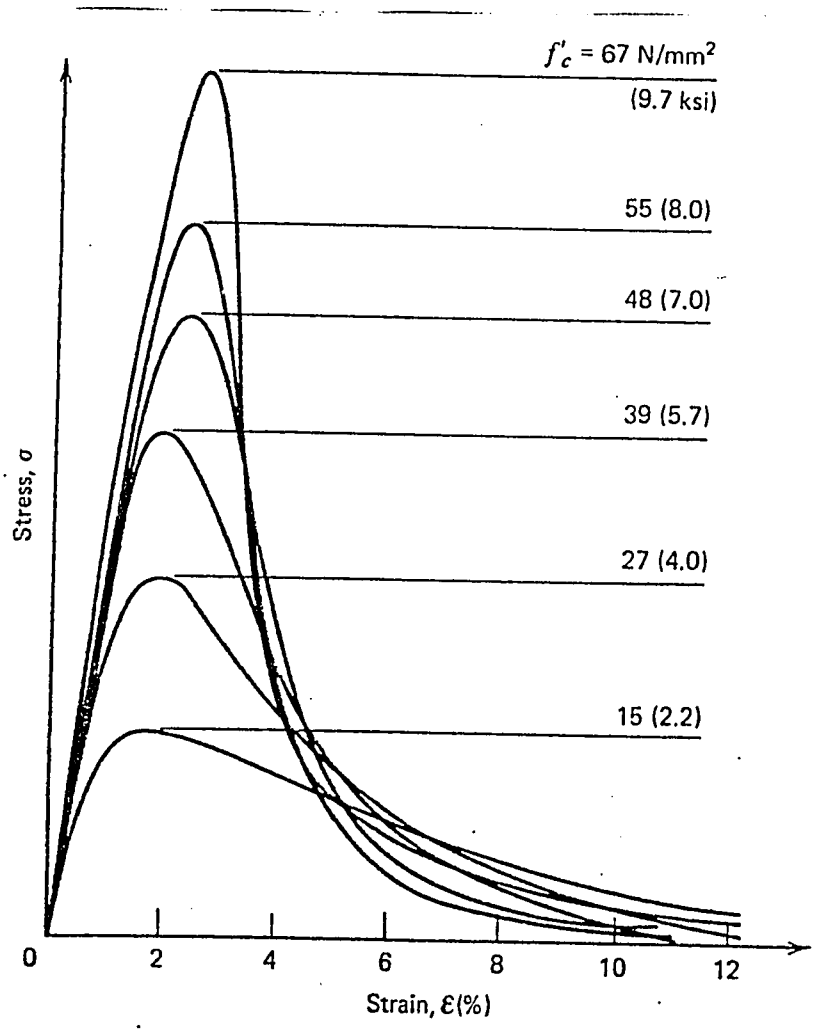

Figure 3.1: Stress-strain curves for concrete in uniaxial compression according to Wischers [35] and adopted from [36].

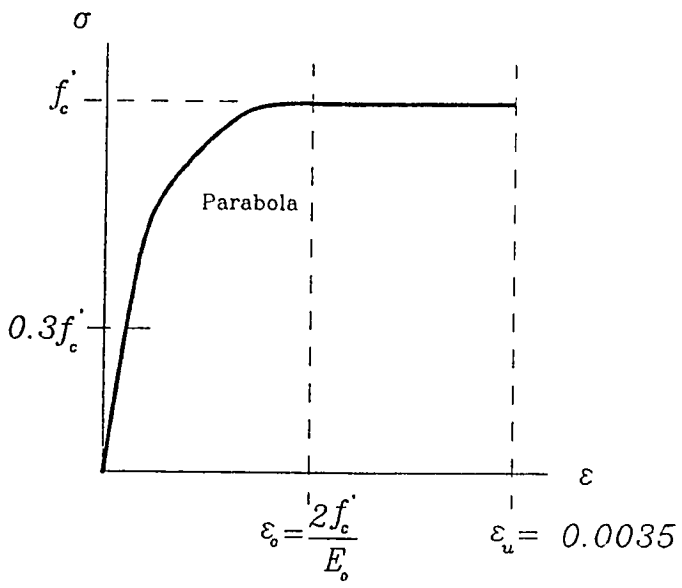

Figure 3.2: Stress-strain curve for concrete in uniaxial compression used in the present model

$$\rho = \sqrt{2J_2}$$

$$\sin\theta = -\frac{3\sqrt{3}J_3}{2J_2^{3/2}}$$

$$-\frac{\pi}{6} \leq \theta \leq \frac{\pi}{6} \tag{3.2}$$

The principle stress are them simply expressed as

$$\begin{Bmatrix} \sigma_1 \\ \sigma_2 \\ \sigma_3 \end{Bmatrix} = \frac{\xi}{\sqrt{3}} \begin{Bmatrix} 1 \\ 1 \\ 1 \end{Bmatrix} + \frac{\rho}{\sqrt{3}} \begin{Bmatrix} \sin(\theta + \frac{2\pi}{3}) \\ \sin\theta \\ \sin(\theta - \frac{2\pi}{3}) \end{Bmatrix}$$

$$-\frac{\pi}{6} \leq \theta \leq \frac{\pi}{6} \tag{3.3}$$

For perfect plastic models, the failure criterion in equation 3.1 is written explicitly in terms of failure stress f_c' as

$$F(I_1, J_2, J_3) = f_c' \tag{3.4}$$

Replacing the right hand side of equation 3.4 by the effective stress σ_0 which is a function of the hardening parameter χ, the perfectly plastic failure criterion is rendered into an isotropic strain hardening model, that is

$$F(I_1, J_2, J_3) = \sigma_0(\chi) \tag{3.5}$$

The Mohr-Coulomb yield criterion used in this study is described as

$$\tau = c - \sigma\tan\phi \tag{3.6}$$

where

τ, σ are shear and normal stresses on any plane and

c, ϕ are material constants. The parameter ϕ is the angle of internal friction for concrete taken as 37° throughout this study.

Equation 3.6 can also be written in terms of stress invariants as

$$F(I_1, J_2, \theta) = \frac{1}{3} I_1 \sin\phi + \sqrt{J_2}\sin(\theta + \frac{\pi}{3}) + \sqrt{\frac{J_2}{3}}\cos(\theta + \frac{\pi}{3})\sin\phi - c\ \cos\phi = 0 \tag{3.7}$$

The material constant c is obtained in terms of $f_c^{'}$ by making the Mohr-Coulomb envelope touch the circle corresponding to the uniaxial compressive test and determined as

$$c = \frac{f_c^{'}(1 - \sin\phi)}{2\cos\phi} \tag{3.8}$$

Using in equation 3.7 results in

$$F(\sigma_{ij}) = \frac{2}{1 - \sin\phi}\left[\frac{I_1}{3}\sin\phi + \sqrt{J_2}\left(\cos\phi - \frac{1}{\sqrt{3}}\sin\phi\cos\phi\right)\right] - f_c^{'} = 0 \tag{3.9}$$

for perfectly plastic models. If $f_c^{'}$ is replaced by $\sigma_0(\chi)$, the model expressed in equation 3.9 can then be used to handle strain hardening.

3.2.1.3 Flow & Hardening Rule

The flow rule defines the incremental plastic stress-strain relation in the plastic range and is related to the plastic potential function, $G(\sigma_{ij})$ [39,40] such that

$$d\varepsilon_{ij}^{p} = d\lambda \frac{\partial G(\sigma_{ij})}{\partial \sigma_{ij}} \tag{3.10}$$

where

$d\varepsilon_{ij}^{p}$ is the plastic strain increment,

$d\lambda$ is a proportionality scalar constant and determines the magnitude of the plastic strain increment and

the gradient $\partial G(\sigma_{ij})/\partial\sigma_{ij}$ termed the flow vector defines the direction of the plastic strain increment normal to the plastic potential function.

In associative plasticity which will be assumed in this study, the plastic function $G(\sigma_{ij})$, may be taken as equal to the yield function $F(\sigma_{ij})$ as given in equation 3.9 and so 3.10 becomes

$$d\varepsilon_{ij}^{p} = d\lambda \frac{\partial F(\sigma_{ij})}{\partial \sigma_{ij}} \tag{3.11}$$

After the initial yield surface where at the onset of plastic flow is defined, the evolution of the subsequent yield surfaces during plastic deformation is specified by the hardening rule. Isotropic hardening is employed in this model and is extrapolated from the assumed uniaxial stress strain relation of concrete in compression as shown in Figure 3.2. In the post-linear stress range of $0.3f_c' \leq \sigma \leq f_c'$, a parabolic relationship of the from expressed in equation 3.12 is assumed [37].

$$\sigma = E_0\varepsilon - 0.5\frac{E_0}{\varepsilon_0}\varepsilon^2$$

$$0.3f_c' \leq \sigma \leq f_c' \tag{3.12}$$

where

E_0 is the initial elasticity modulus,

ε the total strain and

ε_0 the total strain at peak stress f_c'. which may be taken as $2f_c'/E_0$.

The value of E_0 is taken from the equation proposed by ACI committee 363 [41,42] as

$$E_0 = 3320\sqrt{f_c'} + 6900 \tag{3.13}$$

for concrete strengths ranging from 21 MPa to 83 MPa.

The total strain in equation 3.12 may be decomposed into the plastic and elastic components and substitution of the elastic portion $\varepsilon_e = \sigma/E_0$

results in

$$\sigma = -E_0\varepsilon_p + \sqrt{2E_0^2\varepsilon_0\varepsilon_p}$$

$$0.3f_c' \leq \sigma \leq f_c' \tag{3.14}$$

where

ε_p is the plastic strain component

The hardening parameter defined as the derivative of equation 3.14 is therefore expressed as

$$\frac{d\sigma}{d\varepsilon_p} = \chi = H' = -E_0 + E_0\sqrt{\frac{\varepsilon_0}{2\varepsilon_p}} \tag{3.15}$$

3.2.1.4 Elasto-plastic Constitutive Relations

The incremental strain in the post-linear elastic range due to an infinetismal increment in stress is given by

$$\begin{aligned} d\varepsilon_{ij} &= d\varepsilon_{ij}^e + d\varepsilon_{ij}^p \\ &= \frac{ds_{ij}}{2G} + \frac{(1-2\nu)}{E}\delta_{ij}d\sigma_{kk} + d\lambda\frac{\partial F}{\partial\sigma_{ij}} \end{aligned} \tag{3.16}$$

where

s_{ij} is the deviatoric stress tensor,

E, G the elastic normal and shear modulus respectively and

ν the Poisson's ratio.

In matrix form equation 3.16 becomes

$$d\{\varepsilon\} = [D]^{-1}d\{\sigma\} + d\lambda\frac{\partial F}{\partial\{\sigma\}} \tag{3.17}$$

where

$[D]$ is a matrix of elastic material constants.

Since the yield function in equation 3.16 is $F = F(\sigma_{ij}, \chi)$, the total differential is given by

$$dF = \frac{\partial F}{\partial \{\sigma\}} d\{\sigma\} + \frac{\partial F}{\partial \chi} d\chi = 0 \tag{3.18}$$

or in matrix form

$$\{a\}^T d\{\sigma\} - A d\lambda = 0 \tag{3.19}$$

where

$$\{a\}^T = \left\{ \frac{\partial F}{\partial \sigma_x}, \frac{\partial F}{\partial \sigma_y}, \frac{\partial F}{\partial \tau_{xy}}, \right\} \tag{3.20}$$

is termed the flow vector and

$$A = -\frac{1}{d\lambda} \frac{\partial F}{\partial \chi} d\chi \tag{3.21}$$

Premultiplying both sides of equation 3.17 by $\{a\}^T[D]$ and using the expression in 3.19, the proportionality constant is determined to be

$$d\lambda = \frac{1}{A + \{a\}^T[D]\{a\}} \{a\}^T[D]\{\varepsilon\} \tag{3.22}$$

Using equation 3.22 in 3.17 and rearranging, results into the elastoplastic constitutive relation as

$$d\{\sigma\} = [D]_{ep} d\{\varepsilon\} \tag{3.23}$$

where

$$[D]_{ep} = [D] - \frac{[D]\{a\}\{a\}^T[D]}{A + \{a\}^T[D]\{a\}} \tag{3.24}$$

As outlined in reference [39], the value of A can be shown equal to the hardening parameter H' described in equation 3.15. The elastoplastic material matrix then becomes

$$[D]_{ep} = [D] - \frac{[D]\{a\}\{a\}^T[D]}{H' + \{a\}^T[D]\{a\}} \tag{3.25}$$

The flow vector as defined in equation 3.20 can be written as

$$\{a\} = \frac{\partial F(I_1, \sqrt{J_2}, \theta)}{\partial\{\sigma\}} = \frac{\partial F}{\partial I_1}\frac{\partial I_1}{\partial\{\sigma\}} + \frac{\partial F}{\partial \sqrt{J_2}}\frac{\partial \sqrt{J_2}}{\partial\{\sigma\}} + \frac{\partial F}{\partial \theta}\frac{\partial \theta}{\partial\{\sigma\}}$$

$$= C_1\{a_1\} + C_2\{a_2\} + C_3\{a_3\} \tag{3.26}$$

where on eliminating θ in terms of J_2 and J_3,

$$\{a_1\} = \frac{\partial I_1}{\partial\{\sigma\}} = \begin{Bmatrix} 1 \\ 1 \\ 0 \\ 1 \end{Bmatrix}$$

$$\{a_2\} = \frac{\partial \sqrt{J_2}}{\partial\{\sigma\}} = \frac{1}{2\sqrt{J_2}} \begin{Bmatrix} s_x \\ s_y \\ 2\tau_{xy} \\ s_z \end{Bmatrix}$$

$$\{a_3\} = \frac{\partial J_3}{\partial\{\sigma\}} = \begin{Bmatrix} s_y s_z + J_2/3 \\ s_x s_z + J_2/3 \\ -2\tau_{xy} s_z \\ s_x s_y - \tau_{xy}^2 + J_2/3 \end{Bmatrix} \tag{3.27}$$

For Mohr-Coulomb yield criteria used in this study, the constants C_i in equations 3.26 are evaluated as [43]

$$C_1 = \frac{\partial F}{\partial I_1} = \frac{2\sin\phi}{3(1-\sin\phi)}$$

$$C_2 = \frac{\partial F}{\partial \sqrt{J_2}} - \frac{\tan 3\theta}{\sqrt{J_2}}\frac{\partial F}{\partial \theta}$$

$$= \frac{2}{1-\sin\phi}\cos\theta\left[1 + \tan\theta\tan 3\theta + \sin\phi\frac{\tan 3\theta - \tan\theta}{\sqrt{3}}\right]$$

$$C_3 = -\frac{\sqrt{3}}{2\cos 3\theta}\frac{1}{J_2\sqrt{J_2}}\frac{\partial F}{\partial \theta}$$

$$= \frac{2}{1-\sin\phi}\frac{\sqrt{3}\sin\theta + \cos\theta\sin\phi}{2J_2\cos\theta} \tag{3.28}$$

For $\theta = \pm 30°$, the quantities C_i in equations 3.28 cannot be uniquely determined due to the singularities at the corners of the yield surface in the stress space. The problem can however be overcome if the original expressions of the yield criteria are written using explicit expressions of θ as $\pm 30°$. The values C_i in the neighborhood of singular points thus do become

$$\begin{aligned} C_1 &= \frac{2\sin\phi}{3(1-\sin\phi)} \\ C_2 &= \frac{2}{1-\sin\phi}\left(\frac{\sqrt{3}}{2} \pm \frac{\sin\phi}{2\sqrt{3}}\right) \\ C_3 &= 0 \end{aligned} \tag{3.29}$$

3.2.1.5 Concrete Crushing

After the concrete has reached its effective peak stress, it is assumed to undergo perfect plasticity until it crushes at a specific effective strain value. The crushing type of concrete fracture is thus a strain controlled type phenomenon and a strain criterion need be developed in terms of strain invariants. One way of doing this is to simply convert yield criterion described in terms of stresses directly into strains as follows [44,37]:

$$f(\varepsilon_{ij}) = \bar{\varepsilon} = \varepsilon_u \tag{3.30}$$

where

$\bar{\varepsilon}$ is the effective strain and

ε_u is the ultimate total strain extrapolated from uniaxial test results and taken as equal to 0.0035

The loading function has the same form as stress loading function. When the $\bar{\varepsilon}$ reaches the value of 0.0035, the material is assumed to loose all characteristics of strength at the sampling point concerned. The constitutive

relations thus become

$$d\{\sigma\} = [0]d\{\varepsilon\}$$

$$\{\sigma\} = [0]\{\varepsilon\} \tag{3.31}$$

The effective strain criterion is evaluated using the Mohr-Coulomb yield criteria as

$$\bar{\varepsilon} = \sqrt{3\left[\varepsilon_x^2 + \varepsilon_y^2 + \varepsilon_x\varepsilon_y + \frac{3}{4}\left(\gamma_{xy}^2\right)\right]} \tag{3.32}$$

3.2.2 Behavior in Tension

The behavior of concrete in tension is predominantly that of cracking. The smeared crack model [31] is adopted in this study because of its generality in permitting crack propagation and predicting crack directions, independent of mesh configurations and element type used. The smeared crack representation implies that the cracks are not discrete but distributed across a region of finite element. As discussed in the sections below, tension stiffening and degradation of the shear modulus as cracks open are two aspects included in the smeared crack model used in this study.

Cracking is governed by a maximum tensile stress criterion (or tension cut-off). Cracks are assumed to form in a direction perpendicular to the maximum principal tensile stress. The principal stresses are calculated as

$$\sigma_{1/2} = \frac{\sigma_x + \sigma_y}{2} \pm \sqrt{\left(\frac{\sigma_x - \sigma_y}{2}\right)^2 + \tau_{xy}^2} \tag{3.33}$$

The concrete may thus crack in one direction if σ_1 reaches the specified tensile strength f_t' [39,36]. Depending on whether the value of σ_2 reaches or exceeds the tensile strength f_t', a second crack may develop in the orthogonal direction. The angle α between the direction of σ_1 and the x-axis

is calculated as

$$\tan 2\alpha = \frac{2\tau_{xy}}{\sigma_x - \sigma_y} \tag{3.34}$$

and the angle indicating the direction of the principal crack with respect to the x-axis thus becomes

$$\theta = \alpha + \frac{\pi}{2} \tag{3.35}$$

After cracking the material is assumed to be orthotropic with Poisson's effect playing no role.

3.2.2.1 Concrete Behavior in Uniaxial Tension

The stress-strain curve for concrete in tension is linear up to about 60% of its maximum tensile strength f_t'. In the present study therefore, the stress-strain relationship is assumed linear with the initial elastic modulus of concrete up to the maximum tensile strength f_t', whereafter cracking occurs and the stress is reduced to a value determined by the tension stiffening parameter α (see section 3.2.2.2). On subsequent loading, the curve follows a descending branch as discussed in section 3.2.2.2. The value of f_t' used in this study is taken as a function of f_c' using an equation proposed by ACI [45] or

$$f_t' = 0.324(f_c')^{\frac{2}{3}} \tag{3.36}$$

expressed in MPa.

3.2.2.2 Tension Stiffening

Part of the tensile load between the cracks is inevitably carried by concrete due to adherence or bond between the reinforcement and the concrete and thus contributes to the overall stiffness of the structure [46]. This phenomenon termed 'tension stiffening' has to be incorporated into a cracking model to correctly simulate the load carrying capacity of a reinforced member in tension. The average stress over a cracked region is thus not zero,

but as the load is further increased more cracking occurs and the capacity of the cracked region to carry more stresses decreases. A gradual release of the stresses normal to the cracked plane, depending on the cracking opening ('cracking strain') is adopted in this study.

The stress-strain relation used in the computational model is shown in figure 3.3 and is essentially similar to the one proposed by Owen and Figueiras [47]. The loading and unloading of cracked concrete is assumed to be linear elastic with a reduced elastic modulus, E_i given by

$$E_i = \alpha f_t' \left(1 - \frac{\varepsilon_{grtst}}{\varepsilon_m}\right) \frac{1}{\varepsilon_{grtst}}$$

$$\varepsilon_t \leq \varepsilon_{grtst} \leq \varepsilon_m \tag{3.37}$$

where

α, ε_m are tension stiffening parameters and

ε_{grtst} the maximum value of strain ever reached at the sampling point under consideration.

The parameter ε_m, or the cracking strain beyond which stress cannot be carried across the cracks, was assumed constant at 0.002 [37]. The tension stiffening parameter $\alpha = \alpha(f_c')$ was calibrated against f_c' using results of beams tested by Mphonde in his experimental studies on shear strength of beams without stirrups [48], and was found to vary between 0.01 and 0.6. Figure 3.4 shows the derived relation between the compressive strength f_c' and the tension stiffening parameter α for a range of beams with a shear span $a/d \geq 3.6$.

The normal stress thus becomes

$$\sigma_i = E_i \varepsilon_i \tag{3.38}$$

where

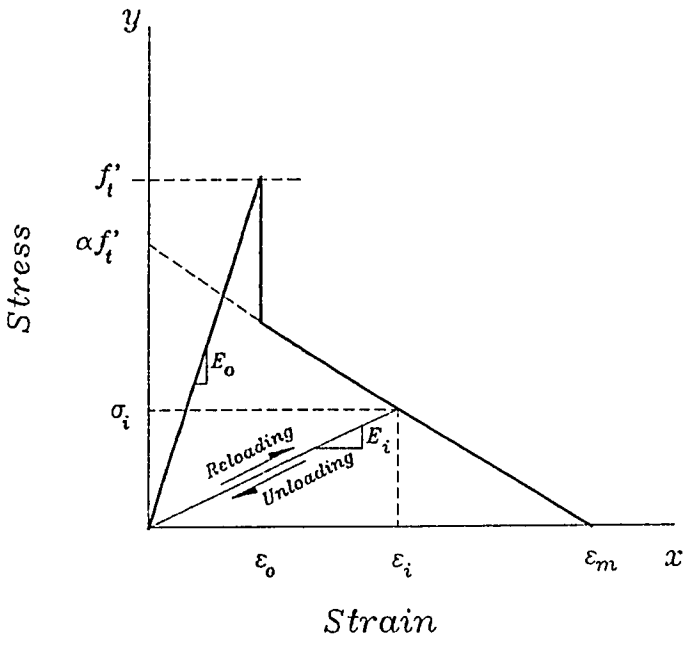

Figure 3.3: Tension stiffening behavior in cracked concrete

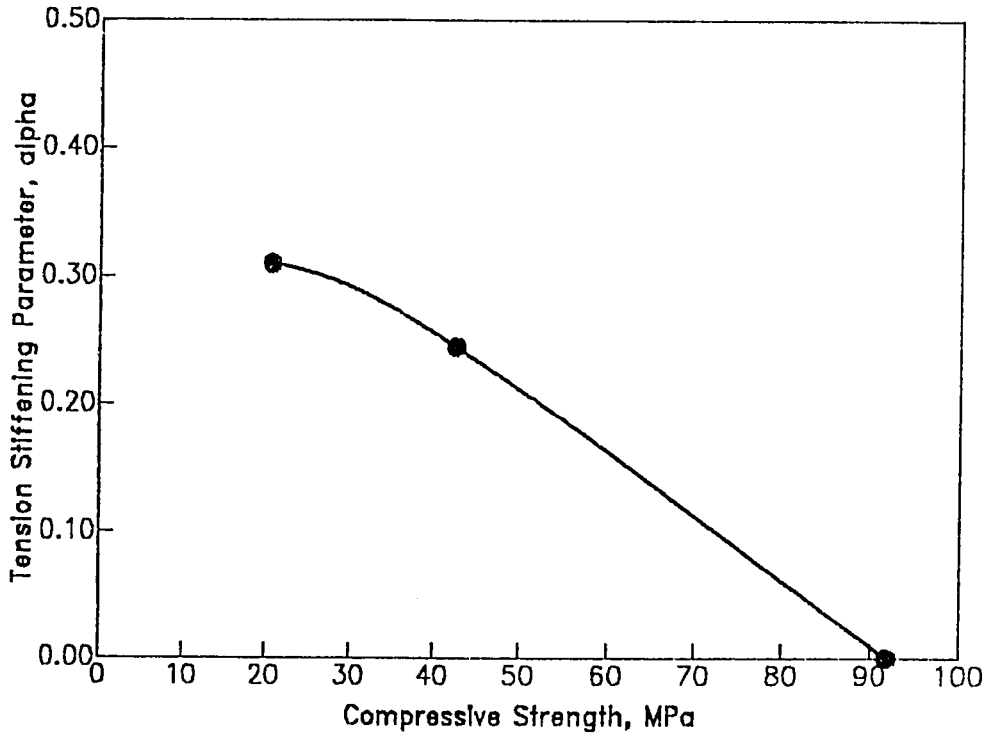

Figure 3.4: Variation of Tension stiffening parameter α, with the compressive strength f_c' $(a/d \geq 3.6)$

ε_i is the current value of strain in direction i.

If the strain component becomes zero or negative, the crack is assumed to have closed and the concrete is made to acquire the uncracked characteristics in the corresponding direction, but the crack direction as well as ε_{grtst} are stored. On further reloading however, the modulus E_i dependent on ε_{grtst} is used.

3.2.2.3 Shear Degradation

Experimental results indicate that a considerable amount of shear stress can be transferred across the rough surfaces of cracked concrete [49,50] due to the rough nature and due to dowel action of steel bars. These tests have shown that the primary variable in the shear transfer mechanism is the crack width. In smeared cracking model the best way to account for aggregate interlock and dowel action is to attribute an appropriate value to the cracked shear modulus G^c. In the present work an approach similar to that used in Ref [51] is adopted, where the cracked shear modulus is assumed to be a function of the current tensile strain. For concrete cracked in the 1 direction

$$G_{12}^c = \begin{cases} 0.25G(1 - \varepsilon_1/0.005) & \varepsilon_1 < 0.005 \\ 0 & \varepsilon_1 \geq 0.005 \end{cases} \tag{3.39}$$

where G is the uncracked concrete shear modulus and ε_i is the tensile strain in the 1 direction [51]. For concrete cracked in both directions, the shear modulus evaluated in equation 3.39 is further reduced by 50 perfecnt. If the crack closes the uncracked shear modulus is again assigned to the corresponding direction.

3.2.2.4 Constitutive Relations for Cracked Concrete

The constitutive relations for cracked concrete are given with respect to the local material coordinate system 1, 2. For Gauss points cracked in one direction the relations become

$$\begin{Bmatrix} \sigma_1 \\ \sigma_2 \\ \tau_{12} \end{Bmatrix} = \begin{bmatrix} E_1 & 0 & 0 \\ 0 & E & 0 \\ 0 & 0 & G_{12}^c \end{bmatrix} \begin{Bmatrix} \varepsilon_1 \\ \varepsilon_2 \\ \gamma_{12} \end{Bmatrix} \tag{3.40}$$

When a second crack develops in the orthogonal direction on σ_2 reaching f_t' the material matrix is modified such that

$$\begin{Bmatrix} \sigma_1 \\ \sigma_2 \\ \tau_{12} \end{Bmatrix} = \begin{bmatrix} E_1 & 0 & 0 \\ 0 & E_2 & 0 \\ 0 & 0 & 0.5G_{12}^c \end{bmatrix} \begin{Bmatrix} \varepsilon_1 \\ \varepsilon_2 \\ \gamma_{12} \end{Bmatrix} \tag{3.41}$$

The modulii E_1 and E_2 are equal to zero while loading but for unloading and reloading cycles they are evaluated using equation 3.37. The shear modulus G_{12} is calculated from equation 3.39.

The material matrices expressed in the local cracked coordinate systems, have to be transformed to the global x-y system. The stresses and strains in the local system are given in terms of the global values as

$$\begin{aligned} \{\sigma^L\} &= [A]\{\sigma^G\} \\ \{\varepsilon^L\} &= [B]\{\varepsilon^G\} \end{aligned} \tag{3.42}$$

where

$$[A] = \begin{bmatrix} \cos^2\theta & \sin^2\theta & 2\sin\theta\cos\theta \\ \sin^2\theta & \cos^2\theta & -2\sin\theta\cos\theta \\ -\sin\theta\cos\theta & \sin\theta\cos\theta & \cos^2\theta - \sin^2\theta \end{bmatrix} \tag{3.43}$$

and

$$[B] = \begin{bmatrix} \cos^2\theta & \sin^2\theta & \sin\theta\cos\theta \\ \sin^2\theta & \cos^2\theta & -\sin\theta\cos\theta \\ -2\sin\theta\cos\theta & 2\sin\theta\cos\theta & \cos^2\theta - \sin^2\theta \end{bmatrix} \tag{3.44}$$

Inverting equation 3.42 results in

$$\begin{aligned} \{\sigma^G\} &= \left[D^G\right]\{\varepsilon^G\} \\ \left[D^G\right] &= [A]^{-1}\left[D^L\right][B] \end{aligned} \tag{3.45}$$

3.3 Steel

3.3.1 Internal Steel Reinforcement

A one dimensional elastoplastic material model ia assumed for the internal flexural and shear steel reinforcement. The yield is defined by the uniaxial yield stress σ_Y and further loading results in elastoplastic behavior with linear strain hardening as depicted in Figure 3.5. An increment in stress $d\sigma$ results in a strain increment $d\varepsilon$ which may be considered to consist of the elastic and plastic components as

$$d\varepsilon = d\varepsilon_e + d\varepsilon_p \tag{3.46}$$

Defining the strain hardening parameter as

$$H' = \frac{d\sigma}{d\varepsilon_p} \tag{3.47}$$

and using equation 3.46 results in

$$\begin{aligned} H' &= \frac{d\sigma}{d\varepsilon - d\varepsilon_e} = \frac{d\sigma/d\varepsilon}{1 - \left(\frac{d\sigma}{d\varepsilon}\right)/\left(\frac{d\sigma}{d\varepsilon_e}\right)} \\ &= \frac{E_T}{1 - E_T/E} \end{aligned} \tag{3.48}$$

where

E, E_T are respectively the initial elastic modulus and the tangential modulus after yielding as shown in Figure 3.5.

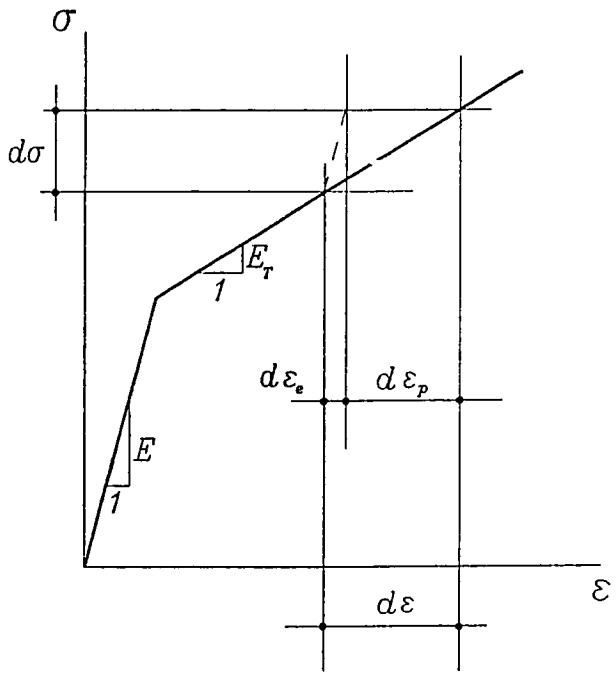

Figure 3.5: Material behavior for internal steel reinforcement

The resulting increment in displacement $d\delta$ is expressed as

$$d\delta = (d\varepsilon_e + d\varepsilon_p)L \tag{3.49}$$

and the corresponding increment in the force, using equation 3.47

$$dF = Ad\delta = AH'd\varepsilon_p \tag{3.50}$$

where

A, L are the cross-sectional area and length of the element respectively.

The elastoplastic stiffness thus becomes

$$K_{ep} = \frac{dF}{d\delta} = \frac{AH'd\varepsilon_p}{L(d\sigma/E + d\varepsilon_p)} \tag{3.51}$$

which on using equation 3.47 results in

$$K_{ep} = \frac{EA}{L}\left(1 - \frac{E}{E+H'}\right) \tag{3.52}$$

The elastoplastic constitutive relation can thus be expressed as

$$\sigma = D_{ep}\varepsilon \tag{3.53}$$

where

$$D_{ep} = \left(1 - \frac{E}{E+H'}\right)E \tag{3.54}$$

3.3.2 External Steel Plate

A two dimensional elastoplastic material model with linear strain hardening is adopted in this study to simulate the behavior of the externally bonded plate. The two dimensional model is essential to allow for the development of peeling stresses at plate curtailment.

The Von-Mises yield criterion is used and is expressed as

$$\sqrt{3J_2} = \sigma_Y(\chi) \tag{3.55}$$

where

J_2 is the second deviatoric stress tensor and

$\sigma_Y = \sigma_Y(\chi)$ is the yield stress dependent on the strain hardening parameter χ.

The constitutive relation is given as

$$\{\sigma\} = [D_{ep}]\{\varepsilon\} \tag{3.56}$$

with the elastoplastic material matrix $[D_{ep}]$ given as

$$[D_{ep}] = [D] - \frac{\{d_D\}\{d_D^T\}}{H' + \{d_D^T\}\{a\}} \tag{3.57}$$

where

$\{d_D\} = [D]\{a\}$,

$[D]$ is the elastic material matrix and

$\{a\}$ is the flow vector evaluated using equations 3.26 and 3.27

3.4 Interface Material Behavior

3.4.1 Concrete/Glue/Steel Interface

3.4.1.1 Material & Cracking Behavior of the Interface

Prior to the cracking of the interface, the material property matrix is taken as

$$[D]_{s-n} = \frac{1}{1-\nu^2}\begin{bmatrix} E & \nu E & 0 \\ \nu E & E & 0 \\ 0 & 0 & G(1-\nu^2) \end{bmatrix} \tag{3.58}$$

where E, ν are the modulus of elasticity and Poissons's ratio, respectively, of the interface and G the shear modulus. The response of the interface

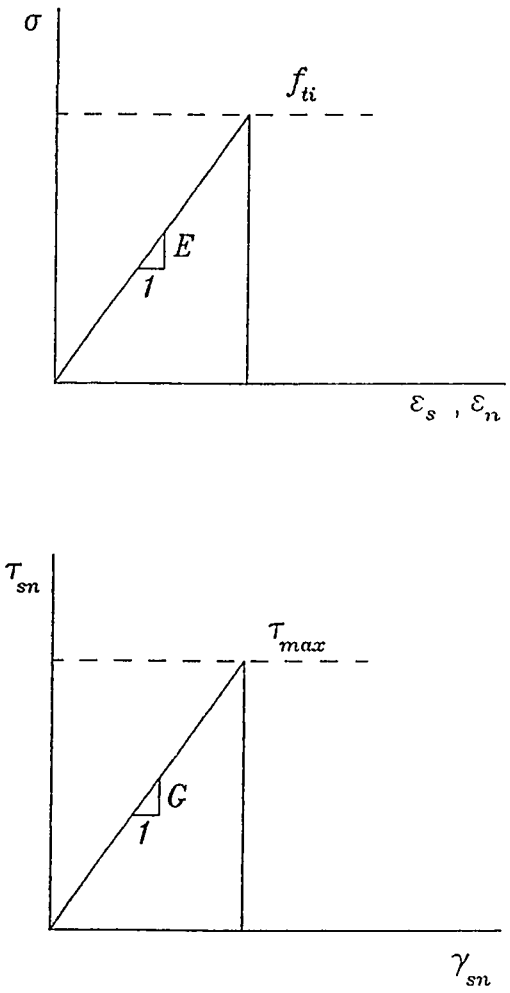

Figure 3.6: Material behavior of the interface element in tension and shear

element under tensile and shear stresses is assumed linear until a failure or fracture surface is reached (see Figure 3.6), whereafter, the element is made to crack. Due to its special thin geometry however, the interface element can crack in only two directions, one parallel to the glue line and the other perpendicular to it. Cracks perpendicular to the glue line will occur as soon as the corresponding normal stress reaches the specified tensile strength f_{ti} of the interface. After cracking has occurred, the stress as well as the elasticity modulus in the corresponding direction are set equal to zero. The updated material property matrix for the interface becomes,

$$[D]_{s-n} = \begin{bmatrix} 0 & 0 & 0 \\ 0 & E & 0 \\ 0 & 0 & 0.25G \end{bmatrix} \tag{3.59}$$

The interface could also crack parallel to the glue line under combined shear and normal stress, which has been shown in the experimental component of this thesis (section 5.2.6) and reported in Ref [52] to follow a Mohr-Coulomb type fracture criterion given by

$$\tau = c - \sigma tan\phi \tag{3.60}$$

where for a steel/epoxy/concrete interface, cohesion c was found to be in the range between 4.8 and 9.5 MPa with the angle of internal friction $\phi = 28°$. The wide range of c is attributed to variation in surface preparation and properties of adhesive and concrete. If the normal stress perpendicular to the glueline is tensile, in which case it is referred to as a peeling stress, all stress components and elements of the material matrix $[D]_{s-n}$, are reduced to zero.

However, if at the instant of failure governed by Mohr-Coulomb law, the normal stress is compressive, then only the shear stress and the corresponding shear modulus are set equal to zero. In this case the material

property matrix is updated to,

$$[D]_{s-n} = \frac{1}{1-\nu^2}\begin{bmatrix} E & \nu E & 0 \\ \nu E & E & 0 \\ 0 & 0 & 0 \end{bmatrix} \tag{3.61}$$

3.4.1.2 Material Properties for the Interface Elements

The material properties needed in the model for the interface element are the normal and shear elasticity modulii (E, G), Poisson's ratio ν and the tensile strength f_{ti}. As is expected, these quantities will depend on the material constants of the parent materials, namely concrete, epoxy glue and steel. The shear modulus of the interface has been determined from the slope of the line relating the average shear stress to slip using a new half-beam specimen [52]. This was found to be 120.1 MPa, and is quite close to the value reported by Charif [4]. Assuming the Poisson's ratio (ν) for the interface to be the same as that of concrete, the modulus of elasticity of the interface was established from the relationship

$$E = 2G(1+\nu) \tag{3.62}$$

With ν taken as 0.16, equation 3.62 yields an interface modulus $E = 278.6$ MPa. Reference [52] also established the tensile cutoff strength of the interface f_{ti} to be 4 MPa.

3.4.2 Steel/Concrete Bond

To model bond and bond deterioration between steel and concrete, two types of finite elements are used including the link element [29] and the more generalized interface element [53,54]. In this study, a thin interface element based on the latter formulation is used. The stress τ_{xy} at the Gauss point is compared with the limiting value of bond slip stress, from which bond deterioration is determined. If this stress exceeds the limiting value, the corresponding shear modulus is made equal to zero at the Gauss point.

Regarding the material parameters uesd to characterize bond behavior between concrete and steel, different values are reported in the literature particularly regarding the shear modulus, G. Based on the values reported in references [55,56,57,58], an average value of $G = 1200$ MPa was used in this study. Assuming Poisson's ratio $\nu = 0.16$, the elasticity modulus was calculated as $E = 2784$ MPa from equation 3.62. Also from experimental results [58,59], the bond strength was determined to be 7.5 MPa.

Chapter 4

Finite Element Model

4.1 Introduction

A two dimensional non-linear finite element model depicting the global behavior of the externally reinforced RC beam up to failure, which may be precipitated by a breakdown in any single component of the multi-phase structural system, is developed in this study. The model involves introduction of a six noded element to capture the characteristics of the interface between the concrete and external steel plate as well as the bond between the internal reinforcement and concrete. The finite element computer program written uses nine noded Lagrangian elements or eight noded Serendipity elements for concrete components of the structure as well as the external steel plate. The internal flexural and shear reinforcement is represented by three noded elements.

In this chapter the governing equilibrium equations are derived using the minimization of the total potential energy. For each of the elements mentioned above, the finite element discretization, the strain displacement relations as well as numerical integration schemes used are discussed.

4.2 Finite Element Formulation

Consider a structural system subjected to a set of body forces $\vec{b}$ over the volume Ω and boundary surface tractions $\vec{t}$ on the surface Γ. The potential energy can be written as

$$\Pi = \frac{1}{2}\int_{\Omega} \vec{\varepsilon}^T \vec{\sigma}\, d\Omega - \int_{\Omega} \vec{u}^T \vec{b}\, d\Omega - \int_{\Gamma} \vec{u}^T \vec{t}\, d\Gamma \tag{4.1}$$

where

$\vec{u}$ is the global displacement field and

$\vec{\varepsilon}, \vec{\sigma}$ are respectively the strain and stress vectors.

In a finite element discretization, the displacement and strain vectors can be expresses as

$$\begin{aligned} \vec{u} &= [N]\vec{d} \\ \vec{\varepsilon} &= [B]\vec{d} \end{aligned} \tag{4.2}$$

where

$\vec{d}$ is the vector of the global nodal displacements,

$[N]$ is the matrix of shape functions and

$[B]$ is the strain displacement matrix essentially containing derivatives of the shape functions.

Using equation 4.2 into 4.1, the potential energy can now be written as

$$\Pi = \frac{1}{2}\int_{\Omega} \vec{d}^T [B]^T \vec{\sigma}\, d\Omega - \int_{\Omega} \vec{d}^T [N]^T \vec{b}\, d\Omega - \int_{\Gamma} \vec{d}^T [N]^T \vec{t}\, d\Gamma \tag{4.3}$$

The stress vector

$$\vec{\sigma} = [D]\vec{\varepsilon} \tag{4.4}$$

where

$[D]$ is the elastic or elastoplastic material matrix

Minimizing the potential energy expression 4.3 that is

$$\frac{d\Pi}{d\vec{d}} = 0 \tag{4.5}$$

and using 4.4 yields

$$\int_\Omega [B]^T [D] [B] \vec{d}\, d\Omega - \int_\Omega [N]^T \vec{b}\, d\Omega - \int_\Gamma [N]^T \vec{t}\, d\Gamma = 0 \tag{4.6}$$

or

$$[K]\vec{d} = \vec{f} \tag{4.7}$$

where $[K]$ is the global stiffness matrix given as

$$[K] = \int_\Omega [B]^T [D] [B]\ d\Omega \tag{4.8}$$

and $\vec{f}$ is the global force vector and equal to

$$\vec{f} = \int_\Omega [N]^T \vec{b}\, d\Omega + \int_\Gamma [N]^T \vec{t}\, d\Gamma \tag{4.9}$$

If the total potential energy is taken as a sum of the contributions of the elements in the discretized finite element mesh, then

$$\Pi = \sum_{e=1}^{n} \Pi^e \tag{4.10}$$

Minimization of the potential energy thus implies that for each element

$$\frac{d\Pi^e}{d\vec{d}^e} = 0 \tag{4.11}$$

yielding the element stiffness matrix as

$$[K^e] = \int_\Omega [B^e]^T [D^e] [B^e]\ d\Omega^e \tag{4.12}$$

and the element load vector as

$$\vec{f}^e = \int_\Omega [N^e]^T \vec{b}^e\, d\Omega^e + \int_\Gamma [N^e]^T \vec{t}^e\, d\Gamma^e \tag{4.13}$$

For solution of non-linear problems equation 4.6 will not generally be satisfied at any stage of the computation and so

$$\Psi = \int_\Omega [B]^T [D] [B] \vec{d} d\Omega - \int_\Omega [N]^T \vec{b} d\Omega - \int_\Gamma [N]^T \vec{t} d\Gamma \neq 0 \qquad (4.14)$$

where

Ψ is the residual force vector.

The solution of equation 4.7 has to be obtained iteratively till convergence when the residual force Ψ has a minimum value as determined by the level of tolerance.

4.3 Element Stiffness Matrices

4.3.1 Eight & Nine Noded Elements

The strain vector in two dimensional elements as shown in Figure 4.1 is written as

$$\vec{\varepsilon} = \left\{ \begin{array}{c} \varepsilon_x \\ \varepsilon_y \\ \gamma_{xy} \end{array} \right\} = \left\{ \begin{array}{c} \partial u/\partial x \\ \partial v/\partial y \\ \partial u/\partial y + \partial v/\partial x \end{array} \right\} \qquad (4.15)$$

where

u, v are respectively the global x and y components of the element displacement field.

The displacements are determined by interpolation using shape functions N_i as

$$u = \sum_{i=1}^{n} N_i u_i$$

and

$$v = \sum_{i=1}^{n} N_i v_i \qquad (4.16)$$

where

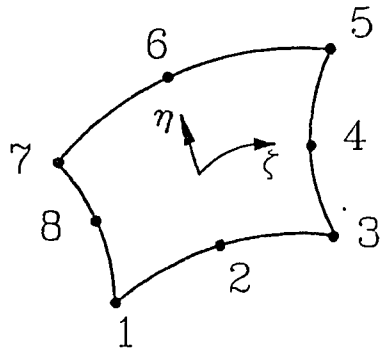

(a). Eight Noded Serendipity Element

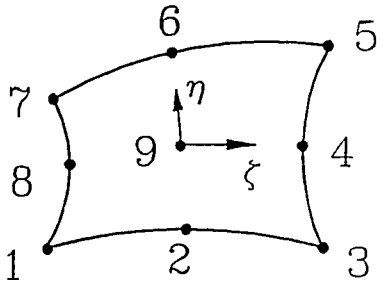

(b). Nine Noded Lagrangian Element

Figure 4.1: Two dimensional finite elements

u_i, v_i are respectively the x and y components of the element nodal displacements and,

n the number of element nodes.

Equation 4.15 thus becomes

$$\vec{\varepsilon} = \begin{Bmatrix} \varepsilon_x \\ \varepsilon_y \\ \gamma_{xy} \end{Bmatrix} = \sum_{i=1}^{n} \begin{Bmatrix} \left(\frac{\partial N_i}{\partial x}\right) u_i \\ \left(\frac{\partial N_i}{\partial y}\right) v_i \\ \left(\frac{\partial N_i}{\partial y}\right) u_i + \left(\frac{\partial N_i}{\partial x}\right) v_i \end{Bmatrix} \tag{4.17}$$

or in matrix form

$$\vec{\varepsilon} = [B]\vec{u} \tag{4.18}$$

where

$$\vec{u}^T = \{u_1\ v_1\ u_2\ v_2\ \cdots\ u_n\ v_n\} \tag{4.19}$$

and $n = 8$ for the 8-noded element and $n = 9$ for the 9-noded element. The strain displacement matrix $[B]$, therefore is given as

$$[B]^T = \left[\bar{N}_1\ \bar{N}_2\ \cdots \bar{N}_n\right] \tag{4.20}$$

where the submatrices $\bar{N}_i$ are given as

$$[\bar{N}_i] = \begin{bmatrix} \partial N_i/\partial x & 0 \\ 0 & \partial N_i/\partial y \\ \partial N_i/\partial y & \partial N_i/\partial x \end{bmatrix} \tag{4.21}$$

The shape functions N_i are usually expressed in terms of the natural coordinates (ξ,η) to facilitate numerical integration. For the eight noded element

the shape functions are given as

$$N_i = \tfrac{1}{4}(1+\xi\xi_i)(1+\eta\eta_i)(\xi\xi_i+\eta\eta_i-1) \qquad i = 1,\ 3,\ 5,\ 7$$

$$N_i = \tfrac{\xi_i^2}{2}(1+\xi\xi_i)(1-\eta^2) + \tfrac{\eta_i^2}{2}(1+\eta\eta_i)(1-\xi^2) \qquad i = 2,\ 4,\ 6,\ 8 \tag{4.22}$$

and for the nine noded element,

$$N_i = \tfrac{1}{4}(\xi^2+\xi\xi_i)(\eta^2+\eta\eta_i) \qquad i = 1,\ 3,\ 5,\ 7$$

$$N_i = \tfrac{1}{2}\eta_i^2(\eta^2+\eta\eta_i)(1-\xi^2) + \tfrac{1}{2}\xi_i^2(\xi^2+\xi\xi_i)(1-\eta^2) \qquad i = 2,\ 4,\ 6,\ 8$$

$$N_i = (1-\xi^2)(1-\eta^2) \qquad i = 9 \tag{4.23}$$

The element stiffness matrix is then evaluated as in equation 4.12. To be able to use the numerical integration, the elemental volume $d\Omega$ in equation 4.12 as well as the strain-displacement matrix $[B]$ in equations 4.20 and 4.21 must be transformed into the natural coordinates $(\xi,\ \eta)$. For isoparametric representation as is employed in this study, the coordinates for any point inside the element can be interpolated using similar shape functions as given in 4.22 and 4.23, that is

$$\begin{Bmatrix} x \\ y \end{Bmatrix} = \sum_{i=1}^{n} \begin{bmatrix} N_i & 0 \\ 0 & N_i \end{bmatrix} \begin{Bmatrix} x_i \\ y_i \end{Bmatrix} \tag{4.24}$$

The Cartesian shape function derivatives needed in equation 4.21 can be found by starting with the fact that

$$\begin{aligned} \frac{\partial N_i}{\partial \xi} &= \frac{\partial N_i}{\partial x}\frac{\partial x}{\partial \xi} + \frac{\partial N_i}{\partial y}\frac{\partial y}{\partial \xi} \\ \frac{\partial N_i}{\partial \eta} &= \frac{\partial N_i}{\partial x}\frac{\partial x}{\partial \eta} + \frac{\partial N_i}{\partial y}\frac{\partial y}{\partial \eta} \end{aligned} \tag{4.25}$$

or

$$\begin{pmatrix} \frac{\partial N_i}{\partial \xi} \\ \\ \frac{\partial N_i}{\partial \eta} \end{pmatrix} = \begin{bmatrix} \frac{\partial x}{\partial \xi} & \frac{\partial y}{\partial \xi} \\ \\ \frac{\partial x}{\partial \eta} & \frac{\partial y}{\partial \eta} \end{bmatrix} \begin{pmatrix} \frac{\partial N_i}{\partial x} \\ \\ \frac{\partial N_i}{\partial y} \end{pmatrix}$$

$$= [J] \begin{pmatrix} \frac{\partial N_i}{\partial x} \\ \\ \frac{\partial N_i}{\partial y} \end{pmatrix} \tag{4.26}$$

where

$$J = \begin{bmatrix} \frac{\partial x}{\partial \xi} & \frac{\partial y}{\partial \xi} \\ \\ \frac{\partial x}{\partial \eta} & \frac{\partial y}{\partial \eta} \end{bmatrix} = \begin{bmatrix} \sum_{i=1}^{n} \frac{\partial N_i}{\partial \xi} x_i & \sum_{i=1}^{n} \frac{\partial N_i}{\partial \xi} y_i \\ \\ \sum_{i=1}^{n} \frac{\partial N_i}{\partial \eta} x_i & \sum_{i=1}^{n} \frac{\partial N_i}{\partial \eta} y_i \end{bmatrix} \tag{4.27}$$

is the Jacobian of the coordinate transformation. Solving for the Cartesian derivatives from equation 4.26 yields

$$\begin{pmatrix} \frac{\partial N_i}{\partial x} \\ \\ \frac{\partial N_i}{\partial y} \end{pmatrix} = [J]^{-1} \begin{pmatrix} \frac{\partial N_i}{\partial \xi} \\ \\ \frac{\partial N_i}{\partial \eta} \end{pmatrix} \tag{4.28}$$

where the inverse of the Jacobian matrix can be shown to be

$$[J]^{-1} = \begin{bmatrix} \frac{\partial \xi}{\partial x} & \frac{\partial \eta}{\partial x} \\ \\ \frac{\partial \xi}{\partial y} & \frac{\partial \eta}{\partial y} \end{bmatrix} = \frac{1}{\|J\|} \begin{bmatrix} \frac{\partial y}{\partial \eta} & -\frac{\partial y}{\partial \xi} \\ \\ -\frac{\partial x}{\partial \eta} & \frac{\partial x}{\partial \xi} \end{bmatrix} \tag{4.29}$$

The element volume needed in equation 4.12 thus becomes

$$\Omega = t\, dx\, dy = t\, \|J\|\, d\xi\, d\eta \tag{4.30}$$

where t is the thickness of the element for plane stress conditions. The integration to obtain the element stiffness matrix can now be performed in natural coordinates where the submatrix K_{ij} linking nodes i and j of the element is given as

$$\begin{aligned} K_{ij} &= \int_{-1}^{1}\int_{-1}^{1} [B]_i^T [D][B]_j \, t\|J\| \, d\xi \, d\eta \\ &= \int_{-1}^{1}\int_{-1}^{1} M_{ij} \, d\xi \, d\eta \end{aligned} \tag{4.31}$$

The three point integration rule is used and so 4.31 becomes

$$K_{ij} = \sum_{p=1}^{3}\sum_{q=1}^{3} M(\xi_p, \eta_q)_{ij} W_p W_q \tag{4.32}$$

where W_p and W_q are the Gauss weighing factors at the sampling point (ξ_p, η_q).

4.3.2 Three Noded Truss Elements

The strains in the truss element shown in Figure 4.2 are written as

$$\varepsilon = \frac{\partial \bar{u}}{\partial s} \tag{4.33}$$

where

$\bar{u}$ is the longitudinal displacement at any point in the element and

s is the local coordinate along the element axis.

The displacements are approximated using shape functions N_i as

$$u = \sum_{i=1}^{3} N_i \bar{u}_i \tag{4.34}$$

where

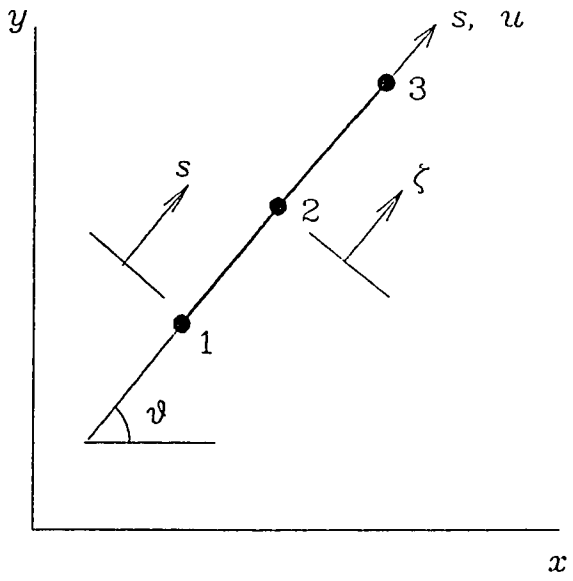

Figure 4.2: Three noded truss element

$\bar{u}_i$ are nodal displacements along s.

Using equation 4.34 into 4.33 results into the strains as

$$\varepsilon = \sum_{i=1}^{3} \frac{\partial N_i}{\partial s} \tag{4.35}$$

The shape functions N_i in terms of the natural coordinates (ξ,η) are given as

$$N_1 = -\frac{1}{2}\xi(1-\xi)$$

$$N_2 = 1-\xi^2$$

$$N_1 = \frac{1}{2}\xi(1+\xi) \tag{4.36}$$

The coordinate at any point in the element is interpolated as

$$s = \sum_{i=1}^{3} N_i s_i \tag{4.37}$$

where

s_i are the local nodal coordinates.

The Jacobian of the transformation

$$J = \frac{\partial s}{\partial \xi} = \sum_{i=1}^{3} \frac{\partial N_i}{\partial \xi} s_i \tag{4.38}$$

and the inverse

$$J^{-1} = \frac{\partial \xi}{\partial s} = \frac{1}{\partial s/\partial \xi} \tag{4.39}$$

The strains in equation 4.35 can now be expressed as

$$\varepsilon = \sum_{i=1}^{3} \frac{\partial N_i}{\partial \xi}\frac{\partial \xi}{\partial s}\bar{u}_i \tag{4.40}$$

or in matrix form as

$$\vec{\varepsilon} = [B]\{\bar{u}\} \tag{4.41}$$

where the strain displacement matrix $[B]$ is given as

$$[B] = J^{-1}\left[\frac{\partial N_1}{\partial \xi} \quad \frac{\partial N_2}{\partial \xi} \quad \frac{\partial N_3}{\partial \xi}\right] \tag{4.42}$$

and

$$\{\bar{u}\}^T = [\bar{u}_1 \quad \bar{u}_2 \quad \bar{u}_3] \tag{4.43}$$

The element volume needed in equation 4.12 is written as

$$\Omega = A\,ds = A\,\|J\|\,d\xi \tag{4.44}$$

where A is the element cross-sectional area.

The submatrix linking nodes i and j of the element is now evaluated as

$$\begin{aligned} K_{ij} &= \int_{-1}^{1} [B]_i^T [D][B]_j\, A\,\|J\|\,d\xi \\ &= \int_{-1}^{1} M_{ij}\,d\xi \\ &= \sum_{p=1}^{3} M(\xi_p)_{ij} W_p \end{aligned} \tag{4.45}$$

The assembled element stiffness matrix calculated from equation 4.45 has to be transformed from the local coordinates to global ones. The stiffness equation in the local coordinate system

$$\{u_L\} = [K]_L\{f_L\} \tag{4.46}$$

The local displacements $\{u_L\}$ are related the global ones $\{u_G\}$, by

$$\{u_L\} = [T]\{u_G\} \tag{4.47}$$

Similarly the nodal force vectors are related as

$$\{f_L\} = [T]\{f_G\} \tag{4.48}$$

Substituting equations 4.47 and 4.48 in 4.46, premultiplying each side by $[T]^{-1} = [T]^T$ results into the global stiffness equation as

$$\begin{aligned} \{u_G\} &= [K]_G\{f_G\} \\ [K]_G &= [T]^T[K]_L[T] \end{aligned} \tag{4.49}$$

where the vector of local displacements is given by equation 4.43 and that of global displacements is given as

$$\{u_G\}^T = [u_1 \quad v_1 \quad u_2 \quad v_2 \quad u_3 \quad v_3 \quad] \tag{4.50}$$

and the transformation matrix $[T]$ given by

$$[T]^T = \begin{bmatrix} \cos\theta & 0 & 0 \\ \sin\theta & 0 & 0 \\ 0 & \cos\theta & 0 \\ 0 & \sin\theta & 0 \\ 0 & 0 & \cos\theta \\ 0 & 0 & \sin\theta \end{bmatrix} \tag{4.51}$$

4.3.3 Six Noded Interface Elements

This section describes the formulation of a new thin interface element that has been developed as part of this thesis to characterize the essential features as well as the failure mechanisms of RC beams strengthened with steel plates on their tensile faces. Not only can the element pick up the normal and shear stress concentrations at the plate curtailment, but is also capable of separation if the peak normal and shear stresses are exceeded.

Since the glue-line thickness as well as its strength are much smaller compared to the other components of the plate bonded beam, a six noded

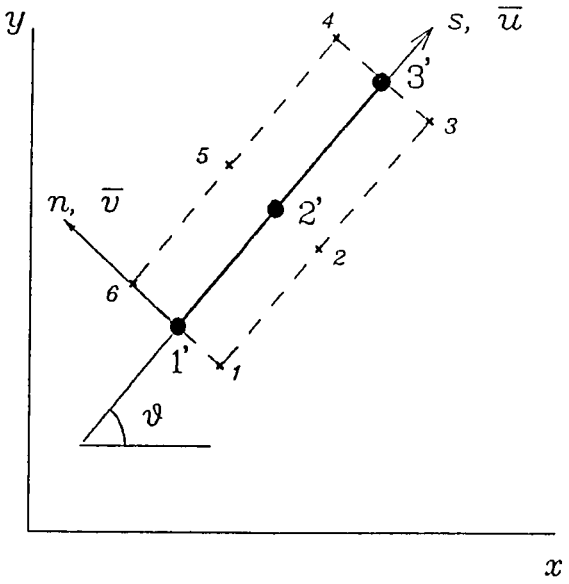

Figure 4.3: Six noded interface element

element, as shown in figure 4.3, was deemed sufficient to represent the steel-glue-concrete interface. By defining equivalent pseudo nodes $1'$, $2'$ and $3'$, isoparametric formulation with parabolic shape functions was possible. A three point Gaussian-integration rule is used for the element.

The strains in the glue element can be written as,

$$\vec{\varepsilon} = \begin{Bmatrix} \varepsilon_s \\ \varepsilon_n \\ \gamma_{sn} \end{Bmatrix} = \begin{Bmatrix} \partial u/ds \\ \partial v/dn \\ \partial u/dn + \partial v/ds \end{Bmatrix} \tag{4.52}$$

The strain ε_s along the s-direction may be approximated as,

$$\varepsilon_s = \frac{\partial u}{\partial s} = \frac{\partial}{\partial s}\sum_{i=1}^{3} N_i'(s)\bar{u}_i = \sum_{i=1}^{3} \frac{dN_i'(s)}{ds}\bar{u}_i \tag{4.53}$$

where $N_i' = N_i'(s)$ are the shape functions given by equations 4.36 at the three equivalent nodal points $1'$, $2'$ and $3'$ as shown in figure 4.3, and $\bar{u}_i$ are the average nodal displacements along line $n = 0$. Equation 4.53 can be written in terms of the element nodal displacements u_i as,

$$\varepsilon_s = \frac{dN_1'}{ds}\left(\frac{u_1+u_6}{2}\right) + \frac{dN_2'}{ds}\left(\frac{u_2+u_5}{2}\right) + \frac{dN_3'}{ds}\left(\frac{u_3+u_4}{2}\right) \tag{4.54}$$

The strain in the normal direction ε_n, is given by

$$\varepsilon_n = \frac{\partial v}{\partial n} \tag{4.55}$$

and can be expressed in terms of nodal normal strains by

$$\begin{aligned} \varepsilon_n &= \sum_{i=1}^{3} N_i'(s)\left(\frac{\partial v}{\partial n}\right)_i \\ &= \sum_{i=1}^{3} N_i'(s)\left(\frac{\Delta v}{t}\right)_i \\ &= \frac{1}{t}\left[N_1'(v_6 - v_1) + N_2'(v_5 - v_2) + N_3'(v_4 - v_3)\right] \end{aligned} \tag{4.56}$$

where t is the element thickness.

The shear strain γ_{sn} is approximated as

$$\begin{aligned}
\gamma_{sn} &= \frac{\partial \bar{u}}{dn} + \frac{\partial \bar{v}}{ds} \\
&= \sum_{i=1}^{3} N_i'(s) \left(\frac{\partial u}{\partial n}\right)_i + \frac{d}{ds} \sum_{i=1}^{3} N_i'(s) \bar{v}_i \\
&= \frac{1}{t} \left[N_1'(u_6 - u_1) + N_2'(u_5 - u_2) + N_3'(u_4 - u_3) \right] \\
&+ \left[\frac{dN_1'}{ds} \left(\frac{v_1 + v_6}{2}\right) + \frac{dN_2'}{ds} \left(\frac{v_2 + v_5}{2}\right) + \frac{dN_3'}{ds} \left(\frac{v_3 + v_4}{2}\right) \right] \quad (4.57)
\end{aligned}$$

Substituting equations 4.54, 4.56 and 4.57 in equation 4.52 results in,

$$\vec{\varepsilon} = [B]\,\vec{v} \quad (4.58)$$

where B, the strain matrix in its transposed form is given as,

$$B^T = \begin{bmatrix} \frac{1}{2}dN_1'/ds & 0 & -N_1'/t \\ 0 & -N_1'/t & \frac{1}{2}dN_1'/ds \\ \frac{1}{2}dN_2'/ds & 0 & -N_2'/t \\ 0 & -N_2'/t & \frac{1}{2}dN_2'/ds \\ \frac{1}{2}dN_3'/ds & 0 & -N_3'/t \\ 0 & -N_3'/t & \frac{1}{2}dN_3'/ds \\ \frac{1}{2}dN_3'/ds & 0 & N_3'/t \\ 0 & N_3'/t & \frac{1}{2}dN_3'/ds \\ \frac{1}{2}dN_2'/ds & 0 & N_2'/t \\ 0 & N_2'/t & \frac{1}{2}dN_2'/ds \\ \frac{1}{2}dN_1'/ds & 0 & N_1'/t \\ 0 & N_1'/t & \frac{1}{2}dN_1'/ds \end{bmatrix} \tag{4.59}$$

and the displacement vector $\vec{v}$ given as,

$$\vec{v}^T = \left\{ \begin{array}{cccccccccccc} u_1 & v_1 & u_2 & v_2 & u_3 & v_3 & u_4 & v_4 & u_5 & v_5 & u_6 & v_6 \end{array} \right\} \tag{4.60}$$

The Jacobian is evaluted as in equation 4.38 using the coordinates s_i of the three nodal points $1'$, $2'$ and $3'$ as shown in figure 4.3. After defining the elemental volume of integration as

$$\Omega = t\, b \, \| J \| \, d\xi \tag{4.61}$$

where b is the width of the interface element. The stiffness submatrix

linking nodes i and j of the element is now evaluated as

$$\begin{aligned} K_{ij} &= \int_{-1}^{1} [B]_i^T [D][B]_j \, t \, b \, \|J\| \, d\xi \\ &= \int_{-1}^{1} M_{ij} \, d\xi \\ &= \sum_{p=1}^{3} M(\xi_p)_{ij} W_p \end{aligned} \tag{4.62}$$

The transformation of the element stiffness matrix to the global coordinate system is carried out using equation 4.49 where u_G is defined by $\vec{v}$ given in equation 4.60. The transformation matrix now becomes

$$T = \begin{bmatrix} \bar{T} & 0 & 0 & 0 & 0 & 0 \\ 0 & \bar{T} & 0 & 0 & 0 & 0 \\ 0 & 0 & \bar{T} & 0 & 0 & 0 \\ 0 & 0 & 0 & \bar{T} & 0 & 0 \\ 0 & 0 & 0 & 0 & \bar{T} & 0 \\ 0 & 0 & 0 & 0 & 0 & \bar{T} \end{bmatrix} \tag{4.63}$$

where

$$\bar{T} = \begin{bmatrix} \cos\theta & \sin\theta \\ -\sin\theta & \cos\theta \end{bmatrix} \tag{4.64}$$

Chapter 5

Experimental Program and Determination of Interface Material Law

5.1 Introduction

External bonding of steel plates to damaged reinforced concrete beams and slabs as a means of strengthening them has been shown to be quite an efficient repair technique by virtue of its simplicity, ease in construction and minimum disruptive features (see [6,5,8,9,60]). In recent years, extensive experimental investigations of the factors influencing the structural performance of epoxy bonded plated concrete beams have been reported by Swamy et. al.(see [14] to [17]). The variables studied include plate thickness, epoxy type and thickness of the adhesive layer. These investigations show that bonding of thin steel plates on the tension faces of concrete beams can lead to significant improvements in the structural performance under both service and ultimate load conditions. However, the investigations also show that premature failure may occur because of shear and normal stress concentrations at the ends of the steel plates resulting in debonding of the plate or ripping off of the concrete cover.

To achieve a realistic design and prediction of ultimate loads for plate bonded beams, an accurate determination of shear and peeling stresses becomes necessary. The magnification of shear stress due to stress concentration occurring in the zone of plate curtailment, and the accompanying transverse normal stress have been determined using a strength of materials approach, independently by researchers at University of Sheffield and at University College, Cardiff (see [18] to [25])

In a non-linear finite element model for the plate bonded beam, material characterization of the concrete/glue/steel interface becomes even more significant. Experimental study into the behavior of steel/glue/concrete interface has been carried out by Swamy, Jones and Charif [4,63] using pull out specimens, and for steel/glue/steel interface using double lap specimens.

In this study, as is shown in Figure 5.1, several geometries and loading conditions were tried out in an attempt to come up with a suitable test specimen to simulate the material behavior of the steel/glue/concrete interface. The test setups were quite elaborate and except for the half beam specimen, the measures results were inconsistent and irreproduceable. In this work therefore, a half beam specimen, believed to simulate the curtailment zone in a plate bonded beam more realistically, is introduced and used to characterize the steel/glue/concrete interface.

There are however limitations in experimental characterization of the glue interface due to errors in the experiment and more significantly due to the inability of measuring the 'hidden' quantities, particularly the peeling stresses. A combined experimental/numerical technique is proposed to overcome this difficulty. The technique is built around a non-linear finite element discretization of various test specimens used to characterize interface behavior and the relevant interface stresses are obtained from the numerical model that correspond to experimentally measured loads at failure of the test specimens.

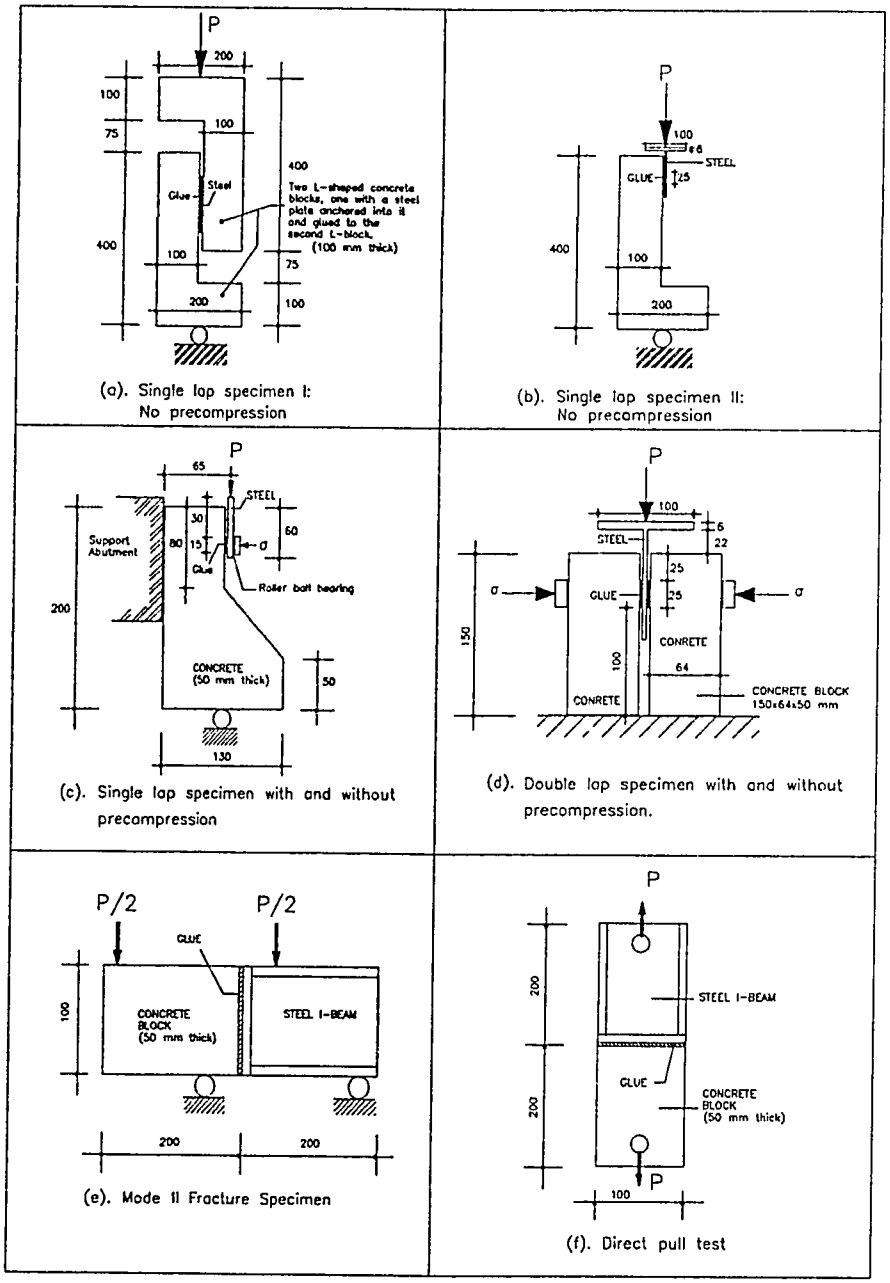

Figure 5.1: Specimen geometries and test-setups for the determination of Steel/Glue/Concrete interface properties, tried out in this study

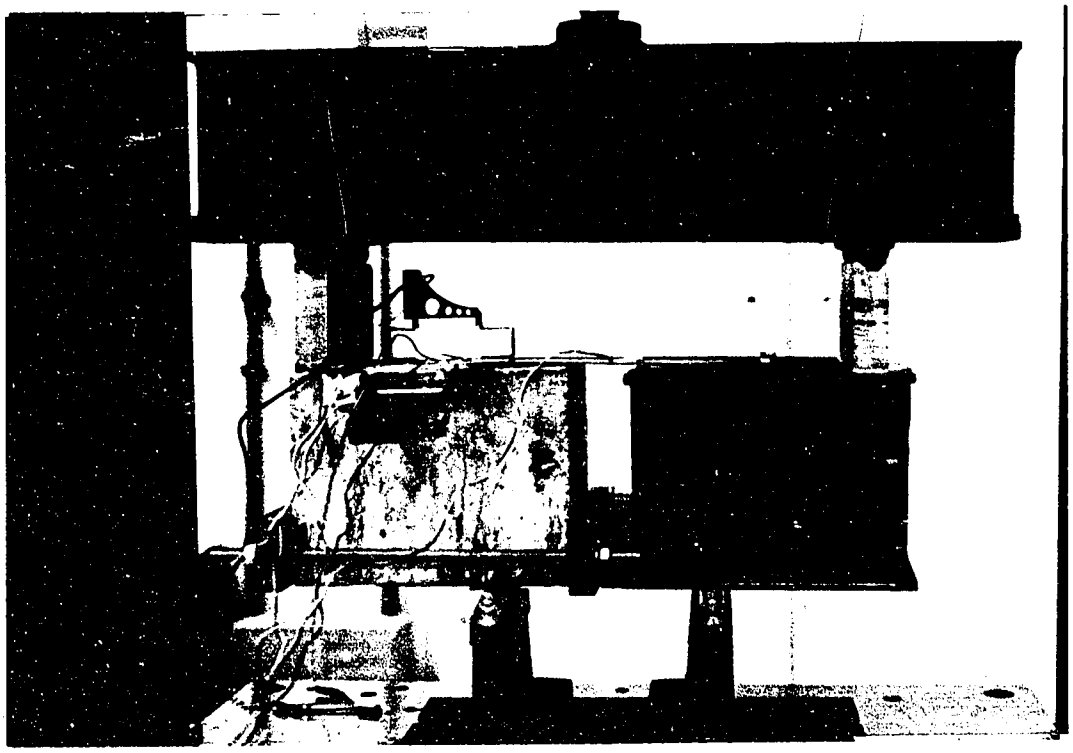

Plate 1: Experimental setup

5.2 Experimental Details

This section describes the experimental set up of the proposed half beam specimen for characterization of the interface. Details regarding the materials used as well as the instrumentation and test procedure are stated. The procedure used to bond the plates to concrete surface is also described in detail.

5.2.1 Half Beam Specimen

Figure 5.2 and Plate 1 show the details of the specimen proposed to characterize the material properties of the steel/glue/concrete interface. The specimen essentially consists of a plane concrete block on the tension side of which is bonded a steel plate 3 mm thick and 15 mm wide. The distance along the glued line was kept constant at 100 mm. The width of the unglued part of the plate is kept constant for an extra length of 200 mm and then enlarged to 100 mm and secured to the top of a steel I-beam section by two bolts. Near the bottom of the concrete block the two halves are connected through a simple hinge.

The whole assembly subjected to a four point loading in a flexural test (Figure 5.2) more closely simulates a reinforced concrete beam bonded with a plate on its tensile face, especially the regions near the plate curtailment. Other advantages include its small size and the fact that it can be reused. The only test variable studied was the concrete compressive strength which ranged from 28 to 58.5 MPa. For each concrete strength, average values of quantities of interest based on six specimens tested is reported.

5.2.2 Materials

The concrete mix design used in the manufacture of the concrete block component of the half beam test specimen is shown in Table 5.1. Ordinary

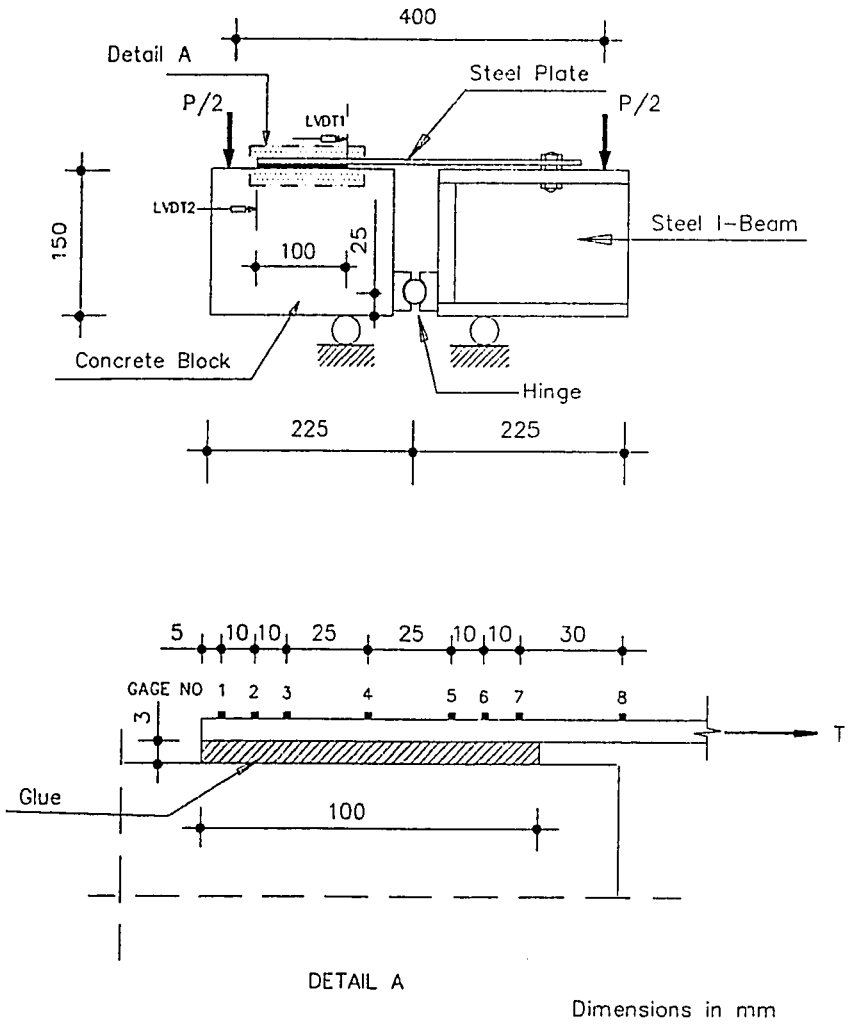

Figure 5.2: Half Beam Test Details

Mix Constituent		*Weight, kg.*
Coarse aggregate		
Passing	$\frac{3}{4}in$ (19 mm)	8.40
	$\frac{1}{2}in$ (12.7 mm)	16.40
	$\frac{3}{8}in$ (9.5 mm)	13.20
	$\frac{3}{16}in$ (4.8 mm)	2.0
Sand		25.0
Cement		15.0

Table 5.1: Concrete mix design

portland cement Type I, crushed limestone aggregate and natural beach sand were the constituents used in the concrete. Table 5.1 also shows the coarse aggregate grading. To obtain concrete of varying strengths, different water/cement ratios were used ranging from 0.38 to 0.65. A dosage of 1.5 liters of superplasticizer per 50 kg. cement was added for low water cement ratios to obtain high concrete strengths.

The 3 mm thick plates used were of mild steel with an elastic modulus of 200 GPa and a yield stress of 269 MPa. A two component epoxy adhesive was used to bond the plates to the surface of the concrete block.

5.2.3 Bonding Procedure

The concrete blocks were cured in the laboratory by immersing in water and after a period of four weeks removed and dried for twenty four hours prior

to gluing of the steel plates. The concrete surface was roughened by the use of a small pick hammer. During this process, not only was the laitance removed but most of the exposed aggregates were further roughened as small particles were chipped off their surfaces. All loose particles were then removed using a vacuum cleaner. The surface of the steel plate to receive the epoxy glue was shot-blasted using coarse sand. The two component epoxy adhesive was mixed in a ratio of resin to hardener of 2 to 1 by weight as per manufacturer recommendations. Due to the relatively small quantities of surface areas involved, the mixing was done by hand till an acceptable level of consistency in terms of color and viscosity was achieved.

A constant glue thickness was maintained by using spacers which were essentially small length wires of stainless steel of diameter 3 mm. The glue was applied on both the concrete block and steel plate surfaces, and after aligning them properly, the plates were held in position with a series of weights. The excess glue was extruded by the weights and was scraped off before the specimens were left to cure.

5.2.4 Instrumentation

To determine the relative slip between the steel plate and concrete block surfaces, the half-beam specimen was instrumented with two linear variable differential transducers (LVDT), one fixed on the steel plate surface and the other on the concrete surface at the ends of the glue line as shown in Figure 5.2. Electrical strain gages, 2 mm length were fixed along the center line of the steel plate to assess the variation of normal stress along the length of the steel plate. The interface shear stress is then obtained as a gradient measure of the normal stress in the plate. The exact location of the gages is also shown in Figure 5.2. Since the stress gradient in the regions near the plate end is high, the gage spacing was made smaller to ensure greater accuracy in the computed forces and stresses. Using a data

logger and a computerized data acquisition system, continuous recording of the readings was possible.

5.2.5 Test Procedure

The test setup is shown in Figure 5.2. The half beam specimen, composed of a concrete block fixed through a hinge mechanism to the other half made of an I-beam steel section, was loaded in an Instron machine. The loading was at a constant strain rate provided by a crosshead movement of 0.5 mm per minute. The data acquisition system scanned the load cell, LVDT's and electric strain gages and recorded the data every 0.20 kN. The data acquisition system also allowed simultaneous graphical display of values being scanned, hence facilitating an easier monitoring of the experiment.

5.2.6 Results of Experimental Study

Figure 5.3 shows a typical plot of the average interface shear stress determined as the load divided by the glued area, versus the slip as determined from the LVDT readings (see Figure 5.2). The slope of the plot G_1, multiplied by the glue line thickness gives an indication of the shear modulus for the interface G_{int}. As outlined in section 5.2.4, the strains were measured along the steel plate and Figure 5.4 shows typical plots of the normal strain in the plate for four different load levels including the ultimate load. Figure 5.5 shows the resulting interface shear stress evaluated from

$$\tau = \frac{\Delta\varepsilon E t_p}{\Delta L} \tag{5.1}$$

where

$\Delta\varepsilon$ difference in strain readings of any two consecutive gages

E elasticity modulus for the steel plate

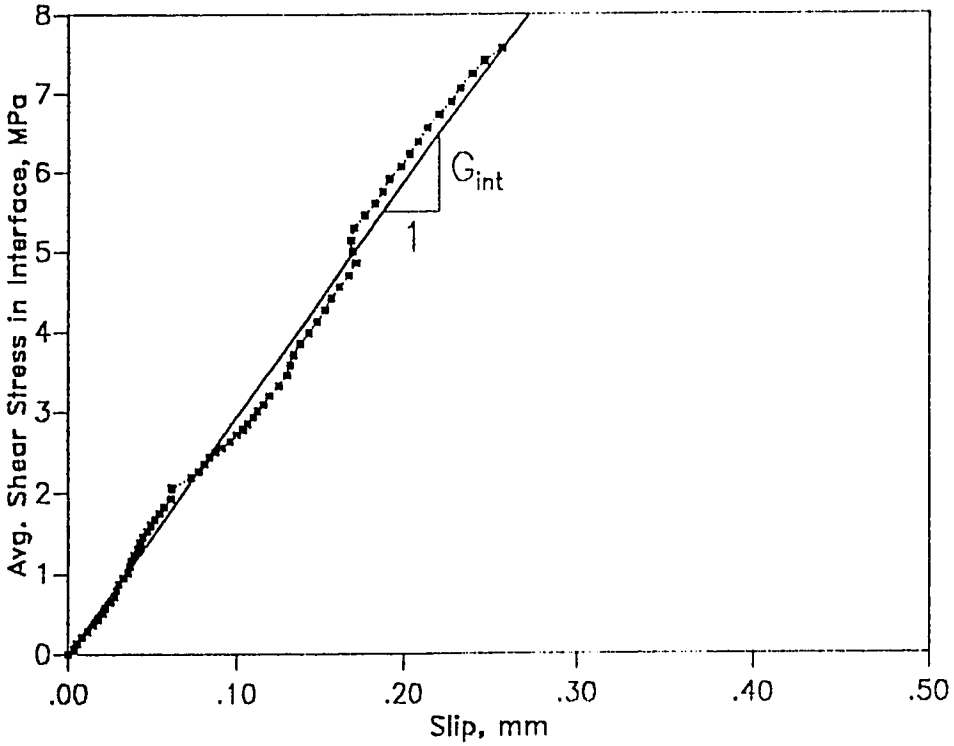

Figure 5.3: Shear modulus of the interface (Experimental)

t_p plate thickness

ΔL distance between the two consecutive gages.

Table 5.2 lists the ultimate loads and corresponding interface shear strength for half beam specimens with concrete blocks of varying compressive strength. The ultimate load levels appear to be independent of the concrete compressive strength for the strength range considered. This finding lends credibility to the hypothesis that the concrete/glue/steel interface material behavior is truly a surface phenomenon. The nature of the surface, including its preparation, may be the significant factor affecting the ultimate strength. Similar results have been obtained by Swamy et al [63].

5.3 Experimental-Numerical Technique

The experimental determination of the interface shear stress at failure is not sufficient in itself to characterize the phenomenological response of a plate bonded beam. This is confirmed by the fact that with the use of same component materials, the measured shear stress at failure is dependent on specimen geometry. This occurence can be attributed to the existence of a transverse normal stress at the interface whose sense and magnitude plays a vital role in determining the magnitude of the interface shear stress at ultimate load conditions.

Inasmuch as a transverse normal or peeling stress is difficult to measure experimentally, the procedure adopted utilized a combined experimental-numerical approach. Use was made of a non-linear finite element analysis of various specimen configurations in vogue for interface characterization together with experimental data for failure loads to estimate combinations of shear and normal stresses causing interface failure. Details of the non-linear finite element model have already been provided in Chapter 4, and

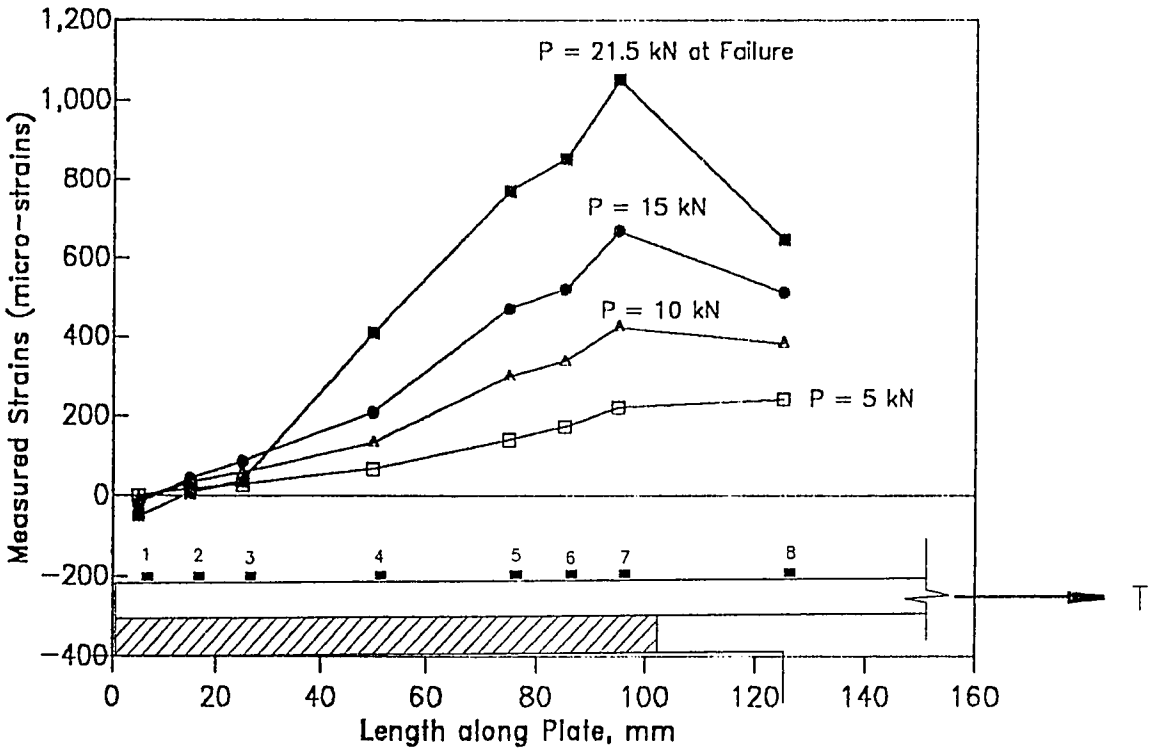

Figure 5.4: Distribution of the strains in steel plate (Experimental)

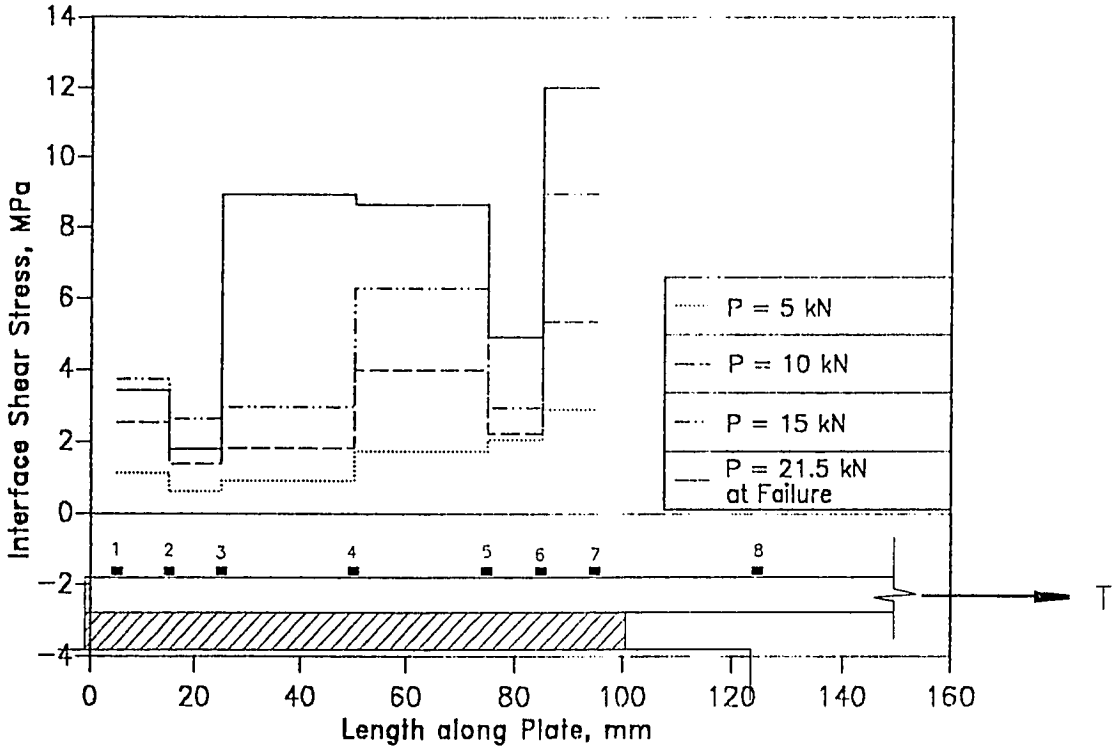

Figure 5.5: Distribution of the shear stress in glue interface (Experimental)

Compressive cylinder strength f_c' *Mpa.*	*Load at failure P kN.*	*Load in plate T kN.*	*Average shear stress at failure* τ_{avg} *MPa.*	*Shear rigidity* G_{int} *MPa.*
28	23.05	10.14	6.76	123
36.8	23.25	10.23	6.82	145
45.4	22.30	9.81	6.54	110
52.4	23.84	10.49	6.99	125
58.5	21.85	9.62	6.41	101
Avg.			6.704	120.2

Table 5.2: Variation of shear strength with concrete compressive strength

are consequently not repeated.

Prior to presenting results from the finite element analysis of the half beam specimen, attention is focussed in the next section on the experimental details for various interface characterization test specimens as developed by researchers elsewhere.

5.3.1 Existing Test Specimens for Interface Characterization

Pull Out Specimen (Ref [63])

Figure 5.6 shows a pull out specimen used by Swamy, Jones and Charif [63] to determine the shear adhesiveness of the concrete-glue-steel interface. The average interface shear stress at failure was reported in the range of 2.17 MPa to 3.33 MPa for concrete compressive strength $f_c^{'}$ ranging from 25.1 MPa to 71.3 MPa and a glue line thickness of 1.0 mm. For a fixed $f_c^{'}$ of 45 MPa, the average shear stress varied from 2.42 MPa to 2.83 MPa for glue line thickness ranging from 0.5 mm to 3.0 mm.

The reported values for the average shear stress at failure appear to be not greatly affected by the magnitude of $f_c^{'}$ and glue line thickness and is essentially affected only by the the nature of the surface. For the finite element analysis of this specimen, an ultimate load corresponding to an average shear stress of 2.83 MPa (25.47 kN), an $f_c^{'}$ of 45 MPa and a glue line thickness of 3.0 mm were taken as the parameters. In addition the elastic modulus for steel was taken as 200 GPa with a yield strength of 265 MPa.

Beam F31 (Ref [4])

Of the several beams tested by Charif [4], beam F31 is reported to have failed by plate separation and thus presents an opportunity to determine the

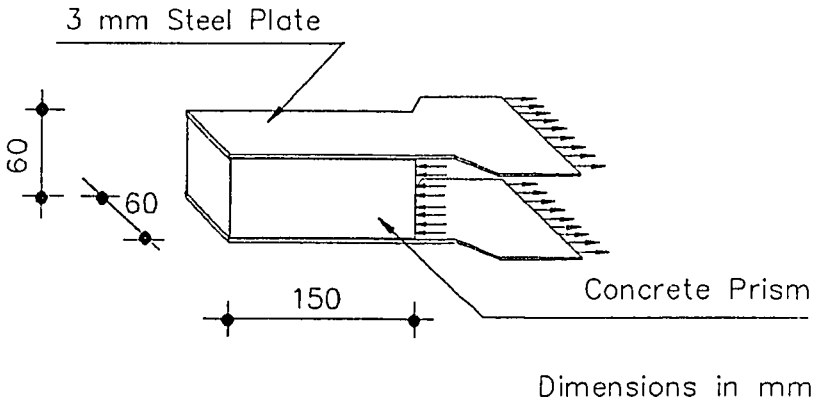

Figure 5.6: Pull out test specimen

shear strength of an interface in the presence of peeling or tensile stresses. Figure 5.7(a) shows the geometric details of beam F31. The beam failed at a load of 182 kN, the mode of failure being that of debonding in the zone of plate curtailment. According to the reported experimental values, the concrete strength used in the finite element analysis was 53 MPa. An elastic modulus of 200 GPa and a yield strength of 291 MPa was assumed for the steel plate.

Beams URB4 and URB5 (Ref [14])

Beams URB4 and URB5 whose details are shown in Figure 5.7(b) both are reported to have failed by plate separation at loads of 57.5 kN and 53.1 kN, respectively [14]. Beam URB4 is bonded externally with a 5 mm plate and beam URB5 with a 10 mm plate. The concrete compressive strength used in the numerical analysis was 58.3 MPa. The elastic modulus for the steel plate was 200 GPa with a yield strength of 240 MPa.

Beams B209 and B218 (Ref [15])

Beams B209 and B218 were part of a series of beams tested by Swamy et al [15] that failed by plate separation. The geometric details for such beams are shown in Figure 5.7(c). Beam B209 failed at a load of 220 kN and beam B218 at 194 kN. The concrete strength in compression used in the numerical analysis was 58 MPa with the steel plate having an elastic modulus of 200 GPa and a yield strength of 248 MPa.

5.3.2 Results of Experimental-Numerical Study

Figures 5.8, 5.9 and 5.10 show typical stress distributions in the glue interface from the finite element analysis for the proposed half beam specimen and for some of the case studies outlined in section 5.3.1, at ultimate load levels as recorded experimentally. For all specimen geometries, it is noted

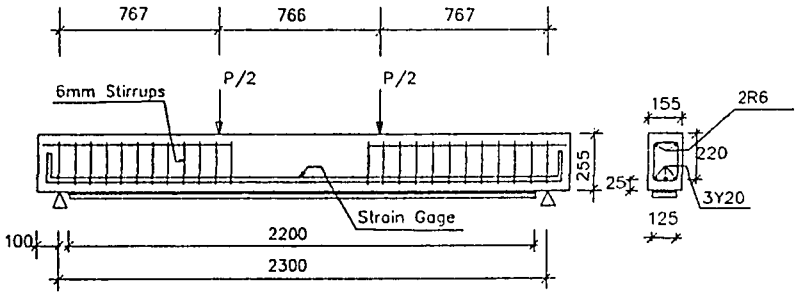

a) Beam F31

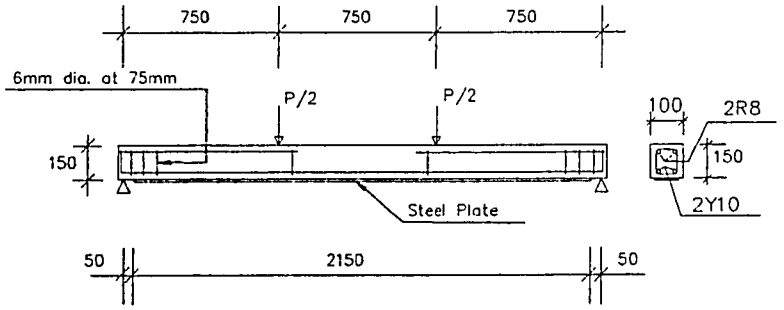

b). Beams URB4 and URB5 (5 and 10 mm plates)

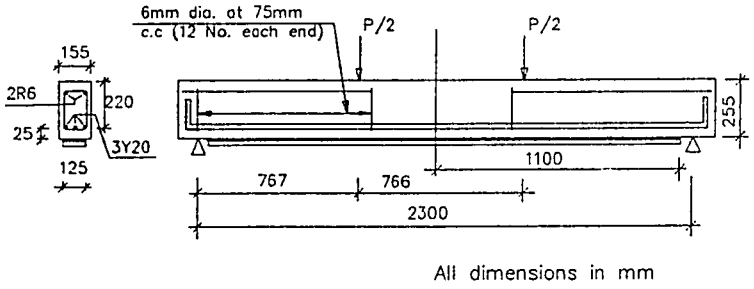

c). Beams B209 and B218

Figure 5.7: Details of beams used as case studies

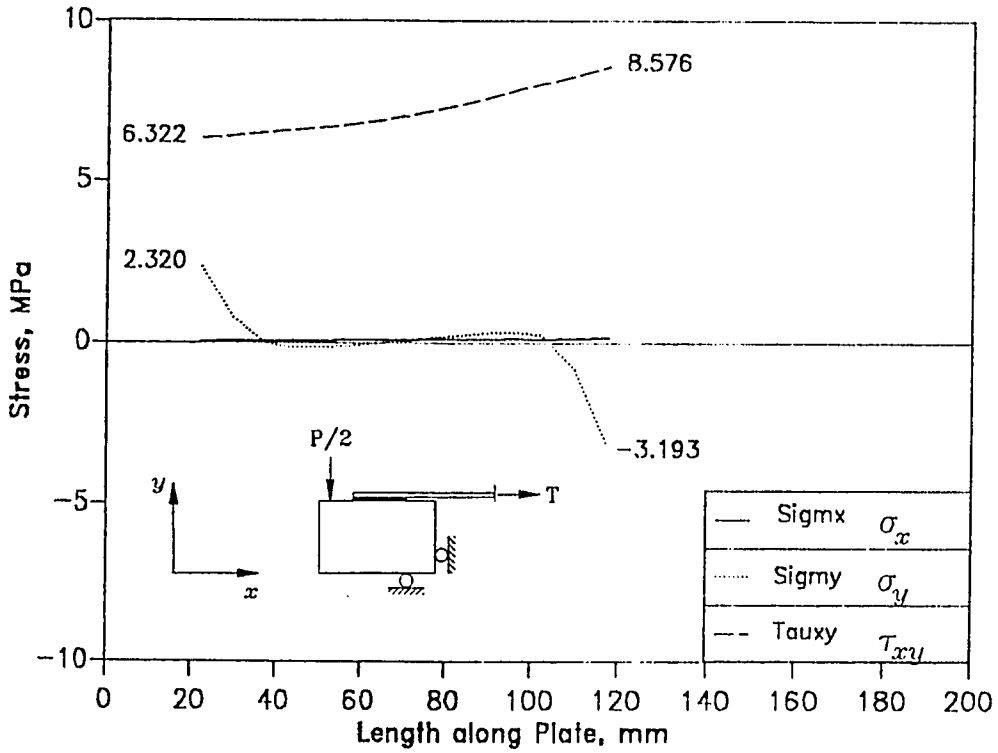

Figure 5.8: Stress distribution in the glue interface for half beam specimen at a load of 10.6 kN (Numerical Model).

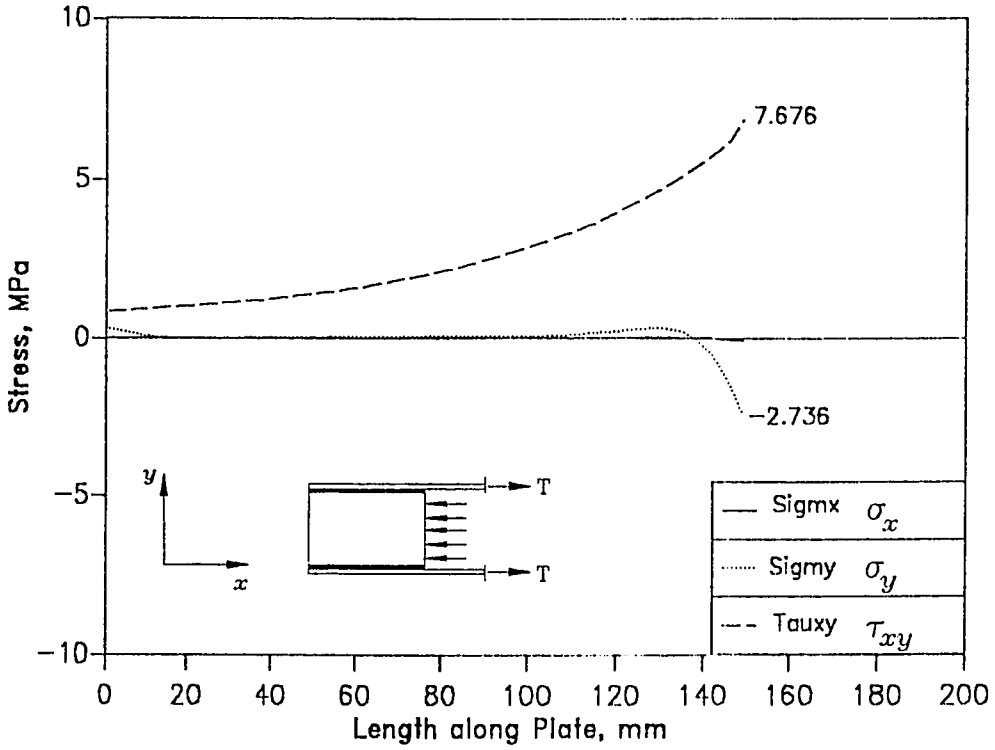

Figure 5.9: Stress distribution in the glue interface for pull out specimen [63] at a load of 25.47 kN (Numerical Model).

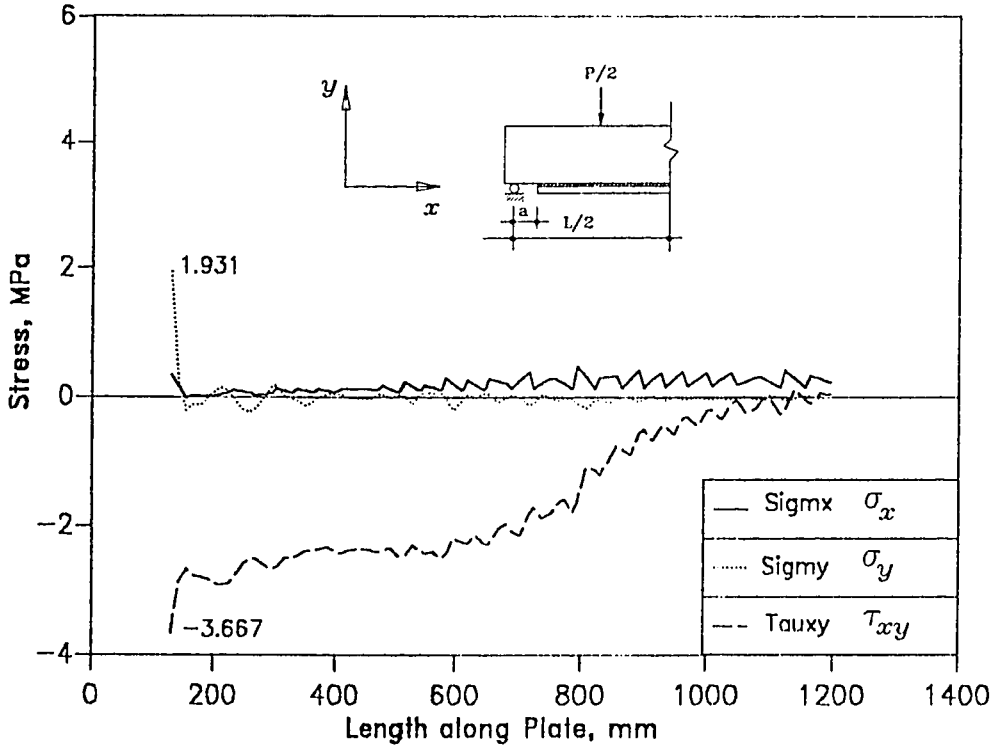

Figure 5.10: Stress distribution in the glue interface for beam URB5 [14] at a load of 53.1 kN (Numerical Model).

that the peak shear stress is accompanied by transverse normal tensile or compressive stress. This is the prime reason why different specimen geometries, although using the same component materials and interface glue, yield varying average shear strengths. A specimen inducing a compressive transverse normal stress in contrast to a peeling or tensile normal stress at the interface would yield a higher concomitant shear stress at failure. Although considerable work has been carried out in interface characterization, the role of compression transverse normal stress in yielding higher shear strength has not been recognized hithertofore.

A plot of the peak shear stress and the transverse normal stress for all specimens studied is shown in Figure 5.11. A linear regression of the data results in a proposed universal failure law for the interface in the form of the classical Mohr-Coulomb as

$$\begin{aligned} \tau_{max} &= c - \sigma tan\phi \\ \sigma &\leq 4.0MPa \end{aligned} \tag{5.2}$$

where

τ_{max} ultimate shear strength of the interface,

c cohesion

σ stress normal to the glue line

ϕ angle of internal friction.

The value of the cohesion c, was found to lie between 4.80 and 9.50 MPa and appears to depend primarily on surface preparation. The angle of internal friction ϕ was determined to be 28°. A cluster of data points in Figure 5.11 suggests a tension cutoff of approximately 4 MPa.

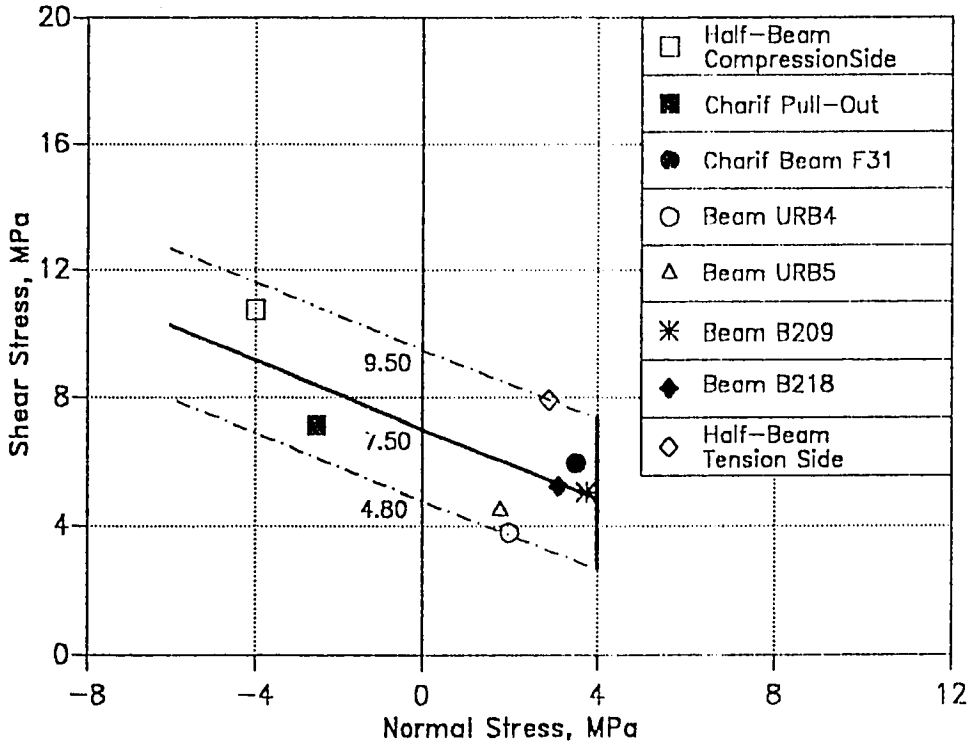

Figure 5.11: Proposed failure law for the glue interface

Chapter 6

Computer Program Implementation

6.1 Introduction

In this chapter, the implementation of the material model as discussed in chapter 3 and the finite element discretization model (see chapter 4), into a computer program is presented. The program developed follows a modular concept similar to the classic programs presented by Hinton and Owen for a variety of subjects [64,39,37,65].

To obtain the solution of the plate bonded beam, not only has the emphasis been put on plane stress idealization, but new elements namely the three noded truss element to represent the internal reinforcement and the six noded element to simulate the behavior of the steel/glue/concrete interface as well as the bond between the concrete and steel have had to be incorporated into the program.

The program has been provided with restart options to enable the non-linear analysis to be broken down into separate distinct runs. In one such option, the program can be restarted from any level of loading with a modified finite element mesh. This facility, using the acronym 'REPAIR' is essential in simulating repair of beams subjected to a certain level of

damage.

A user's manual for the program in which all the options are explained is presented in Appendix A. A powerful pre-processor named 'MeshGen' was written and prepares the nodal coordinates and element incidences for the beam, hence generating the complete input file for the main 'Plas2dR' program. The use of the 'MeshGen' program is explained in Appendix B.

A graphical post-processing program 'Plas2dP' was also written to assist in the interpretation of the results from the analysis. With this program, it is possible to plot undeformed and deformed meshes, material status, and stresses and strains along any section of the structure. The user's manual for the 'Plas2dP' program is presented in Appendix C.

In the sections below is presented a summary of the 'Plas2dR' program options, the methodology employed in the solution algorithm as well as the flow of execution. The last section discusses the pre- & post processing and 'Repair' programs.

6.2 Program Options

Types of elements

Figure 6.1a shows a library of elements available for use with the 'Plas2dR' program. As is shown in Figure 6.1b eight noded Serendipity elements and the nine noded Lagrangian elements are used for concrete and the external steel plate. The internal flexural and shear reinforcement is modeled by the three noded elements while the six noded elements are used to represent the steel-glue-concrete interface as well as the bond between the internal steel and concrete.

Solution Algorithm

Four solution algorithms are available namely

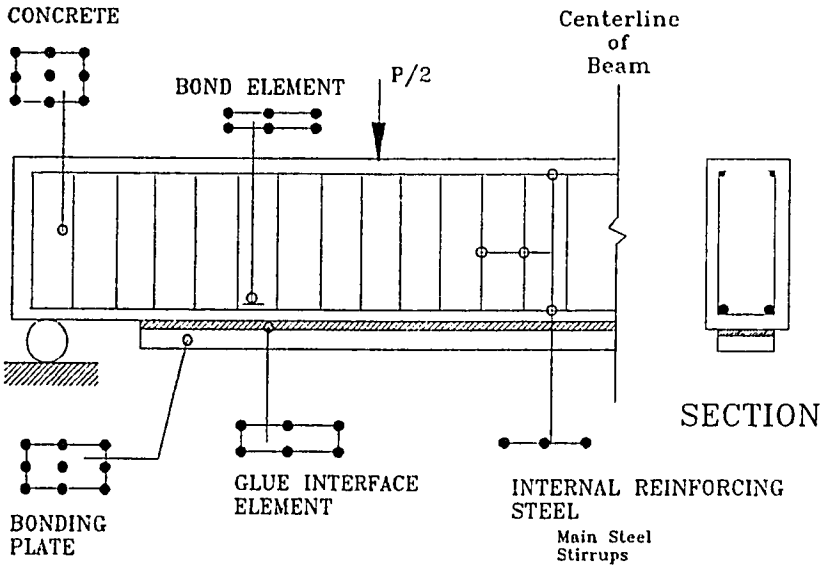

Figure 6.1: Library of finite elements

a). Initial stiffness method where the structural stiffness matrix is evaluated only once at the beginning of the analysis.

b). Tangential stiffness method where the stiffness matrix is evaluated at every iteration.

c). Combined solution algorithm I where the stiffness matrix is evaluated only at the first iteration of each load increment.

d). Combined solution algorithm II where the stiffness matrix is evaluated at both the first and second iterations of every load increment.

In the combined solution algorithms, the stiffness matrix may also be recalculated at any iteration if any crack closure is experienced at a given sampling point. The initial stiffness method is unconditionally stable.

Load Cases

Three loading situations are possible namely

a). Concentrated loads applied at the nodes.

b). Gravity loading.

c). Distributed loading at an element edge.

Convergence Criteria

It is possible to select a convergence criterion based on the norm of the residual forces or nodal displacements, although in this study no significant difference among the two was found. A convergence norm based on nodal displacements though, was used throughout this study.

Data Output

The output from the 'Plas2dR' program consists of three files namely

a). one standard output file,

b). one file containing data for graphical post-processing and

c). one file storing the data to be read on restarting the 'Plas2dR' program

Standard Output Files

The standard output file can be printed at any iteration of any load increment and selective output is possible where for instance only

- displacements or
- displacements and reactions or
- displacements, reactions, stresses, stress resultants and material status

are listed. Generation of the standard output file may be suppressed to save storage space, particularly if the graphical post-processing program is to be used to study the results.

Output File for Graphical Post-processing

The file containing data required for graphical post-processing is usually generated at the end of a selected converged load increment. It is possible however, to generate several such files for different load increments but there is a limit as to how many due to space restrictions. The most convenient option though is the one where the file is generated at the end of every converged load increment thus overwriting the previous one. This way, if

for some reason the execution stops, there exists an output file from the latest previous increment.

The graphical post-processing file can also be output at any iteration of any load increment but in this case, the program automatically stops execution immediately at the end of the iteration. This feature is useful in two situations. First a graphical post-processing file is required on the very first iteration to check the discretized mesh and secondly at the iteration beyond which the solution diverges in order to check the material status, stresses and strains at the ultimate conditions.

Data for Restart

The file containing data to be read when the 'Plas2dR' program is restarted is usually generated at the end of a selected converged load increment. Similar to the graphical post-processing files described above, it is possible to generate several restart files for different load increments but the limitation of storage space will usually restrict the maximum number files that can be prepared to very few. This is overcome by generating the restart file at the end of every converged load increment and overwriting the previous one.

6.3 Methodology

In this section the main features of the methodology used in the finite element solution are presented. At the beginning of the n^{th} load increment the displacements $\vec{u}^{n-1}$ and the stresses $\vec{\sigma}^{n-1}$ are known, as well as the unbalanced nodal forces $\vec{\Psi}^{n-1}$ resulting from the previous converged load increment. The incremental nodal forces are calculated according to

$$\vec{\Psi}^{n} = \vec{\Psi}^{n-1} + \Delta\vec{f}^{n} \tag{6.1}$$

where $\Delta\vec{f}^{n}$ is the n^{th} load increment. The iterative process is performed with the following steps for a generic iteration, i:

1. The stiffness matrix $[K]$ is updated or not according to the solution algorithm adopted.

2. The incremental displacements $\Delta\vec{u}_i$ are evaluated using the equilibrium equations

$$\Delta\vec{u}_i = -[K]^{-1}\vec{\Psi}_{i-1} \tag{6.2}$$

where $\vec{\Psi}_{i-1}$ are the unbalanced nodal forces resulting from the previous iteration. The total displacement vector $\vec{u}^i$ is then updated as,

$$\vec{u}_i = \vec{u}_{i-1} + \Delta\vec{u}_i \tag{6.3}$$

3. The incremental strains $\Delta\vec{\varepsilon}_i$ and the total strains $\vec{\varepsilon}_i$ are evaluated according to,

$$\Delta\vec{\varepsilon}_i = [B]\Delta\vec{a}_i \tag{6.4}$$

$$\vec{\varepsilon}_i = [B]\vec{a}_i \tag{6.5}$$

where $[B]$ is the strain matrix.

4. The incremental stresses $\Delta\vec{\sigma}_i$ and the total stresses $\vec{\sigma}_i$ are calculated as,

$$\Delta\vec{\sigma}_i = [D]\Delta\vec{\varepsilon}_i \tag{6.6}$$

$$\vec{\sigma}_i = \vec{\sigma}_{i-1} + \Delta\vec{\sigma}_i \tag{6.7}$$

where $[D]$ is the elasticity matrix or the corresponding matrix of the cracked concrete.

5. The stresses are corrected according to the material constitutive equations. For concrete sampling points, using the total stresses $\vec{\sigma}_i$, the maximum principal stress σ_1 is calculated. If $\sigma_1 > f_t'$ or, if the concrete is already cracked, the stresses are updated according to the tension modelling constitutive law. The effective stress $\bar{\sigma}$ is then calculated according to the yield function. If $\bar{\sigma}$ is greater than the initial

yield stress or if the material has already yielded, the stresses are corrected according to the elasto-plastic behaviour. If the stress in the reinforcing steel σ_s is greater than the steel yield stress f_y or if the steel has already yielded at the Gauss point, the stresses are treated elastoplastically.

6. The equivalent internal nodal forces $\vec{p}_i$ are evaluated using numerical integration, as

$$\vec{p}_i = \int_V [B]^T \vec{\sigma}_i \, dV \tag{6.8}$$

where $\vec{\sigma}_i$ are the total stress components corrected according to the constitutive equations.

7. The out of balance forces $\vec{\Psi}_i$ are calculated as,

$$\vec{\Psi}_i = \vec{f} - \vec{p}_i \tag{6.9}$$

where $\vec{f} = \sum_{j=1}^{n} \Delta \vec{f}^j$ is the current external nodal force vector.

8. The convergence of the process is checked. If convergence has been achieved, proceed to the next load increment otherwise restart the iterative cycle from step 1.

6.4 Program Execution

This section describes the structure and operation of the main fortran program that was written and used in this study. The program consists of a total number of 6125 executable statements in 58 subroutines.

0. START

1. Call DIMEN to preset variables associated with dynamic dimensioning.

2. Call INPUT to input data defining the geometry, boundary conditions and material properties.

   2.1 Read the control cards and call CHECK1 to check the main control data.

   2.2 Read the element material nodal connections, nodal connections and element type.

   2.3 Read some of the nodal coordinates and call NODEXY to interpolate coordinates of midside nodes.

   2.4 Read the support conditions and fixed values.

   2.5 Read the material properties.

   2.6 Call GAUSSQ to set up the Gaussian integration constants.

   2.7 Call CHECK2 to calculate the maximum front width and also to check the rest of the input data.

3. Call LOADPS to calculate the consistent nodal forces for each element depending on whether the the applied load is a point load, a pressure loading or gravity loading.

4. If the analysis is restarting from a given increment and not at the beginning, then call ZERO1 to read from files in which accumulated data was stored.

5. Call ZERO to

   a). set to zero arrays needed for accumulation of data if starting at the beginning.

   b). set to zero the new vacant positions if restarting the analysis with extra elements (as would be needed in strengthening of predamaged beams).

LOOP OVER TOTAL NUMBER OF LOAD INCREMENTS.

6. Call INCREM to increment the applied loads according to specified load factors.

LOOP OVER TOTAL NUMBER OF ITERATIONS.

7. Call ALGOR to set indicators that identify the type of solution algorithm.

8. If the stiffness matrix at the current iteration is to be evaluated, call STIFFP,

   a). to calculate and store on a file the element stiffnesses.

   b). except for element type 0, element stiffnesses for other types of elements are calculated by calling specialized subroutines.

   LOOP OVER THE TOTAL NUMBER OF ELEMENTS

   8.1 If element type, LELTP(IELEM)=2, Call STFC02 which evaluates stiffness matrix for concrete type elements taking into account elastoplastic yielding and concrete cracking.

   8.2 Else if element type, LELTP(IELEM)=4, Call STFC04 which evaluates stiffness matrix for truss type elements taking into account elastoplastic yielding.

   8.3 Else if element type, LELTP(IELEM)=5 or LELTP(IELEM)=6, Call STFC05 which evaluates stiffness matrix for steel-glue-concrete interface element or the steel-concrete bond type elements.

   8.4 Else: in which case element type, LELTP(IELEM)=0, evaluate stiffness matrix for the general elastoplastic 2D element using the rest of the subroutine STIFFP.

END LOOP OVER THE TOTAL NUMBER OF ELEMENTS

9. Call FRONT to solve the system equations using the frontal method.

10. Call RESIDU,

    a). to reduce the stresses to the yield surface and also calculate the equivalent nodal forces at the end of the current iteration.

    b). except for element type 0, stress reduction and equivalent nodal force evaluation for other types of elements are done by calling specialized subroutines.

    LOOP OVER THE TOTAL NUMBER OF ELEMENTS

    10.1 If element type, LELTP(IELEM)=2, Call RTFC02 which evaluates the stresses and equivalent nodal forces for concrete type elements..

    10.2 Else if element type, LELTP(IELEM)=4, Call RTFC04 which evaluates the stresses and equivalent nodal forces for truss type elements taking into account elastoplastic yielding.

    10.3 Else if element type, LELTP(IELEM)=5 or LELTP(IELEM)=6, Call RTFC05 which evaluates the stresses and equivalent nodal forces for steel-glue-concrete interface element or the steel-concrete bond type elements.

    10.4 Else: in which case element type, LELTP(IELEM)=0, evaluate the stresses and equivalent nodal forces for the general elasto-plastic 2D element using the rest of the subroutine RESIDU.

    END LOOP OVER THE TOTAL NUMBER OF ELEMENTS

11. Call routines that calculate the norms of residuals and checks the convergence.

11.1 If ISWCH(1)=1, then call CONV02 which checks convergence using displacement norms.

11.2 Else call CONVER which checks convergence using residual forces norm.

12. If requested from the input data (see A.13), Call OUTPUT to output displacements, reactions and stresses for the first iteration or when the solution is converged.

13. Exit the iteration loop if,

a). the maximum number of iterations are exceeded; in which case the program execution terminates.

b). the solution is converged.

END LOOP OVER TOTAL NUMBER OF ITERATIONS.

14. Call routines that dump data for graphical post-processing, when the solution is converged in the current load increment.

14.1 If ISWCH(2)=1, then call DMP which dumps detailed data for graphical postprocessing.

14.2 Else if ISWCH(2)=2, then call DMP1 which dumps limited data especially the deflection of any given node being monitored as the structure is loaded to failure.

15. If requested for the current increment call RESTAT to store on file the accumulated arrays, which will be read in case the analysis is to restart from this increment.

END LOOP OVER TOTAL NUMBER OF LOAD INCREMENTS.

16. STOP

6.5 Pre- & Post Processing

6.5.1 MeshGen Program

The program 'MeshGen' generates the nodal coordinates and element incidences and also prepares a data file that can be used as input file for the 'Plas2dR' program. The mesh generation routine does the node and element numbering starting from a basic rectangular grid, and through a series of on/off switches as explained in Appendix B quite sophisticated meshes are possible.

The basic rectangular grid is defined by specifying the spacings along both the x and y axes. By inputting switches, one for 'on' and zero for 'off' the program is instructed as to which of the nodes on the basic rectangular grid to number or not to number. A similar procedure is followed for element numbering except that in this case the element type is also specified.

The restrained nodes are generated from the coordinates specified in the input file. The material properties as well as the loading type are specified in the input to the 'MeshGen' program.

6.5.2 Program for Graphical Post Processing

The program 'Plas2dP' is a powerful post-processing program that uses the data from the output plot file generated by the main 'Plas2dR' program to present the results of the analysis in a graphical format. The program interfaces with the 'CALCOMP' graphics package for drawings and the 'ICUSYS' or Interactive Chart Utility for charts, two packages available at the KFUPM Data Processing Center. The program is however, written in a straight forward fortran language and can easily be interfaced to any other graphics package.

The program offers several graphics functions and a particular function

is selected by specifying an option number as explained in Appendix C and as stated below:

Option 1. Undeformed discretized mesh.

Option 2. Deformed structure

Option 3. Material status at the sampling points. Using different plotting symbols, yielding and crushing of concrete in compression, cracked concrete points, yielded steel as well as plate separation at the interface is indicated.

Option 4. Plot of stresses. The section along which the stresses are plotted is specified by inputting the number of the two sampling points at the beginning and end of the section.

Option 5. Deflection of any node vs. the load.

Option 6. The coordinates of the Gauss points are listed in a convenient format which also gives the element types. This is very useful in helping choose the sampling points required say in option 4.

6.5.3 Repair Program

The 'Repair' program was written to simulate the repair of beams subjected to a certain level of damage. The program accomplishes this in several steps. First, the program reads the status of the damaged unrepaired beam, the information of which is contained in the corresponding restart file. Secondly it reads the geometry and element incidences of the discretized mesh of the unrepaired beam.

Thirdly the geometry and element incidences of the repaired beam are input. Inevitably, this mesh contains more nodes and elements corresponding to the added glue interface and external plate elements. However, by

equating the coordinates, a correspondence between the old unrepaired mesh and the new mesh representing the repaired beam is made, thereby permitting the inheritance of the material status, stresses, strains and equivalent nodal forces into the new beam.

The transfer of the nodal displacements however, do require special consideration. The damaged beam has a deflected shape and as the repair is carried out, the added elements must conform to the existing deformed form. This is achieved by allowing any new node assume the displacements of the node among the old ones closest to it. Finally, the repair is complete when a new restart file is prepared. This restart file is used with the input file corresponding to the mesh of the repaired beam, and which can now be reloaded.

Chapter 7

Program Verification

7.1 Introduction

In this chapter, the ability of the numerical model developed in this study to predict the structural response of a reinforced concrete beam externally strengthened or repaired with plates of sufficient strength and rigidity, is verified. Results from the numerical computations are compared with experimental data derived from experiments done both at the University of Sheffield and at KFUPM. Whereas experiments at Sheffield were primarily concerned with strengthening of undamaged RC beams, those at KFUPM were more related to strengthening of damaged beams, more appropriately referred to as repair.

In the sections that follow in this chapter, ultimate loads, load-deflection curves, stresses and failure mechanisms as predicted by the numerical model and how they compare with the experimental results are discussed. The material parameters assumed in the numerical model are also stated.

7.2 Beams Strengthened with Steel Plates

To verify the present numerical model with regard to beams strengthened with external steel plates, beams tested at the University of Sheffield by Jones, Swamy and Ang [14] have been selected. In the following sections, the beam details and material characteristics as used in the numerical computations are outlined. Comparisons between the numerical and experimental results are made.

7.2.1 Beam Details & Material Parameters

Four of the beams tested at the University of Sheffield by Jones, Swamy and Ang [14] have been selected to verify the present numerical model. The beams are URB1, URB2, URB3 and URB4, and the details regarding the experimental program and material properties can be found in their paper [14]. Figure 7.1 presents an overall summary of the geometry of the beams studied.

Beam URB1 is an ordinary under-reinforced concrete beam with no external steel plate reinforcement and sufficient shear reinforcement to ensure a ductile flexural type failure. Beams URB2, URB3 and URB4 are similar to URB1 except that each beam is reinforced by a steel plate of 1.5 mm, 3 mm and 5 mm, respectively, epoxy bonded externally. In all cases the glue thickness is fixed at 3 mm.

The material properties used in the model were identical to those reported in the experimental investigation [14] and are stated below for each material type. As explained in [14], the concrete material properties for beam URB3 were different from the other beams.

Concrete

- Compressive was strength taken as 0.85 of the reported cube com-

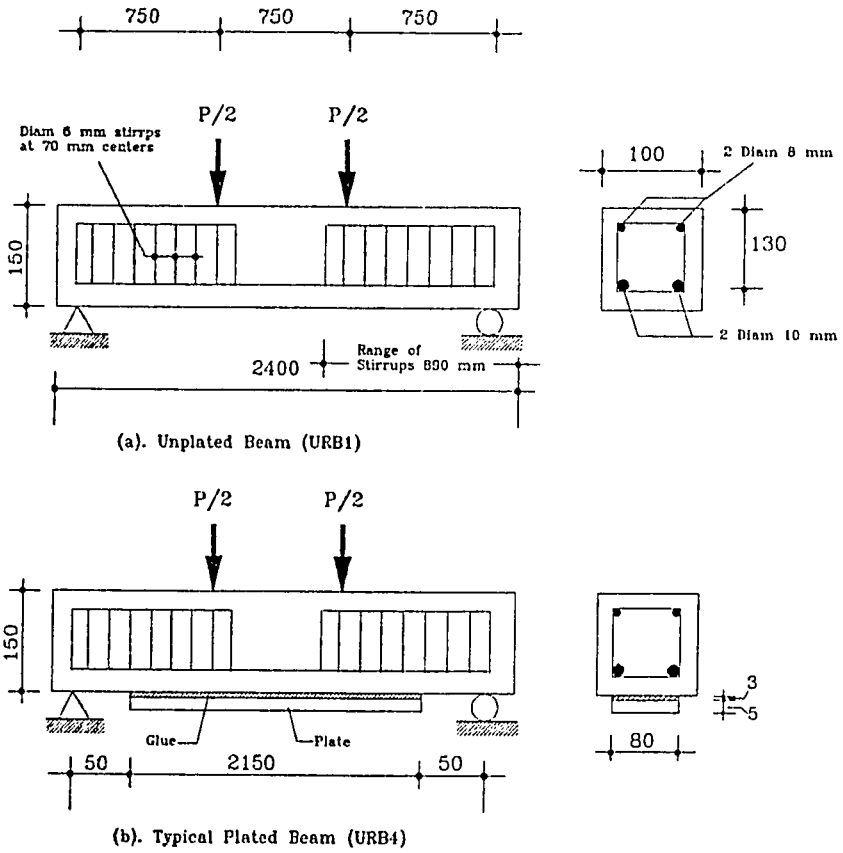

Figure 7.1: Details of beams: URB# Series

pressive strength

$$f_c' = 53.89 \quad MPa$$

and for beam URB3

$$f_c' = 82.79 \quad MPa$$

- Elasticity modulus was calculated from equation 3.13,

$$E_c = 31272 \quad MPa$$

and for beam URB3

$$E_c = 37108 \quad MPa$$

- Tensile strength was evaluated from equation 3.36,

$$f_t' = 4.62 \quad MPa$$

and for beam URB3

$$f_t' = 6.12 \quad MPa$$

- Poisson's ratio

$$\nu_c = 0.15$$

- Ultimate crushing strain

$$\varepsilon_u = 0.0035$$

- Tension stiffening parameter α read from Figure 3.4

$$\alpha = 0.189 \quad \alpha_{URB3} = 0.045$$

and

$$\varepsilon_m = 0.002$$

Internal Steel

- Elasticity modulus

$$E_s = 200 \quad GPa$$

- Yield stress

$$\sigma_y = 530 \quad MPa$$

- Strain hardening parameter

$$H' = 200 \quad MPa$$

External Steel Plate

- Elasticity modulus

$$E_p = 200 \quad GPa$$

- Yield stress

$$\sigma_y = 240 \quad MPa$$

- Strain hardening parameter

$$H' = 200 \quad MPa$$

- Poisson's ratio

$$\nu = 0.30$$

Concrete/Glue/Steel Interface

The derivation of the properties for the concrete-glue-steel interface are explained in sections 3.4 and 5.3.2 and the particular material parameter values in this part of the study are

- Elasticity modulus

$$E_i = 278.9 \quad MPa$$

- Shear modulus

$$G_i = 120.2 \quad MPa$$

- Coefficient of interface shear cohesion

$$c = 5.362 \quad MPa$$

- Tensile stress cut-off

$$f_{ti} = 4.0 \quad MPa$$

- Poisson's ratio

$$\nu_i = 0.16$$

Steel/Concrete Bond

The material parameters needed for the modelling of the steel/concrete bond are explained in section section 3.4.2 and here these values are taken as

- Elasticity modulus

$$E_b = 2784 \quad MPa$$

- Shear modulus

$$G_b = 1200 \quad MPa$$

- Bond strength

$$\tau_{bond} = 7.5 \quad MPa$$

- Tensile stress cut-off

$$f_{tb} = 4.2 \quad MPa$$

- Poisson's ratio

$$\nu_b = 0.16$$

7.2.2 Results & Discussion

Comparisons regarding the ultimate loads, deflections, cracking patterns and stresses between the numerical results and the experimental data as reported by Jones, Swamy and Ang [14] as well as a discussion of failure modes is presented in the following sections.

7.2.2.1 Ultimate Loads

Table 7.1 shows the comparisons between the numerical and the reported experimental values of the ultimate loads for the various beams under study.

The results show close connection between the ultimate loads based on the finite element model and those obtained experimentally. Also shown is the flexural capacity of beam URB1 as obtained from the strength theory based on the ACI code. No such code formulations exist presently for predicting ultimate capacities of R/C beams reinforced externally.

7.2.2.2 Load-Deflection Curves

Figures 7.2 and 7.3 show comparisons between the numerical and experimental load-deflection curves , where close agreement is indicated.

7.2.2.3 Stresses

Figures 7.4 and 7.5 show the stress at the ultimate load conditions in the internal reinforcing steel and the external plate for beams URB2 and URB4 bonded with 1.5 mm and 5 mm, external plates respectively. Both the external and internal reinforcing steels for beam URB2 are yielded indicating a flexural failure with no plate separation. Although the external plate in beam URB4 yields in the constant moment region, the internal steel remains unyielded. The stress peak in the internal steel near the plate cutoff

Beam designation	*Plate thickness mm*	*Ultimate Loads (kN)*		
		Finite Element Model	*Experimental Ref [14]*	
URB1	-	29	27	26.83[a]
URB2	1.5	41	40	
URB3	3	53	55	
URB4	5	59	57.5	

[a]According to ACI

Table 7.1: Ultimate loads of beams studied

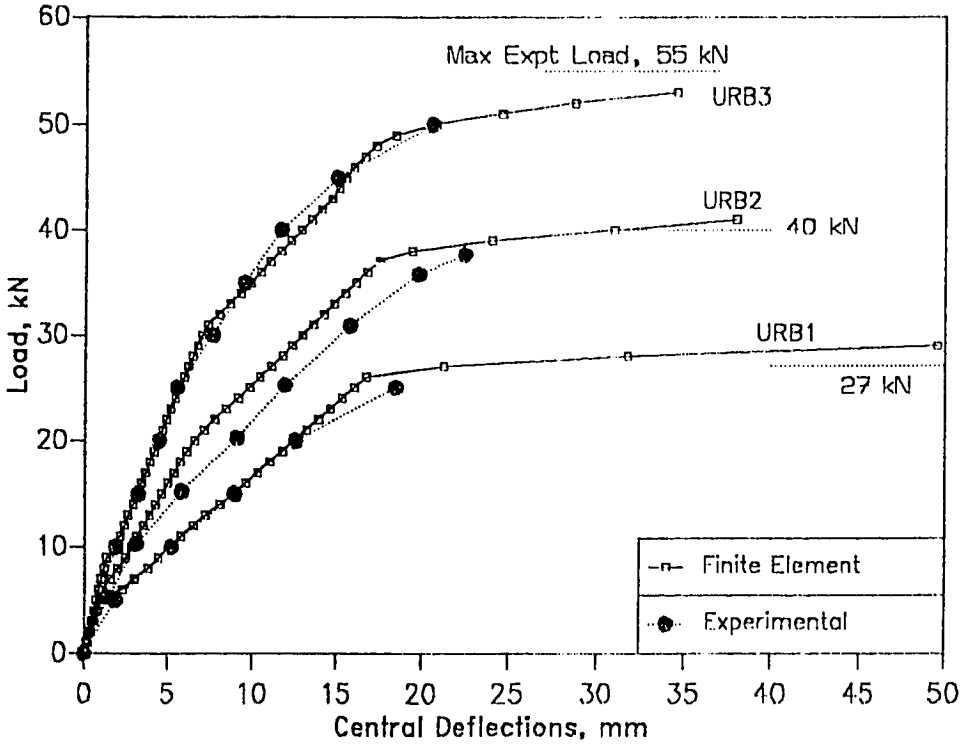

Figure 7.2: Load/deflection characteristics for beams URB1, URB2 and URB3

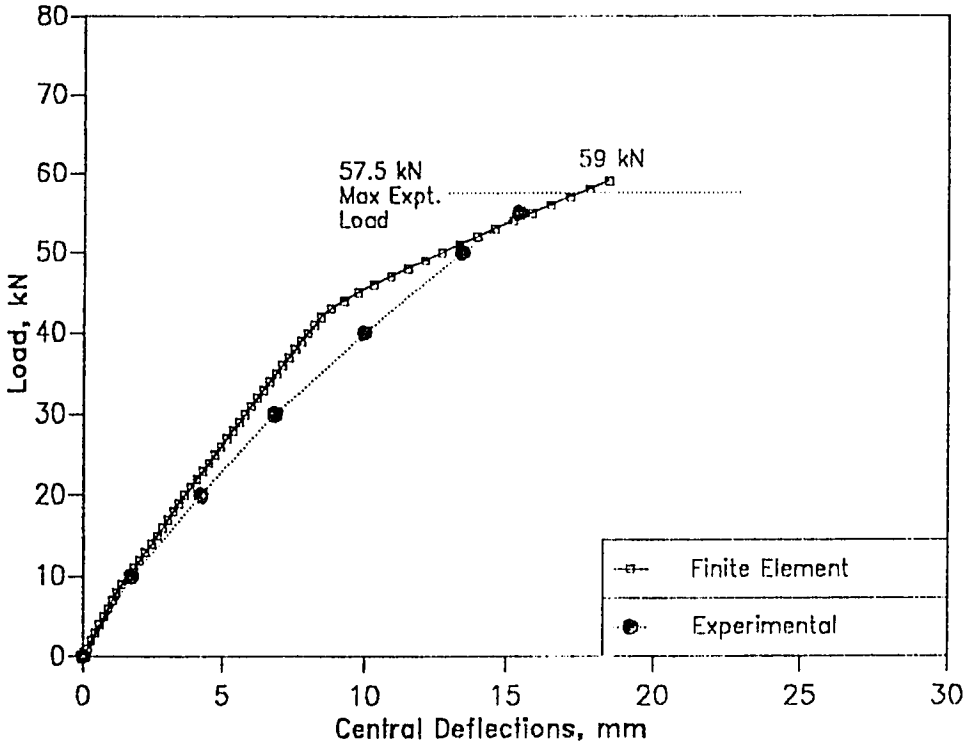

Figure 7.3: Load/deflection characteristics for beam URB4

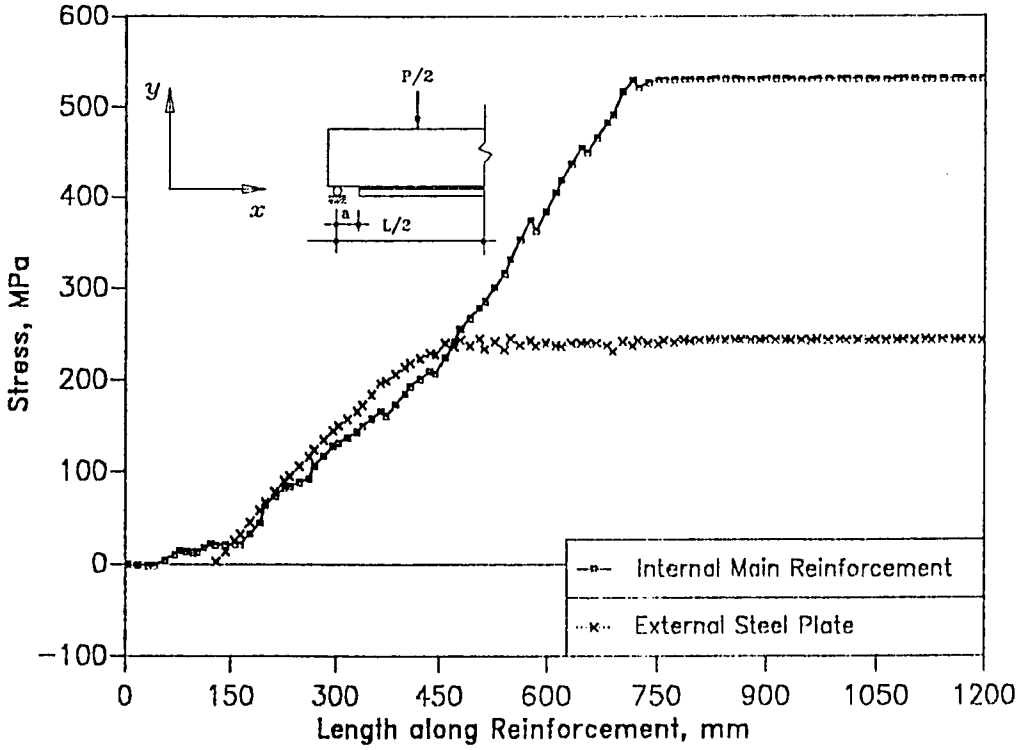

Figure 7.4: Normal stresses in internal main steel and external plate for beam URB2 at a load of 41 kN.

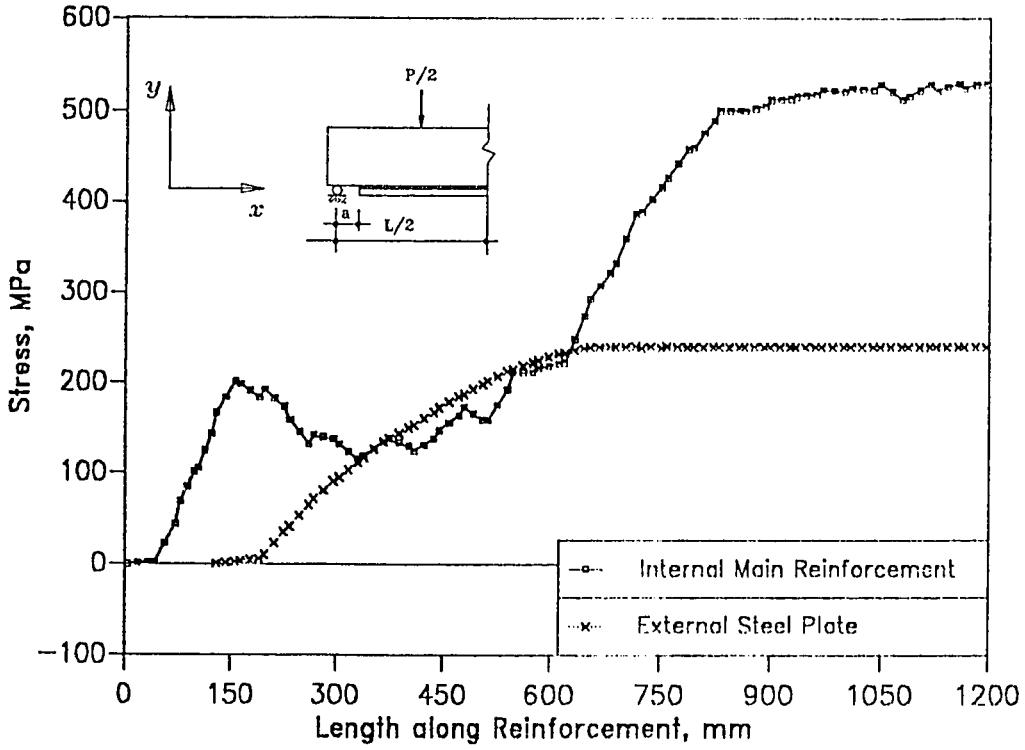

Figure 7.5: Normal stresses in internal main steel and external plate for beam URB4 at the ultimate load of 59 kN.

indicates a transfer of tensile force from the external plate to the main reinforcement, by virtue of plate separation.

Figure 7.6 shows the interface normal and shear stresses for URB2 at ultimate conditions. The low stresses indicate complete composite behavior. The stresses for a relatively thicker plate bonded beam URB4 (see Figure 7.7) are much higher and for the sampling points near the plate end, the interface is cracked indicating a plate separation in this region.

7.2.2.4 Cracking Patterns

Figures 7.8 and 7.9 respectively show the locations of concrete microcracking and zones of concrete compression yielding for beams URB2 and URB4 at their ultimate load conditions. The cracking in the constant moment region of beam URB2 is quite extensive and reaches the yielded concrete in compression. This confirms the flexural mode of failure. On the other hand, the concrete material status of beam URB4 consists of vertical cracking in the constant moment region to a lesser degree, and distinct inclined cracking emanating from the region where the plate is curtailed.

Figure 7.10 shows the material status of the steel/glue/concrete interface for beam URB4 at the ultimate conditions. Plate separation is indicated by the failure of the sampling points in the interface elements close to the plate end. Figure 7.11 shows the deformed shape of beam URB4 at ultimate load conditions as well as the discretization mesh used in the study.

7.2.2.5 Metamorphosis of Failure Modes

To understand the effect of the interface strength on the ultimate failure mechanism of beams bonded with relatively thicker plates, the finite element solution for beam URB4 is obtained for different values of interface cohesion, c. Table 7.2 shows the ultimate load values obtained in such

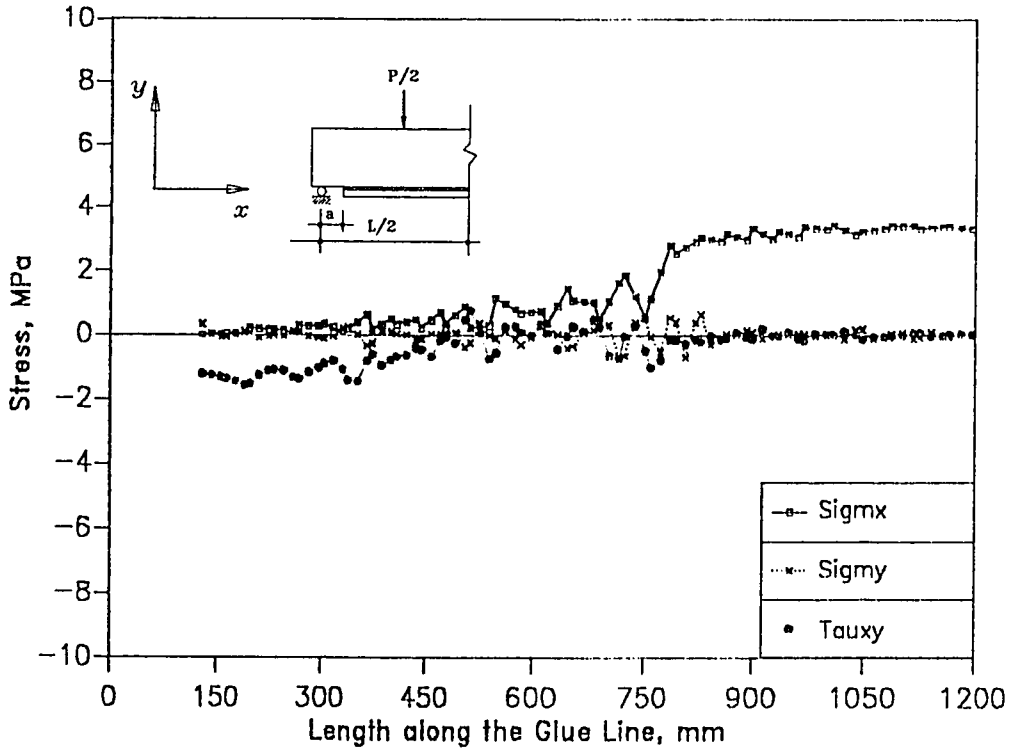

Figure 7.6: Normal and shear stresses in steel/glue/concrete interface for beam URB2 at a load of 41 kN.

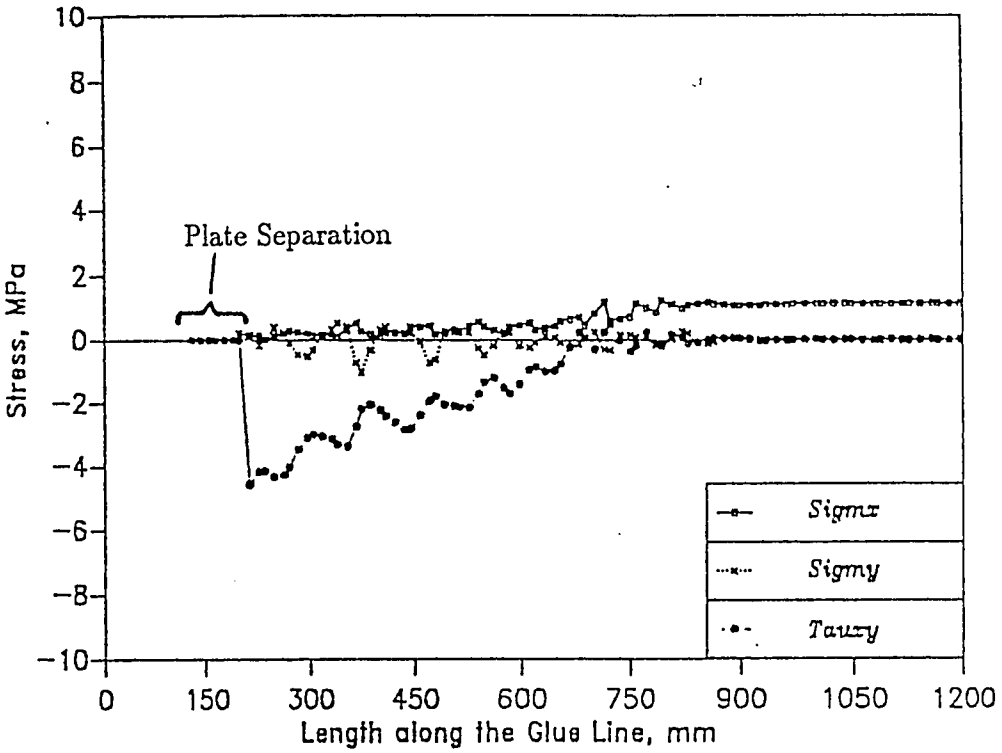

Figure 7.7: Normal and shear stresses in steel/glue/concrete interface for beam URB4 at a load of 59 kN.

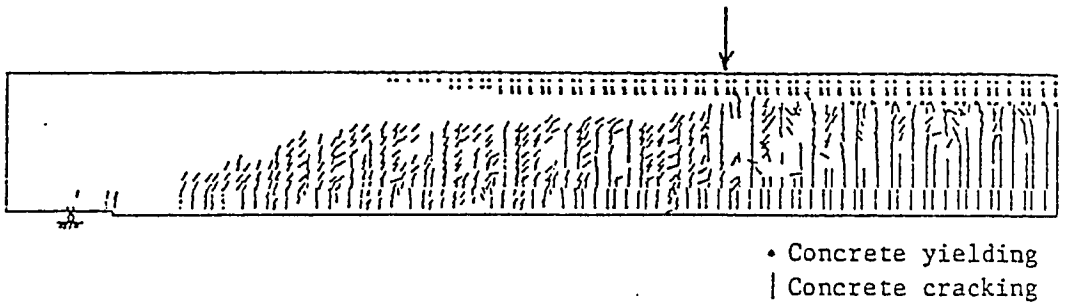

Figure 7.8: Zones of concrete microcracking and compression yielding for beam URB2 at a load of 41 kN.

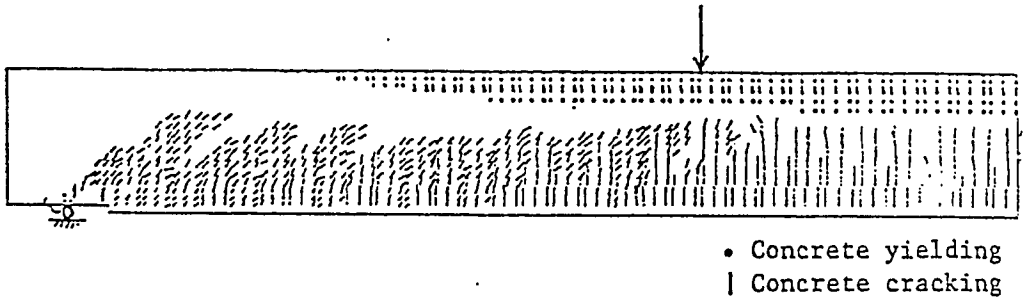

Figure 7.9: Zones of concrete microcracking and compression yielding for beam URB4 at a load of 59 kN.

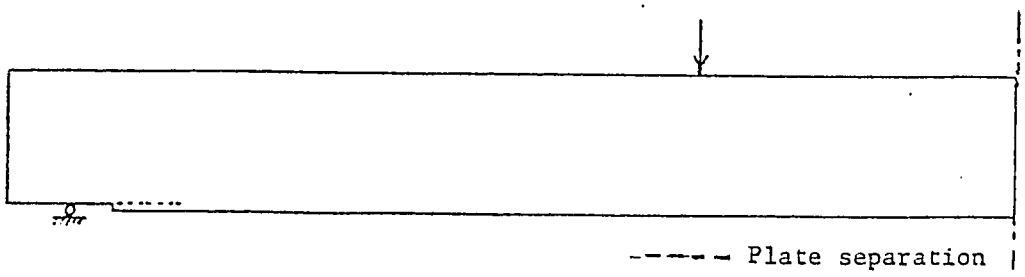

Figure 7.10: Material status for the steel/glue/concrete interface for beam URB4 at a load of 59 kN.

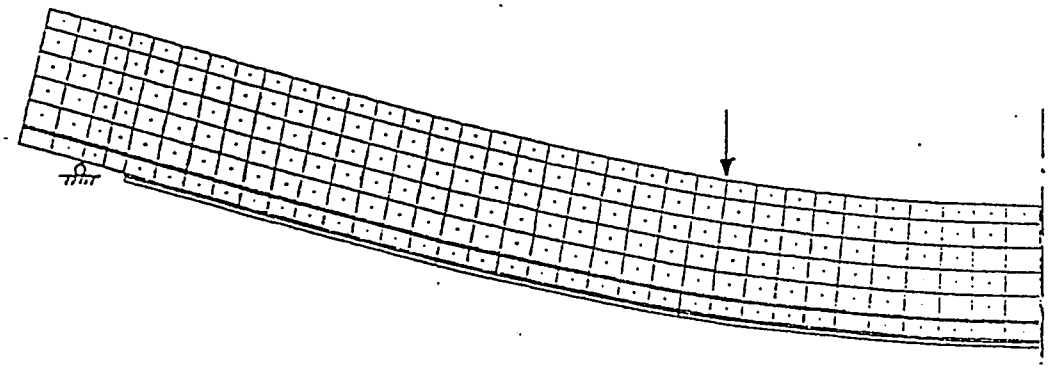

Figure 7.11: Deformed shape of beam URB4 at a load of 59 kN.

a study. Beyond some value of c, the interface is fully composite at the ultimate load conditions and the beam fails at the same load, in a mode interpreted as a diagonal tension failure. For values of c lower than this, the beam fails by plate separation. In order to confirm the hypothesis that the ultimate load beyond a certain interface cohesion corresponded to a diagonal tension failure for full composite action, beam URB4 was analysed assuming perfect bond between the plate and the RC beam i.e. with no interface element. The model yielded on ultimate load of 59.5 kN, which is 1.65% smaller than the case for $c = 15$ MPa, and is attributed to a reduced depth of the beam due to the absence of the 3 mm interface layer.

Table 7.3 attempts to highlight the relative interplay of the various mechanisms as the external plate thickness is increased from 1.5 mm to 5 mm. For beams bonded with thin plates, failure is dominated by extensive cracking in the constant moment region and yielding of both reinforcing steels. Bonding with thicker steel plates leads to higher interface stresses at the plate curtailment region thus resulting in plate separation as confirmed experimentally [14].

7.2.3 Conclusions

The non-linear finite element model to predict response of RC beams strengthened by epoxy bonding of steel plates externally to the beam has been shown to capture the essential characteristics of behavior up to failure. Reinforced Concrete beams strengthened in this manner are noted to undergo a metamorphosis of failure modes as the thickness of the external steel plate, t_p, is increased.

An underreinforced RC beam strengthened by a plate of nominal thickness is noted to fail in a manner similar to a classical failure of an unplated underreinforced RC beam i.e intrusion of deep flexural cracking with concomitant yielding of internal reinforcement and external plate. As t_p is

Interface Cohesion c MPa	*Ultimate Load, P_u kN*	*Mode of Failure*
1.5	28	Plate Separation
2.6	46	Plate Separation
5.4	59 (URB4)	Plate Separation
7.0	60.5	Diagonal Tension
15.0	60.5	Diagonal Tension
No Interface Element	59.5	Diagonal Tension

Table 7.2: Effect of interface cohesion c on the ultimate load (external plate thickness $t_p = 5$ mm).

Beam	*Material Status at Ultimate Load*				*Finite Element Model*	*Observed Experimental Failure Mode [14]*
	Internal Steel	*External Plate*	*Interface*	*Dominant Concrete Cracking*		
URB1	Extensive yielding HYZ=463mm	-	-	Flexural cracking	Internal steel yielding	Steel yielding
URB2	Extensive yielding HYZ=486mm	Extensive yielding HYZ=747mm	Fully intact SZ= 0 mm	Flexural cracking	Yielding of internal and external reinforcement	Steel yielding
URB3	Extensive yielding HYZ=518mm	Extensive yielding HYZ=718mm	Fully intact SZ= 0 mm	Flexural cracking	Yielding of internal and external reinforcement	Steel yielding
URB4	No yielding HYZ=0mm	Moderate yielding HYZ=425mm	Separation near plate cutoff SZ=82mm	Flexure-shear cracking	Plate separation	Plate separation

Table 7.3: Failure mechanisms of bonded beams (see figure 7.12 for illustration of HYZ & SZ)

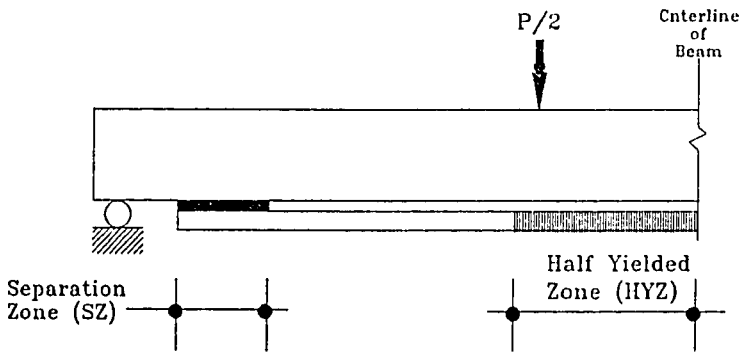

Figure 7.12: Illustration of yielded and plate separation zones in plated beam

increased, depth of flexural cracks in concrete are arrested but with accompanying increase in zone of cracking along length of beam. For weak interfaces between concrete and external plate, failure is now initiated by separation of the plate from the main beam and culminated by diagonal tension cracking in the neighborhood of the zone of plate separation. Numerical experiments for beams with artificially strong interfaces (so as to ensure complete composite action) reveal that beyond a certain magnitude of the interface cohesion, the collapse load of the beam reaches a plateau, which is interpreted as being the load required to cause a diagonal tension failure of the RC beam fully composite with the external steel plate.

7.3 Beams Repaired with GFRP Plates

Experiments done at KFUPM [66] on repair and elsewhere [67,68,69,70] on strengthening of RC beams using plates made of fiber glass composites have revealed that fiber glass composites of sufficient thickness, strength and rigidity offer similar advantages as of steel plates. In addition resistance to corrosion of the glass fiber plates gives an impetus into their use.

Field application of the repair by bonding externally plates made of glass fiber composites is expected to increase in the near future and its successful performance will depend on the understanding of the interactive behavior of different material components making up the repair system. A rational design of the repair system must be based on an analytical model capable of accounting for the non-linear material behavior of a bonded reinforced concrete beam and accurately predict the ultimate load as well as failure mode which may be precipitated by any of the various component materials reaching a limiting state of stress or strain.

In this section, the nonlinear finite element model which has been developed to depict the behavior of externally reinforced RC beams and verified for external reinfrocement in the form of steel plates (see section 7.2) is now

tested for beams repaired with GFRP plates. These plates have a relatively low elastic modulus, linear up to the fracture strength with no strain hardening [66,71]. The numerical algorithm is modified to handle the repair by loading and unloading an unrepaired beam and then adding the plate elements to the deformed mesh of the damaged beam (see section 6.5.3).

7.3.1 Beam Details & Material Parameters

7.3.1.1 Experimental Details

This subsection summarizes the experimental program and test set up as used by Badr [66] details of which are required for use in the numerical model. Types of materials used, the procedure used to bond the plates to the damaged beams and the instrumentation and test setup are discussed.

Figure 7.13 shows the dimensions of the beams used in the experimental study as well as details of the internal reinforcement and external fiber glass plates. The beams were under-reinforced with a reinforcement ratio $\rho_s = 0.0093$ ($\rho_b = 0.037$) and adequately reinforced in shear to ensure a flexural failure. Four series of beams were tested namely one with no fiber glass plate repair to act as control, and the remaining three repaired respectively, with 1 mm, 2 mm and 3 mm plates. The glue thickness was kept constant at 1 mm.

The internal reinforcement was made up of mild steel with an elasticity modulus of 180 GPa and a yield stress of 360 Mpa. The two component epoxy structural adhesive used to bond the fiber glass plates consisted of an EP-CA resin (white) and an EP-CA hardener (black). The fiber glass material used in the experiments was in form of plates manufactured by the hand lay-up method, which is considered the oldest, but the most common technique. The type selected for the experiments consisted of 3 layers of woven roving and 1 layer of surface mat.

The beams were damaged by preloading them up to a central deflection

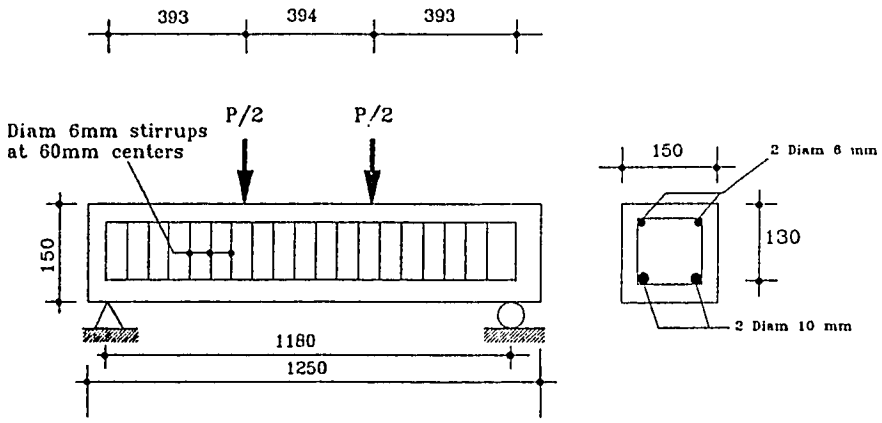

Figure 7.13: Detail of beams repaired with GFRP plates

of 10 mm. The damaged beams were then unloaded and strengthened by epoxy bonding the fiber glass plates. In order to achieve a good bond between concrete surface and the glass fiber plates, the beam surfaces were roughened by sand blasting. The fiber glass plate surface was sufficiently rough due to the surface mat finishing.

7.3.1.2 Material Parameter Values

Referring to the experimental details described in sub-section 7.3.1.1, the material properties used in the model were taken as.

Concrete

- Compressive strength

$$f_c' = 37.7 \quad MPa$$

- Elasticity modulus calculated from equation 3.13,

$$E_c = 27074 \quad MPa$$

- Tensile strength evaluated from equation 3.36,

$$f_t' = 3.64 \quad MPa$$

- Poisson's ratio

$$\nu_c = 0.15$$

- Ultimate crushing strain

$$\varepsilon_u = 0.0035$$

- Tension stiffening parameter α read from Figure 3.4

$$\alpha = 0.286$$

and

$$\varepsilon_m = 0.002$$

Internal Steel

- Elasticity modulus

$$E_s = 180 \quad GPa$$

- Yield stress

$$\sigma_y = 360 \quad MPa$$

- Strain hardening parameter

$$H' = 200 \quad MPa$$

External GFRP Plate

- Elasticity modulus

$$E_p = 14870 \quad MPa$$

- Rupture stress

$$\sigma_y = 294 \quad MPa$$

- Poisson's ratio

$$\nu = 0.30$$

Bond and Glue Interface Materials

The material properties adopted for the bond and glue interface are identical to those assumed in section 7.2.1 above.

7.3.2 Results & Discussion

In this section the results of the non-linear finite element analysis are compared with the experimental values [66] regarding the ultimate loads, deflections, cracking patterns and stresses as well failure mechanisms.

Plate thickness (mm)	*Ultimate Loads (kN)*	
	Finite Element Model	*Experimental*
1	63.5	66.96
2	67	66.03
3	66	66.07

Table 7.4: Ultimate loads of plated beams

7.3.2.1 Ultimate Loads

Table 7.4 shows the comparisons between the numerical and the experimental values of the ultimate loads for the reinforced concrete beams repaired with glass fiber plates of various thicknesses.The results show close agreement between the ultimate loads based on the finite element model and those obtained experimentally.

7.3.2.2 Deflections

Figures 7.14, 7.15 and 7.16, compare the load deflection curves resulting from experimental and numerical analysis for beams repaired with GFRP plates and close agreement is seen to exist between the two. The virgin unrepaired beams are first damaged by loading them to a deflection of 10 mm after which they are unloaded to zero load. The experimental loading-unloading curve show slight variations due to the inevitable differences in the virgin beams used. The same numerical loading-unloading curve is however used throughout the three cases.

Although the ultimate loads are not significantly affected by the plate thickness, the ultimate deflections do show a significant reduction in the ductility as the plate thickness is increased.

7.3.2.3 Stresses

Figures 7.17 to 7.19 show normal stresses in internal steel and external fiber glass plate for beams plated with 1, 2 and 3 mm plates, respectively. In all the three cases, the internal steel reinforcement is yielded at the ultimate load levels. However, the stress in the external GFRP plates reduces as the plate thickness is increased.

The normal and shear stresses in the glue interface for beams plated with 1, 2 and 3 mm plates are shown in Figures 7.20 to 7.22 respectively.

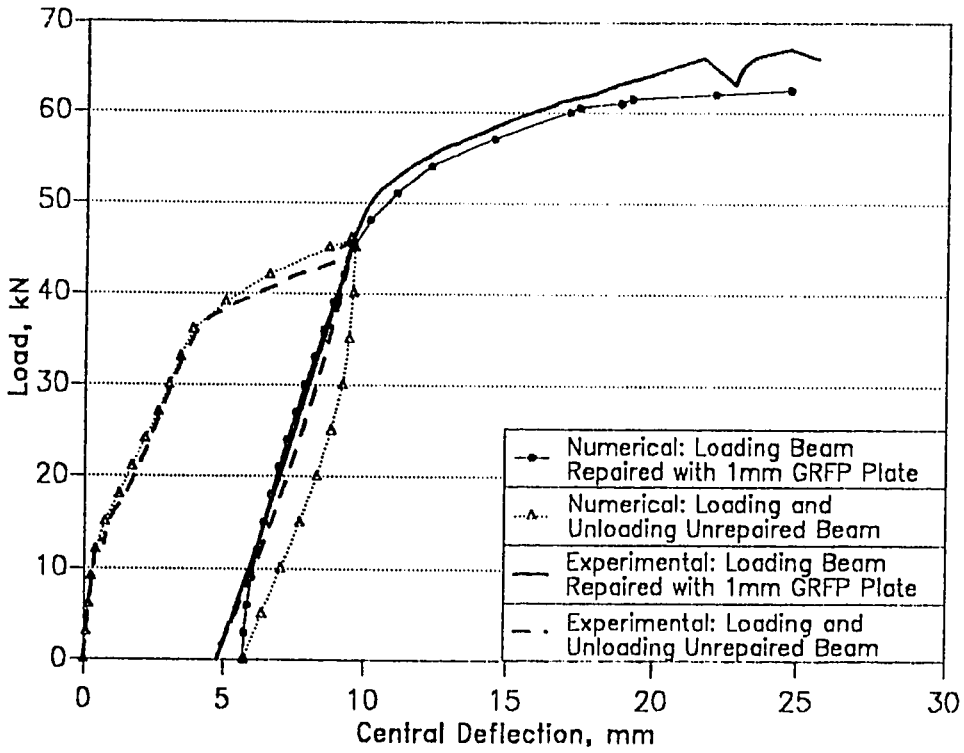

Figure 7.14: Load/deflection characteristics for 1 mm glass fiber plated beam

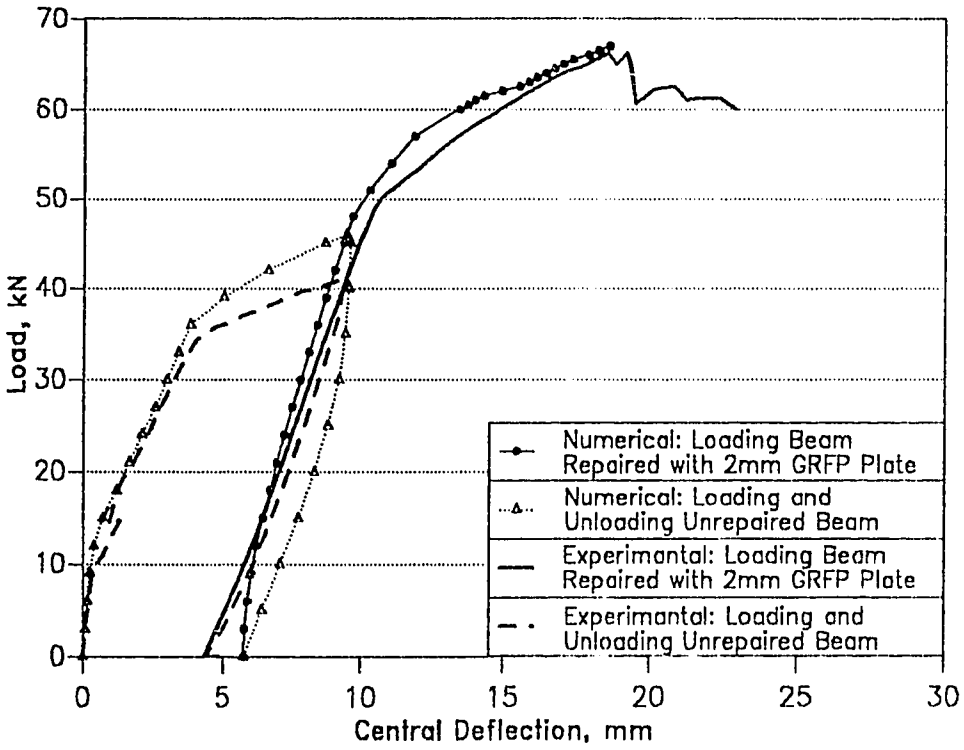

Figure 7.15: Load/deflection characteristics for 2 mm glass fiber plated beam

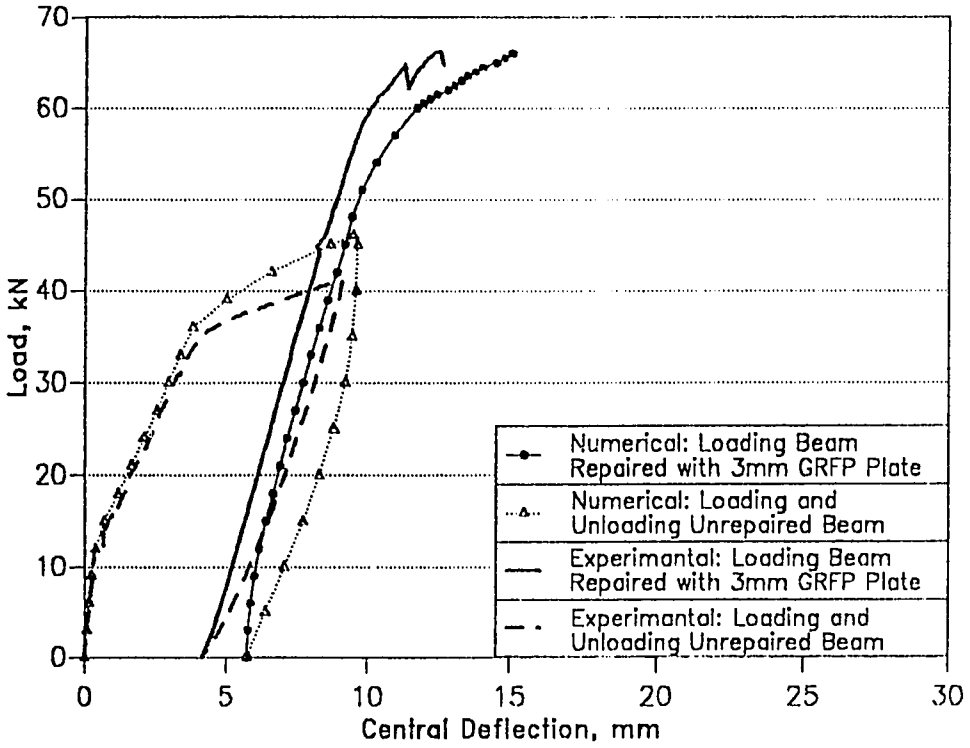

Figure 7.16: Load/deflection characteristics for 3 mm glass fiber plated beam

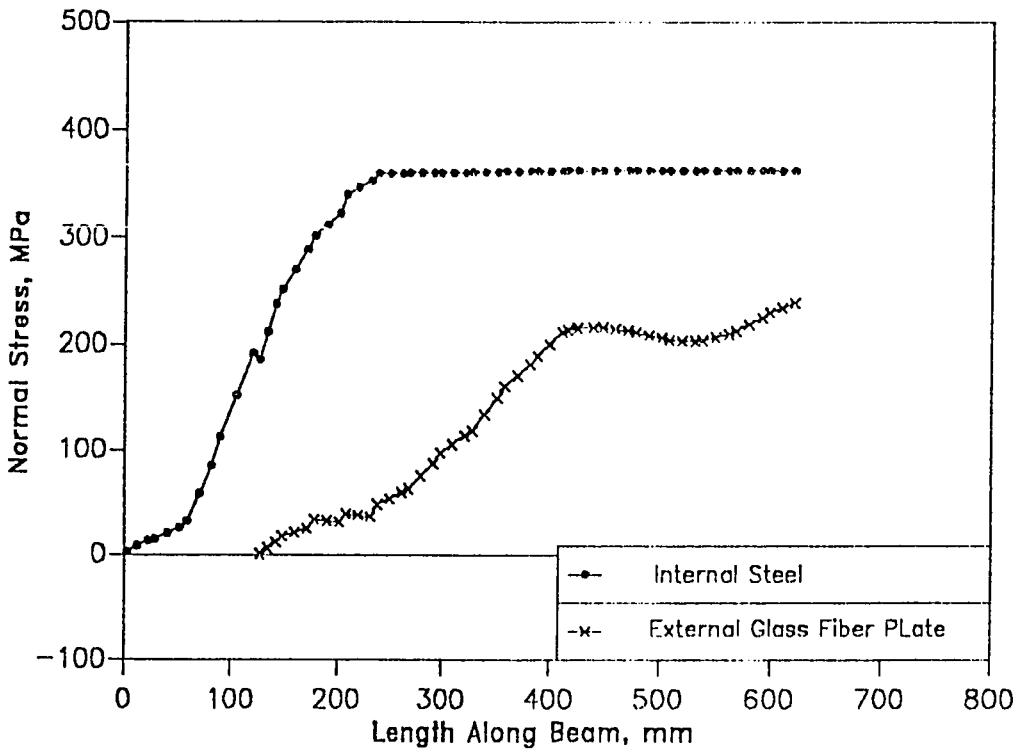

Figure 7.17: Normal stresses in internal steel and external plate for 1 mm plated beam at an ultimate load of 62.5 kN.

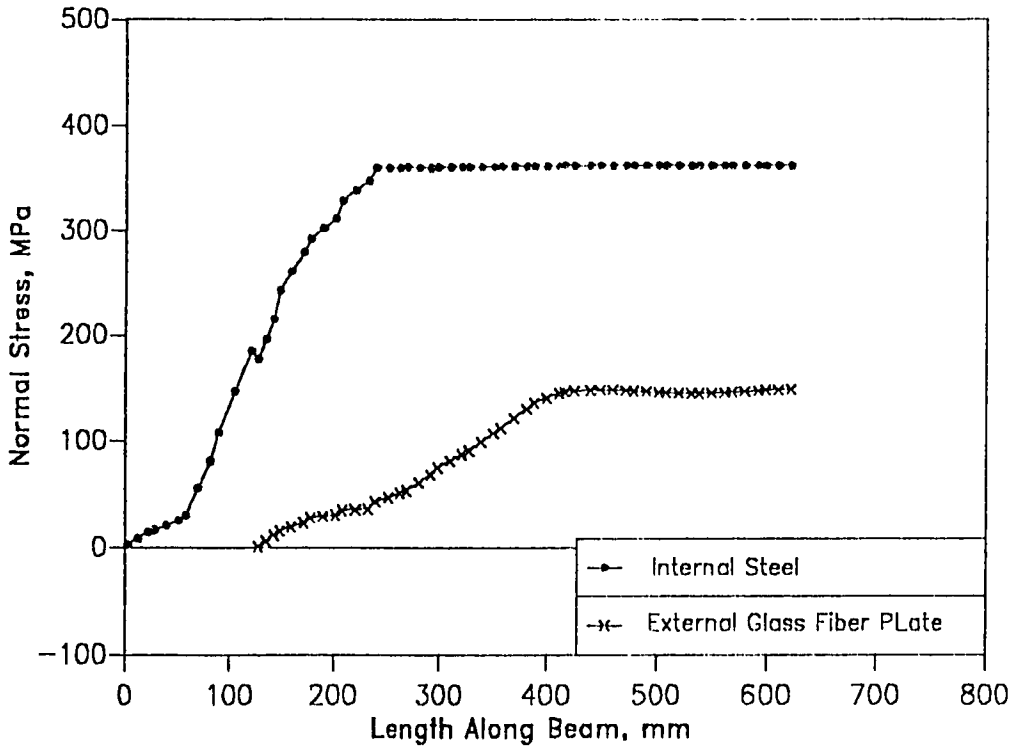

Figure 7.18: Normal stresses in internal steel and external plate for 2 mm plated beam at an ultimate load of 67 kN.

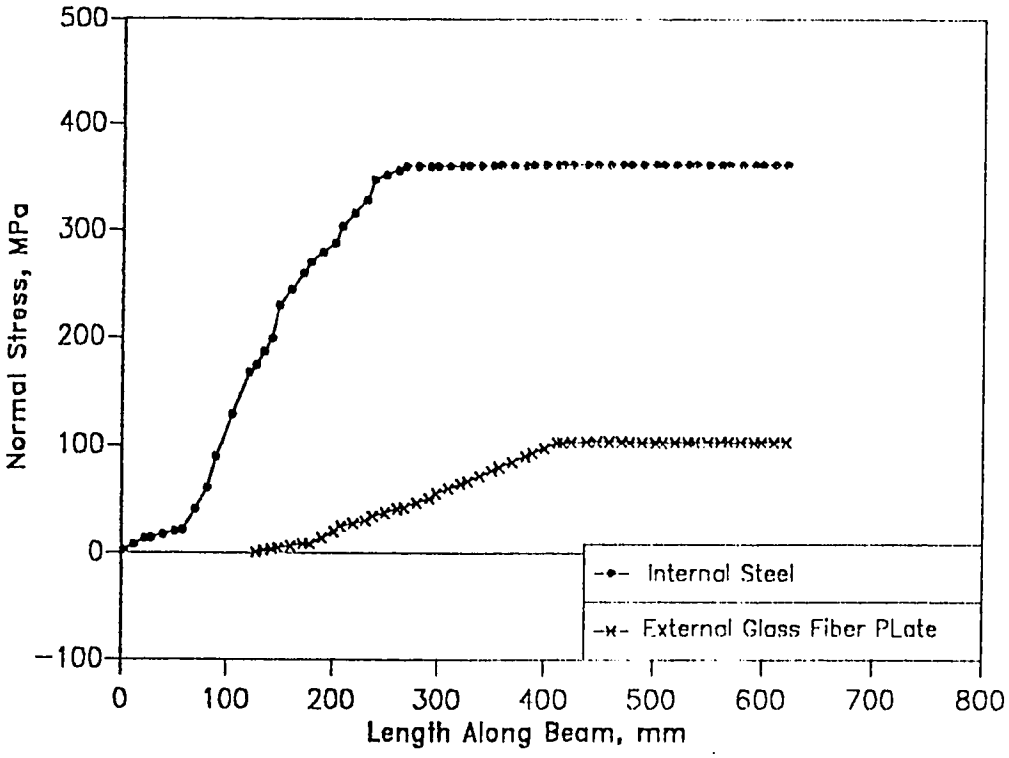

Figure 7.19: Normal stresses in internal steel and external plate for 3 mm plated beam at an ultimate load of 66 kN.

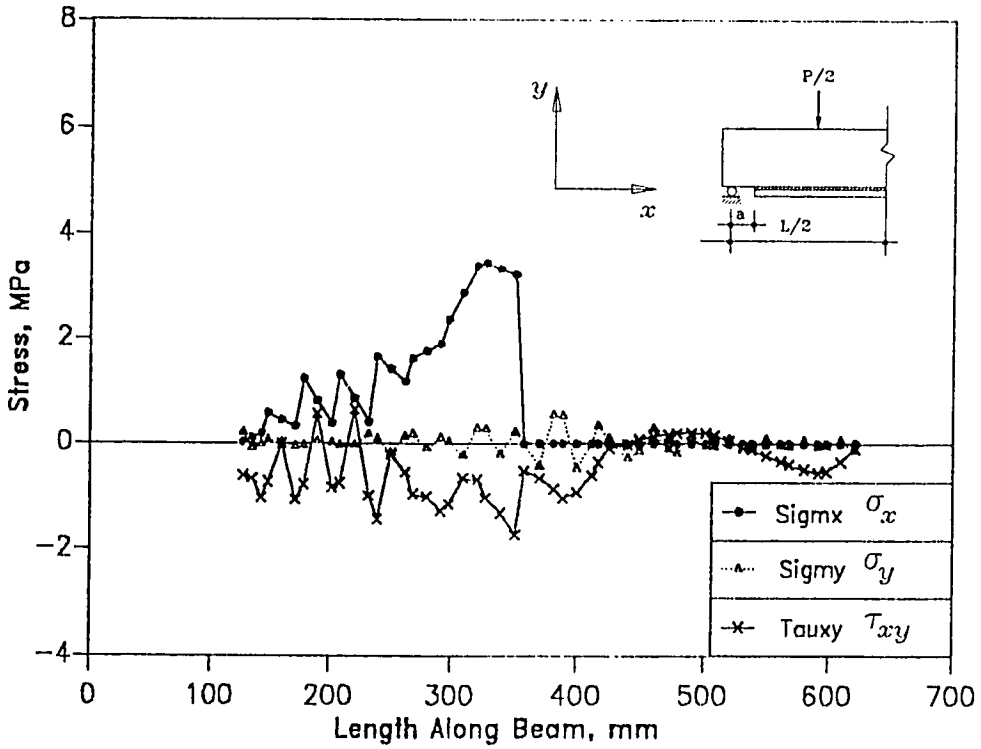

Figure 7.20: Normal and shear stresses in the glue interface for 1 mm plated beam at an ultimate load of 62.5 kN.

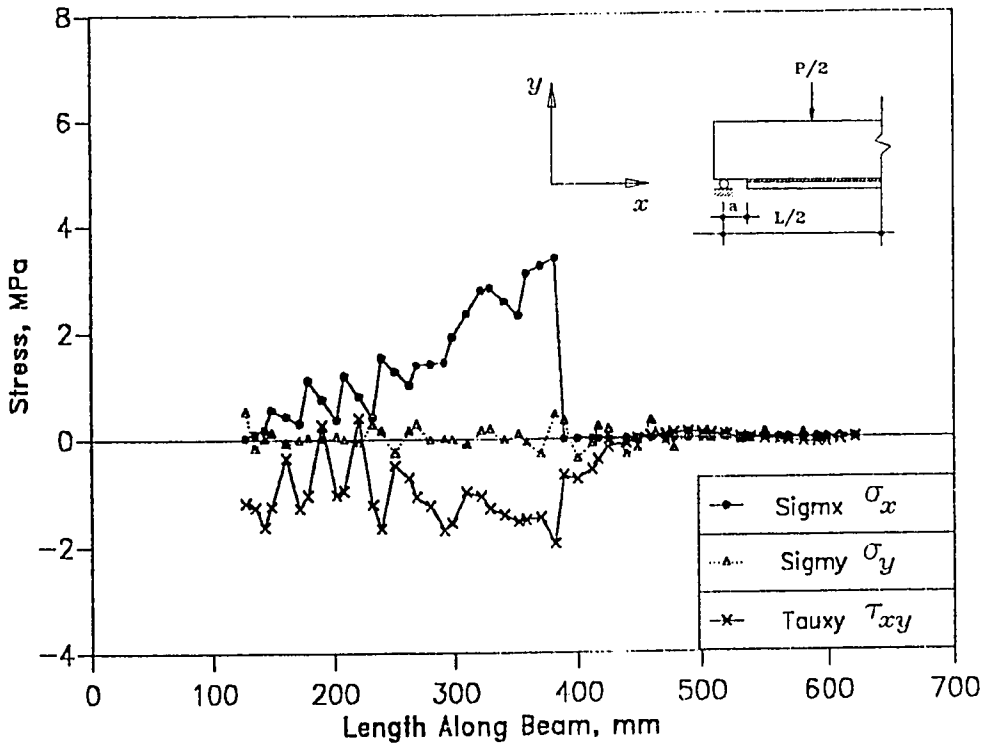

Figure 7.21: Normal and shear stresses in the glue interface for 2 mm plated beam at an ultimate load of 67 kN.

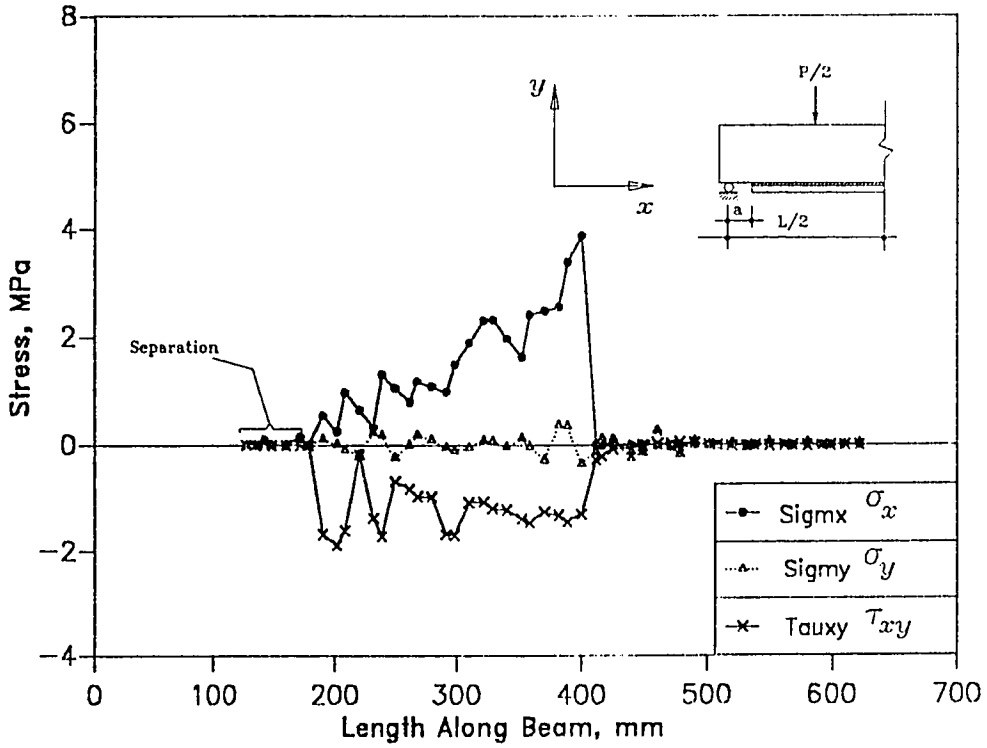

Figure 7.22: Normal and shear stresses in the glue interface for 3 mm plated beam at an ultimate load of 66 kN.

For beams repaired with one and two mm plates, the interface shear stresses are relatively low but are high enough for the case of the beam with 3 mm plate as to induce interface failure.

7.3.2.4 Cracking Patterns

Figure 7.23 shows zones of microcracking and compression yielding for the plated beams. The crack patterns of the three beams do not show significant variation and this is due to the fact that all the beams were essentially pre-cracked to the same degree prior to repair, and in the numerical model, the crack status yields information on location of cracks but not their widths. What is noticeable however, is the fact that the cracking towards the compression zone becomes more extensive as the plate thickness is reduced.

7.3.2.5 Failure Modes

Experimentally, the beam repaired with 1 mm plate is reported to have collapsed by rupturing of the plate whereas plate separation occurred in the case of the beam reinforced with a 3 mm plated beam. In the numerical model, the program was written to stop execution at the instant the stress in the external plate reached or exceeded the rupture stress and this is what happened precisely in the case of the 1 mm plated beam.

The beams reinforced with 2 and 3 mm GFRP plates both stopped execution due to divergence in the solution. Inspection of the interface stresses (Figure 7.22) and the material status at the glue interface (Figure 7.24), indicated that the interface exceeded its limiting capacity. The phenomenon of plate separation in case of the 3 mm plated beam was also observed experimentally [66].

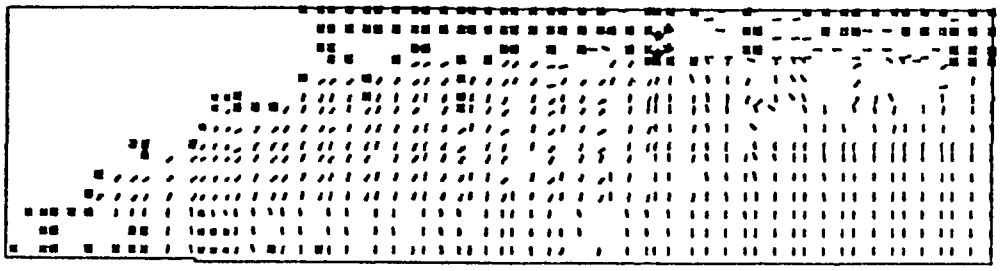

(a). 1 mm plated beam at the ultimate load of 62.5 kN.

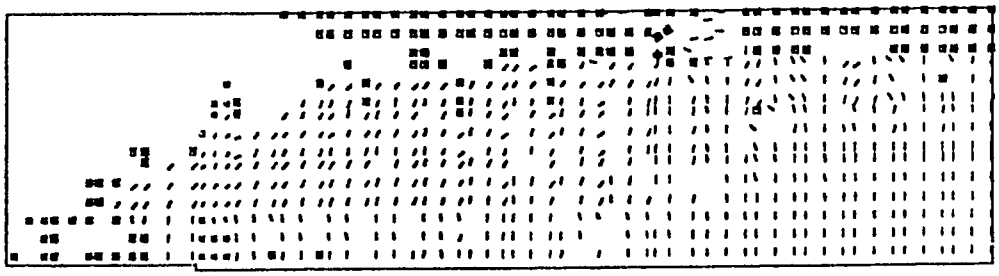

(b). 2 mm plated beam at the ultimate load of 67 kN.

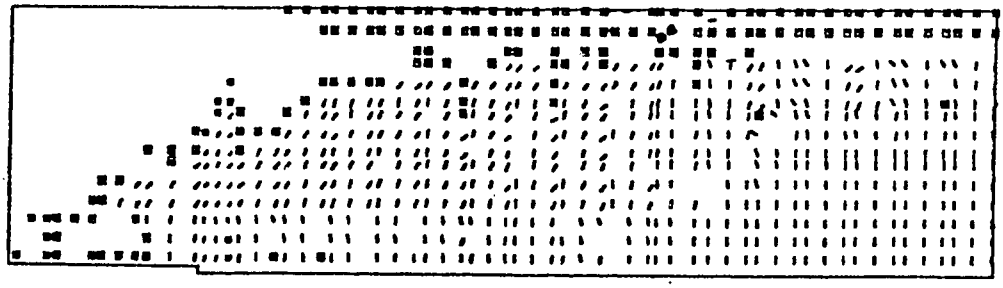

(c). 3 mm plated beam at the ultimate load of 66 kN.

Figure 7.23: Zones of microcracking and compression yielding.

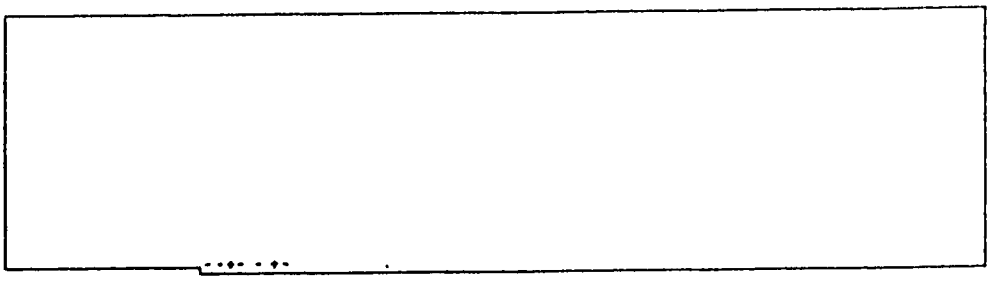

Figure 7.24: Material status at the glue interface for 3 mm plated beam at an ultimate load of 66 kN.

7.3.3 Conclusion

The non-linear finite element model developed to predict response of RC beams reinforced with externally bonded plates and already shown to capture the essential characteristics of behavior in monotonic loading up to failure for steel plates (see section 7.2) has now been verified for beams repaired by plates made of glass fiber reinforced plastics. In addition, this verification included a cycle of loading/unloading (of the unrepaired beam) followed by loading to failure of the repaired beam. The failure mechanism has been shown to be dependent on the plate thickness. For relatively thin plates, the interface stresses are low and if the beam is sufficiently under-reinforced, the plated beam will fail under a classical flexural mode with rupture of the GFRP plate. As the plate thickness is increased however, the interface stresses increase resulting in plate separation.

Chapter 8

Parametric Study

8.1 Introduction

In this chapter, numerical experiments are performed to determine the influence of various parameters on the structural response and ultimate behavior of beams to the tensile side of which is bonded external plates, either as means of repairing or strengthening them. Most of the variables considered relate to the geometry of the beam components, particularly the external plate. Aspects considered are the cross-sectional dimensions of the plate and location of its curtailment. In some of the case studies, the plate has been tapered in order to assess its effect on the peak interface stresses. One other geometrical factor considered is the amount of internal reinforcement. The effect of the glue stiffness on the magnitude and distribution of the interface stresses was also investigated.With regard to repair, one factor has been chosen for consideration in this study and that is the level of damage of the virgin beam prior to repair.

To assess the sensitivity of the finite element solution to the discretization parameters, the effect of the mesh size has been considered and led to the basis of the mesh used in the rest of the parametric study.

The ultimate loads, ultimate deflections, failure mechanisms, interface

shear and peeling stresses are all used to compare the relative performance of the plate bonded beam as the parameters are varied. Such comparisons are detailed in the sections below.

8.2 Mesh Size

The placement of the internal steel in the reinforced concrete beam particularly the concrete cover to the main reinforcement as well as stirrup spacing, dictates the possible maximum mesh size in a finite element discretization, if the aspect ratio of the concrete elements is to be kept within limits. To test the effect of the mesh size on the numerical results, three discretizations have been used. In the first case, shown in Figure 8.1a, an extra fine mesh is used. Another relatively fine mesh mesh (Figures8.1b) together with a coarse mesh (Figures8.1c) are employed for comparison purposes. Table 8.1 summarizes the characteristics of the discretization.

Figure 8.2 shows the deflections resulting from three discretizations studied, and Figure 8.3 shows the concrete microcracking and yielding at ultimate load levels. As can be seen from Figure 8.2 the difference in deflections between the extra fine mesh and the fine mesh is minimal. The very coarse mesh however tends to underestimate the load at higher load levels. Figure 8.3 shows the cracking patterns at the ultimate load levels for each of the three mesh discretizations. Table 8.2 shows the stresses resulting from the three different mesh discretizations for top most concrete fiber and for the internal steel at the beam center. These results indicate insignificant differences in the stresses between the extra fine mesh I and mesh II. For the rest of the parametric study therefore, Mesh II (Table 8.1) was used.

Discretization	*No. of Elements*			*No. of Nodes*
	Concrete	*Steel*	*Bond*	
Extra Fine Mesh I	204	118	68	1035
Fine Mesh II	68	59	34	385
Coarse Mesh III	51	45	34	315

Table 8.1: Mesh discretization summary

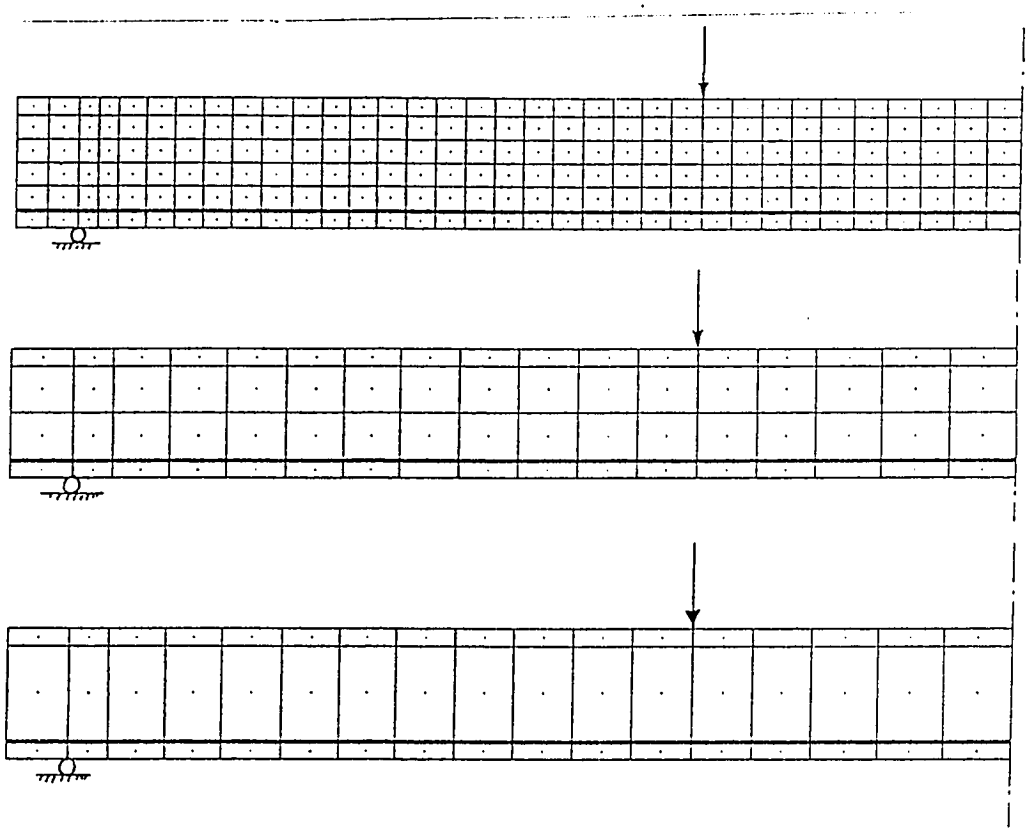

Figure 8.1: Mesh discretization sketches

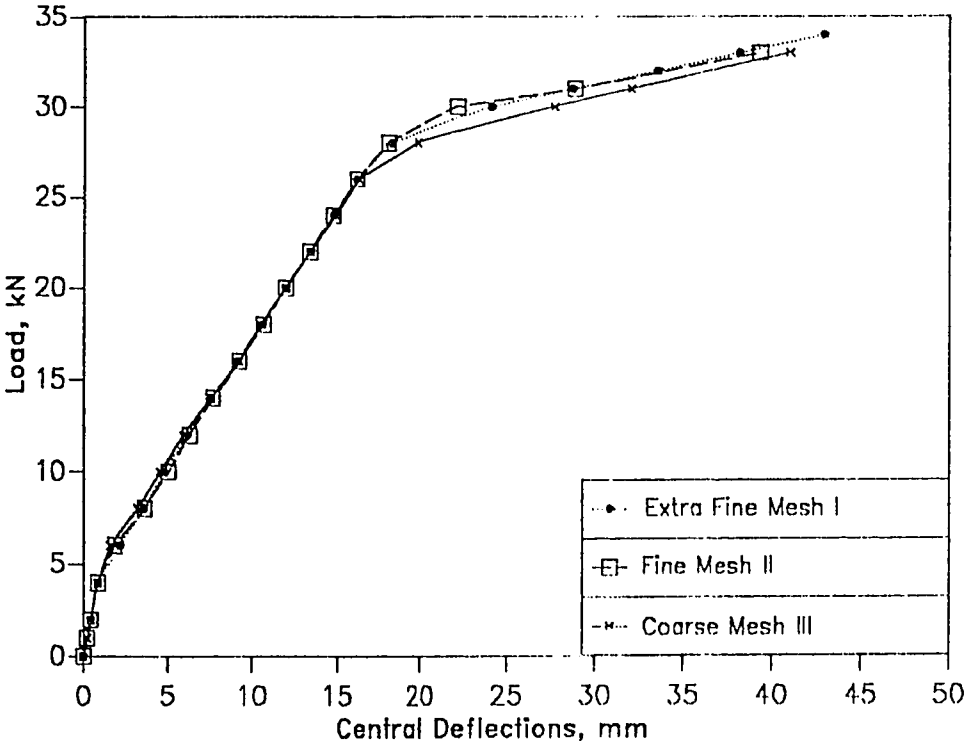

Figure 8.2: Deflections for different mesh discretizations

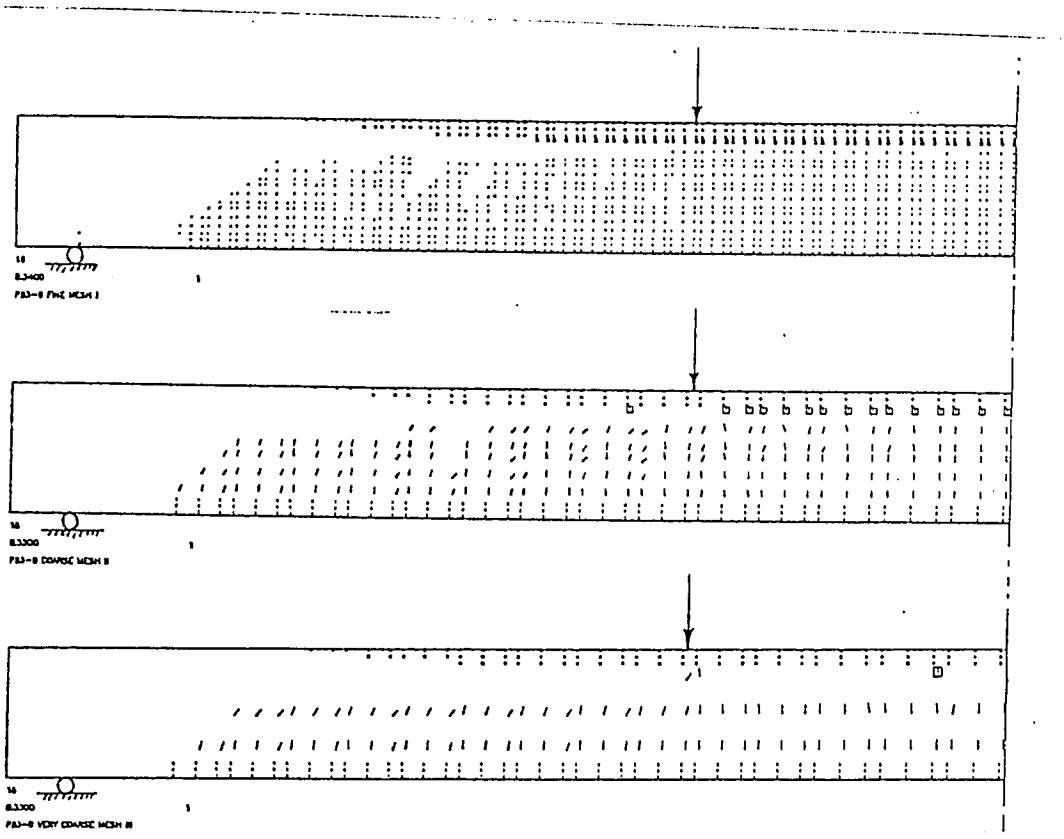

Figure 8.3: Concrete microcracking for different mesh discretizations

Load Level kN	*Stresses, MPa*					
	Concrete MPa			*Internal Steel* MPa		
	Extra Fine Mesh I	Fine Mesh II	Coarse Mesh III	Extra Fine Mesh I	Fine Mesh II	Coarse Mesh III
4	-3.751	-3.756	-3.756	16.86	16.94	16.94
20	-27.23	-27.21	-25.62	382.2	382.9	402.6
33	-53.91	-53.90	-54.21	530.9	531.2	531.2

Table 8.2: Stresses for the different mesh discretizations

8.3 Effect of Level of Damage

In this section the effect of level of damage of the virgin beam prior to repair is investigated. The presentation starts with a description of the beam geometry, material parameters and the loading procedure used. This is followed by comparison of the results with respect to the ultimate loads and load deflection curves.

8.3.1 Beam Geometry, Material Parameters and Loading Procedure

The overall geometry as well as the loading pattern for beams used in this parametric study is similar to those used in the experimental studies conducted at KFUPM [72] and is also reproduced in Figure 8.4. The beams are repaired with 1.5 mm plates and a glue thickness of 2 mm.

In the numerical studies the unrepaired beam is loaded to various central deflections, unloaded to a zero load, repaired with the 1.5 mm plate in a manner described in section 6.5.3 and finally, the repaired beam is loaded till failure. Levels of damage were selected to correspond to a central deflection of 5, 10, 15 and 27 mm.

The material properties used in the numerical experiments are similar to the experimental ones [72] and are enumerated below:

Concrete: $f_c' = 31$ MPa, $E_c = 25385$ MPa (see equation 3.13), $f_t' = 3.20$ MPa (see equation 3.36), $\nu_c = 0.15$, $\varepsilon_u = 0.0035$, $\alpha = 0.0287$ (from Figure 3.4), $\varepsilon_m = 0.002$ and $\phi = 37°$.

Internal Steel: $E_s = 200$ GPa, $\sigma_y = 360$ MPa and $H' = 200$ MPa.

External Steel Plate: $E_p = 200$ GPa, $\sigma_y = 269$ MPa, $\nu = 0.30$ and $H' = 200$ MPa.

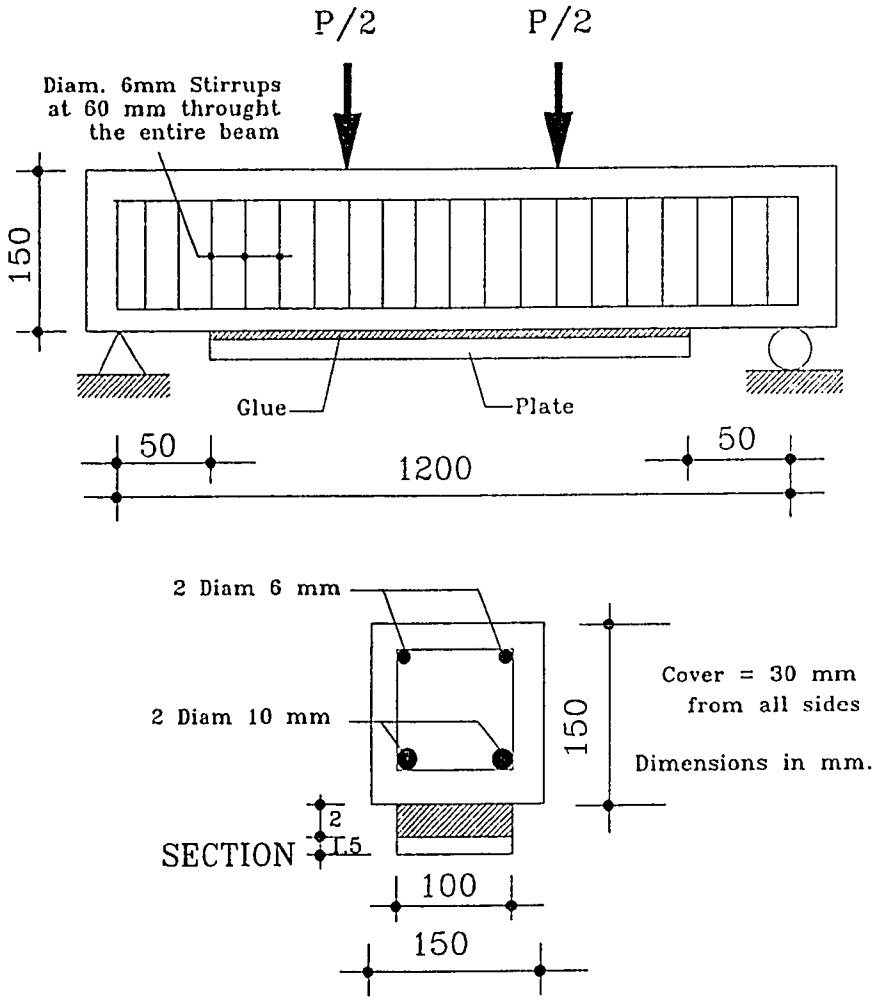

Figure 8.4: Beam and testing details for the study of the effect of level of damage prior to repair

Concrete/Glue/Steel Interface: (see section 3.4) $E_i = 278.9$ MPa, $G_i = 120.2$ MPa, $c = 5.362$ MPa, $f_{ti} = 4.0$ MPa and $\nu_i = 0.15$

Steel/Concrete Bond: (see section 3.4.2) $E_b = 2784$ MPa, $G_b = 1200$ MPa, $\tau_{bond} = 7.5$ MPa, $f_{tb} = 3.20$ MPa and $\nu_b = 0.16$

8.3.2 Results

Figure 8.5 shows the load-deflection curves of beams repaired after different levels of damage. The figure depicts

(i). the monotonic loading curves of the virgin RC beam (without plate) to failure.

(ii). unloading curves of virgin beam at predetermined levels of damage.

(iii). loading curves of damaged beams repaired by external plates.

Table 8.3 lists the ultimate loads and deflections attained by beams after repairing at different levels of damage. There is a nominal decrease in the ultimate capacity of the repaired beam with increasing levels of damage prior to repair.

8.4 Effect of Plate Dimensions

In the sections that follow below numerical experiments are performed to determine the effect of plate dimensions on the ultimate loads, failure mechanisms and peak interface stresses of plated beams. For any given R/C beam, the plate width is normally dictated by the beam width and for this reason, the major thrust in this part of the study has been concentrated on the effect of the plate thickness. However two beam cases have been analyzed to study the effect of beam width.

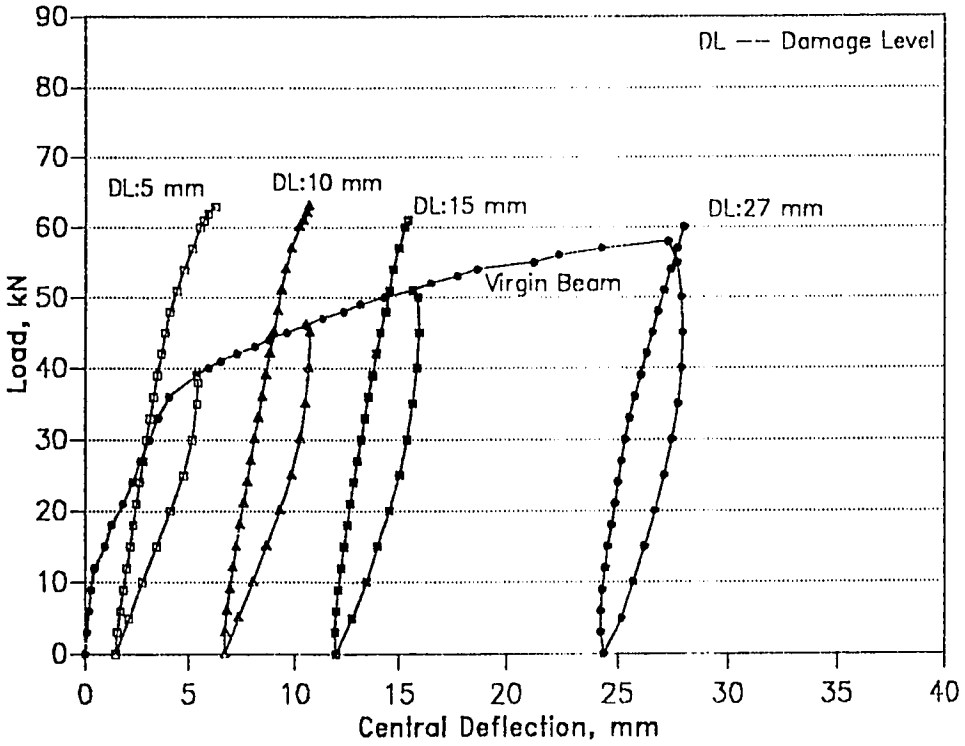

Figure 8.5: Load-deflection curves for beams repaired after different levels of damage

Damage Level (mm)			*Load (kN)*	
Δ_{max} *on Loading an Unrepaired Beam*	Δ *on Unloading*	Δ_{max} *on Loading*	*Repaired*	*% Increase based on unrepaired* $P_{ult} = 58$ *kN*
5.35	1.48	6.24	63	8.62
10.51	6.71	11.36	63	8.62
15.62	11.99	17.44	61	5.17
27.30	24.42	32.48	60	3.45

Table 8.3: Failure loads of beams repaired after different levels of damage

8.4.1 Plate Thickness

The beam geometry adopted in this part of the study is identical to the beam shown in Figure 7.1 with varying plate thicknesses. The parameters investigated and beam designations are shown in Table 8.4.

The material parameters used in the analysis are

Concrete: $f_c' = 54$ MPa, $E_c = 31272$ MPa (see equation 3.13), $f_t' = 4.62$ MPa (see equation 3.36), $\nu_c = 0.15$, $\varepsilon_u = 0.0035$, $\alpha = 0.189$ (from Figure 3.4), $\varepsilon_m = 0.002$ and $\phi = 37°$.

Internal Steel: $E_s = 200$ GPa, $\sigma_y = 530$ MPa and $H' = 200$ MPa.

External Steel Plate: $E_p = 200$ GPa, $\sigma_y = 240$ MPa, $\nu = 0.30$ and $H' = 200$ MPa.

Concrete/Glue/Steel Interface: (see sections 3.4) $E_i = 278.9$ MPa, $G_i = 120.2$ MPa, $c = 7.0$ MPa, $f_{ti} = 4.0$ MPa and $\nu_i = 0.16$

Steel/Concrete Bond: (see section 3.4.2) $E_b = 2784$ MPa, $G_b = 1200$ MPa, $\tau_{bond} = 7.5$ MPa, $f_{tb} = 4.62$ MPa and $\nu_b = 0.16$

The beams are loaded monotonically in increments of 3 kN which are reduced to 0.25 kN near the ultimate load levels. Figure 8.6 shows the typical material status of a plated beam (in this case beam PB50-10) at ultimate conditions. The extent of steel yielding for the plate and internal reinforcing steel (HYZ) and the plate separation zone (SZ) as defined in Figure 8.6 may be used to evaluate the effect of various parameters on the failure mechanism of the plated beam. Table 8.5 shows these values for different plate thicknesses. The ultimate loads are also indicated.

It can be concluded from the table that in general the ultimate load increases as the plate thickness increases and at the same time, the extent at which both the external and internal steels yield are reduced. Plate

Internal Steel Reinf. Ratio ρ_s	*Beam Designations* Plate Thickness t_p, mm						
	$t_p = 0$	$t_p = 1$	$t_p = 2$	$t_p = 3$	$t_p = 4$	$t_p = 5$	$t_p = 10$
$0.25\rho_b$	PB25-0	PB25-1	PB25-2	PB25-3	PB25-4	PB25-5	PB25-10
$0.50\rho_b$	PB50-0	PB50-1	PB50-2	PB50-3	PB50-4	PB50-5	PB50-10
$0.75\rho_b$	PB75-0	PB75-1	PB75-2	PB75-3	PB75-4	PB75-5	PB75-10

Table 8.4: Beam designations for study of effect of plate thickness and internal steel reinforcement ratio.

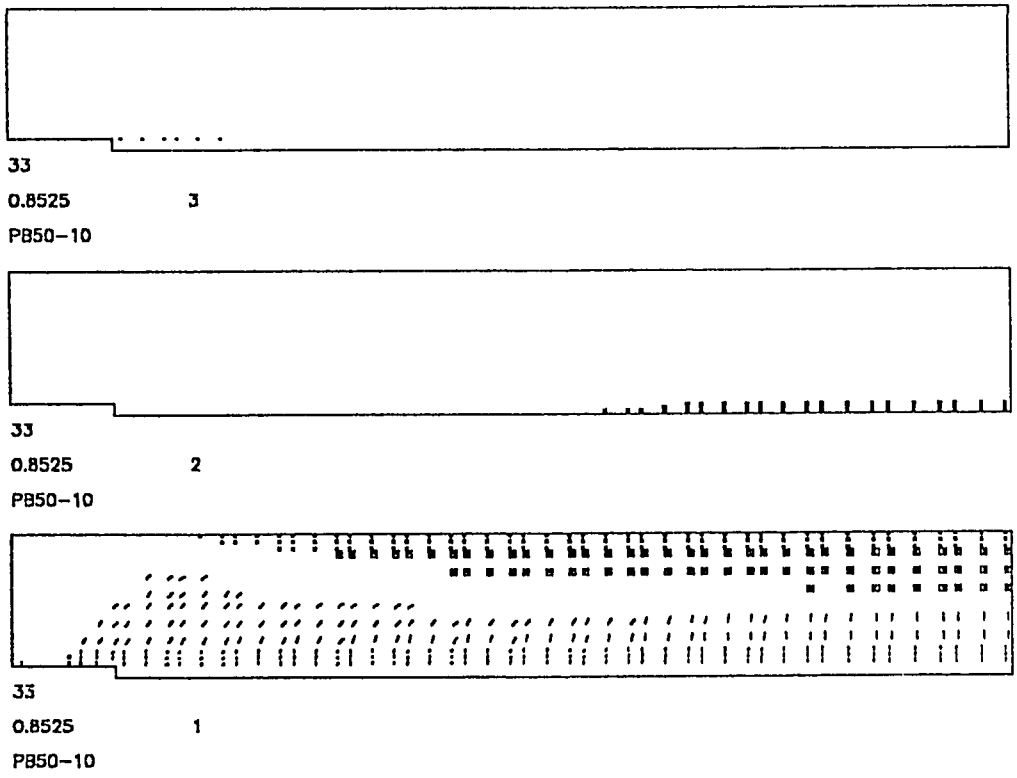

Figure 8.6: Material status at ultimate load conditions: Beam PB50-10

Plate Thickness t_p, mm	*Ultimate Loads & Failure Mechanisms*			
	Ultimate Load kN	HYZ *Plate* mm	HYZ *Int. Steel* mm	SZ
	Amount of Internal Steel $\rho_s = 0.25\rho_b$			
0	30.5		574	
1	37.5	791	552	0
2	44.5	739	526	0
3	50.25	691	480	0
4	56.25	646	455	0
5	62.5	621	439	0
10	76	455	0	66
	Amount of Internal Steel $\rho_s = 0.50\rho_b$			
0	48		477	
1	54.25	804	383	0
2	60.25	739	452	0
3	66	720	414	0
4	70.75	662	381	0
5	75.75	646	314	0
10	85.25	480	0	132
	Amount of Internal Steel $\rho_s = 0.75\rho_b$			
0	64		417	
1	69	848	404	0
2	74	757	317	0
3	75.5	687	0	0
4	78.5	662	0	0
5	81.25	621	0	0
10	93.5	480	0	83

Table 8.5: Effect of plate thickness and internal steel reinforcement ratio of failure mechanisms

separation is noted to occur only in the 10 mm plated beam due to the high value of the interface shear cohesion c used in the analysis.

Figures 8.7 and 8.8 show the effect of plate thickness on the peak shear and normal transverse (or peeling) stresses. In general thicker plates result in higher values of interface stresses at all corresponding load levels. This characteristic of the plated RC beam makes it mandatory that a limit be established for the thickness of a plate that can be installed on a RC beam of known geometry in order to avoid a premature interface failure.

8.4.2 Plate Width

To study the effect of plate width on the interface shear stresses, beams 150 mm wide and 300 mm deep on a simple span of 7 m were used. The geometry of the beams is shown in Figure 8.9. Beams SCHK1, SCHK3 and SCHK4 were plated with 130x5.5 mm, 65x11 mm and 65x5.5 mm plates respectively. So the width is varied keeping the depth constant in beams SCHK1 and SCHK4 whereas in beams SCHK1 and SCHK3, the plate area is left unchanged.

The material parameters used for these beams are

Concrete: $f_c' = 45$ MPa, $E_c = 29171$ MPa (see equation 3.13), $f_t' = 4.10$ MPa (see equation 3.36), $\nu_c = 0.15$, $\varepsilon_u = 0.0035$, $\alpha = 0.250$ (from Figure 3.4), $\varepsilon_m = 0.002$ and $\phi = 37°$.

Internal Steel: $E_s = 200$ GPa, $\sigma_y = 414$ MPa and $H' = 200$ MPa.

External Steel Plate: $E_p = 200$ GPa, $\sigma_y = 269$ MPa, $\nu = 0.30$ and $H' = 200$ MPa.

Concrete/Glue/Steel Interface: (see sections 3.4) $E_i = 278.9$ MPa, $G_i = 120.2$ MPa, $c = \infty$, $f_{ti} = \infty$ and $\nu_i = 0.15$

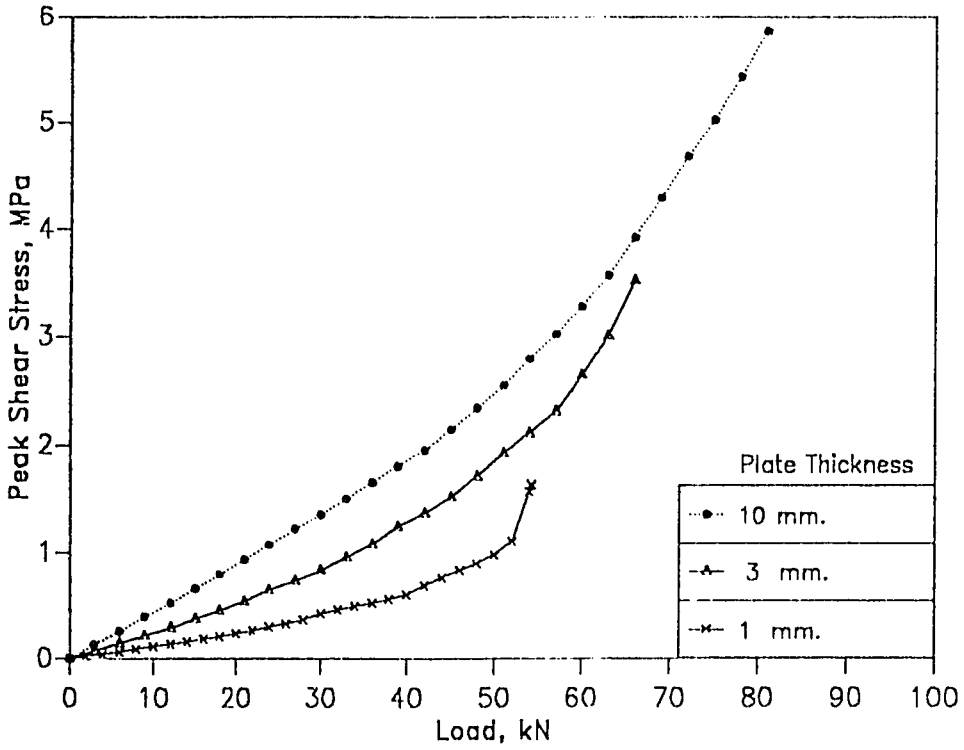

Figure 8.7: Effect of plate thickness on peak interface shear stresses

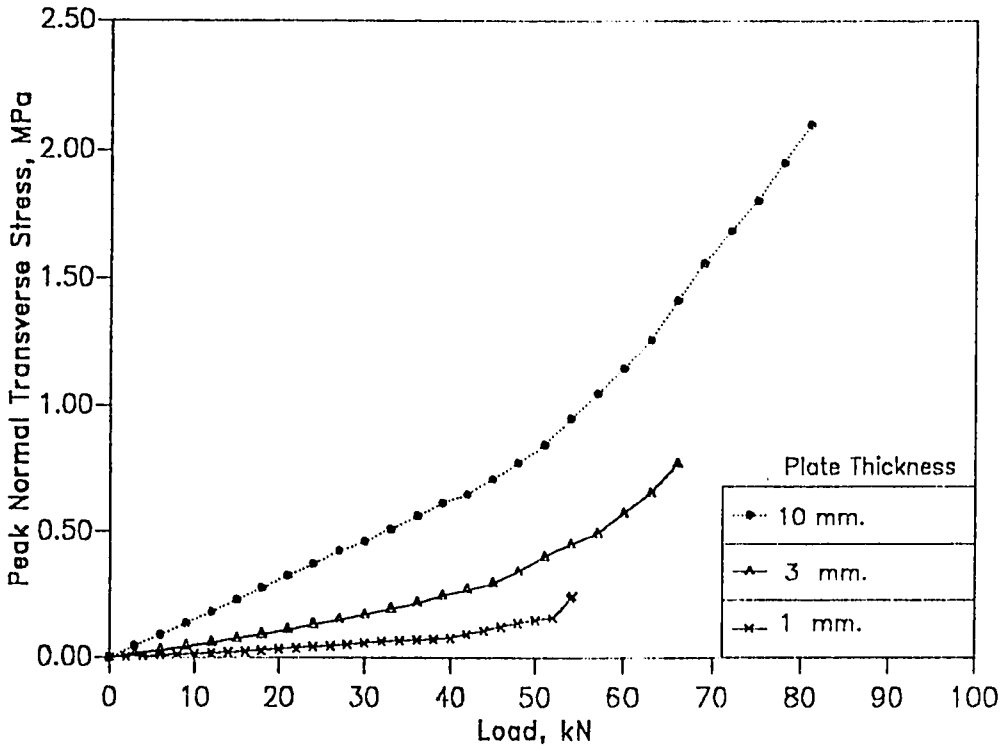

Figure 8.8: Effect of plate thickness on peak peeling stresses

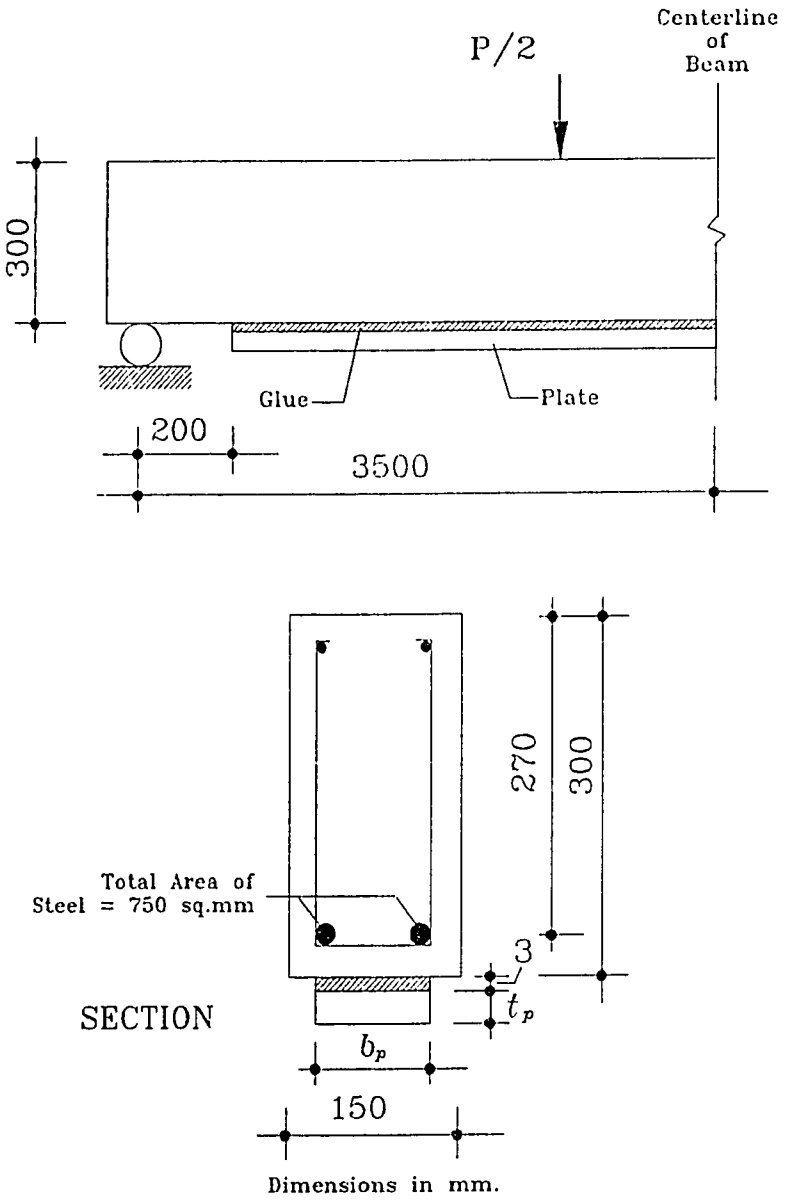

Figure 8.9: Beams to study effect of plate width on behavior of plated beams

Steel/Concrete Bond: (see section 3.4.2) $E_b = 2784$ MPa, $G_b = 1200$ MPa, $\tau_{bond} = 7.5$ MPa, $f_{tb} = 4.10$ MPa and $\nu_b = 0.16$

To prevent plate separation, the value for the interface shear cohesion has been set to a high value.

Figures 8.10 and 8.11 show plots of the variation of peak interface shear and normal transverse stresses with the applied load. The effect of the width of the plate on the peak shear and peeling stress is not as pronounced as that of its thickness. This is due to the fact that change in width affects the interface area mobilized in transmitting shear and peeling whereas change in plate thickness leaves this area unchanged. Also increase in plate width and/or thickness leads to increase in forces in the plate that cause interface shear and peeling stresses.

To keep the interface stresses as low as possible therefore, it is desirable that the reinforcing external plate be as wide and as thin as possible. Similar conclusions have been derived experimentally [13,15] as explained in section 2.2.1 and also using analytical techniques based on the strength of materials [18,25] as shown in section 2.2.3.

8.5 Amount of Internal Steel

Table 8.4 shows the beam designations used to study the effect of the amount of internal reinforcement on the structural response of a plated beam. For each of several plate thicknesses, three reinforcement ratios namely $0.25\rho_b$, $0.50\rho_b$ and $0.75\rho_b$ where ρ_b is the steel ratio at balanced beam conditions were used. Similar material parameters as those listed in section 8.4.1 were employed in the analysis.

The results with respect to the ultimate loads and extent of steel yielding are shown in Table 8.5. For a given plate thickness, increasing the quantity of the internal steel generally results in higher ultimate loads. The higher

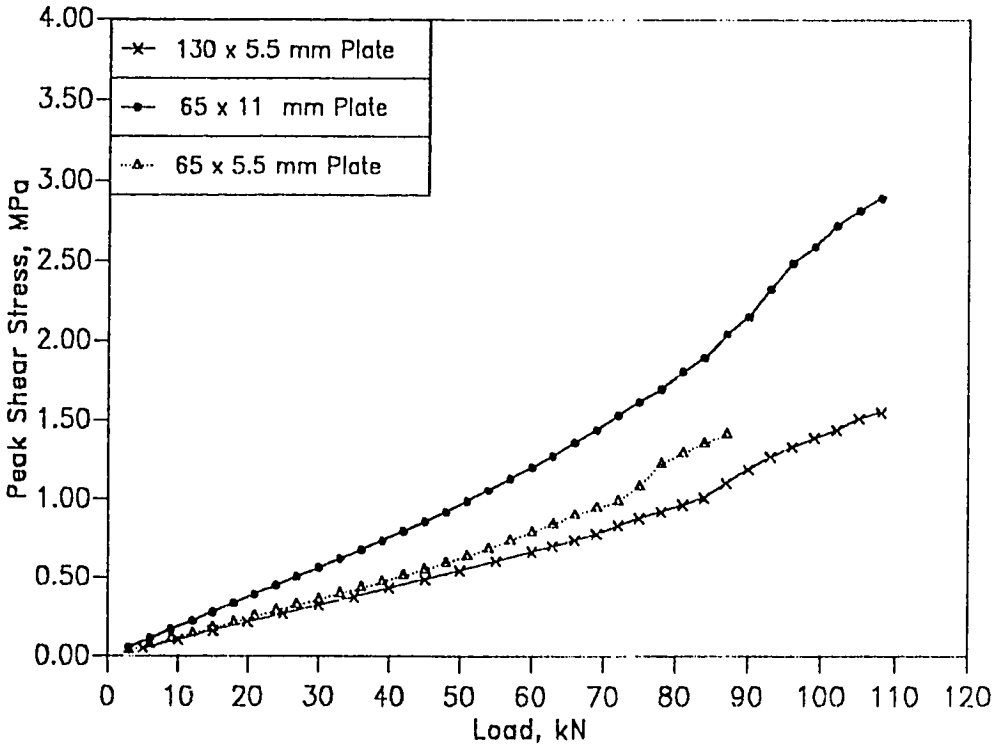

Figure 8.10: Effect of plate width on interface shear stresses

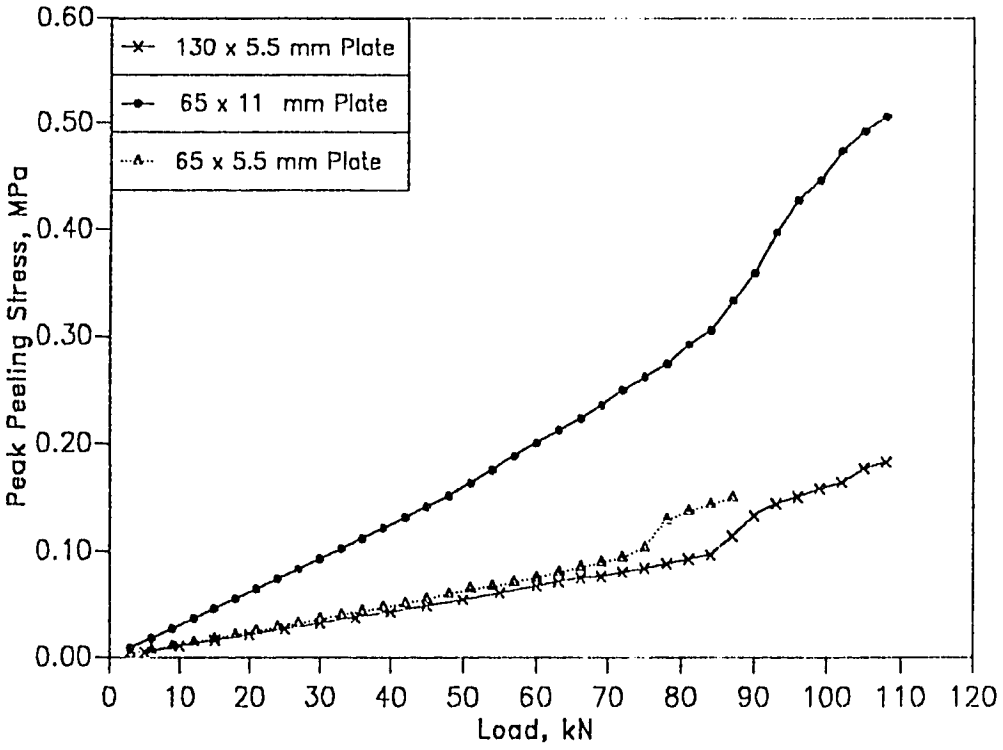

Figure 8.11: Effect of plate width on interface peeling stresses

load values attained result in a higher portion of the plate yielding. The extent of the internal steel yielding however, does reduce consistently with increasing steel ratios and at high steel level, the steel does not yield even for relatively thin external plates.

The effect of the internal steel on the peak interface shear stresses is illustrated in Figures 8.12 and 8.13 for beams plated with 2 mm and 10 mm plates respectively. For a given thickness of plate and a given load level, increasing the amount of internal reinforcement causes a decrease in the amount of tensile force carried by the plate with a corresponding increase in the force in the internal reinforcement. This leads to a reduced interface shear stress. This effect is much more pronounced at high load levels when the concrete around the plate curtailment zone starts to crack. Similar results were observed for the peak peeling stresses.

Another interesting result seen in Figures 8.12 and 8.13 is that the load level at which concrete cracking commences around the plate cutoff (seen as the kink in the load-stress plot), becomes more sensitive to the internal steel reinforcement ratio as the plate thickness is reduced. For thick plates, concrete around the plate curtailment virtually cracks at the same load for all amounts of internal reinforcement. This is attributed to the fact that the higher stresses in the plate cutoff region resulting from relatively thick plates will result in early concrete cracking even before the internal steel is mobilized to any appreciable extent.

8.6 Loading Type

To compare the effect of a uniformly distributed loading to that of four-point concentrated loading on the interface stresses, the beam of a similar geometry as beam SCHK1 described in section 8.4.2 and shown in Figure 8.9 was loaded with a uniform load. The beam designated SCHK2 was subjected to load increments of 1 N/mm corresponding to a total load

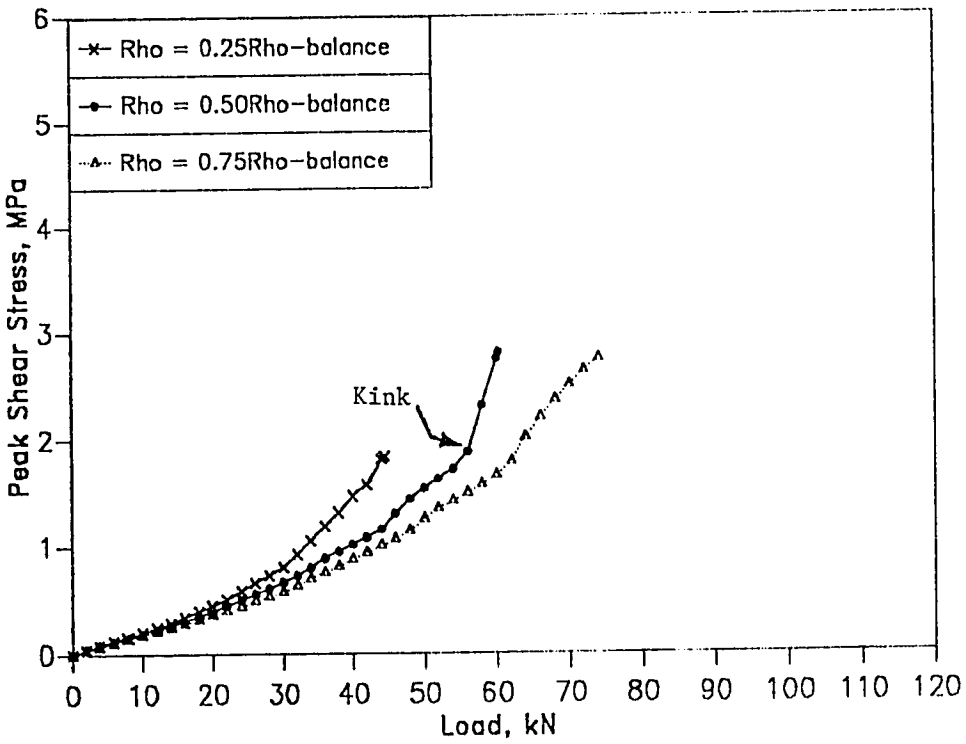

Figure 8.12: Effect of internal steel reinforcement ratio on the peak shear stresses: 2 mm plated beam

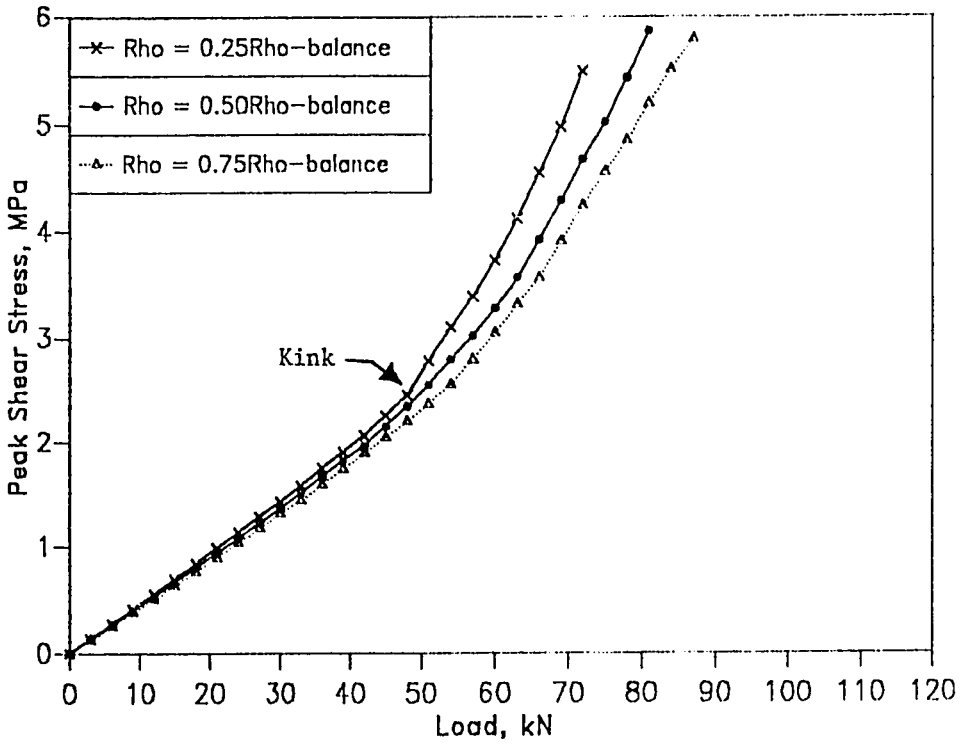

Figure 8.13: Effect of internal steel reinforcement ratio on the peak shear stresses: 10 mm plated beam

of 7 kN. The ultimate total uniformly distributed load on the beam was 231 kN compared to the 108 kN for the beam with concentrated loads.

Figure 8.14 shows respectively the resulting interface shear and normal transverse stresses plotted against the applied load for beams loaded with a uniformly distributed and concentrated loads. There is not much difference in the stresses because as is shown in section 9.6.2, the ratio M_0/V_0 for a uniformly distributed load tends to a as a/L gets smaller, that is,

$$\lim_{a/L\to 0}\left(\frac{M_0}{V_0}\right) = \lim_{a/L\to 0}\left(\frac{La - a^2}{L - 2a}\right) = a \tag{8.1}$$

where

a length from support to the plate curtailment

L beam span.

which is the case for most practical cases. If a/L is large however, like in cases where the plate is curtailed further away from the support, this difference can be significant.

8.7 Location of Plate curtailment

The effect of the length of plate curtailment from the support was investigated using parameters as indicated in Table 8.6 where the beam designations are indicated. For each plate thickness t_p, four different curtailment lengths a were considered. The geometry of the beams are identical to those discussed in section 8.4.1.

Figures 8.15 and 8.16 show respectively the interface shear stresses plotted against the load for 1 mm and 10 mm plated beams and whose plates are curtailed at different lengths from the support. Figure 8.17 shows, for a precracking load of 6 kN, the variation of the peak shear stress with the plate thickness for different plate curtailment lengths. The increase in the

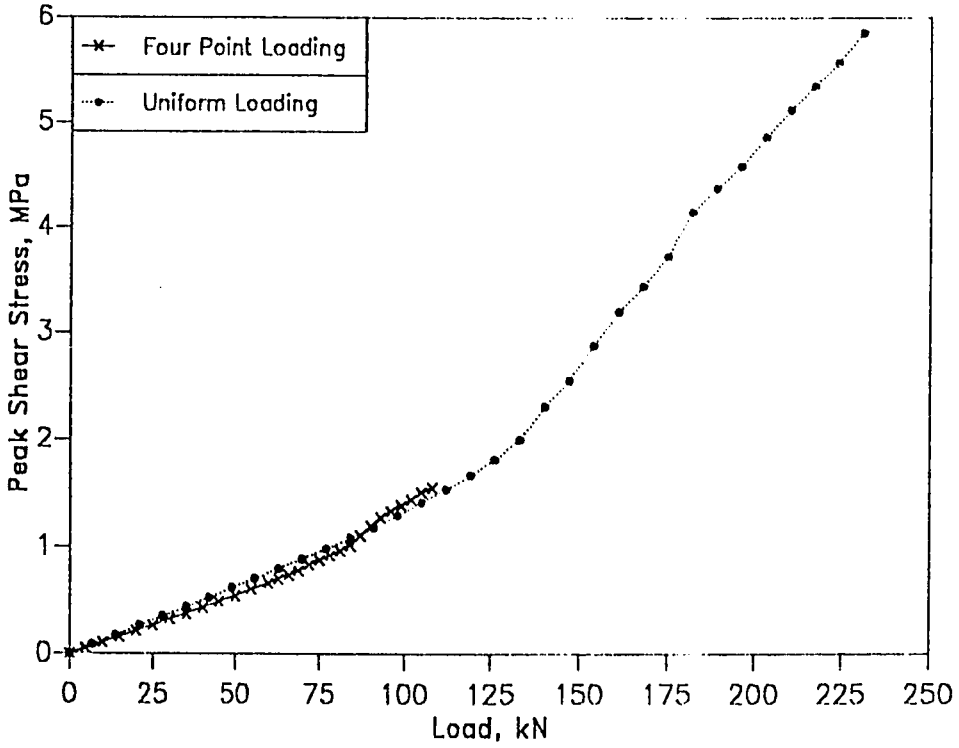

Figure 8.14: Effect of uniform loading on peak shear stresses

Length from Support to the the Plate Curtailment a, mm	*Beam Designations* Plate Thickness t_p, mm					
	$t_p = 1$	$t_p = 2$	$t_p = 3$	$t_p = 4$	$t_p = 5$	$t_p = 10$
50	PB50-1	PB50-2	PB50-3	PB50-4	PB50-5	PB50-10
260	IB2-1	IB2-2	IB2-3	IB2-4	IB2-5	IB2-10
470	IB3-1	IB3-2	IB3-3	IB3-4	IB3-5	IB3-10
680	IB4-1	IB4-2	IB4-3	IB4-4	IB4-5	IB4-10

Table 8.6: Beams used to study effect of length to plate curtailment

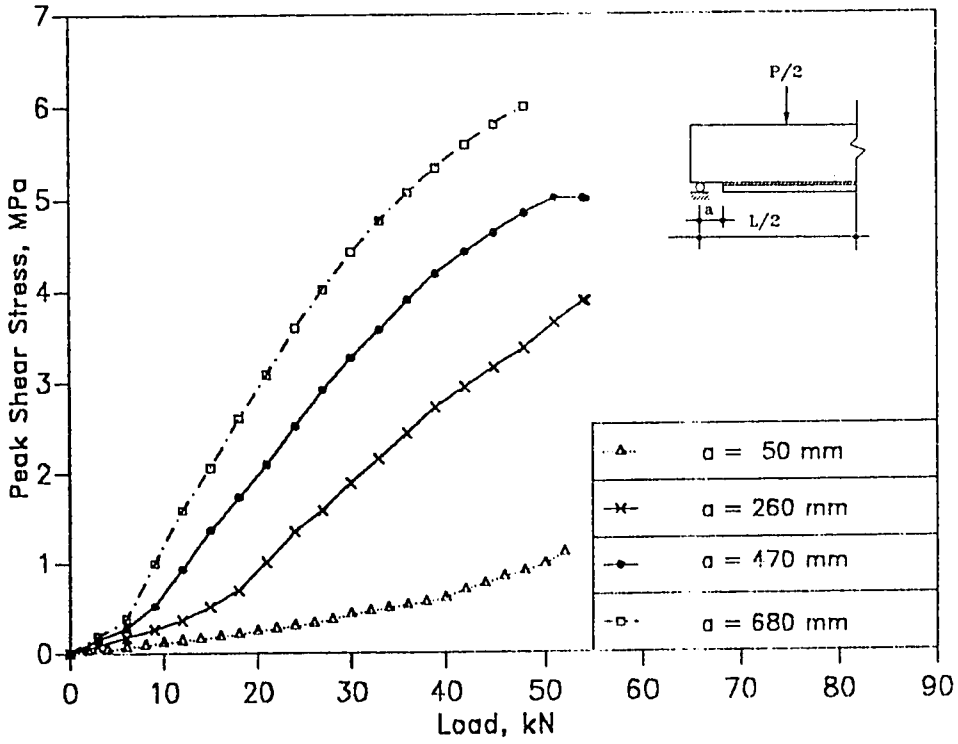

Figure 8.15: Effect of plate curtailment length on peak interface shear stress: 1 mm plated beam

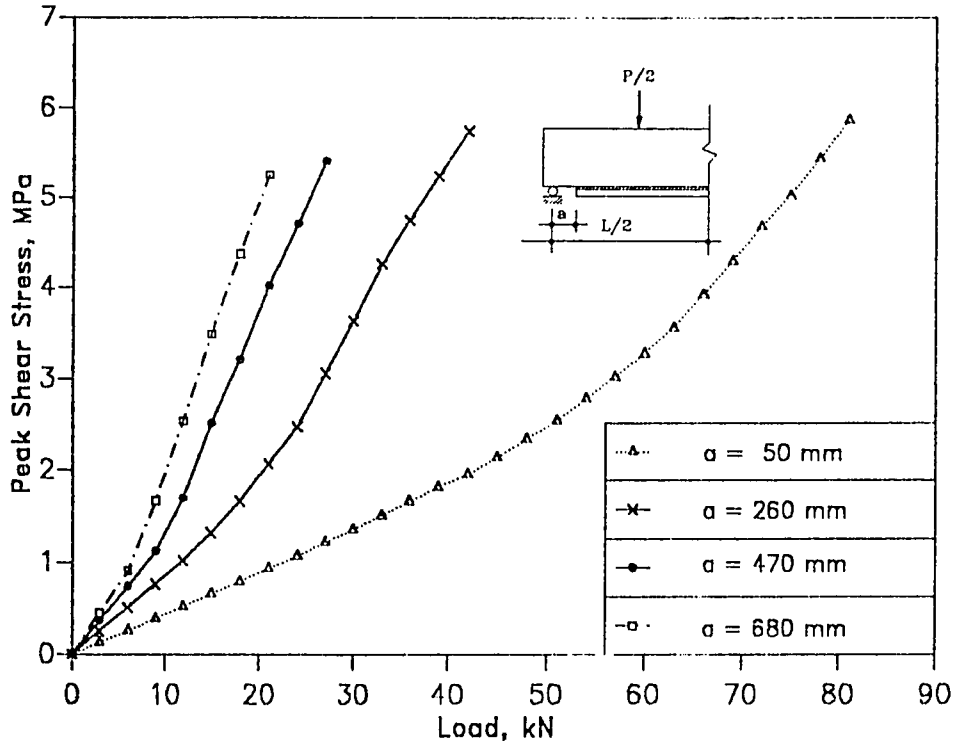

Figure 8.16: Effect of plate curtailment length on peak interface shear stress: 10 mm plated beam

peak stresses due to the plate curtailment are attributed to the fact that as a increases, the global moment increases which in turn necessitates the application of a larger axial force, t_1 (see section 2.2.3.2 and Figure 2.5a) leading to an increase in the interface shear. Also there is a magnification of shear force f_{20} and bending moment m_{20} (see Figure 2.5b) leading to higher peeling stresses.

Alternatively, for the same glue properties, the development length $\bar{x}$, (see Figure 2.3 of section 2.2.3.1) remains unchanged, whereas the force developed in the steel plate at the distance $\bar{x}$ from the curtailed end of the plate increases in the same proportion to the bending moment. This leads to an increase in the interface shear and peeling stresses.

8.8 Plate Tapering

Beam PB50-10 (see Table 8.4) strengthened with a 10 mm plate is used to assess the effect of plate taper on the interface shear stress distribution. Two plate tapers were investigated and are shown in Figure 8.18. In *Taper # 1*, the plate thickness is kept constant at 10 mm but the width is varied from 80 mm at the end of the constant moment region to 40 mm at the plate end. For the case of *Taper # 2*, the width is kept constant but the thickness is linearly reduced from 10 mm to 1 mm at the plate curtailment. The beam with *No Taper* refers to constant width of 80 mm and a constant thickness of 10 mm.

The beams are loaded to a load level of 6 kN and Figure 8.19 shows the resulting interface shear stress distribution for the three types of plate taper. Figure 8.20 shows the interface shear stress distribution at a higher load level of 40 kN. The results indicate that the most effective taper in reducing the shear stresses is the thickness taper. For the thickness taper considered (*Taper # 2*), the peak is translated to a new location. It seems possible therefore, that an optimal thickness profile can be designed to

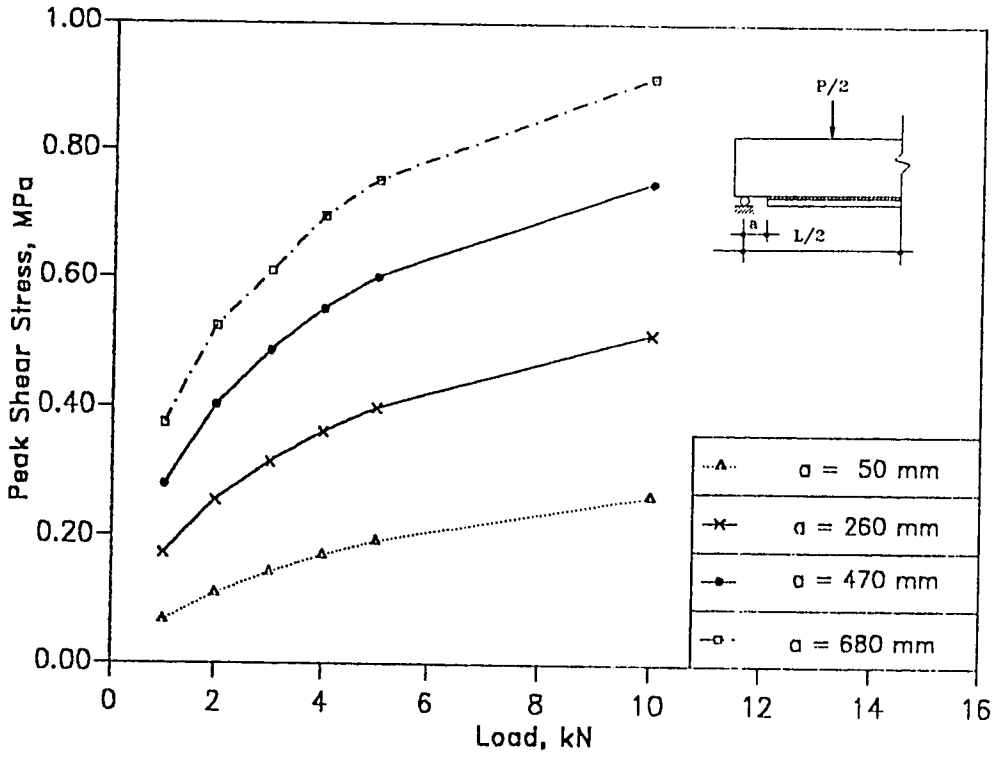

Figure 8.17: Effect of plate curtailment length on peak interface shear stress for different plate thicknesses at a Load of 6 kN

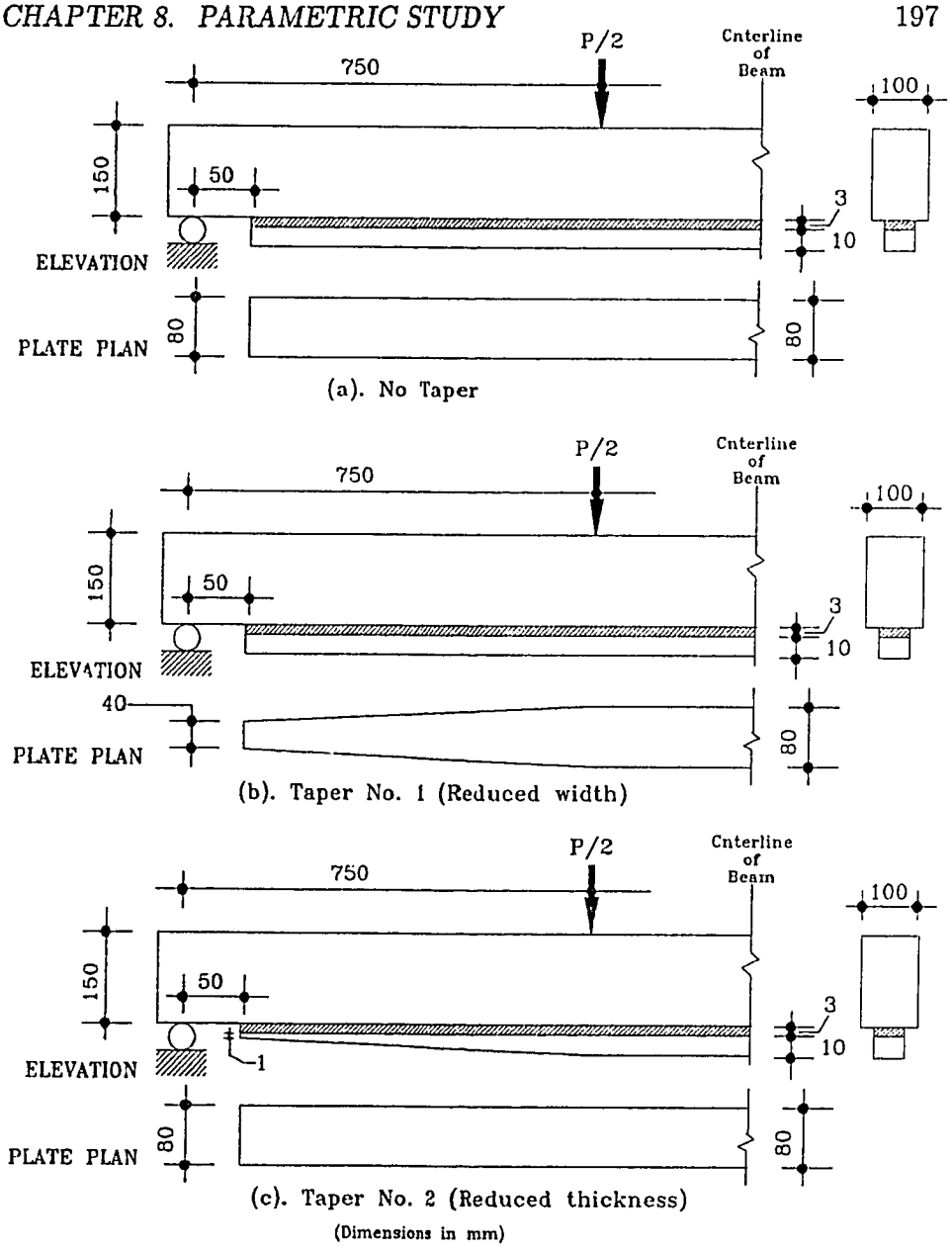

Figure 8.18: Types of plate taper studied

achieve minimum shear stress in the interface.

8.9 Glue Stiffness

To study the effect of the glue stiffness on the peak interface shear stresses, beam PB50-5 (see Table 8.4) was used ranging the glue shear modulus from 40 Mpa to 13500 Mpa. Figure 8.21 plots the distribution of the interface shear stress along the interface layer for glue shear modulii of 40 and 1000 MPa at a load level of 6 kN and shows that increasing the stiffness of the glue has an adverse effect on the peak stresses. A similar trend can be observed in Figure 8.22 where the peak shear and peeling stresses are plotted against the glue shear modulus for a load level of 6 kN.

Figure 8.23 which shows the plot of the normal tensile stress in the external plate at a load level of 6 kN for glue shear modulii of 40 and 1000 MPa reveals that increasing the glue shear modulus in general results in a redistribution of the stresses resulting in higher stress values in the plate.

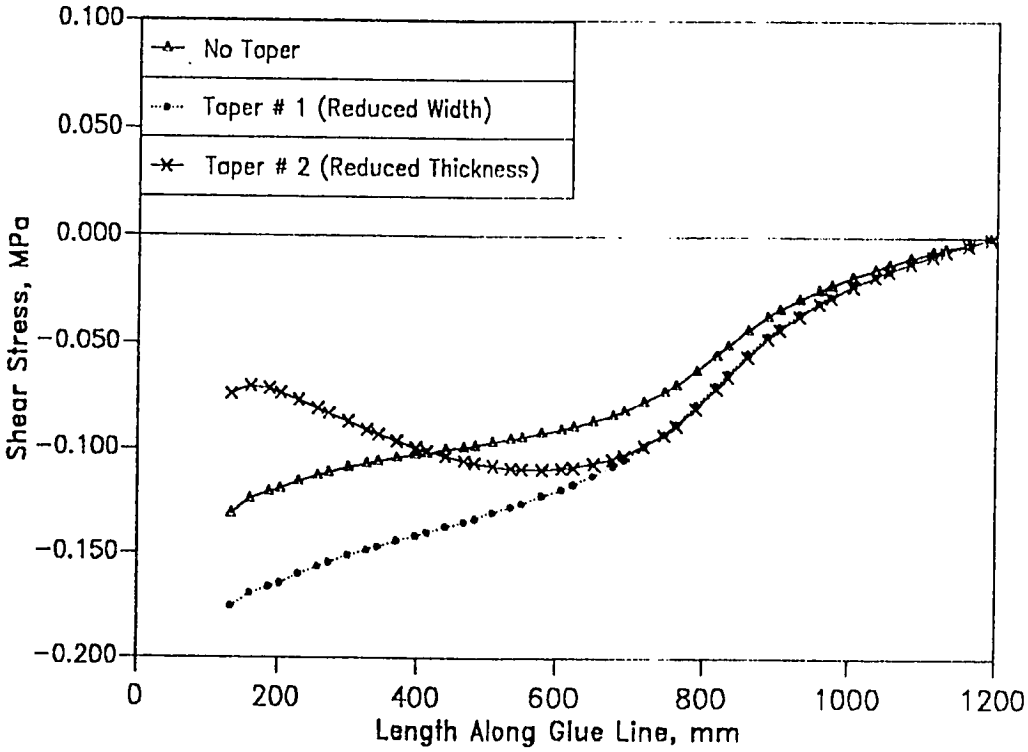

Figure 8.19: Interface shear stress distribution for the different types of plate taper at a load level 6 kN.

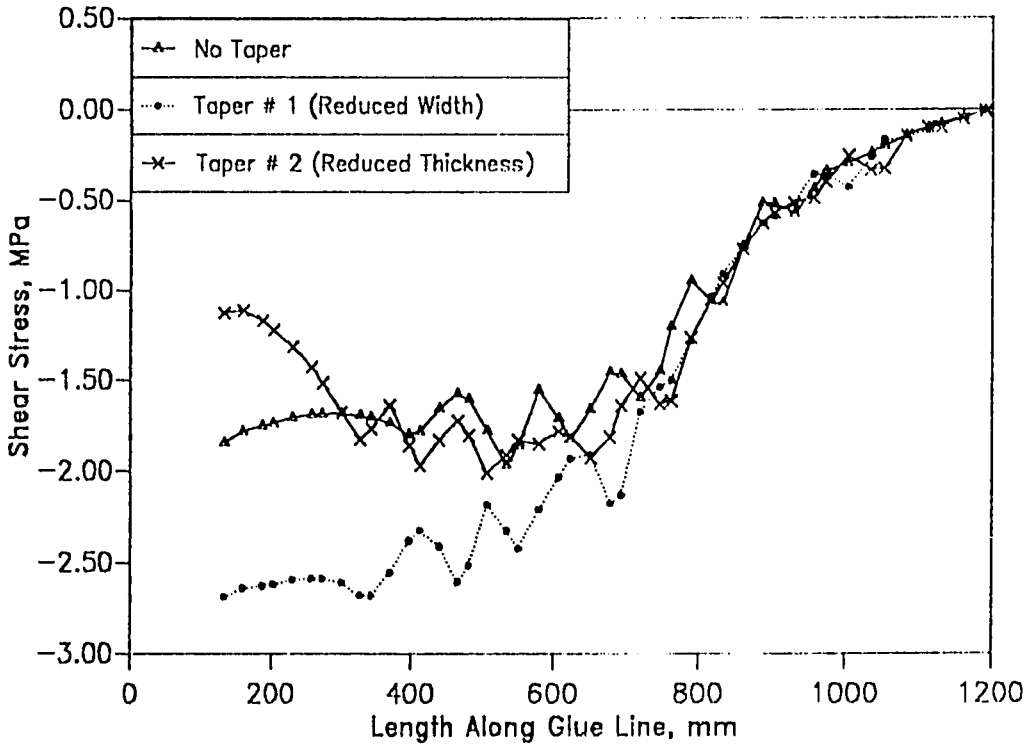

Figure 8.20: Interface shear stress distribution for the different types of plate taper at a load level 40 kN.

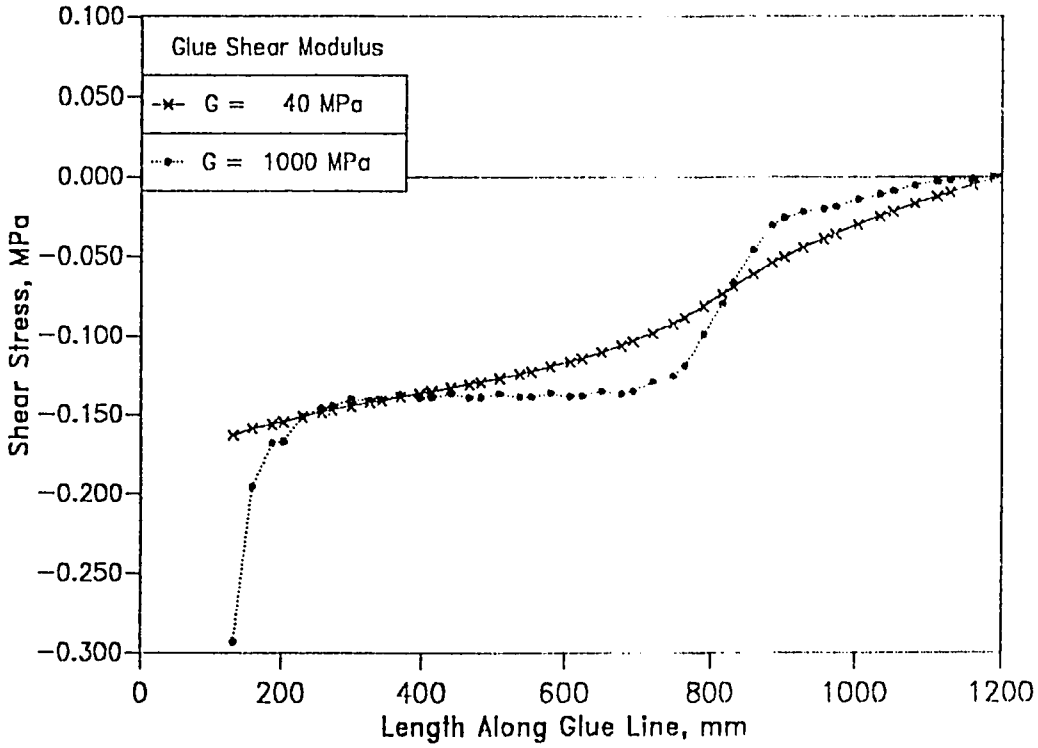

Figure 8.21: Effect of the glue shear modulus on the distribution of shear stress in the interface layer at a load of 6 kN.

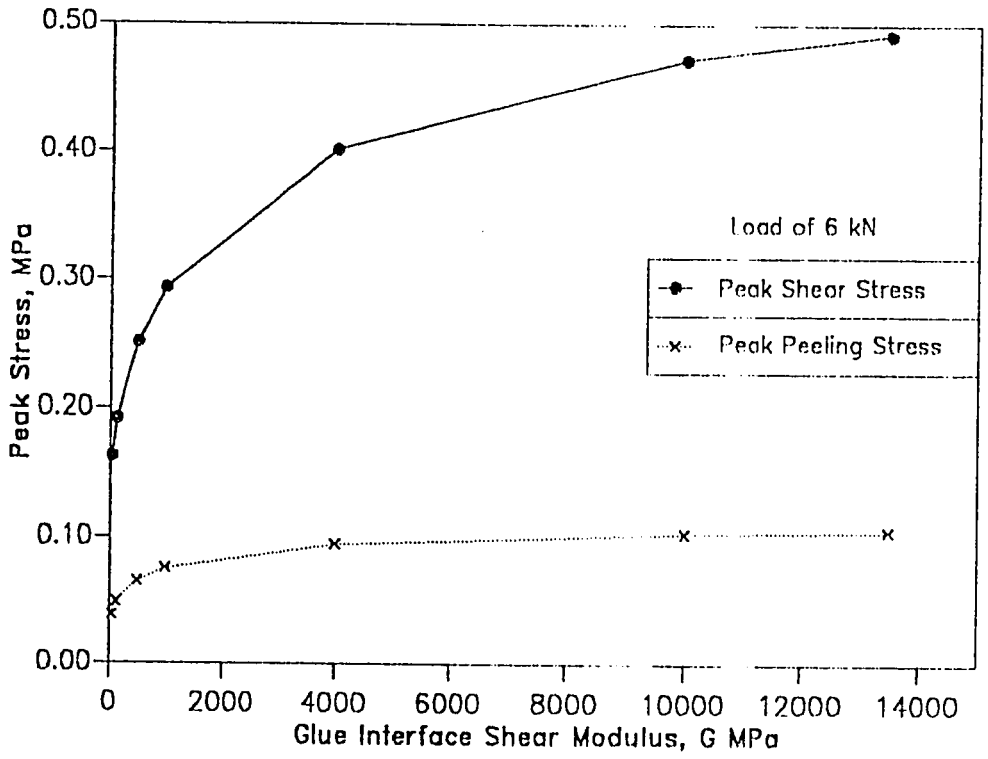

Figure 8.22: Effect of the glue shear modulus on the peak stresses in the interface layer at a load of 6 kN.

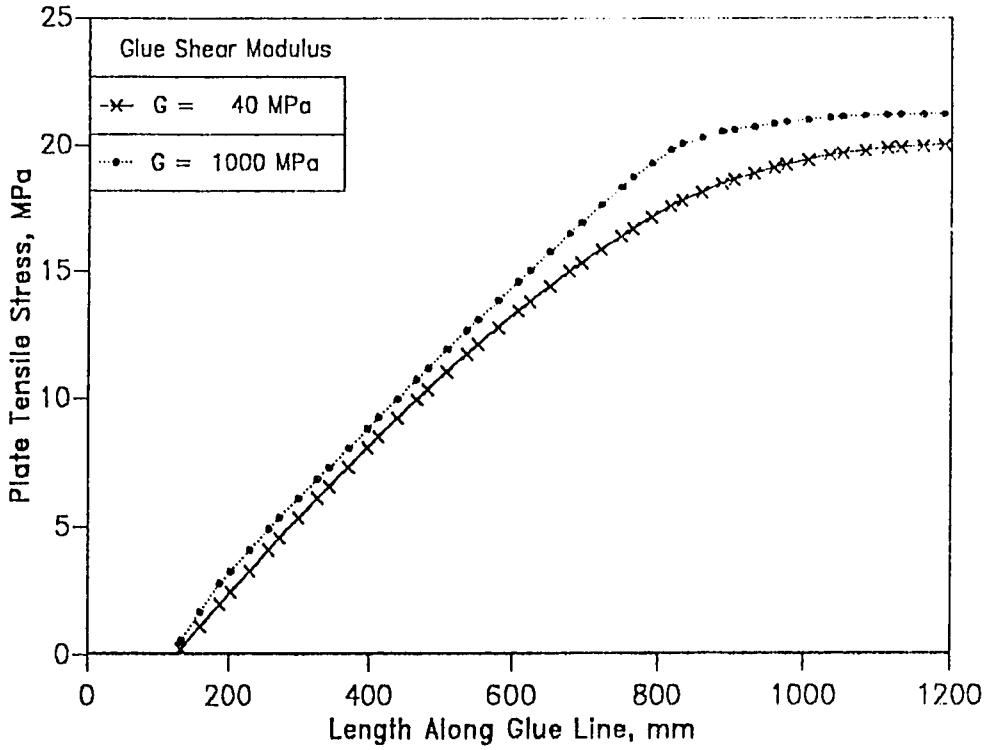

Figure 8.23: Effect of the glue shear modulus on the normal tensile stress in the external plate

Chapter 9

Design Guidelines

9.1 Introduction

In this chapter a procedure for the design of external plates to be bonded to RC beams for purposes of strengthening or repair is presented. The derivation of the suggested design procedure makes use of

- the results of the study of the effect of various geometric and material parameters on the structural response of a plated beam as carried out in chapter 8.
- strength of material formulae for the determination of interface stresses presented in chapter 2 particularly equation 2.18 due to Jones, Swamy and Charif [18] and equations 2.38 and 2.39 due to Roberts [25].
- the results of more numerical experiments in which the effect of the concrete compressive strength f_c' was taken into account.
- surveys of experimental data availabe in the literature with the aim of obtaining an expression for estimating the shear capacity of plated RC beams.

Rational design of external plates to be bonded to undereinforced RC beams, adequately reinforced in shear, hinges on the relative plate thickness where for thin plates, failure of the beam is dominated by extensive flexural concrete cracking, yielding of internal reinforcement and external plate, and crushing of concrete in the compression zone. In this case, the design can be based on strain compatibility and the use of a rectangular compression stress block similar to the ACI method for RC beams in flexure.

As the plate thickness increases however, the interface stresses at the plate curtailment zone increase and if the allowable strength values for the interface are exceeded, the plate may separate resulting in premature failure. If the bonding adhesive is weak or if the gluing is not properly done, this type of failure may be characterized by plate debonding initially emanating from the plate curtailment. As the plate debonding proceeds away from the support and as the effective plate length is reduced, the peak peeling stresses progressively increase (see section 8.7) till such a value that a shear critical crack develops leading to sudden failure (see Figure 9.1a).

If the glueing is strong enough so as to prevent plate debonding, cracking emanates from the location of plate curtailment. The existence of peak peeling and shear stresses at the plate curtailment zone in addition to the bending stress results in a biaxial tensile stress state forcing the crack to move in essentially horizontal direction just below the level of internal reinforcement where the section is weakest. Failure ensues when the moving horizontal crack joins an existing shear flexural crack, culminating in a steep vertical ascent towards the point of loading (see Figure 9.1b).

To determine the external plate thickness sufficient to strengthen or repair an RC beam therefore, the design procedure should consist of three steps namely:

Step I: The plated beam should be designed for flexure assuming plate yielding and concrete crushing on the compression

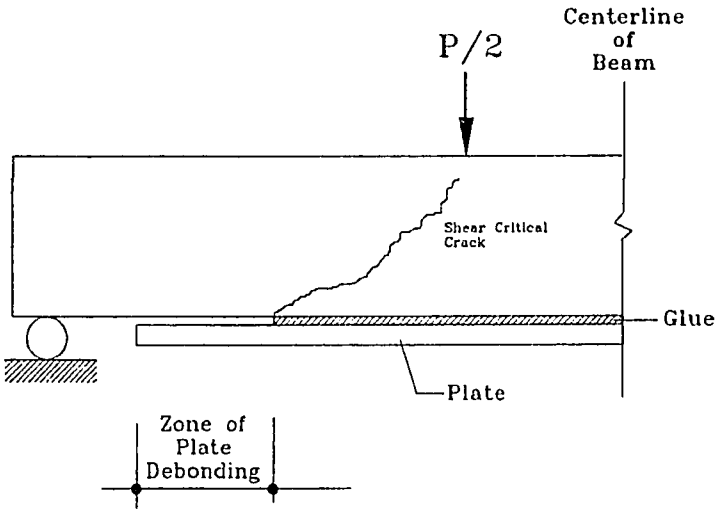

(a). Failure by plate debonding

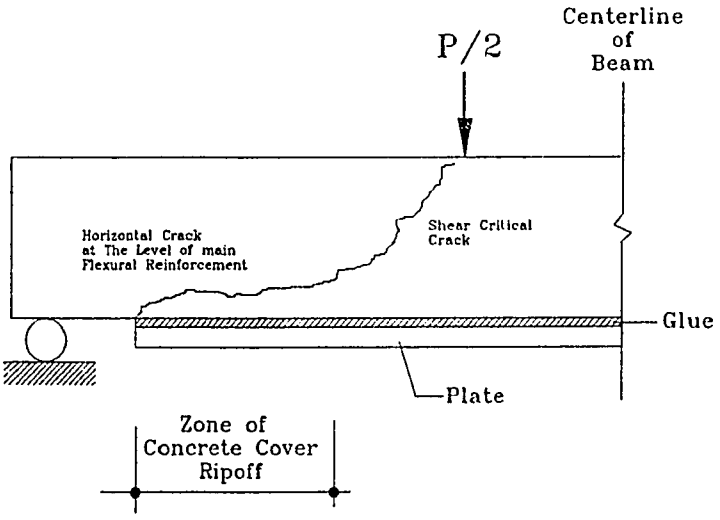

(b). Failure by ripping off
of the concrete cover

Figure 9.1: Sudden shear failures of plated beams.

side.

Step II: The interface stresses must be checked to ensure they are within limits to avoid plate debonding.

Step III: The shear capacity of the plated beam must be checked to safeguard the beam against sudden failure due to concrete cover rip-off.

9.2 Beams Analyzed

The geometry of beams analyzed in this part of the thesis are identical to those shown in Figure 7.1 and the beam designations as well as the parameters varied are shown in Table 9.1. The material parameter values used in the analysis are detailed as below.

Concrete:

1. $f_c' = 25$ MPa

   $E_c = 23500$ MPa (see equation 3.13), $f_t' = 2.77$ MPa (see equation 3.36) and $\alpha = 0.30$ (from Figure 3.4)

2. $f_c' = 45$ MPa

   $E_c = 29171$ MPa, $f_t' = 4.10$ MPa and $\alpha = 0.23$

3. $f_c' = 60$ MPa

   $E_c = 32617$ MPa, $f_t' = 4.96$ MPa and $\alpha = 0.16$

4. For all concrete strengths

   $\nu_c = 0.15$, $\varepsilon_u = 0.0035$, $\varepsilon_m = 0.002$ and $\phi = 37°$.

Internal Steel: $E_s = 200$ GPa, $\sigma_y = 414$ MPa, $\rho = 0.5\rho_b$ and $H' = 200$ MPa.

Concrete Strength MPa	*Distance from Support to Plate Cutoff*	*Beam Designations* Plate thickness, t_p			
f'_c	a	t_p = 1 mm	t_p = 3 mm	t_p = 5 mm	t_p = 10 mm
25	50	S25-1-1	S25-1-3	S25-1-5	S25-1-10
	120	S25-1a-1	S25-2-3	S25-2-5	S25-2-10
	260	S25-2-1	S25-3-3	S25-3-5	S25-3-10
	470	S25-3-1	S25-4-3	S25-4-5	S25-4-10
	680	S25-4-1	—	—	—
45	50	S45-1-1	S45-1-3	S45-1-5	S45-1-10
	120	S45-2-1	S45-2-3	S45-2-5	S45-2-10
	260	S45-3-1	S45-3-3	S45-3-5	S45-3-10
	470	S45-4-1	S45-4-3	S45-4-5	S45-4-10
60	50	S60-1-1	S60-1-3	S60-1-5	S60-1-10
	120	S60-2-1	S60-2-3	S60-2-5	S60-2-10
	260	S60-3-1	S60-3-3	S60-3-5	S60-3-10
	470	S60-4-1	S60-4-3	S60-4-5	S60-4-10

Table 9.1: Parameters varied in the study used to derive the peak interface stress formulae.

External Steel Plate: $E_p = 200$ GPa, $\sigma_y = 269$ MPa, $\nu = 0.30$ and $H' = 200$ MPa.

Concrete/Glue/Steel Interface: (see sections 3.4) $E_i = 278.9$ MPa, $G_i = 120.2$ MPa, $c = \infty$, $f_{ti} = \infty$ and $\nu_i = 0.15$

Steel/Concrete Bond: (see section 3.4.2) $E_b = 2784$ MPa, $G_b = 1200$ MPa, $\nu_b = 0.16$, $\tau_{bond} = 7.5$ MPa, $f_{tb} = 2.77$ MPa ($f_c' = 25$ MPa), $f_{tb} = 4.10$ MPa ($f_c' = 45$ MPa) and $f_{tb} = 4.96$ MPa ($f_c' = 60$ MPa),

Since the study was aimed at evaluating the interface stresses at all load levels, premature interface failure was prevented by setting the shear interface cohesion constant at a very high value. The beams are loaded monotonically in increments of 3 kN which are reduced to 0.25 kN near the ultimate load levels.

9.3 Comparison of Ultimate Numerical and Theoretical Flexural Loads

Tables 9.2, 9.3 and 9.4 show the ultimate loads numerically obtained for beams studied in this part of the thesis (see Table 9.1). The theoretical load values shown in the table are calculated assuming a flexural mode of failure (see section 9.6.1, equations 9.10 and 9.11). Since the coefficient of interface shear cohesion was taken as ∞, the numerical ultimate load values indicated for interface failure correspond to the load instant at which the combination of interface shear and transverse normal stresses satisfied equation 5.2 with critical values of cohesion $c = 5.36$ MPa and angle of internal friction $\phi = 28°$. The results do confirm that for beams where failure is governed by yielding of steel, the ultimate loads can be accurately determined using flexural formulae based on strain compatibility.

Beam	*Ultimate Loads*		*Failure Mechanism*
	Numerical	Theoretical	
S25-1-1	27.75	26.98	Steel Yielding
S25-1-3	41.00	40.84	Steel Yielding
S25-1-5	53.00	52.38	Steel Yielding
S25-1-10	54	71.03	Interface Failure
S25-1a-1	27.75	26.98	Steel Yielding
S25-2-3	41.25	40.84	Steel Yielding
S25-2-5	44.00	52.38	Interface Failure
S25-2-10	42.00	71.03	Interface Failure
S25-2-1	27.75	26.98	Steel Yielding
S25-3-3	32.00	40.84	Interface Failure
S25-3-5	30.00	52.38	Interface Failure
S25-3-10	28.00	71.03	Interface Failure
S25-3-1	27.75	26.98	Steel Yielding
S25-4-3	22.00	40.84	Interface Failure
S25-4-5	20.00	52.38	Interface Failure
S25-4-10	18.00	71.03	Interface Failure
S25-4-1	22.00	26.98	Interface Failure

Table 9.2: Ultimate loads for $f_c' = 25$ MPa

Beam	*Ultimate Loads*		*Failure Mechanism*
	Numerical	Theoretical	
S45-1-1	42.50	42.48	Steel Yielding
S45-1-3	57.25	57.48	Steel Yielding
S45-1-5	68.00	71.31	Interface Failure
S45-1-10	69.00	100.7	Interface Failure
S45-2-1	43.00	42.48	Steel Yielding
S45-2-3	57.50	57.48	Steel Yielding
S45-2-5	57.00	71.38	Interface Failure
S45-2-10	51.00	100.7	Interface Failure
S45-3-1	43.00	42.48	Steel Yielding
S45-3-3	42.00	57.48	Interface Failure
S45-3-5	39.00	71.31	Interface Failure
S45-3-10	36.00	100.7	Interface Failure
S45-4-1	43.00	42.48	Steel Yielding
S45-4-3	30.00	57.48	Interface Failure
S45-4-5	27.00	71.73	Interface Failure
S45-4-10	24.00	100.7	Interface Failure

Table 9.3: Ultimate loads for $f_c' = 45$ MPa

Beam	*Ultimate Loads*		*Failure Mechanism*
	Numerical	Theoretical	
S60-1-1	54.50	54.01	Steel Yielding
S60-1-3	68.00	69.39	Steel Yielding
S60-1-5	77.00	83.93	Interface Failure
S60-1-10	75.00	116.7	Interface Failure
S60-2-1	54.75	54.01	Steel Yielding
S60-2-3	67.25	69.39	Interface Failure
S60-2-5	57.00	83.93	Interface Failure
S60-2-10	54.00	116.7	Interface Failure
S60-3-1	54.75	54.01	Interface Failure
S60-3-3	48.00	69.39	Interface Failure
S60-3-5	42.00	83.93	Interface Failure
S60-3-10	39.00	116.7	Interface Failure
S60-4-1	54.50	54.01	Steel Yielding
S60-4-3	33.00	69.39	Interface Failure
S60-4-5	30.00	83.93	Interface Failure
S60-4-10	27.00	116.7	Interface Failure

Table 9.4: Ultimate loads for $f_c' = 60$ MPa

9.4 Evaluation of Interface Stresses

In the following two sections, new expressions for interface shear and peeling stresses are proposed utilizing data made available from the numerical experimentation and retaining the form as given by Roberts[25] based on a strength of materials model. The suggested expressions include the effect of material non-linearities, especially cracking of concrete, and also the influence of concrete compressive strength f_c'.

9.4.1 Comparison with Roberts Formula

Equations 2.38 and 2.39 presented by Roberts [25] and whose derivation is detailed in section 2.2.3.2 are in this section compared with the data obtained from the numerical experiments for the beams stated in Table 9.1. Four beams have been selected for comparison purposes namely S45-1-1, S45-4-1, S45-1-10 and S45-4-10.

Figures 9.2 and 9.3 show the comparison between the Roberts interface shear stress formula and the results from the numerical model for 1 mm plated beam with curtailment length of 50 mm and 470 mm from the support, respectively. Similarly, corresponding results for the 10 mm plated beams are shown in Figures 9.4 and 9.5.

The Roberts formula for estimating the interface stresses is found to be quite conservative for very thin plates, but does underestimate the stresses for thicker plates. This fact was also mentioned in the paper by Roberts [25] and the problem was overcome by multiplying the computed stress values by a factor approximately equal to 30%. The deviation of the numerical solution from the Roberts formula is attributed to the material non-linearities, particularly cracking occurring near the zone of plate curtailment. This phenomenon cannot be picked up by the Roberts solution by virtue of it being derived from a linear elastic model. In the next section, using the

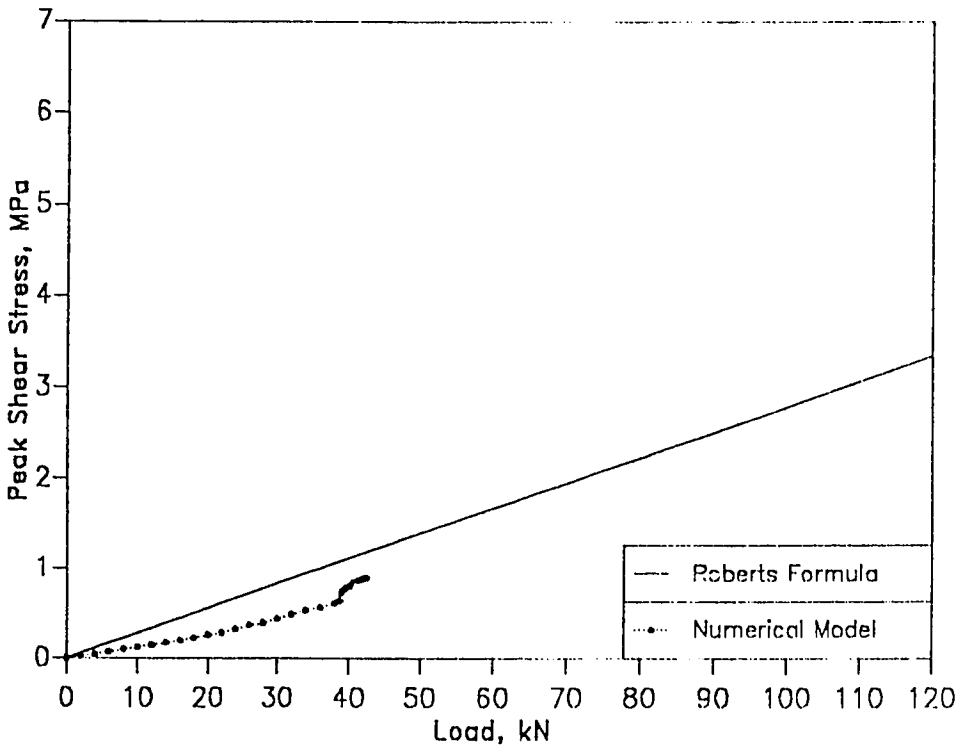

Figure 9.2: Comparison of the peak shear interface stresses with the Roberts formula: 1 mm plate, $a = 50$ mm

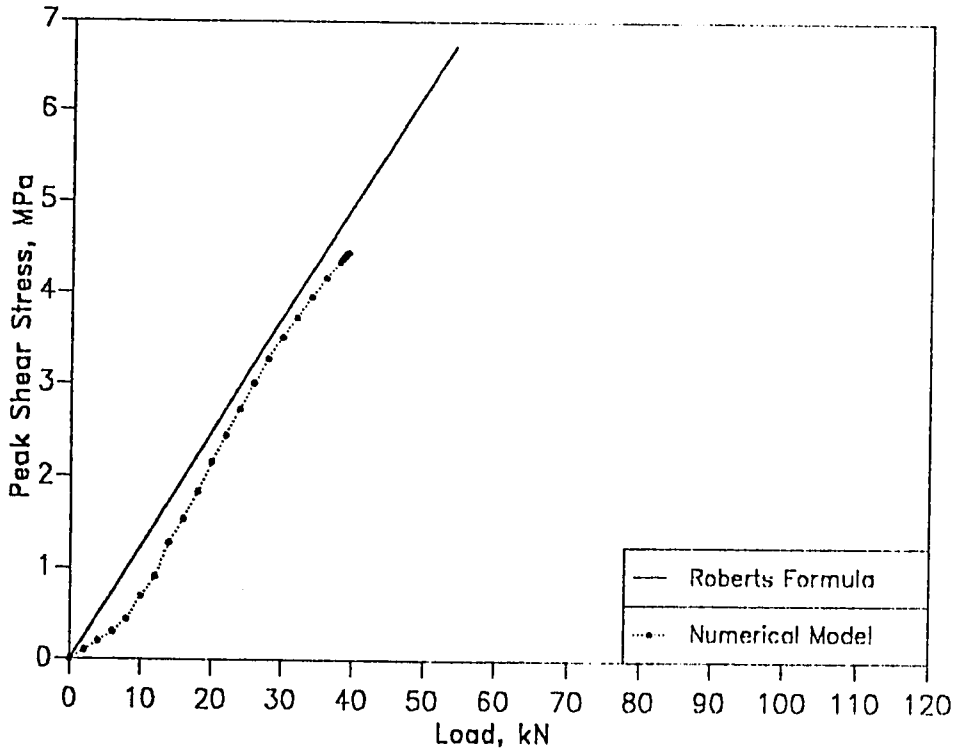

Figure 9.3: Comparison of the peak shear interface stresses with the Roberts formula: 1 mm plate, $a = 470$ mm

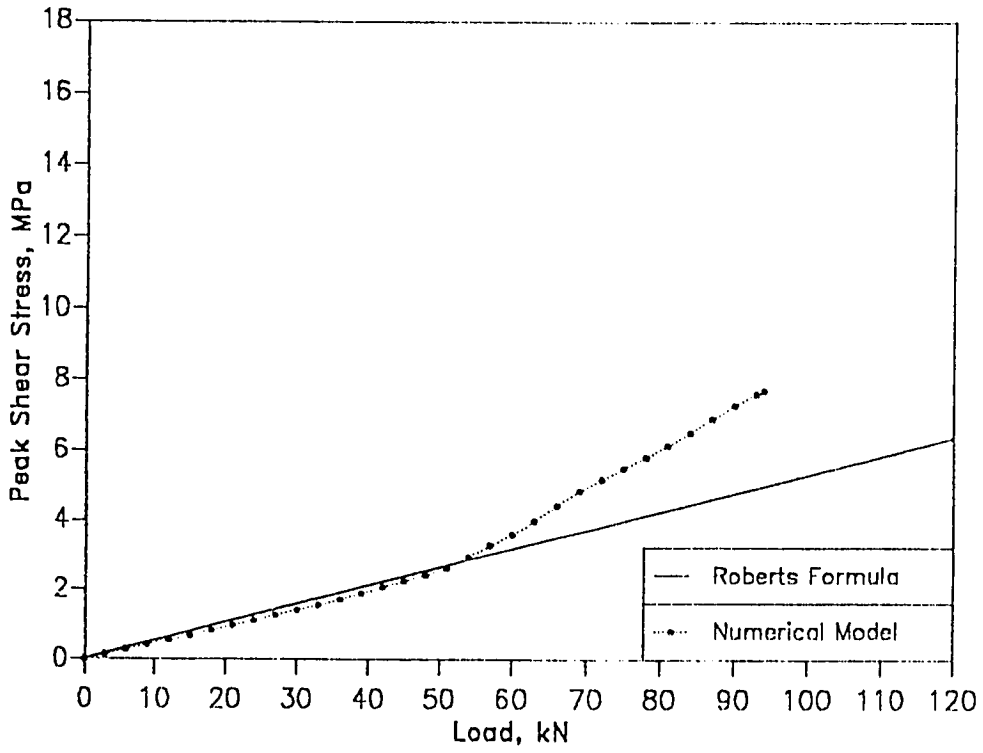

Figure 9.4: Comparison of the peak shear interface stresses with the Roberts formula: 10 mm plate, $a = 50$ mm

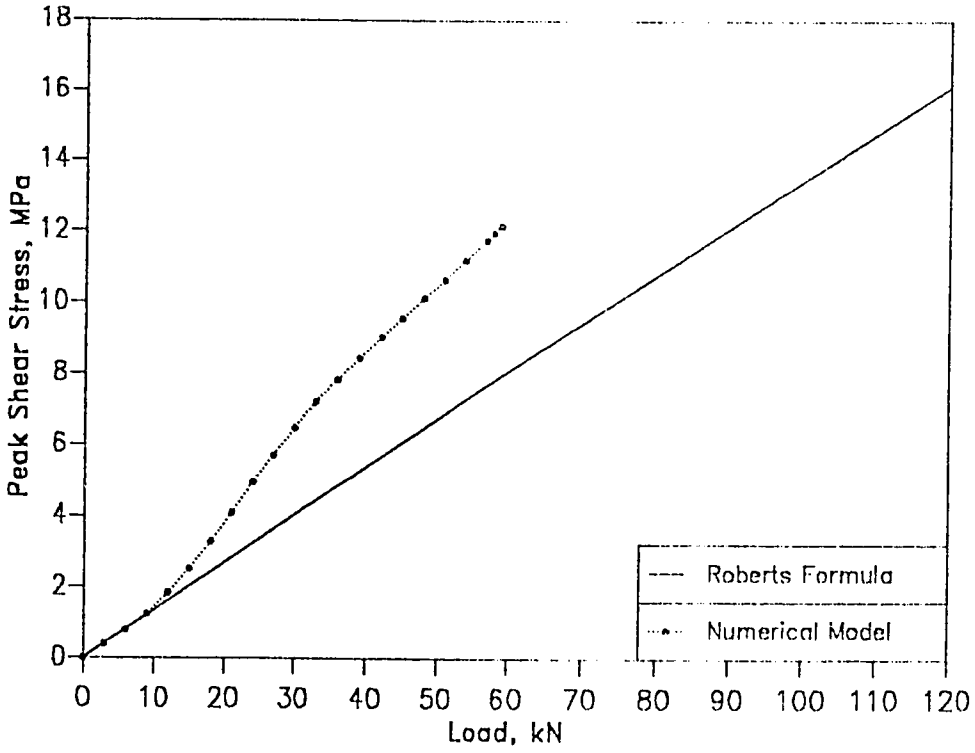

Figure 9.5: Comparison of the peak shear interface stresses with the Roberts formula: 10 mm plate, $a = 470$ mm

regression of extensive numerical results, the Roberts formula is modified.

9.4.2 Suggested Interface Stress Formulae

Figures 9.6, 9.7 and 9.8 respectively show the peak interface shear stress (τ_0) obtained from the numerical model, plotted against $C_{R1}V_o$ (equation 9.18) for concrete strengths f_c' equal to 25, 45 and 60 MPa, respectively, where the factor C_{R1} is calculated using equation 9.19. Each figure includes data for all beam specimens listed in Table 9.1 and corresponding to the specified concrete strengths f_c'

The results from the figures indicate that the deviation from the Roberts formula becomes more pronounced as the concrete compressive strength is lowered. This confirms the supposition that the concrete cracking near the plate curtailment zone plays an important role in the non-linear behavior of the shear stresses. The non-linearity is thus more pronounced for lower concrete strengths since cracking is more extensive.

Data from the three Figures (9.6, 9.7 and 9.8) is combined into one chart resulting in Figure 9.9 where an upper bound regressed equation for the peak interface shear stresses is give by

$$\tau_0 = \alpha_1 f_t' \left(\frac{C_{R1} V_0}{f_c'} \right)^{\frac{5}{4}} \tag{9.1}$$

where

$\alpha_1 = 35$ is regression coefficient

f_t' is the tensile strength in MPa, of concrete and

V_0 is the global shear force in Newtons, at the location of plate cutoff.

Using data from all the beams outlined in Table 9.1, Figure 9.10 depicts the plot of peak transverse normal stress σ_0 obtained from the numerical

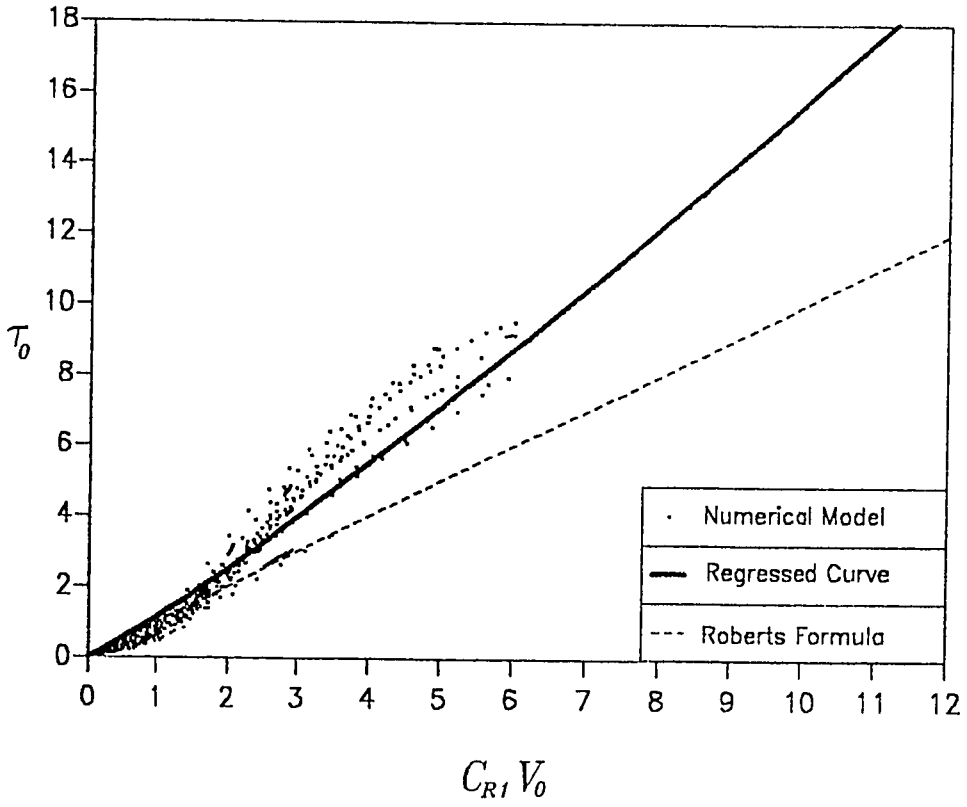

Figure 9.6: Peak interface shear stress for $f_c' = 25$ MPa

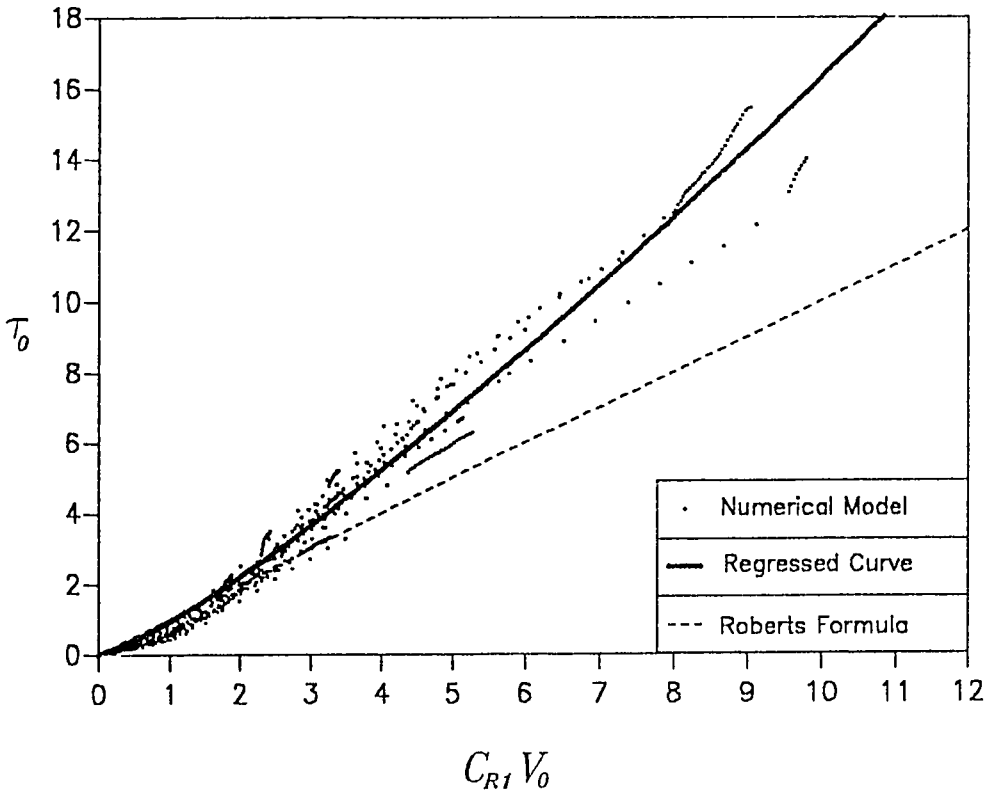

Figure 9.7: Peak interface shear stress for $f_c' = 45$ MPa

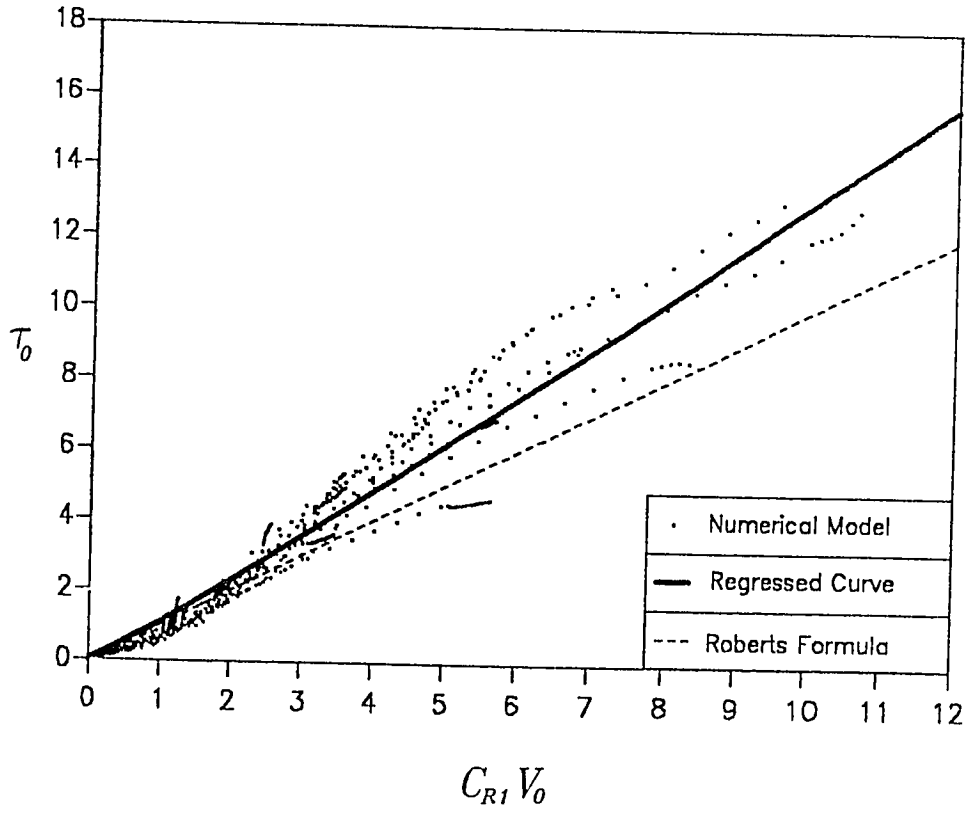

Figure 9.8: Peak interface shear stress for $f_c' = 60$ MPa

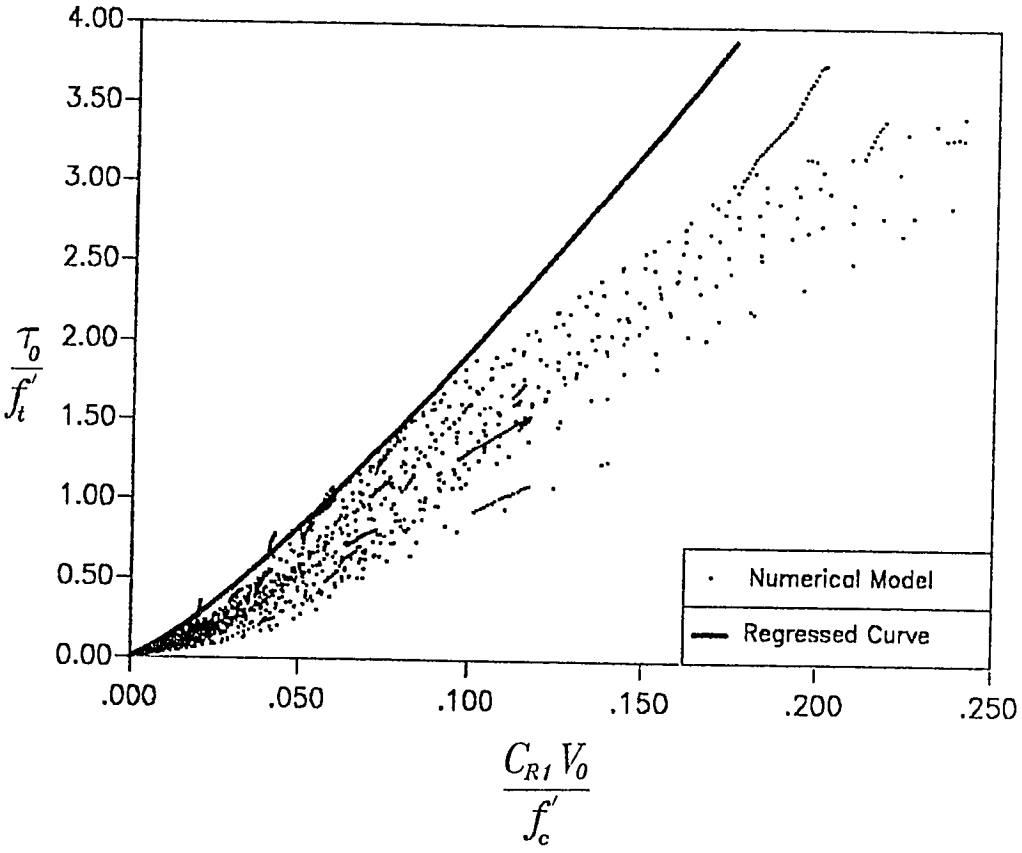

Figure 9.9: Regression curve for the determination of the peak interface shear stress

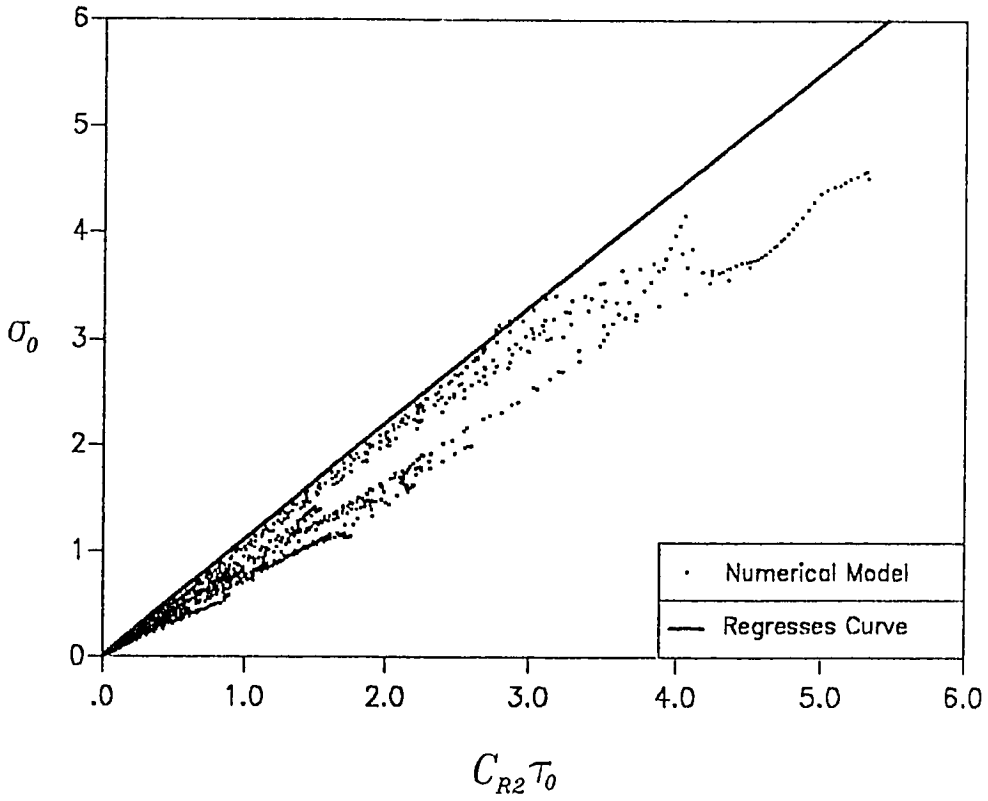

Figure 9.10: Regression curve for the determination of the peak interface transverse normal stress

model, against $C_{R2}\bar{\tau}_0$ (equation 9.25) where the factor C_{R2} is defined in equation 9.26. Regression of the data results in the following predictor equation

$$\sigma_0 = \alpha_2 C_{R2} \tau_0 \tag{9.2}$$

where

$\alpha_2 = 1.10$ is a regression coefficient.

Equations 9.1 and 9.2 may be used to calculate the interface peak stresses. Their use is detailed in section 9.6.2 with a design example explained in section 9.7.

9.5 Shear Capacity of Plated Beams

A novel feature in plated R/C beams is the development of transverse normal stress or peeling stress, along with a high shear stress, at the level of concrete/glue/steel interface, and under certain conditions of plate geometry. This leads to a type of failure not present in unplated R/C beams. This failure is referred to as a shear failure, or more appropriately, a concrete cover rip-off failure.

This sectionr surveys experimental evidence that has been made available in literature over the last ten years, and notes that the cracking pattern in shear failure of plated R/C beams is not identical to the corresponding case for unplated R/C beams. In some cases, the cracking pattern virtually renders all stirrups redundant, leading to a drastically reduced load capacity of the beam in the form of a highly brittle, premature failure. Inasmuch as the ACI expression for determination of shear strength of unplated R/C beams is based on a certain crack profile, it becomes necessary to develop an alternate form to allow for rational design of plated R/C beams.

9.5.1 Survey of Experimental Results

The experimental work surveyed in this paper include those from Ref. [16, 14,4,15,28], with the geometrical and material parameters being summarized in Table 9.5, with symbols referred to in Fig. 9.11. All beams were tested as simply supported either under four-point or three-point loading. The total number of test data included is 26 R/C beams, representing a wide range of cross-section, plate thickness, internal main reinforcement, stirrup spacing, concrete strength and yield strength of reinforcement.

The reported failure loads (P_{expt}) and the accompanying modes of failure are given in Table 9.6. The failure modes are annotated as flexure, flexure/shear and shear. The flexure/shear failure refers to a hybrid mode of failure where there is yielding of internal reinforcement and external plate prior to failure, but failure is precipitated by the horizontal tearing of concrete cover below the level of internal reinforcement [15]. Shear failure (or referred to as shearbond in Ref. [15]) essentially describes a premature, highly brittle failure in the form of shearing off of the concrete along the level of the internal reinforcement with no evidence of debonding of interface prior to failure. In addition, there is no yielding of either the main reinforcement or the steel plate.

Also included in Table 9.6 is the load corresponding to a flexural mode of failure (P_{flex}), and obtained using the ACI strength method

$$\begin{aligned} P_{flex} &= 2\frac{M_u}{L} \\ M_u &= A_s f_{ys}\left(d_s - \frac{a}{2}\right) + d_p b_p f_{yp}\left(h_p - \frac{a}{2}\right) \\ a &= \frac{A_s f_{ys} + b_p d_p f_{yp}}{0.85 f'_c b_c} \end{aligned} \tag{9.3}$$

In order to check on the shear capacity of the plated R/C beams, the

Series of Experiments		Geometrical Parameters									Material Parameters					
		L/a mm/mm	b_c mm	h_c mm	d mm	b_p mm	L_c mm	t_p mm	A_s mm^2	A_{st}/s mm^2/mm	f'_c MPa	f_y MPa	f_{yst} MPa	f_{yp} MPa	E_c kN/mm^2	E_s kN/mm^2
Ref 16	C3, C5, C7, C16	1100/550	100	150	125	80	50	1.6	100.5	56.5/100	74.4	490	410	175	40	200
	C11	1100/250	100	150	125	80	50	1.6	100.5	56.5/100	74.4	490	410	175	40	200
	C12	1100/365	100	150	125	80	50	1.6	100.5	56.5/100	74.4	490	410	175	40	200
Ref 14	URB2	2250/750	100	150	130	80	50	1.5	157	56.5/70	53.9	530	410	210.6	35.8	192
	URB3	2250/750	100	150	130	80	50	3.0	157	56.5/70	82.8	530	410	263	44.4	198
	URB4	2250/750	100	150	130	80	50	5.0	157	56.5/70	53.9	530	410	217.5	35.8	200
	URB5	2250/750	100	150	130	80	50	10.0	157	56.5/70	53.9	530	410	240	35.8	200
Ref 4	F11	2300/767	155	255	220	125	50	1.5	942	56.5/75	45.3	430	324	246	32	200
	F31	2300/767	155	255	220	125	50	6.0	942	56.5/75	46.3	432	324	291	32	200
Ref 15	203, 207, 216	2300/767	155	255	220	125	50	1.5	942	56.5/75	57.8	470	250	236	36	200
	204, 208, 217	2300/767	155	255	220	125	50	3.0	942	56.5/75	57.8	470	250	258	36	200
	205, 209, 218	2300/767	155	255	220	125	50	6.0	942	56.5/75	57.8	470	250	248	36	200
Ref 28	B1	1200/400	150	150	120	100	50	3.0	157	56.5/60	37.7	414	414	276	27.3	200
	FRB2	1200/400	150	150	120	100	50	1.0	157	56.5/60	37.7	414	414	276	27.3	200
	FRB5	1200/400	150	150	120	100	50	2.0	157	56.5/60	37.7	414	414	276	27.3	200
	B10	1200/400	150	150	120	100	50	1.5	157	56.5/60	37.7	414	414	276	27.3	200
	MF1	1200/400	150	150	120	100	50	3.0	226	56.5/60	39.9	414	414	269	27.8	200

Table 9.5: Geometry and Material Description of Beams Surveyed

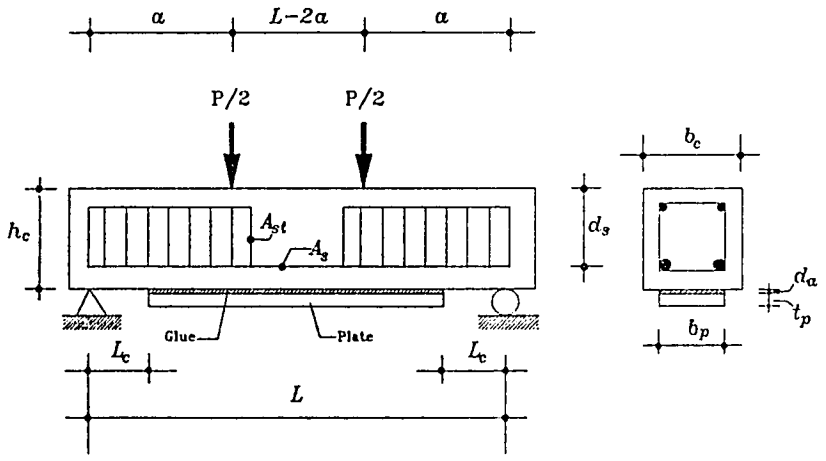

Figure 9.11: Typical R/C beam strengthened externally by plate

following quantities were computed:

$$V_c = \frac{1}{6}\left(\sqrt{f'_c} + 100\rho_w\right) b_c d_s$$

$$V_s = \frac{A_v f_{yst} d_s}{s}$$

$$V_u = 0.5\, P_{expt} \tag{9.4}$$

To check the efficiency of the stirrups associated with the crack resulting from concrete rip off failure at or below the level of reinforcement prior to a steep ascent to the point of loading, the quantity k_{SF}, defined as:

$$k_{SF} = (0.5\, P_{expt} - V_c)\,/V_s \tag{9.5}$$

was computed only for those beams identified to have failed in shear or flexure/shear. From the values listed in Table 9.6, it is very interesting to note that for specimen MF1, $k_{SF} = 0.0$, implying no participation of stirrups in resisting the concrete rip off failure. For beams yielding $k_{SF} > 1.0$, the implication is that the ACI shear strength for such beams could be conservative. However, for those beams with $k_{SF} < 1.0$, it becomes apparent that a modified expression should be made available to the designers to estimate the shear capacity of plated R/C beams.

9.5.2 Proposed Expression for Shear Capacity

As a first step, it is essential to identify what factors make the beam more vulnerable to a rip-off failure. It is likely that the horizontal cracking is precipitated by the biaxial tension field induced at the location of plate curtailment due to creation of the transverse normal stress or more popularly known as the peeling stress. The peeling stress can be approximated

by [25]

$$\sigma_0 = \left\{ \left[1 + \left(\frac{K_s}{E_p b_p d_p} \right)^{0.5} L_c \right] \frac{b_p d_p}{I b_a} (h_p - h) \right\} d_p \left[\frac{K_n}{4 E_p I_p} \right]^{0.25} V_0 \qquad (9.6)$$

where

$K_s = G_a \frac{b_a}{d_a}$ is the shear stiffness of the interface layer and

G_a, b_a and d_a are respectively the shear modulus, width and depth of the adhesive,

$L_c = M_0/V_0$ at plate cutoff location,

M_0, V_0 are the moment and shear force at the location of plate cutoff,

E_p is the elastic modulus of the plate,

b_p, d_p is the width and thickness of the external plate,

h_p is the distance from top of beam to center of plate,

h is the distance from top of beam to the neutral axis of the equivalent transformed steel section,

I is the second moment of area of the equivalent transformed steel section about the neutral axis for a cracked section,

I_p is the second moment of inertia of the external plate about its own centroid,

$K_n = E_a \frac{b_a}{d_a}$ normal stiffness of the interface layer and

E_a the elastic modulus of the adhesive.

Using the abbreviations

$$C_{R1} = \left[1 + \left(\frac{K_s}{E_p b_p d_p}\right)^{0.5} L_c\right] \frac{b_p d_p}{I b_a}(h_p - h)$$

$$C_{R2} = d_p \left[\frac{K_n}{4 E_p I_p}\right]^{0.25} \tag{9.7}$$

two figures have been plotted. Fig. 9.12 is a plot of the ratio P_{expt}/P_{flex} vs. $\frac{1000\, A_s\, C_{R1}\, C_{R2}}{(a/d)}$ where A_s is the amount of internal steel, a the distance from support to the loaded point and d the effective depth of the concrete section; whereas Fig. 9.13 is a plot of k_{SF} vs. $C_{R1}\, C_{R2} * 10^6$. Fig. 9.12 depicts P_{expt}/P_{flex} for all beams surveyed, and there appears to be zones in which either flexural failure is most likely or where shear failure is the more probable. Naturally, there is also a transition zone. The results of Fig. 9.13 portray an interesting trend, with k_{SF} showing great sensitivity to the $C_{R1}\, C_{R2}$ parameter. One may recall that k_{SF} has only been computed for those beams reported to have failed in shear or flexure/shear as evidenced by concrete cover rip-off. The variation of k_{SF} has been captured as an experimentally decaying function

$$k = 2.4\, e^{-0.08 C_{R1}\, C_{R2} * 10^6} \tag{9.8}$$

Using this predictor equation, the factor k has been computed for all the beams and reported in Table 9.6. Based on k, P_{shear} has been calculated for all the beams surveyed as

$$V_u = \frac{P_{shear}}{2} = V_c + k\, V_s \tag{9.9}$$

where V_c and V_s are as defined in equation 9.4. The results of Table 9.6 can now be interpreted from a design point of view. In order to carry out a rational design of a plated R/C beam, one carries out the following checks:

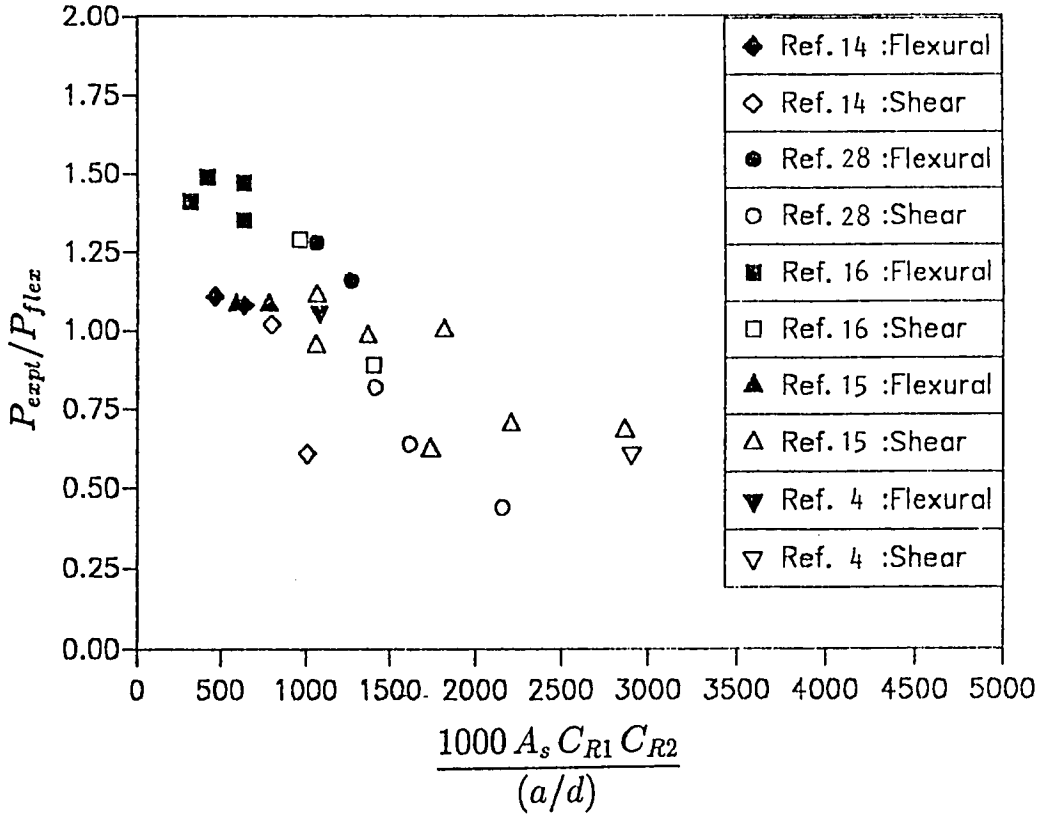

Figure 9.12: Failure Loads and Modes for Plated Beams Surveyed

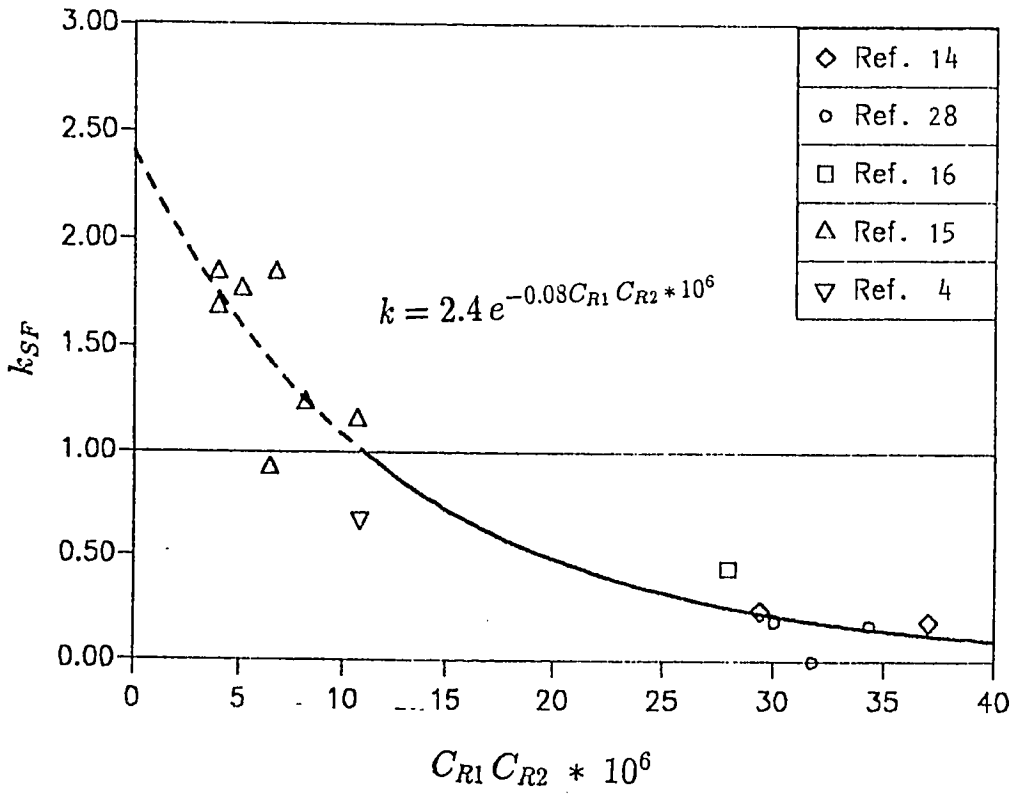

Figure 9.13: Determination of the stirrup efficiency factor k for plated beams

(i). find P_{flex} based on the ACI strength model

(ii). find P_{shear} based on equation 9.9 and where k is given by equation 9.8.

(iii). actual failure load and mode will be controlled by the lower of the two values $< P_{flex}, P_{shear} >$.

It appears that the magnitude of the peeling stress plays a significant role in the shear capacity of plated R/C beams. For beams with low values of $C_{R1}C_{R2}$, the shear cracking remains similar to the diagonal tension cracking of unplated R/C beams, enabling sufficient number of stirrups to be mobilized to intercept 45° cracking ($k_{SF} \geq 1.0$). However, as $C_{R1}C_{R2}$ increases, the extent of horizontal cracking increases, with the final movement of the crack being quite steep close to the point of loading. Thus, the ACI diagonal tension model developed for unplated R/C beams and which assumes cracks moving across at 45° cannot be directly used for plated R/C beams. For certain beam specimens (see MF1), the load at failure is virtually due only to shear capacity of plain concrete. This can have disastrous consequences in actual practice, where an R/C member reinforced with a plate of sufficient thickness so as to increase $C_{R1}\,C_{R2} * 10^6$ beyond a safe level could fail at a lower load (in an explosive manner) than the capacity of the unplated, originally ductile, R/C beam.

9.6 Design Procedure for Plated Beams

The design is carried out in two stages. The first step of the design ensures that the plate and the internal steel yield to achieve a ductile failure and the second step, the interface peak stresses at location of plate curtailment are checked against allowable values to avoid plate separation.

9.6.1 Step I: Flexural Design

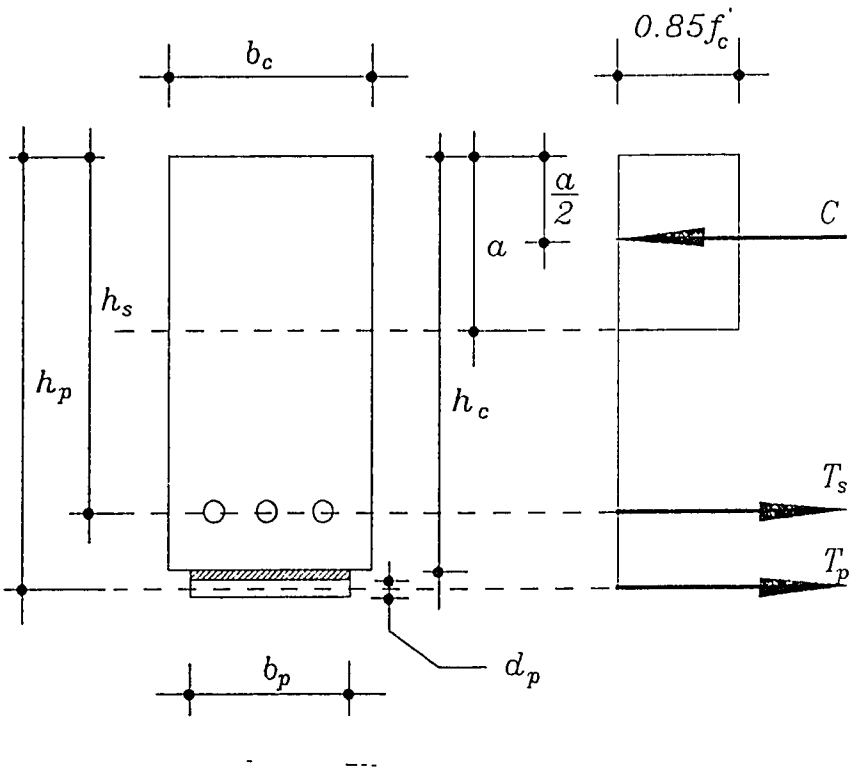

Figure 9.14: Ultimate forces acting on a plated beam section

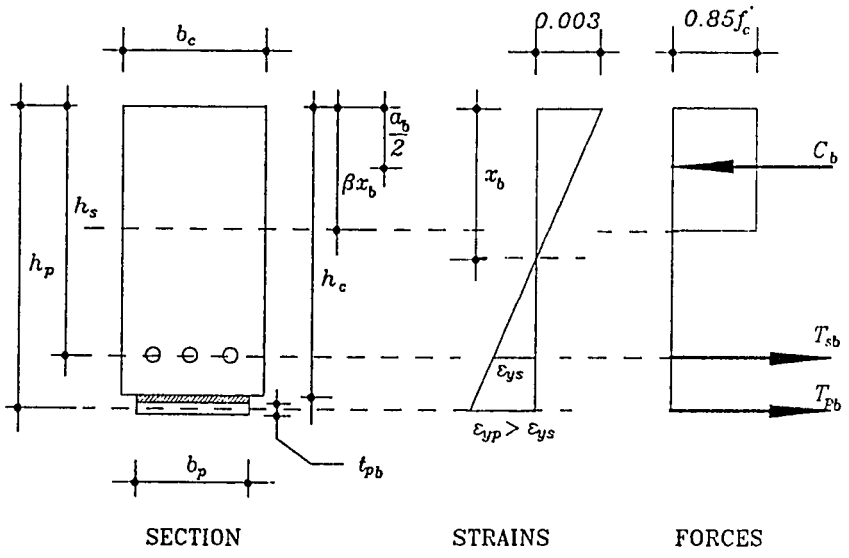

Figure 9.15: Balanced Load Condition

Equilibrium at ultimate load conditions of a plated beam as shown in Figure 9.14 result in

$$T_s\left(d_s - \frac{a}{2}\right) + T_p\left(h_p - \frac{a}{2}\right) = \frac{M_u}{\phi} \tag{9.10}$$

where

$T_s = A_s f_{ys}$ is the force in internal reinforcing steel,

$T_p = A_p f_{yp}$ is the force in external steel plate,

h_p is the distance from top of beam to center of plate,

M_u is the maximum ultimate moment after applying the load factors,

$\phi = 0.9$ is the ACI strength factor in flexure,

A_s is the area of the internal steel,

$A_p = b_p d_p$ is the area of the external plate and

b_p, d_p is the width and thickness of the external plate.

The depth of the concrete rectangular stress block a, in equation 9.10 is given as

$$a = \frac{A_s f_{ys} + b_p d_p f_{yp}}{0.85 f'_c b_c} \tag{9.11}$$

where

f_{ys}, f_{yp} are the yield stresses of the internal reinforcing steel and external plate respectively,

f'_c is the concrete compressive strength and

b_c is the width of the concrete section.

Substituting 9.11 in equation 9.10 results in

$$A_1 d_p^2 + A_2 d_p + A_3 = 0$$

where

$$\begin{aligned} A_1 &= \frac{b_p f_{yp}}{2}\left(1 - \frac{b_p f_{yp}}{0.85 f_c' b_c}\right) \\ A_2 &= b_p f_{yp}\left(h_c + d_c - \frac{A_s f_{ys}}{0.85 f_c' b_c}\right) \\ A_3 &= A_s f_{ys}\left(d_s - \frac{A_s f_{ys}}{2(0.85) f_c' b_c}\right) - \frac{M_u}{\phi} \end{aligned} \tag{9.12}$$

and

d_c is the depth of the concrete section and

d_s the effective depth to the internal steel.

Solving equation 9.12 leads to the formula for the plate thickness as

$$d_p = \frac{-A_2 + \sqrt{A_2^2 - 4A_1 A_3}}{2A_1} \leq t_{pb} \tag{9.13}$$

where t_{pb} is the plate thickness at balanced load conditions and thus the maximum plate thickness to ensure a ductile flexural failure. From Figure 9.15, equilibrium of forces results in

$$C_b = \beta x_b \left(0.85 f_c^{'}\right) b_c = T_{sb} + T_{pb} = A_s f_{ys} + t_{pb} b_p f_{yp} \tag{9.14}$$

leading to

$$t_{pb} = \frac{\beta x_b \left(0.85 f_c^{'}\right) b_c - A_s f_{ys}}{b_p f_{yp}} \tag{9.15}$$

and x_b is found from known strain variation at balanced conditions.

9.6.2 Step II: Plate/Concrete Interface Stresses

In this part of the design process, the stresses at the region of plate cutoff are checked to ensure that plate separation does not occur. The design formulas are presented in such a way that for a given level of allowable coefficient of cohesion of the steel/glue/concrete interface c_{all}, a maximum cutoff distance from the beam support is evaluated. The interface stresses for a given load, in general increase as the plate thickness and its cross-sectional area become larger and so for a given area the minimum thickness is achieved by selecting the largest plate width, which for a plated beam is limited by the concrete beam width.

The interface stresses τ_0, σ_0 at the plate cutoff region are limited to an acceptable level if

$$\tau_0 + \sigma_0 \tan 28^o \leq c_{all} \tag{9.16}$$

where

c_{all} is the allowable coefficient of shear cohesion in MPa, for the epoxy concrete/steel surface.

The peak shear stress τ_0 is given as

$$\tau_0 = \alpha_1 f_t' \left(\frac{C_{R1} V_0}{f_c'} \right)^{\frac{5}{4}} \tag{9.17}$$

where

$\alpha_1 = 35$ is an empirical regression coefficient determined from numerical parametric study undertaken in this work,

f_t' is the tensile strength in MPa, of concrete and

V_0 the global shear force in Newtons, at the location of plate cutoff.

In contrast, using a linear strength of materials model, Roberts [25] suggested the use of the expression to evaluate the peak shear interface stress as

$$\bar{\tau}_0 = C_{R1} V_0 \tag{9.18}$$

where C_{R1} in equations 9.17 and 9.18 is calculated using equation 9.19.

$$C_{R1} = \left(1 + \left[\frac{K_s}{E_p b_p d_p}\right]^{\frac{1}{2}} a^*\right) \frac{b_p d_p}{I b_a}(h_p - h) \tag{9.19}$$

where

$a^* = M_0/V_0$ indicates the location of plate cutoff,

I is the second moment of area of the equivalent transformed steel section about the neutral axis for a cracked section

K_s is the shear stiffness of the interface layer as given in equation 2.21.

The value of a^* is a function of the loading type. For a uniformly distributed load on a simple span,

$$a^* = \frac{La - a^2}{L - 2a} \tag{9.20}$$

where

a distance from the support to the plate cutoff,

L the span.

For a four point loading on a simple span,

$$a^* = a \tag{9.21}$$

For a given level of the load, the shear force at the plate curtailment is also a function of the distance from the support, a. For example the shear force for a uniformly distributed load on a simple span is given as,

$$V_0 = w_s \left(\frac{L}{2} - a\right) \tag{9.22}$$

where

w_s is the uniformly distributed load at service load conditions.

On the other hand, the shear force for a four point loading on a simple span is given simply as,

$$V_0 = \frac{P_s}{2} \tag{9.23}$$

where

P_s is the total load applied on the beam at service load conditions.

The peak peeling stress σ_0 required in the inequality 9.16 is given by

$$\sigma_0 = \alpha_2 C_{R2} \tau_0 \tag{9.24}$$

where

$\alpha_2 = 1.10$ is an empirical regression coefficient determined from numerical parametric study undertaken in this work to obtain a conservative estimate of the peeling stresses.

The expression given by Roberts [25] using the strength of materials for the peeling stress is

$$\bar{\sigma}_0 = C_{R2} \bar{\tau}_0 \tag{9.25}$$

where the factor C_{R2} in equations 9.24 and 9.25 is calculated using equation 9.26.

$$C_{R2} = d_p \left(\frac{K_n}{4 E_p I_p} \right)^{\frac{1}{4}} \tag{9.26}$$

where

I_p the second moment of area of the steel plate about its own centroid and

K_n normal stiffness of the interface layer as given in equation 2.31.

Substitution of the equations 9.17 and 9.24 in equation 9.16 results in an equation which can be solved for $a = a_{max}$, or the maximum distance from the support beyond which, for a given plate thickness and load level, the plate should not be curtailed. For a uniformly distributed load w_s on a simple span, the resulting equation is a cubic in a;

$$\left[1 + \left(\frac{K_s}{E_p b_p d_p}\right)^{\frac{1}{2}} \left(\frac{La - a^2}{L - 2a}\right)\right] w_s \left(\frac{L}{2} - a\right) =$$

$$f_c' \left(\frac{c_{all}}{(1 + \alpha_2 C_{R2} tan28^o)\alpha_1 f_t'}\right)^{\frac{4}{5}} \frac{I b_a}{b_p d_p (h_p - h)} \tag{9.27}$$

Equation 9.27 is best solved on a trial and error basis as shown in the following design example.

For a four point loading the expression for the length to the plate cutoff is much simpler and can be explicitly written as

$$a = \left[\frac{2}{P_s} \frac{I b_a}{b_p d_p (h_p - h)} f_c' \left(\frac{c_{all}}{(1 + \alpha_2 C_{R2} tan28^o)\alpha_1 f_t'}\right)^{\frac{4}{5}} - 1\right] \left(\frac{E_p b_p d_p}{K_s}\right)^{\frac{1}{2}} \tag{9.28}$$

Due to the range of validity of the parametric study done in this work, the maximum cutoff length must satisfy

$$\frac{a_{max}}{h_c} \leq 3.0 \tag{9.29}$$

where

h_c is the depth of the concrete section

9.6.3 Step III: Evaluation of the Shear Capacity of Plated Beams

The shear capacity of plated beams V_{up} can be approximated (in units of N-mm) as

$$
\begin{aligned}
V_{up} &= V_c + kV_s \\
V_c &= \frac{1}{6}\left(\sqrt{f_c'} + 100\rho_w \frac{V_u d}{M_u}\right) b_w d \\
V_s &= \frac{A_v f_{yst} d}{s} \\
k &= 2.4e^n \\
n &= -0.08 C_{R1}\, C_{R2} * 10^6
\end{aligned}
\tag{9.30}
$$

where

f_c' is the concrete strength, MPa,

ρ_w the main steel reinforcement ratio,

$\frac{V_u d}{M_u}$ is taken as 1.0,

b_w, d the width and effective depth of the unplated RC section,

A_v the amount of shear reinforcement,

f_{yst} the stirrup yield strength,

s the stirrup spacing and

C_{R1}, C_{R2} are evaluated using equations 9.19 and 9.26 respectively.

9.7 Design Example

Problem

A simply supported beam spanning 12 m has a section as shown in Figure 9.16 and was originally designed to carry a live load of 18 kN/m and

a dead load of 10 kN/m (not including the beam self weight). It is now required the beam be strengthened to carry an extra live load of 15 kN/m and a superimposed dead load 10 kN/m.

Given that $f_c' = 30$ MPa and $f_{ys} = 414$ MPa, design a plate size needed to carry the extra load. Assume $f_{yp} = 270$ MPa and the allowable coefficient of cohesion for the epoxy glue/steel/concrete interface $c_{all} = 2.68$ MPa. The beam has $\phi 6$ mm stirrups at 75 mm spacing for shear reinforcement.

Solution

The design parameters in this example using units of N–mm are:

Concrete	E_c=25084 MPa, b_c=450 mm, h_c=850 mm, f_c'=30 MPa, f_t'=3.13 MPa
Internal Steel	A_s=5000 mm^2, d_s=800 mm, f_{ys}=414 MPa
Stirrups	A_v=56.5 mm^2, s=75 mm, f_{yst}=250 MPa
Interface Layer	d_a=3 mm, E_a=278.6 MPa, G_a=120.1 MPa, c_{all}=2.68 MPa
External Plate	E_p=200000 MPa, f_{yp}=270 MPa
Beam Span	L=12000 mm

I: Flexural Design

The width of the plate and thus of the interface layer is limited by the size of the concrete section and is recommended that it should be at most 20 mm less than the concrete beam width. So choose

$$b_p = b_a = 450 - 20 = 430 \quad \text{mm}$$

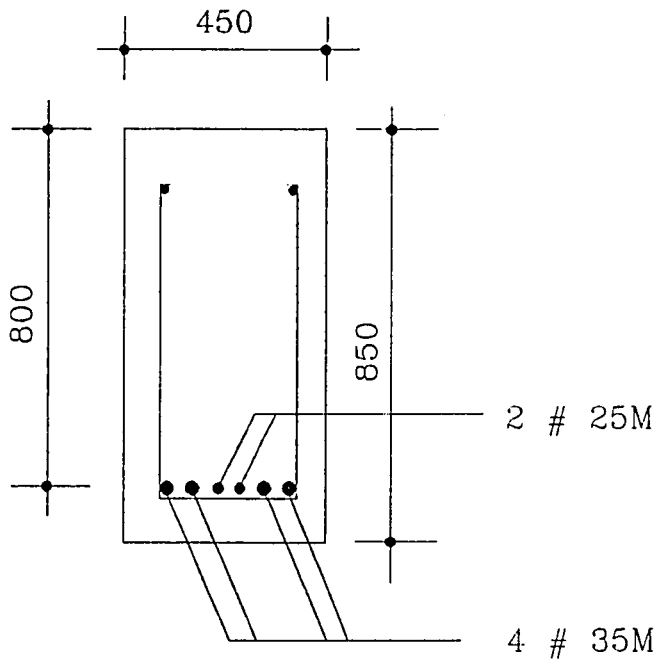

Figure 9.16: Design example

The ultimate load in Newtons per mm length

$$w_u = 1.7(18+15)+1.4[10+10+(850 * 450 * 2.351(10)^{-5})] = 96.7 \quad \text{N/mm}$$

The maximum moment in Nmm

$$M_u = w_u \frac{L^2}{8} = 1740.6 * 10^6 \quad \text{Nmm}$$

Calculate the factors A_i in equation 9.12

$$A_1 = -529279.4$$

$$A_2 = 78089770.6$$

$$A_3 = -464705882.4$$

Use of equations 9.13 and 9.15 result in

$$d_p = 6.213 \leq t_{pb} = 6.5 \quad \text{mm}$$

Use a plate thickness of 6.5 mm with a width of 430 mm.

II: Check Interface Stresses

The service load in Newtons per mm length

$$w_s = (18+15)+[10+10+(850 * 450 * 2.351(10)^{-5})] = 62.0 \quad \text{N/mm}$$

Calculate the depth to the neutral axis of a cracked section of the plated beam [25] as

$$h = \frac{-B+\sqrt{B^2+4AC}}{2A}$$

where

$$A = E_c b_c / 2E_p = 20.2195$$

$$B = A_s + b_p d_p = 7795$$

$$C = h_s A_s + h_p b_p d_p = 6393218.75$$

So

$$h = 357.5 \quad \text{mm}$$

Evaluate the section modulus of the cracked section as

$$I = \frac{E_c b_c h^3}{3E_p} + A_s (h_s - h)^2 + b_p d_p (h_p - h)^2 = 2533871652.5 \quad \text{mm}^4$$

Similarly calculate the section modulus of the external plate about its own centrioid as

$$I_p = \frac{b_p {d_p}^3}{12} = 9840.73 \quad \text{mm}^4$$

Find the shear and normal stiffness of the interface layer as

$$K_s = G_a \frac{b_a}{d_a} = 17214.3 \quad \text{MPa}$$

$$K_n = E_a \frac{b_a}{d_a} = 39932.7 \quad \text{MPa}$$

Using equation 9.26 calculate

$$C_{R2} = 0.3085$$

Substituting the above values in equation 9.27 results in an equation of the form

$$\left(1 + 0.005549 \frac{La - a^2}{L - 2a}\right) w_s \left(\frac{L}{2} - a\right) - 1055102.5 = 0$$

Solving by trial and error

Trial a	*Result*
100	-484588
400	90310
350	-3355
352	407
351.78	-6.25
351.7833	0

So the maximum distance a 6.5 mm thick plate can be curtailed is 352 mm from the support as shown in Figure 9.17.

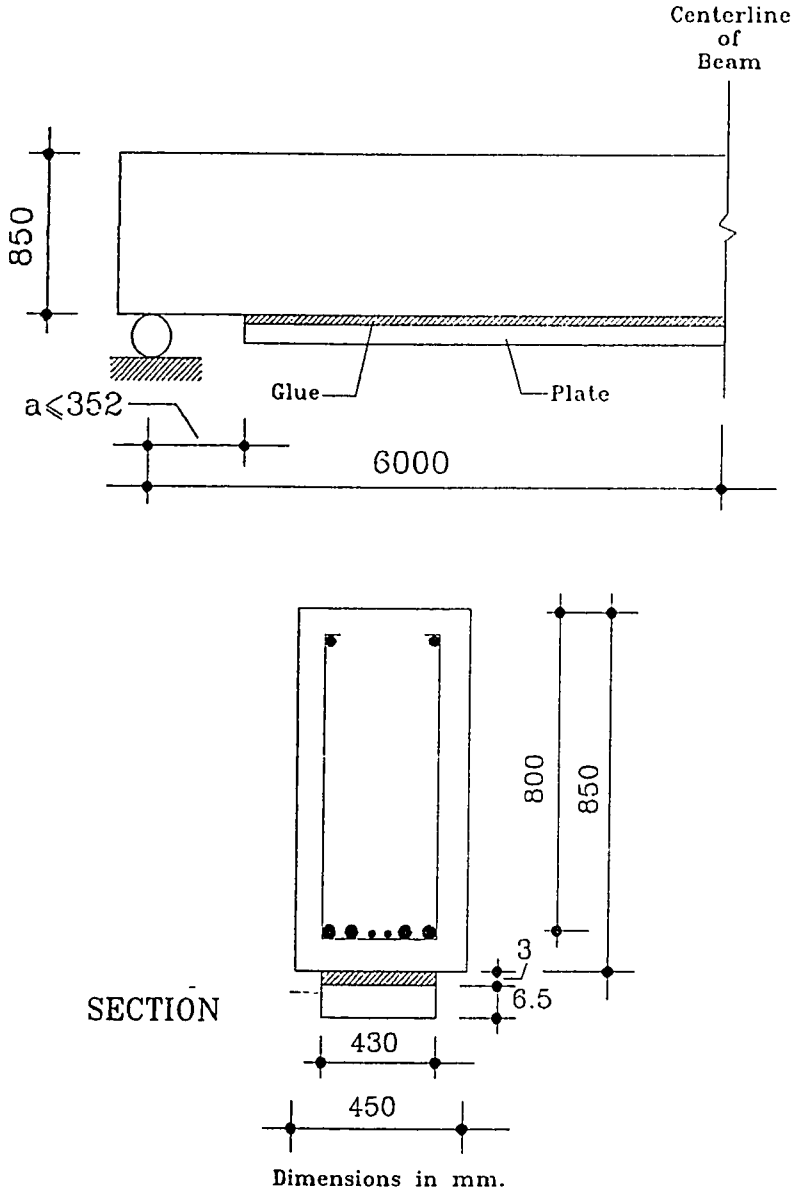

Figure 9.17: Detailing of the plate design example

III: Evaluate the Shear Capacity

From equations 9.19 and 9.26

$$C_{R1} = 3.7786 * 10^{-6}, \quad C_{R2} = 0.3085$$

Using equation 9.30

$$n = -0.09326$$

The coefficient k thus becomes

$$k = 2.4\, e^{-0.09326} = 2.1863$$

The shear capacity for the beam is therefore evaluated as

$$V_c = 412.0 \quad \text{kN}$$

$$V_s = 150.7 \quad \text{kN}$$

$$V_{up} = 412.0 + 2.1863 * 150.7 = 741.4 \quad \text{kN}$$

This is equivalent to a uniformally distributed load

$$w_{up} = 124 > w_u = 96.7 \quad \text{N/mm}$$

confirming the designed plated beam is sufficient in shear.

Beam	k_{SF}	k	P_{shear}	P_{flex}	P_{expt}	Failure Mode
URB2	–	0.61	89.4	36.0	40.0	Flexure
URB3	–	0.36	86.0	50.8	55.0	Flexure
URB4	0.24	0.23	56.7	56.5	57.5	Shear
URB5	0.19	0.12	47.7	87.7	53.1	Shear
B1	0.17	0.15	56.5	90.8	58.0	Shear
B10	–	0.28	68.1	64.5	75.0	Flexure
FRB2	–	0.40	79.1	55.5	71.0	Flexure
FRB5	0.19	0.22	62.4	73.4	60.0	Shear
MF1	0.0	0.19	62.9	102.6	45.0	Shear
C11	0.44	0.26	54.1	73.3	65.0	Shear
C12	0.44	0.26	54.1	50.2	65.0	Shear
C16	–	0.26	54.1	33.3	45.0	Flexure
C3	–	0.26	54.1	33.3	49.0	Flexure
C5	–	0.54	70.6	33.5	50.0	Flexure
C7	–	0.78	84.4	37.2	52.5	Flexure
218	0.92	1.43	236.7	314.3	194.0	Shear
217	1.68	1.75	263.1	270.4	257.0	Flexure/Shear
203	1.84	1.75	262.9	243.1	270.0	Flexure/Shear
207	–	1.90	275.6	243.2	262.0	Flexure
216	–	2.01	284.6	243.6	262.0	Flexure
204	1.84	1.40	234.0	269.2	270.0	Flexure/Shear
208	1.76	1.60	250.2	269.2	264.0	Flexure/Shear
205	1.15	1.03	203.0	312.1	213.0	Shear
209	1.23	1.25	221.3	312.9	220.0	Shear
F11	–	1.74	294.9	218.6	232.0	Flexure
F31	0.68	1.02	217.8	297.6	182.0	Shear

Table 9.6: Evalution of the factors k and k_{SF} for the beams surveyed

Chapter 10

Conclusions

The main conclusions drawn from this study are

1. The new half-beam test setup introduced was shown to be a reliable specimen for measuring of parameters neccessary for the characterization of the steel/glue/concrete interface.

2. Test data in terms of average interface shear stress at failure from the half beam specimen revealed the lack of influence of concrete compressive strength indicating taht the interface failure was a surface phenomenon. This conclusion is contingent upon adoption of normal means of surface preparation.

3. Apparent dichtomy in results obtained in literature regarding shear strength of interface glue has been explained as being a phenomenon influenced by the sense of accompanying transverse normal stress i.e. whether it is tensile (or peeling) or compressive (or bearing). The nature of the transverse normal stresses is shown to be a function of specimen geometry.

4. Data from the half beam specimen and other existing data in literature for characterization of the interface failure has been noted to follow the Mohr-Coulomb constitutive law with a tension cutoff.

5. A nominal decrease in the ultimate capacity of the repaired beam was noted with increasing levels of damage prior to repair.

6. Injudicious selection of plate size may lead to radical change in behavior of RC beam transforming it from a ductile to a brittle mode of failure.

7. Increase in plate thickness leads to increase in the ultimate loads. This phenomenon however is constrained by the limiting condition of failure of the interface.

8. Thicker plates result in higher values of interface stresses at corresponding load levels, making it mandatory that a limit be established for the thickness of a plate for a specific RC beam in order to avoid a premature interface failure.

9. In order to keep the interface stresses to a low level, it is desirable that the external plate be as wide as possible and as thin as is practically feasable.

10. Increased levels of internal reinforcement leads to a reduction in the interface stresses for the same load levels, the effect being more pronounced for RC beams reniforced with thin external plates.

11. Type of loading does not influence significantly the magnitude of the interface stresses for standard plate curtailment lengths.

12. Increase in plate curtailment lengths as measured from the support leads to significant magnification in interface shear and peeling stresses.

13. Plate tapering in elevation was noted to be the optimal form of reducing plate area towards the plate curtailment zone in terms of decreasing the interface stress.

14. Using softer glues leads to a decrease in peak interface shear and peeling stresses.

15. In cases of beams where failure is governed by yielding of external steel plate and internal reinforcement, the ultimate loads can be predicted by using flexural formulae based on strain compatibility.

16. Numerical model revealed that the Roberts formula for estimating interface stresses was found to be conservative for very thin plates but underestimates the stresses for thicker plates, especially at high loads.

17. Interface stresses are noted to deviate from Roberts formula as the concrete compressive strength is lowered. This is attributed to the influence of concrete cracking on interface stresses, a phenomenon not accounted for in Roberts linear elastic model.

18. Modified expressions for interface stress are proposed as a design aid in the form of equations

$$\tau_0 = \alpha_1 f_t' \left(\frac{C_{R1} V_0}{f_c'} \right)^{\frac{5}{4}}$$

$$\alpha_1 = 35$$

$$C_{R1} = \left(1 + \left[\frac{K_s}{E_p b_p d_p} \right]^{\frac{1}{2}} a^* \right) \frac{b_p d_p}{I b_a} (h_p - h)$$

$$\sigma_0 = \alpha_2 C_{R2} \tau_0$$

$$\alpha_2 = 1.10$$

$$C_{R2} = d_p \left(\frac{K_n}{4E_p I_p} \right)^{\frac{1}{4}}$$

19. Based on evidence from experiments conducted by several groups of researchers over a period of ten years, it is established that the shear strength of plated R/C beams cannot be safely estimated by the ACI formula as used for shear strength of unplated R/C beams, as the parameter controlling peeling stress magnitude, $C_{R1}\,C_{R2}$, is increased. In the presence of peeling stress, a biaxial tension field is developed at location of plate curtailment, leading to formation of a horizontal crack which rips the concrete cover at the level of internal reinforcement. The horizontal crack progresses and moves up in a steep ascent to the point of loading. This crack path, in contrast to the 45° path in classical diagonal tension failure in unplated R/C beams, renders the function of stirrups redundant to a large extent.

20. Based on experimental evidence of beams noted to have failed by concrete cover rip off, an exponentially decaying function is noted to represent the degree of efficiency of stirrups.

As a result of the extensive parametric study carried out in this work, it is recommended that more experimental work should be carried out with properly designed specimens so as to obtain a more complete function representing the degree of stirrup efficiency, and thus shear capacity of plated beams.

Appendix A

Program User's Manual

A.1 Title Card

One card is required.

Location	*Variable*	*Description Details*	*Note*
1-60	TITLE	Descriptive Title of the Problem	1

Reference Notes

1 Consists of 60 alphanumeric characters

A.2 Control Card I

One card is required.

Location	*Variable*	*Description Details*	*Note*
1–5	NPOIN	Total number of nodal points	
6–10	NELEM	Total number of elements	
11–10	NVFIX	Total number of restrained boundary nodes	1
16–21	NTYPE	Problem type parameter: 1—Plane stress, 2—Plane strain and 3—Axis-symmetric	2
22–25	NNODE	Number of nodes per element: 8—Quadratic Serendipity element and 9—Quadratic Lagrangian element	3
26–30	NMATS	Total number of different materials	
31–35	NGAUS	Order of integration rule: 2—Two-Point Gauss quadrature rule and 3—Three-Point Gauss quadrature rule	4
36–40	NALGO	Non-linear solution algorithm parameter: • 1—Initial stiffness method • 2—Tangential stiffness method • 3—Combined algorithm I • 4—Combined algorithm II	5
41–45	NCRIT	Yield criterion parameter: 1—Tresca, 2—Von Misses, 3—Mohr-Coulomb and 4—Drucker-Prager	6

46–50	NINCS	Number of increments in which the total loading is to be applied.	
51–55	NSTRE	Number of stress components: 3—Plane stress or strain and 4—Axisymmetric	
56	ISWCH(1)	Convergence criteria switch: 0—Residual force criteria and 1—Displacement criteria	
57	ISWCH(2)	Dumping of output data for for graphic post-processing: 0—No damping, 1—Dump the complete data for detailed post-processing and 2—Damp limited data	7
58	ISWCH(3)	Restarting Switch: 0—Initial start, 1—Restarting from a given increment and 2—Restarting from the previous increment	8
59	ISWCH(4)	Suppress output file switch: 0—Suppress output file and 1—Output a detailed file	9
60	ISWCH(5)	Inactive	

Reference Notes

1 Nodes where one or more degrees of freedom are restrained.

2 Plane strain and axis-symmetric problem types are yet to be fully completed.

3 Applicable to concrete type elements only.

4 To be compatible with other element types, only NGAUS=3 should be used

5 In the initial stiffness method, element stiffnesses are evaluated at the beginning and remain unchanged thereafter. For the tangential stiffness method, the element stiffnesses are re-evaluated at every iteration of each load increment. In the combined algorithm type I element stiffnesses are re-evaluated at *first* iteration of each load increment only. For the combined algorithm type II, element stiffnesses are re-evaluated at *second* iteration of each load increment only.

6 For concrete type elements the Mohr-Coulomb criterion has been used.

7 For ISWCH(2)=1, valid for only one increment run. All information regarding stresses, strains displacements, reactions etc. are output. When ISWCH(2)=2, Load and displacement for a given node are monitored for all increments.

8 For ISWCH(3)=2 ensures that restart files are dumped at conclusion of each increment and overwrites the previous restart files. Before this option can be used, the first increment must be run with ISWCH(3)=0 to set the initial restart file.

9 Refers to the normal output file. Not needed if the graphical post-processing program is to be used.

A.3 Control Card II

One card is required.

Location	*Variable*	*Description Details*	*Note*

1–5	JNNOD	Node for which deflection is to be monitored for all increments	1
6–10	INIFL	Initial increment from which you are restarting	2
11–15	NTRST	Total number of increments for which restart files are to be stored	
16–20	JREST(1)	First increment number for which a restart file is to be kept	3,4
21–25	JREST(2)	Second increment number for which a restart file is to be kept	
—	—	—	
—	JREST(NTRST)	Last increment number for which a restart file is to be kept	

Reference Notes

1 Limited to one node.. Normally required in the initial runs to get the load-deflection curves

2 Left blank if starting from the beginning

3 The increments for which restart files are to be kept are entered in formats of I5. Keeping restart files at regular intervals avoids the necessity of having to rerun the problem from the start after the initial run.

4 If ISWCH(2) in section A.2 is one, both data for graphical post-processing and corresponding restart files will be generated and stored.

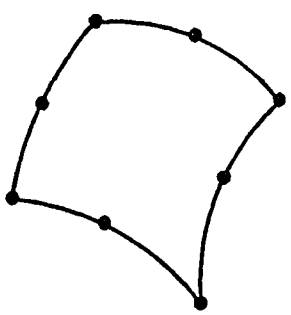

8–Noded Serendipity Element

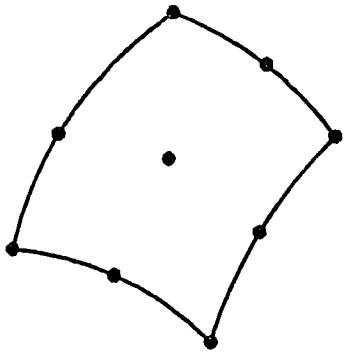

9–Noded Lagrangian Element

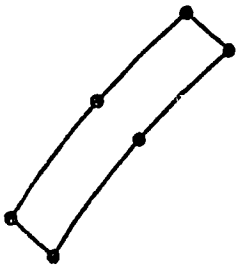

6–Noded Interface Element

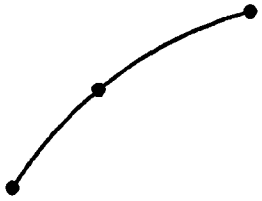

3–Noded Truss Element

Figure A.1: Element Library

A.4 Element Cards

One card for each element.

Location	*Variable*	*Description Details*	*Note*
1-5	NUMEL	Element number	
6-10	MATNO(NUMEL)	Material property number	
11-15	LNODS(NUMEL,1)	1^{st} Nodal connection number	1
16-20	LNODS(NUMEL,2)	2^{nd} Nodal connection number	
—	—	—	2,3
51-55	LNODS(NUMEL,9)	9^{th} Nodal connection number	4
56	LELTP(NUMEL)	Element type parameter	5
57	IECRT(NUMEL)	Mohr-Coulomb criterion switch	6

Reference Notes

1 Node numbers must be listed in an anticlockwise sequence starting at a corner node. See figure A.1 for the element library.

2 For a glue-interface or bond-interface element only the first six nodes need be specified.

3 For a truss element only the first three nodes need be specified.

4 For an eight nodded Serendipity element this position is left blank.

5 Specifies the type of element:

0– Isotropic elastoplastic element

2– Concrete type element

4– Truss element

5– Glue-interface element

6– Bond-interface element

6 IECRT(NUMEL)=1, is usually used for concrete elements to allow them yield according to Mohr-Coulomb yield criterion. For other elements, normally left blank.

A.5 Nodal Cards

One card for each node input.

Location	*Variable*	*Description Details*	*Note*
1–5	IPOIN	Node number	
6–15	COORD(IPOIN,1)	x or r coordinate of IPOIN	1,2,3
16–25	COORD(IPOIN,2)	y or z coordinate of IPOIN	

Reference Notes

1 Coordinates of the mid-side nodes, if not specified shall be assumed to lie on a straight edge and will be centrally placed using linear interpolation

2 The coordinates of the highest numbered node must be placed last.

3 For Lagrangian elements, the coordinates of the 9^{th} node are never input, being automatically generated

A.6 Boundary Conditions

One card for each node restrained.

Location	*Variable*	*Description Details*	*Note*
1–5	NOFIX(IVFIX)	Restrained node number	1
11–15	IFPRE	Restraint code	2
21–30	PRESC(IVFIX,1)	The prescribed value of the x or r component of nodal displacement.	3
31–40	PRESC(IVFIX,2)	The prescribed value of the y or y component of nodal displacement.	

Reference Notes

1 IVFIX varies from 1 to NVFIX, the total number of restrained nodes.

2 The restraint code should be specified as:

10 nodal displacement restrained in the x or r direction

01 nodal displacement restrained in the y or z direction

11 nodal displacement restrained in both directions

3 Nodes with initial displacement (settlement) must be restrained in that particular direction

A.7 Material Cards

A.7.1 Control Card

Only one card is required.

Location	*Variable*	*Description Details*	*Note*
1–5	NUMAT	Material identification number	1

Reference Notes

1 The material properties to be specified varies depending on the element type as shown in the following cards.

A.7.2 Isotropic Elastoplastic Material: Type 0

This material type would normally be used for bonding plate elements. Two cards needed for each material type.

Location	*Variable*	*Description Details*	*Note*
CARD I			
1–10	PROPS(LPROP,1)	Elastic modulus, E_s	

11–20	PROPS(LPROP,2)	Poisson's ratio, ν	
21–30	PROPS(LPROP,3)	Material width, t	1
31–40	PROPS(LPROP,4)	Mass density, ρ	
41–50	PROPS(LPROP,5)	Uniaxial yield stress, σ_y	2
51–60	PROPS(LPROP,6)	Strain hardening parameter H'	
61–70	PROPS(LPROP,7)	Friction angle, ϕ measured in degrees	3
CARD II			
1–10	PROPS(LPROP,8)	—	4
11–20	PROPS(LPROP,9)	—	4
21–30	PROPS(LPROP,10)	—	4

Reference Notes

1 Leave blank for plane strain and axis-symmetric problems

2 For Mohr-Coulomb and Drucker-Prager materials, the uniaxial stress is the cohesion, c.

3 Only for Mohr-Coulomb and Drucker-Prager materials.

4 Left blank

A.7.3 Concrete Type Material: Type 2

Two cards needed for each material type.

Location	*Variable*	*Description Details*	*Note*
CARD I			
1–10	PROPS(LPROP,1)	Elastic modulus, E_c	
11–20	PROPS(LPROP,2)	Poisson's ratio, ν	
21–30	PROPS(LPROP,3)	Material width, t	1
31–40	PROPS(LPROP,4)	Mass density, ρ	
41–50	PROPS(LPROP,5)	Maximum tensile stress, f_t'	
51–60	PROPS(LPROP,6)	Compressive strength, f_c'	
61–70	PROPS(LPROP,7)	Limiting crushing strain, ε_u	
CARD II			
1–10	PROPS(LPROP,8)	Tension stiffening coefficient, ε_m	
11–20	PROPS(LPROP,9)	Tension stiffening coefficient, α_m	
21–30	PROPS(LPROP,10)	Friction angle, ϕ measured in degrees	2

Reference Notes

1 Leave blank for plane strain and axis-symmetric problems

2 Since Mohr-Coulomb yield criterion is used for concrete type elements.

A.7.4 Material Properies for a Truss Element: Type 4

Two cards needed for each material type.

Location	*Variable*	*Description Details*	*Note*
CARD I			
1–10	PROPS(LPROP,1)	Elastic modulus, E_s	
11–20	PROPS(LPROP,2)	Area of element, A_s	
21–30	PROPS(LPROP,3)	Yield strength, σ_y	
31–40	PROPS(LPROP,4)	Hardness paremeter H'	
41–50	PROPS(LPROP,5)	—	1
51–60	PROPS(LPROP,6)	—	1
61–70	PROPS(LPROP,7)	—	1
CARD II			

—	—	—	2

Reference Notes

1 Positions left blank for truss type elements.

2 The second card must be left blank.

A.7.5 Material Properties for a Glue Interface Element: Type 5

Two cards needed for each material type.

Location	*Variable*	*Description Details*	*Note*
CARD I			
1–10	PROPS(LPROP,1)	Normal elastic modulus of the interface, E_g	1
11–20	PROPS(LPROP,2)	Shear modulus, G_g	2
21–30	PROPS(LPROP,3)	Glue-line thickness, t_g	
31–40	PROPS(LPROP,4)	Width of the glue, perpendicular to the plane of bending, b_g.	
41–50	PROPS(LPROP,5)	Maximum shear stress attainable by the glue interface, τ_{max}	3

51–60	PROPS(LPROP,6)	Maximum direct tensile attainable by the interface, f_{t-max}	4
61–70	PROPS(LPROP,7)	Poisson ratio	5
CARD II			
—	—	—	6

Reference Notes

1 The value E_g assumed equivalent to the normal stiffness perpendicular to the glue-line, may be taken as the elastic modulus of the bulk epoxy glue.

2 The shear stiffness of the steel-glue-concrete interface may be determined from direct shear tests or as in this study, from specially designed specimens.

3 Beyond this value, the glue interface will be deemed to have failed by slipping.

4 Since the tensile strength of the epoxy glue is much more than that of concrete, f_{t-max} may be taken to be that of plane concrete.

5 The Poisson ratio for the glued interface element, taken to be that of plane concrete.

6 The second material card is left blank for glue interface elements.

A.7.6 Material Properties for a Steel Bond Element: Type 6

Two cards needed for each material type.

Location	*Variable*	*Description Details*	*Note*
CARD I			
1–10	PROPS(LPROP,1)	Elastic modulus, E	1
11–20	PROPS(LPROP,2)	Shear modulus, G	1
21–30	PROPS(LPROP,3)	Thickness, t	2
31–40	PROPS(LPROP,4)	Breadth of the bond element, perpendicular to the plane of bending, b_g.	3
41–50	PROPS(LPROP,5)	Bond strength, τ_{bond}	
51–60	PROPS(LPROP,6)	Maximum direct tensile strength, f_{t-max}	4
61–70	PROPS(LPROP,7)	—	5
CARD II			
—	—	—	6

Reference Notes

1 Similar values as the surrounding concrete may be used.

2 A reasonably small value of the order of 2 to 6 mm.

3 Usually the same thickness as that of the structure.

4 Tensile strength of the surrounding concrete.

5 Left blank.

6 The second material card is left blank for bond elements.

A.8 Load Case Title Card

One card rquired.

Location	*Variable*	*Description Details*	*Note*
1-60	TITLE	Title of the load case.	1

Reference Notes

1 Limited to 60 alphanumeric characters

A.9 Load Control Card

Only one card is required.

Location	*Variable*	*Description Details*	*Note*
1–5	IPLOD	Applied point load switch.	1
6–10	IGRAV	Gravity Loading control switch.	2

11-15	IEDGE	Distributed edge load control parameter.	3

Reference Notes

1 0 — No applied nodal loads to be input
1 — Applied nodal loads to be input.
2 0 — No gravity loads to be considered
1 — Gravity loading is to be considered.
3 0 — No distributed edge loads to be input.
1 — Distributed edge loads to be input.

A.10 Applied Load Cards

Only one card is required for each loaded nodal point. If IPLOD = 0, this card set is omitted.

Location	*Variable*	*Description Details*	*Note*
1-5	LODPT	Nodal point at which load is applied.	1
6-15	POINT(1)	Value of the load component in the x or (r) direction.	2
16-25	POINT(2)	Value of the load component in the y or (z) direction.	

Reference Notes

1 The last card should be that of the highest numbered node whether it is loaded or not.

2 For axis-symmetric problems, the loads input should be the *total* loading on the circumferential ring passing through the nodal point concerned.

A.11 Gravity Loading Cards

Only one card is required. If IGRAV = 0, this card set is omitted.

Location	*Variable*	*Description Details*	*Note*
1–10	THETA	Angle of gravity measured from the positive y-axis.	1
11–25	GRAVY	Gravity constant specified as a multiple of the gravitational acceleration, g.	

Reference Notes

1 See figure A.2.

A.12 Distributed Edge Cards

A total of three card types are required. Cards of type II and III are repeated in turn for every element edge. If IEDGE = 0, this card set is omitted.

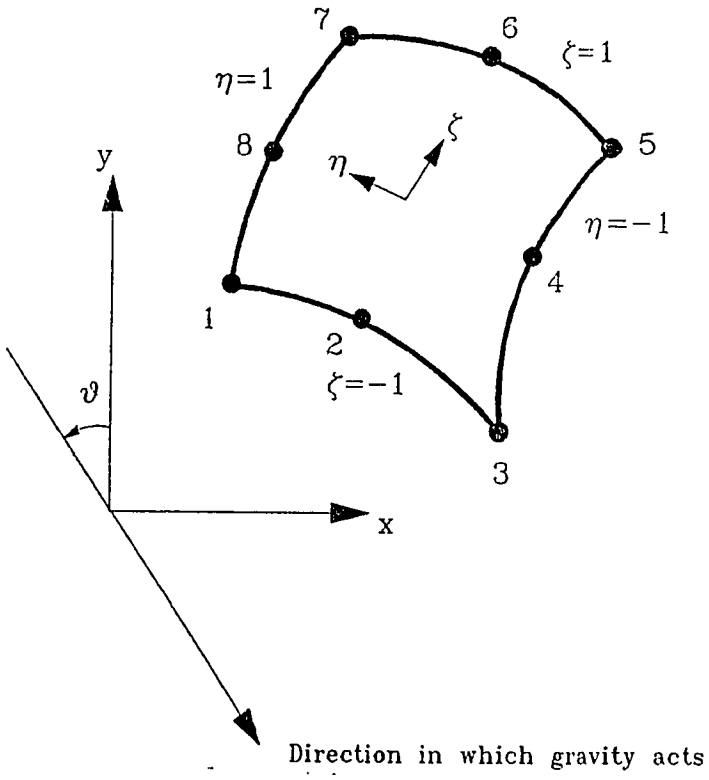

Figure A.2: Specifying the gravity axis for two-dimensional problems.

Location	*Variable*	*Description Details*	*Note*
CARD I		*Control Card*	
1-5	NEDGE	Number of element edges on which distributed loads are to be applied.	
CARD II		*Element Edge Incidence*	
1-5	NEASS	Element number with which the element edge is associated.	
6-10	NOPRS(1)	List of nodal points comprising the loaded edge.	1
11-15	NOPRS(2)	—	
16-20	NOPRS(3)	—	
CARD III		*Distributed Loads*	
1-10	PRESS(1,1)	Value of the normal component of the distributed load at point NOPRS(1)	
11-20	PRESS(1,2)	Value of the tangential component of the distributed load at point NOPRS(1)	
21-30	PRESS(2,1)	Value of the normal component of the distributed load at point NOPRS(2)	

31–40	PRESS(2,2)	Value of the tangential component of the distributed load at point NOPRS(2)	
41–50	PRESS(3,1)	Value of the normal component of the distributed load at point NOPRS(3)	
51–60	PRESS(3,2)	Value of the tangential component of the distributed load at point NOPRS(3)	

Reference Notes

1 The sequence of nodes are placed in an anticlockwise sense.

A.13 Load Increment Cards

One card is required for each load increment.

Location	*Variable*	*Description Details*	*Note*
1–5	KINCS	Increment number.	
6–10	FACTO	Applied load factor for this increment.	1
11–20	TOLER	Convergence tolerance factor.	

21–25	MITER	Maximum number of iterations allowed for the increment.	
26–30	NOUTP(1)	Parameter controlling output of results after the first iteration. 0 — No output 1 — Output displacements 2 — Output displacements and reactions 3 — Output displacements, reactions and stresses.	
31–35	NOUTP(2)	Parameter controlling output of results after convergence has been achieved. 0 — No output 1 — Output displacements 2 — Output displacements and reactions 3 — Output displacements, reactions and stresses.	2

Reference Notes

1 The value FACTO is specified as a factor of the total loading input in sections A.10, A.11 and A.12.

2 Parameter of 3 should always be specified if the graphical post-processing program is to be used, (see ISWCH(2) in section A.2

Appendix B

User's Manual for the Mesh Generation Program

B.1 Introduction

The mesh generation program, whose use is described below, is applicable to nodes and elements that are arranged on a rectangular grid. The nodes and the elements are numbered sequentially along the shorter side to minimize the bandwidth. A typical input file for a typical plate bonded beam and explanatory notes are attached.

B.2 Title Card

One card is required.

Location	*Variable*	*Description Details*	*Note*
1–60	TITLE	Title of the problem.	1

Reference Notes

1 Limited to 60 alphanumeric characters.

B.3 Overall Rectangular Grid Description Card

One card is required.

Location	*Variable*	*Description Details*	*Note*
1–5	NVPOT	Number of grid nodes along the shorter (normally y) direction.	
6–10	NHPOT	Number of grid nodes along the longer (normally x) direction.	
11–15	NNODE	Number of nodes per element.	1

Reference Notes

1 Normally 8–nodes for the quadratic Serendipity element and 9–nodes for the quadratic Lagrangian element.

B.4 Node Generation Switch Cards

Several cards are required in this set.

Location	*Variable*	*Description Details*	*Note*
CARD I			
1–5	NVTYP	Total number of types of vertical grid switch series.	
CARD II			
1–5	KVTYP	Label of the particular grid series.	
CARD III			1
1-NVPOT	NVDSC(KVTYP,IVPOT)	IVPOT=1,NVPOT: A series of switches; 1— to number the node and 0— to skip the numbering.	1
CARD IV			
1–5	NHTYP	Total number of cards describing the arrangement of the switch series described in Cards II & III along the longer side of the problem being discretized.	
CARD V			2
1–5	KHTYP(IHTYP)	Total number of repititions of the following numbering sequence.	3

6–10	NUMBR(IHTYP)	Total number of vertical grid switch types in the sequence.	
11–	NHDSC(IHTYP,IHPOS)	IHPOS=1,NUMBR(IHTYP): Series of vertical grid switch types in the particular sequence.	

Reference Notes

1 Cards II & III are repeated as many times as NVTYP.

2 Card series V is repeated as many times as NHTYP.

3 Note IHTYP=1,NHTYP.

B.5 Vertical Spacing Cards

Several cards are required in this set.

Location	*Variable*	*Description Details*	*Note*
CARD I			
1–5	NSPCV	Total number of cards describing the spacing in the vertical direction.	
CARD II			1

1–5	KSPCV(ISPCV)	Number of equal spaces consecutively following one another.	2
6–15	DY(ISPCV)	The value of the spacing.	

Reference Notes

1 Cards set II are as many as NSPCV.
2 The arithmetic sum of KSPCV(ISPCV) must equal (NVPOT-1).

B.6 Horizontal Spacing Cards

Several cards are required in this set.

Location	*Variable*	*Description Details*	*Note*
CARD I			
1–5	NSPCH	Total number of cards describing the spacing in the horizontal direction.	
CARD II			1
1–5	KSPCH(ISPCH)	Number of equal spaces consecutively following one another.	2

6–15	DX(ISPCH)	The value of the spacing.	

Reference Notes

1 Cards set II are as many as NSPCH.
2 The arithmetic sum of KSPCH(ISPCH) must equal (NHPOT-1).

B.7 Element Numbering Cards

Several cards are required in this set.

Location	*Variable*	*Description Details*	*Note*
CARD I			
1–5	NELMV	Total number of elements in the vertical direction on the master rectangular grid.	
CARD II			
1–5	NELTP	Total number of cards that describe the different types of element numbering in the grid.	
CARD III			1

1-5	KELTP	Label of the particular element numbering sequence.	
CARD IV			1
1	CVELM(KELTP,IELMV)	Parameter describing the element type to be numbered.	2
2	NVELM(KELTP,IELMV)	Element material number.	3,4
3	'blank' or ','	Left blank or a comma is placed to help in the readability.	
—	—	Continuing description of the element types to be numbered.	5

Reference Notes

1 Cards set III & IV are repeated as many times as NELTP.

2 These consist of upper case alphabetical letters namely:

E Element on the master rectangular grid not to be numbered,

C Concrete element,

B Bond element,

T Truss element, normally for horizontal main or top steel,

V Vertical stirrup,

G Glued interface,

P Bonding plate element,

3 For the 'E' or un-numbered element, the material number is 0.

4 The material numbers are placed in a sequence such that the total number of materials in the structure is equal to the maximum number.

5 On the same card, the first three positions on the Card IV are repeated as many times as NELMV.

B.8 Sequence of Element Numbering Cards

Several cards are required in this set.

Location	*Variable*	*Description Details*	*Note*
CARD I			

1–5	NTPEL	Total number of cards describing the element numbering sequence.	
CARD II			1
1–5	KTPEL(ITPEL)	Total number of repetitions of the following numbering sequence.	2
6–10	NOELM(ITPEL)	Total number of vertical element numbering types in the sequence.	
11–	NELSC(ITPEL,IHPOS)	IHPOS=1,NOELM(ITPEL): Series of vertical element numbering types in the particular sequence.	

Reference Notes

1 Cards series II are repeated as many times as NTPEL.

2 Note ITPEL=1,NTPEL.

B.9 Cards Relating to Numbering of Vertical Stirrups

Two cards are required in this set.

Location	*Variable*	*Description Details*	*Note*
CARD I			
1–5	NVTOT	Total number of vertical grid lines onto which is placed vertical stirrups.	
6–	NVERT(IVTOT)	IVTOT=1,NVTOT: Sequence of particular vertical grid numbers onto which is placed vertical stirrups in formats of I5.	
CARD II			
1–5	IBEGN	The grid number at which numbering of vertical stirrup members commences.	
6–10	IENDS	The grid number at which numbering of vertical stirrup members ends.	

B.10 Cards for Generation of Restrained Nodes

Several cards are required in this set.

Location	*Variable*	*Description Details*	*Note*

CARD I			
1–5	NVFIX	Total number of restrained nodes.	
CARD II			
1–5	NCARD	Total number of cards describing the details regarding the generation of restrained nodes.	
CARD III			1
1–10	X	The x coordinate of the restrained node.	
11–20	Y	The y coordinate of the restrained node.	
21	—	Left blank.	
22–25	RESTR	Character string parameter determining along which line the restrained nodes are to be generated.	2
26–28	—	Left blank.	
29	IX	Parameter indicating the nature of restraint in the x direction.	3
30	IY	Parameter indicating the nature of restraint in the y direction.	3

31–40	DX1	Value of prescribed displacement in the x direction.
41–50	DY1	Value of prescribed displacement in the y direction.

Reference Notes

1 Cards series III are repeated as many times as NCARD.

2 The character string RESTR can be one of the following:

XALL All nodes with the given x coordinate are to be restrained. In this case the value for Y need not be input.

YALL All nodes with the given y coordinate are to be restrained. In this case the value for X need not be input.

The location for RESTR must be left empty if both X & Y are given.

3 Specified by:

0 Free to move in the particular direction.

1 Fixed with respect to movement the particular direction, except for the prescribed amount.

B.11 Deflection Monitoring Card

One card is required.

Location	*Variable*	*Description Details*	*Note*
1–10	XMONI	x coordinate of the node to be monitored.	1
11–20	YMONI	y coordinate of the node to be monitored.	

Reference Notes

1 Only one node can be monitored as the structure is monotonically loaded to failure.

B.12 Material Properties Cards

Several cards are required in this set. The explanation regarding the meaning of the various material property values for different element types are detailed in sections A.7.2 to A.7.6.

B.12.1 Material Properties Cards for Concrete Elements

Several cards are required in this set.

Location	*Variable*	*Description Details*	*Note*
Card I			

1	KMATS	Character string identifying type of element for which material properties are to be read. In this case KMATS='C', for concrete type element.	
2	IMATS	Material number.	
Card II			
1–10	DESCR	DESCR='E'.	1
11–20	PROPS(IMATS,1)	Elastic modulus of concrete.	
Card III			
1–10	DESCR	DESCR='NU'.	1
11–20	PROPS(IMATS,2)	Poisson's ratio for concrete.	
Card IV			
1–10	DESCR	DESCR='WIDTH'.	1
11–20	PROPS(IMATS,3)	Width of the concrete element.	
Card V			
1–10	DESCR	DESCR='DENSITY'.	1

11–20	PROPS(IMATS,4)	Density of concrete element. Usually set to 0.	
Card VI			
1–10	DESCR	DESCR='TENSILE'.	1
11–20	PROPS(IMATS,5)	Tensile strength of concrete, f_t'.	
Card VII			
1–10	DESCR	DESCR='COMPRSV'.	1
11–20	PROPS(IMATS,6)	Compressive strength of concrete, f_c'.	
Card VIII			
1–10	DESCR	DESCR='EPSILON-U'.	1
11–20	PROPS(IMATS,7)	Limiting crushing strain, ε_u.	
Card IX			
1–10	DESCR	DESCR='EPSILON-M'.	1
11–20	PROPS(IMATS,8)	Tension stiffening coefficient, ε_m.	
Card X			

1–10	DESCR	DESCR='ALPHA-M'.	1
11–20	PROPS(IMATS,9)	Tension stiffening parameter, α_m.	
Card XI			
1–10	DESCR	DESCR='PHI'.	1
11–20	PROPS(IMATS,9)	Friction angle, ϕ measured in degrees.	

Reference Notes

1 Descriptive title of the property being input. Not needed in the program, but may assist in the readability of the input file.

B.12.2 Material Properties Cards for Bond Elements

Several cards are required in this set.

Location	*Variable*	*Description Details*	*Note*
Card I			
1	KMATS	Character string identifying type of element for which material properties are to be read. In this case KMATS='B', for bond type element.	

2	IMATS	Material number.	
Card II			
1–10	DESCR	DESCR='E'.	1
11–20	PROPS(IMATS,1)	Elastic modulus.	
Card III			
1–10	DESCR	DESCR='G'.	1
11–20	PROPS(IMATS,2)	Shear modulus.	
Card IV			
1–10	DESCR	DESCR='THICKNS'.	1
11–20	PROPS(IMATS,3)	Thickness, t.	
Card V			
1–10	DESCR	DESCR='WIDTH'.	1
11–20	PROPS(IMATS,4)	Breadth of the bond element perpendicular to the plane of bending, b_g.	
Card VI			
1–10	DESCR	DESCR='TAU-MAX'.	1

11–20	PROPS(IMATS,5)	Bond strength, τ_{bond}.	
Card VII			
1–10	DESCR	DESCR='FT-MAX'.	1
11–20	PROPS(IMATS,6)	Maximum direct tensile strength, f_{t-max}.	
Card VIII			
1–10	DESCR	DESCR='NU'.	1
11–20	PROPS(IMATS,6)	Poisson's ratio, ν.	

Reference Notes

1 Descriptive title of the property being input. Not needed in the program, but may assist in the readability of the input file.

B.12.3 Material Properties Cards for Truss Elements

Several cards are required in this set.

Location	*Variable*	*Description Details*	*Note*
Card I			

1	KMATS	Character string identifying type of element for which material properties are to be read. In this case KMATS='T' or 'V', for truss type element.	
2	IMATS	Material number.	
Card II			
1–10	DESCR	DESCR='ES'.	1
11–20	PROPS(IMATS,1)	Elastic modulus, E_s	
Card III			
1–10	DESCR	DESCR='AS'.	1
11–20	PROPS(IMATS,2)	Area of element, A_s	
Card IV			
1–10	DESCR	DESCR='TENSILE'.	1
11–20	PROPS(IMATS,3)	Yield strength, σ_y	
Card V			
1–10	DESCR	DESCR='HARDNESS'.	1
11–20	PROPS(IMATS,4)	Hardness paremeter H'	

Reference Notes

1 Descriptive title of the property being input. Not needed in the program, but may assist in the readability of the input file.

B.12.4 Material Properties Cards for Glue Interface Elements

Several cards are required in this set.

Location	*Variable*	*Description Details*	*Note*
Card I			
1	KMATS	Character string identifying type of element for which material properties are to be read. In this case KMATS='G', for glue interface type element.	
2	IMATS	Material number.	
Card II			
1–10	DESCR	DESCR='E'.	1
11–20	PROPS(IMATS,1)	Normal elastic modulus of the interface, E_g	
Card III			

1-10	DESCR	DESCR='G'.	1
11-20	PROPS(IMATS,2)	Shear modulus, G_g	
Card IV			
1-10	DESCR	DESCR='THICKNS'.	1
11-20	PROPS(IMATS,3)	Glue-line thickness, t_g	
Card V			
1-10	DESCR	DESCR='WIDTH'.	1
11-20	PROPS(IMATS,4)	Width of the glue, perpendicular to the plane of bending, b_g.	
Card VI			
1-10	DESCR	DESCR='TEN-CUTOFF'.	1
11-20	PROPS(IMATS,5)	Maximum tensile stress attainable by the glue interface, σ_{max}	
Card VII			
1-10	DESCR	DESCR='COHESSION'.	1

11–20	PROPS(IMATS,6)	The shear stress at $\sigma = 0$ intercept of the material law for the glued interface, c	
Card VIII			
1–10	DESCR	DESCR='NU'.	1
11–20	PROPS(IMATS,6)	Poisson's ratio, ν.	
Card IX			
1–10	DESCR	DESCR='ANGLE-PHI'.	1
11–20	PROPS(IMATS,6)	Angle of internal friction for the glued interface, ϕ.	

Reference Notes

1 Descriptive title of the property being input. Not needed in the program, but may assist in the readability of the input file.

B.12.5 Material Properties Cards for Bonding Plate Elements

Several cards are required in this set.

Location	*Variable*	*Description Details*	*Note*
Card I			

1	KMATS	Character string identifying type of element for which material properties are to be read. In this case KMATS='P', for plate bonding type element.	
2	IMATS	Material number.	
Card II			
1–10	DESCR	DESCR='E'.	1
11–20	PROPS(IMATS,1)	Elastic modulus, E_s	
Card III			
1–10	DESCR	DESCR='NU'.	1
11–20	PROPS(IMATS,2)	Poisson's ratio, ν	
Card IV			
1–10	DESCR	DESCR='WIDTH'.	1
11–20	PROPS(IMATS,3)	Material width, t	
Card V			
1–10	DESCR	DESCR='DENSITY'.	1
11–20	PROPS(IMATS,4)	Mass density, ρ	

Card VI			
1–10	DESCR	DESCR='TENSILE'.	1
11–20	PROPS(IMATS,5)	Uniaxial yield stress, σ_y	
Card VII			
1–10	DESCR	DESCR='HARDNESS'.	1
11–20	PROPS(IMATS,6)	Strain hardening parameter H'	

Reference Notes

1 Descriptive title of the property being input. Not needed in the program, but may assist in the readability of the input file.

B.13 Loaded Point Card

One card is required.

Location	*Variable*	*Description Details*	*Note*
1–10	XLODP	x coordinate of the loaded node.	1
11–20	YLODP	y coordinate of the loaded node.	1

Reference Notes

1 For the moment, only one node can be loaded as this was suffiient for the most of the verification study.

B.14 Characteristic Filename Card

One card is required.

Location	*Variable*	*Description Details*	*Note*
1-60	FNAME	Characteristic Filename.	1

Reference Notes

1 Limited to 8 alphanumeric characters, this characteristic filename is tagged on all files that are handled during the execution of the program.

B.15 Mesh Generation Example

The input file listed below will generate nodal coordinates, element incidences, material properties etc, for a typical plate bonded beam structure as shown in figure B.15. Explanatory notes and reference sections for each portion of input are given after the listing.

```
                                                          Line #
MESH GENERATION PROBLEM: TRIAL                              1
  14   15    8    DATA RELATING TO NODE GENERATION          2
   4                                                        3
```

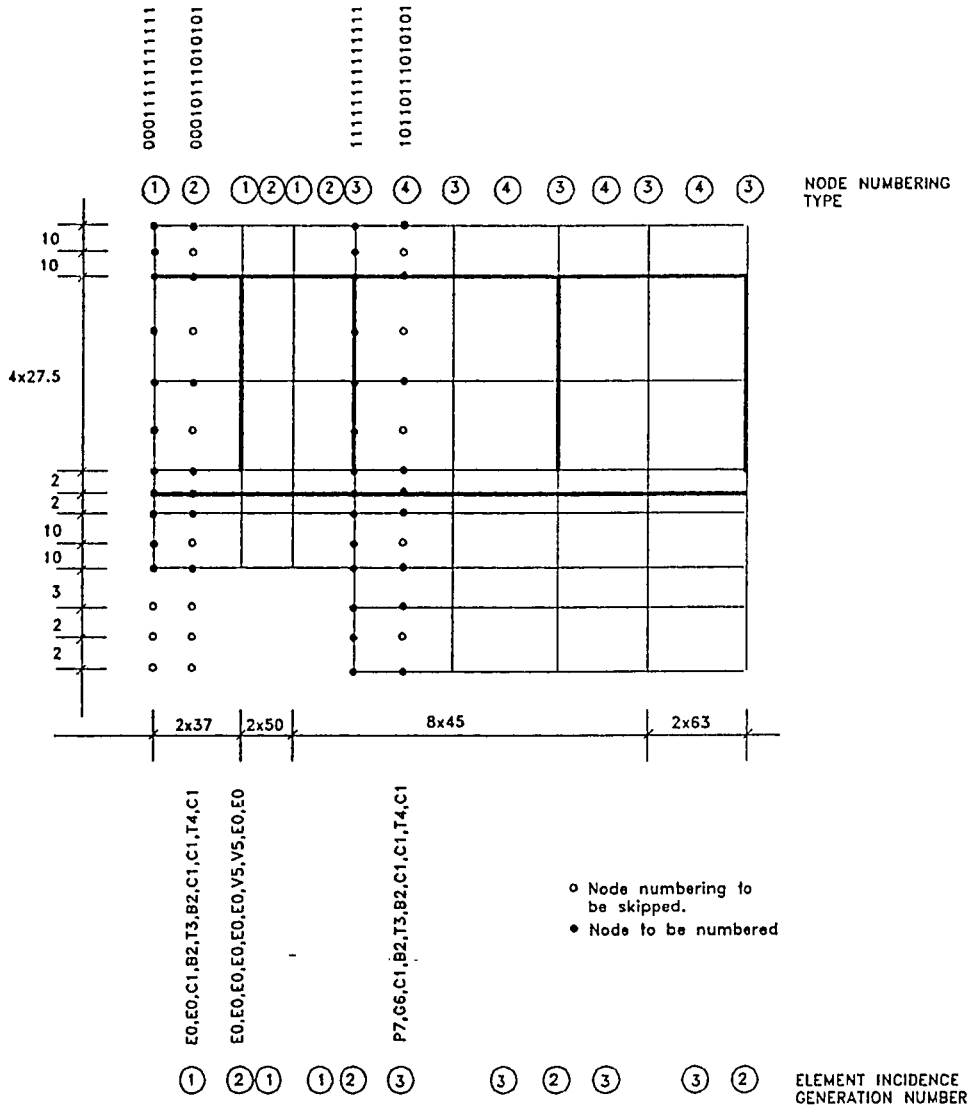

Figure B.1: Mesh generation example.

```
    1                                                          4
00011111111111                                                 5
    2                                                          6
00010111010101                                                 7
    3                                                          8
11111111111111                                                 9
    4                                                         10
10110111010101                                                11
    3                                                         12
    3     2     1     2                                       13
    4     2     3     4                                       14
    1     1     3                                             15
    6                                                         16
    2    2.0000                                               17
    1    3.0000                                               18
    2   10.0000                                               19
    2    2.0000                                               20
    4   27.5000                                               21
    2   10.0000                                               22
    4                                                         23
    2   37.0000                                               24
    2   50.0000                                               25
    8   45.0000                                               26
    2   63.0000                                               27
   10   DATA RELATING TO ELEMENT INCIDENCE GENERATION         28
    3                                                         29
    1                                                         30
E0,E0,C1,B2,T3,B2,C1,C1,T4,C1                                 31
    2                                                         32
E0,E0,E0,E0,E0,E0,V5,V5,E0,E0                                 33
```

```
    3                                                          34
P7,G6,C1,B2,T3,B2,C1,C1,T4,C1                                  35
    4                                                          36
    1    2    1    2                                         37
    1    2    1    1                                         38
    2    3    2    3    3                                    39
    1    1    2                                              40
    4    3    7   11   15  VERTICAL STIRRUPS                  41
    8   12                                                    42
   15        NVFIX OR RESTRAINED NODES                        43
    2                                                          44
 660.0000            XALL   10   0.0        0.0              45
  74.0       7.0            01   0.0        0.0              46
 660.0       0.0       DEFL. TO BE  MONITORED.               47
C1     CONCRETE                                              48
E          20000.0                                           49
NU          0.145                                            50
WIDTH       100.0                                            51
DENSITY       0.0                                            52
TENSILE      3.20                                            53
COMPRSV     37.70                                            54
EPSILON-U  0.0035                                            55
EPSILON-M  0.002                                             56
ALPHA-M     0.6                                              57
PHI         37.0                                             58
B2       BOND ELEMENT                                        59
E           20000.                                           60
NU           8733.                                           61
THICKNS       2.0                                            62
WIDTH       100.0                                            63
```

```
TAU-MAX        5.5                                    64
FT-MAX         4.8                                    65
T3        MAIN STEEL                                  66
ES          200000.                                   67
AS           157.0                                    68
TENSILE      530.0                                    69
HARDNESS     200.0                                    70
T4        TOP STEEL                                   71
ES          200000.                                   72
AS           100.0                                    73
TENSILE      530.0                                    74
HARDNESS     200.0                                    75
V5        VERTICAL STIRRUPS                           76
ES          200000.                                   77
AS            56.55                                   78
TENSILE      530.0                                    79
HARDNESS     200.0                                    80
G6        GLUE INTERFACE                              81
E             278.9                                   82
G             120.2                                   83
THICKNS         3.0                                   84
WIDTH          80.0                                   85
COHESSION       7.0                                   86
TEN-CUTOFF      4.0                                   87
ANGLE-PHI      28.0                                   87
P7        BONDING PLATE                               87-A
E           198000.                                   89
NU           0.30                                     90
WIDTH          80.0                                   91
DENSITY         0.0                                   92
```

#30–#35	Each of the 3 different types of element numbering series, is labeled and typed in.	B.7
#36	Total number of cards describing the order of element numbering along the x direction are 4.	B.8
#37–#40	This block implies an element numbering sequence of once of (1 2), once of (1 1), twice of (2 3 3) and once of (2), or 1 2 1 1 2 3 3 2 3 3 2	B.8
#41	Stirrups are placed on 4 vertical grid lines, namely 3, 3, 11 and 15, on the x axis.	B.9
#42	Stirrups commence at grid #8 and end on #12 along the y direction.	B.9
#43	Total number of restrained nodes are 15.	B.10
#44	There is a total of 2 cards describing the location and type of restraint.	B.10
#45	All nodes with an x coordinate value of 660.0 mm. are restrained from movement in the x direction.	B.10
#46	Node with an x coordinate value of 74.0 mm. and a y coordinate value of 7.0 mm. is restrained from movement in the y direction.	B.10
#47	Node with an x coordinate value of 660.0 mm. and a y coordinate value of 0.0 mm. is to have its deflection monitored as the beam is loaded to failure.	B.11
#48–#58	Material property parameters for material #1, which happens to be concrete.	B.12.1
#59–#65	Material property parameters for material #2, which happens to be that of a steel-to-concrete bond element.	B.12.2
#66–#70	Material property parameters for material #3, which happens to be main tensile steel reinforcement.	B.12.3
#71–#75	Material property parameters for material #4, which happens to be the top compression steel.	B.12.3
#76–#80	Material property parameters for material #5, which happens to be the vertical stirrups.	B.12.3

#81–#87	Material property parameters for material #6, which happens to be that of the glue interface element.	B.12.4
#88–#94	Material property parameters for material #7, which happens to be the bonding plate.	B.12.5
#95	Node with an x coordinate value of 444.0 mm. and a y coordinate value of 161.0 mm. is loaded with a downward force of 50000 N.	B.13
#96	Characteristic name to be tagged on most files during file handling operations is 'TRIAL'.	B.14

Appendix C

User's Manual for the Graphical Post Processing Program

C.1 Introduction

This chapter of the appendix explains the preparation of the input file that controls the functioning and output of the graphical post processing program. A particular graphical function is selected by inputting an option parameter. Subsequent cards that must be provided vary with each option and are explained in the sections below.

The post-processing program reads data from a file generated from the main non-linear finite element program when the switch option ISWCH(2) in section A.2 is selected as one.

C.2 Undeformed Mesh

One card is required.

Location	*Variable*	*Description Details*	*Note*
1–5	IOPTN	Post processing option for undeformed mesh set to 1.	1

Reference Notes

1 Before running the post processing program with other options, the undeformed mesh should be plotted first to confirm it does match the expected discretized mesh.

C.3 Deformed Mesh

Several cards are required.

Location	*Variable*	*Description Details*	*Note*
CARD I			
1–5	IOPTN	Post processing option for deformed mesh set to 2.	
CARD II			
1–5	NINCS	Total number of increments to plot.	1
6–15	FMAGN	Magnification factor.	2
CARD III			

1–5	NPLOT	Total number of plots required.	3
6–	KINCS(IPLOT)	Typed in a series of I5 format, the number of the particular increments to be plotted.	4

Reference Notes

1 Although the post processing program can plot the deformed mesh for more than one increment, it is recommended that one increment should be plotted at a time, especially for relatively large jobs, ie NINCS=1.

2 The cumulative incremental displacements are magnified by this factor before being added to the global coordinates.

3 Normally set equal to NINCS in card series II.

4 IPLOT=1,NPLOT.

C.4 Material Status at Sampling Points

Several cards are required.

Location	*Variable*	*Description Details*	*Note*
CARD I			

1–5	IOPTN	Post processing option for plotting of the material status at the sampling points set equal to 3.	
CARD II			
1–5	NINCS	Total number of increments to plot.	1
6–15	FMAGN	Magnification factor.	2
CARD III			
1–5	NPLOT	Total number of plots required.	3
6–	KINCS(IPLOT)	Typed in a series of I5 format, the number of the particular increments to be plotted.	4
CARD IV			
1–5	NSETS	Total number of sets for plotting the outlines.	5
CARD V			
1–5	IPTS(ISETS)	Total number nodal points in the particular set.	6

6-	NPTS(ISETS,I)	I=1,IPTS(ISETS) are the particular nodal points typed in formats of I5.	

Reference Notes

1 Although the post processing program can plot the material status for more than one increment, it is recommended that one increment should be plotted at a time, especially for relatively large jobs, ie NINCS=1.

2 The cumulative incremental displacements are magnified by this factor before being added to the global coordinates.

3 Normally set equal to NINCS in card series II.

4 IPLOT=1,NPLOT.

5 The material status will not be superimposed on the mesh to avoid overcrowding. However, by plotting a series of selected line segments, the structure outline, main reinforcements etc may be highlighted for better clarity.

6 The card series V are to be repeated as many times as NSETS.

C.5 Plot of Stresses

Two cards are required.

Location	*Variable*	*Description Details*	*Note*
CARD I			

1–5	IOPTN	Post processing option for plotting stresses set equal to 4.	1
CARD II			
1–5	NINCS	Total number of increments to plot.	2
6–10	NBEGN	The starting global Gauss point number of the line along which stresses need be plotted.	3
11–15	NNEND	The last global Gauss point number of the line along which stresses need be plotted.	3
16–20	NNCST	Total number of stress plots.	4
21–25	IINCS	The increment number from which the stress components are to be extracted.	

Reference Notes

1 The three components of the stress, σ_x, σ_y, and τ_{xy}, are extracted and placed in an output file that can be directly used in the KFUPM Interactive Chart Utility, ICUSYS, to plot the stresses.

2 Normally set equal to 1.

3 The line can only either be horizontal or vertical.

4 Normally NNCST is set to 1.

C.6 Plot of Deflection for a Given Node

Two cards are required.

Location	*Variable*	*Description Details*	*Note*
CARD I			
1–5	IOPTN	Post processing option for plotting deflections of a given node set equal to 5.	1
CARD II			
1–5	NINCS	Total number of increments to plot.	
6–10	JNODE	Node where deflections need to be plotted.	
14–15	DTYPE	Type and sign of deflections.	2
16–25	TLOAD	Load corresponding to a load factor TFACT=1.	

Reference Notes

1 This option would normally be required if deflections for a node other than that specified in section A.3 needs to be plotted. The file created by this option can be directly used in the KFUPM Interactive Chart Utility, ICUSYS, to plot the load vs. deflections.

2 For example -V deflection to be extracted is negative vertical. For horizontal deflections use letter **H**.

C.7 Gauss Point Coordinates

One card is required.

Location	*Variable*	*Description Details*	*Note*
1–5	IOPTN	Post processing option for printing the coordinates of the gauss points set equal to 6.	1

Reference Notes

1 This option-outputs a file in such a format that associates with each element, a global Gauss number and corresponding coordinates. This is particularly esseentila in identifying the Gauss point numbers for use in section C.5.

Bibliography

[1] Al-Mandil, M. Y., et al. *A study of cracking of concrete bridge decks in Saudi Arabia.* Technical Report, King Fahd Univ. of Petroleum and Minerals, Dhahran, Saudi Arabia, March 1988. National Project Final Report.

[2] Pearson-Kirk, D. et al. Truck loadings for design of concrete bridges in Saudi Arabia. In *Proc., Int. Symp. Concr. Structures in the Middle East*, pages 514–524, King Saudi Univ., Riyadh, Saudi Arabia, 1987.

[3] Pearson-Kirk, D. Characteristics of trucks in Saudi Arabia. In *Third Int. Road Federation (IRF) Regional Meeting, 6*, pages 423–450, 1988.

[4] Charif, A. *Structural Behavior of Reinforced Concrete Beams Strengthened by Epoxy Bonded Steel Plates.* PhD thesis, University of Sheffield, 1983.

[5] L'hermite, R.L. and Bresson, J. Beton arme par collage des armatures. In *Synthetic Resins in Building Construction*, pages 175–203, RILEM International Symposium, Paris, 1967.

[6] Fleming, C. J. and King, G.E.M. The development of strucural adhesives for three original uses in South Africa. In *Synthetic Resins in Building Construction*, pages 75–92, RILEM International Symposium, Paris, 1967.

[7] Hugenschmidt, Felix. *Strengthening of Existing Concrete Structures with Bonded Reinforcements.* Technical Report, CIBA-GEIGY, June 1985.

[8] Lino, T. and Otakawa, K. Application of epoxy resins in strengthening of concrete structures. In *Proc., Third Int. Congress on Polymers in Concrete*, pages 997–1011, Koriyama, Japan, 1981.

[9] Brown, K. Japanese style strengthening for M5 bridges. *Construction News*, 21, October 1973.

[10] Mays, G. C. and Hutchinson, A. R. Engineering property requirements for structural adhesives. *Proc. Instn Civ. Engrs, Part 2* , 485–501, September 1988.

[11] Basunbul, I. A. Examples of plate bonding repair technique in the kingdom of Saudi Arabia. Internal Communication.

[12] Irwin, C. A. K. *The Strengthening of Concrete Beams by Bonded Steel Plates.* TRRL Suplimentary Report 160UC, Department of Environment Department of Transport, Crowthorne, Berkshire, 1975. (Transport and Research Laboratory).

[13] Macdonald, M. D. *The Flexural Behavior of Concrete Beams with Bonded External Reinforcement.* TRRL Suplimentary Report 415, National Technical Information Service, U.S., 1978. (Department of Commerce).

[14] Jones, R., Swamy, R. N., and Ang, T. H. Under- and over-reinforced concrete beams with glued steel plates. *The International Journal of Cement Composites and Lightweight Concrete*, 4(1):19–32, February 1982.

[15] Swamy, R. N., Jones, R., and Bloxham, J. W. Structural behaviour of reinforced concrete beams strengthened by epoxy-bonded steel plates. *The Strucural Engineer*, 65A(2):59–68, February 1987.

[16] Jones, R., Swamy, R. N., Bloxham, J., and Bouderbalah, A. Composite behaviour of concrete beams with epoxy bonded external reinforcement. *The International Journal of Cement Composites and Lightweight Concrete*, 2(2):91–107, May 1980.

[17] Swamy, R. N., Jones, R., and Charif, A. The effect of external plate reinforcement on the strengthening of structurally damaged RC beams. *The Strucural Engineer*, 67(3):45–56, February 1989.

[18] Jones, R., Swamy, R. N., and Charif, A. Plate separation and anchorage of reinforced concrete beams strengthened by epoxy-bonded steel plates. *The Strucural Engineer*, 66(5):85–94, March 1988.

[19] Christoph, W. Long-term behavior of reinforced concrete beams strengthened by subsquently bonded steel plates. In *International Symposium of Future for Plastics in Building and Civil Engineering*, pages 4.ADD.4.1–4.ADD.4.6, Liege, 1984.

[20] Calder, A. J. J. *Exposure Tests on Externally Reinforced Concrete Beams—First Two Years.* TRRL Supplementary Report 529, Department of Environment Department of Transport, Crowthorne, Berkshire, 1979. (Transport and Research Laboratory).

[21] Calder, A. J. J. *Exposure Tests on 3.5 m Externally Reinforced Beams— The First 8 Years.* TRRL Report RR191, Department of Environment Department of Transport, Crowthorne, Berkshire, 1989. (Transport and Research Laboratory).

[22] Calder, A. J. J. *Exposure Tests on Externally Reinforced Beams—Performance After 10 Years.* TRRL Report RR129, Department of Environment Department of Transport, Crowthorne, Berkshire, 1988. (Transport and Research Laboratory).

[23] Van Gemert, D. and Vanden Bosch, M. Long-term performance of epoxy bonded steel-concrete joints. In Sasse, H. R., editor, *Adhesion Between Polymers and Concrete*, pages 518–527, Proceedings of an International Symposium organized by RILEM Technical Committe 52, Paris, September 1986.

[24] Weder, Christoph. Long-term behaviour of reinforced concrete beams strengthened by subsquently bonded steel plates. In *Future for Plastics in Building and Civil Engineering*, Liege, 1984.

[25] Roberts, T. M. Approximate analysis of shear and normal stress concentrations in the adhesive layer of plated RC beams. *The Strucural Engineer*, 67(12):229–233, June 1989.

[26] Newmark, N. M., Siess, C. P., and Viest, I. M. Tests and analysis of composite beams with incomplete interaction. University of Illinois, Urbana, Illinois.

[27] Roberts, T. M. Finite difference analysis of composite beams with partial interaction. *Computers and Structures*, 21(3):469–473, 1985.

[28] Munawar, H. *Flexural and Shear Behavior of Damaged* RC *Beams Repaired by Plate Bonding.* Master's thesis, King Fahd University of Petroleum and Minerals, 1992.

[29] Ngo, D. and Scordelis, A,C. Finite element analysis of reinforced concrete beams. *American Concrete Institute Journal*, 64(3), 1967.

[30] Scordelis, A. C., Ngo, D., and Franklin, H. A. Finite element study of reinforced concrete beams with diagonal tension cracks. In *Proceedings of Symposium on Shear in Reinforced Concrete, American Concrete Institute Publication SP-42*, 1974.

[31] Rashid, Y. R. Analysis of prestressed concrete pressure vessels. *Nucl. Eng. Design*, 7(4):334–344, April 1968.

[32] Scordelis, A. C. Finite element analysis of reinforced concrete structures. In *Proceedings of the Specialty Conference on Finite Element Method in Civil Engineering*, Montreal, Canada, 1972.

[33] ASCE. *State-of-the-Art Report on Finite Element Analysis of Reinforced Concrete.* Technical Report, American Society of Civil Engineering, 1982. Compiled by the ASCE Task Committee on Finite Element Analysis of Reinforced Concrete Structures.

[34] Hsu, T. T. C., Slate, F. O., Sturman, G. M., and Winter, G. Microcracking of plain concrete and the shape of the stress-strain curve. *Journal of the American Concrete Institute*, 60(2):209–224, February 1963.

[35] Wischers, G. Application of effects of compressive loads on concrete. *Bentontechnische Berichte, No.2 & 3*, 1978.

[36] Chen, W. F. and Saleeb, A. F. *Constitutive Equations for Engineering Materials.* Volume 1, John Wiley & Sons, Inc., 1982.

[37] Hinton, E. and Owen, D. R. J. *Finite Elements Software For Plates and Shells.* Pineridge Press Limited, 91 West Cross Lane, Swansea, U.K., 1984.

[38] Jiang, D. H. and Shen, J. H. . Strength of concrete slabs in punching shear. *Journal of Structural Engineering*, 112(12), December 1986.

[39] Owen, D. R. J. and Hinton, E. *Finite Elements in Plasticity: Theory and Practice.* Pineridge Press Limited, 91 West Cross Lane, Swansea, U.K., 1980.

[40] Zienkiewcz, O. C. *The Finite Element Method.* MaGraw- Hill Book Company, 1977.

[41] ACI. State-of-the-art report on high strength concrete. *Journal of American Concrete Institute*, 81(4):361–411, 1984.

[42] Massicotte, B., Elwi, A. E., and MacGregor, J. G. Tension-stiffening model for planar reinforced concrete members. *Journal of Structural Engineering*, 116(11):3039–3058, November 1990.

[43] Abbasi, M. S. A. *Non-linear Finite Element Modelling of Reinforced Concrete Slabs.* PhD thesis, King Fahd University of Petroleum and Minerals, 1991.

[44] Chen, W. F. *Plasticity in Reinforced Concrete.* MaGraw- Hill Book Company, 1982.

[45] Raphael, J.M. Tensile strength of concrete. *Journal of the American Concrete Institute*, 81(2):158–165, 1984.

[46] Goto, Y. Cracks formed in concrete around deformed tension bars. *ACI Journal*, 244–251, April 1971.

[47] Figueiras J. A. and Owen, D. R. J. *Finite Elements Software For Plates and Shells*, chapter Analysis of elasto-plastic and geometrically non-linear anisotropic plates and shells, pages 235–326. Pineridge Press Limited, 91 West Cross Lane, Swansea, U.K., 1984.

[48] Mphonde, A. G. and Frantz, G. C. Shear tests of high- and low-strength concrete beams without stirrups. *ACI Journal*, 350–357, July-August 1984.

[49] Fenwick, R. C. and Paulay, T. Mechanics of shear resistance of concrete beams. *ASCE Journal of the Structural Division*, 94(ST10):2325–2350, October 1968.

[50] Hamadi, Y. D. and Regan, P. E. Behaviour in shear of beams with flexural cracks. *Magazine of Concrete Research*, 32(111):67–78, June 1980.

[51] Cedolin, L. and Del Poli, S. Finite element studies of shear-critical R/C beams. *ASCE Journal of the Engineering Mechanics Division*, 103(EM3):395–410, June 1977.

[52] Ziraba, Y.N., Baluch, M.H., Azad, A.K., Basunbul, I.A., Al-Sulaimani, G.J., and Sharif, A.M. Combined experimental-numerical approach to characterization of steel/glue/concrete interface. Submitted for Publication.

[53] Ngo, D. *A Network-Topological Approach to the Finite Element Analysis of Progressive Crack Growth in Concrete Members.* PhD thesis, University of California, Berkeley, June 1975.

[54] Saouma, V. E. *Interactive Finite Element Analysis of Reinforced Concrete: A Fracture Mechanics Approach.* PhD thesis, Cornell University, Ithaca N. Y., January 1981.

[55] Glemberg, R. *Dynamic Analysis of Concrete Structures.* Technical Report, Dept. of Structural Mechanics, Chalmers University of Technology, Sweden, 1984.

[56] Channakeshava, C., Elwi, A. E., and Murray, D. W. Effect of modeling on NLFE analysis of concrete strucures. *Journal of Structural Engineering*, 114(7):1467–1487, July 1988.

[57] Balakrishnan, S. and Iyengar, K. T. S. R. Elasto-plastic cracking analysis of reinforced concrete. *Journal of Structural Engineering*, 114(11):2421–2438, November 1988.

[58] Ziraba, Y. N., Baluch, M. H, Al-Sulaimani, G. J., and Basunbul, I. A. Bond slip analysis of epoxy coated bars. In *Proceedings of the Third Saudi Engineers Conference*, pages 85–94, College of Engineering, King Saudi University, Riyadh, November 1991.

[59] Al-Sulaimani, G. J., Al-Mandil, M. Y. Basunbul, I. A., and Kaleemullah, M. Effect of epoxy coating of reinforcing bars on their bond behavior with surrounding concrete. In *Proceedings, Third International Conference on Deterioration and Repair of Concrete Structures in the Arabian Gulf*, pages 369–377, October 1989.

[60] Raithby, K. D. *External Strengthening of Concrete Bridges with Bonded Steel Plates*. TRRL Supplementary Report 612, Department of Environment Department of Transport, Crowthorne, Berkshire, 1980. (Transport and Research Laboratory).

[61] Swamy, R. N. and Jones, R. Behavoir of plated reinforced concrete beams subjected to cyclic loading during glue hardening. *The International Journal of Cement Composites and Lightweight Concrete*, 4(1):223–234, November 1983.

[62] Roberts, T. M. and Haji-Kazemi, H. A theoretical study of the behavior of reinforced concrete beams strengthened by externally bonded steel plates. *Proc., Institution of Civil Engineers*, 87(2):39–55, March 1989.

[63] Swamy, R. N., Jones, R., and Charif, A. Shear adhesion properties of epoxy resin adhesives. In Sasse, H. R., editor, *Adhesion Between*

[63] Roberts, T. M. and Haji-Kazemi, H. A theoretical study of the behavior of reinforced concrete beams strengthened by externally bonded steel plates. *Proc., Institution of Civil Engineers*, 87(2):39–55, March 1989.

[64] Hinton, E. and Owen, D. R. J. *An Introduction to Finite Element Computations.* Pineridge Press Limited, 91 West Cross Lane, Swansea, U.K., 1980.

[65] Owen, D. R. J. and Fawkes, A. J. *Engineering Fracture Mechanics: Numerical Methods and Applications.* Pineridge Press Limited, 91 West Cross Lane, Swansea, U.K., 1983.

[66] Ghaleb, B. M. N. *Strengthening of Damaged Reinforced Concrete Beams by External Fiber Glass Plates.* Master's thesis, King Fahd University of Petroleum and Minerals, July 1992.

[67] Saadatmanesh, H. and Ehsani, M. R. Fiber composite plates can strengthen beams. *Concrete International*, 65–70, March 1990.

[68] Saadatmanesh, H. and Ehsani, M. R. *Fiber Composite Plates for Strengthening Birdge Beams.* Elsevier Science Publishers Ltd., England., 1990.

[69] Saadatmanesh, H. and Ehsani, M. R. Strengthened with GFRP Plates I: Experimental Study. *J. Struct. Engrg., ASCE*, 117(11), 1991.

[70] Phillip, A. Ritchie, David, A. Thomas, Le-Wu Lu, and Guy M. Connelly. External reinforcement of concrete beams using fiber glass reinforced plastics. *ACI Structural Journal* , 88(4):490–500, July-August 1991.

[71] Sharif, A.M., Al-Sulaimani, G.J., Basunbul, I., Baluch, M.H., and Ghaleb, B.N. Strengthening of initialy loaded R/C beams using GFRP plates. Accepted for Publication in the ACI Structural Journal.

[72] Gubati, A. A. S. *Study of Various Repair Methods for Reinforced Concrete Flexural Members.* Master's thesis, King Fahd University of Petroleum and Minerals, June 1988.